COMPREHENSIVE ANALYSIS OF DESIGN STORM FORMULATION ACROSS NEWFOUNDLAND UNDER CLIMATE CHANGE WITH SCARCE DATA

by

©Abena Owusua Amponsah

A Thesis submitted to the School of Graduate Studies in partial fulfillment of the requirements for the degree of

Doctor of Philosophy

Faculty of Engineering and Applied Science
Memorial University of Newfoundland
St. John's, Newfoundland and Labrador

May 30, 2023

Abstract

Urban and rural watersheds are becoming increasingly vulnerable to extreme weather events and their consequences. One such consequence is flooding. Stormwater management systems need to be efficiently designed to handle both the quantity and quality of floodwaters. Efficient stormwater systems can be achieved when design parameters are set to their optimum. The design parameters for proper sizing of stormwater infrastructure are obtained from design storms, a combination of Intensity-Duration-Frequency (IDF) curves and a rainfall temporal distribution. IDF curves are developed using rainfall data; as such, changes to the climate will affect these curves. There is a need to re-evaluate the current design storms to determine how they will be affected by the changing climate. Evaluating a design storm from a chaotic variable such as precipitation is complex, and the variation in climate makes it more complicated.

Information on IDF curves is challenging to obtain, especially at locations where precipitation data is lacking or for which there is little data. The focus of this study is the use of models for data generation and analysis of data for appropriate temporal distribution identification. The application of the work in this thesis provides information to guide engineering design and other hydrological studies under climate change. This thesis presents a series of studies that: assess the impact of climate variations on temporal distributions used in design storm analysis; analyzes how these temporal distribution patterns - when combined with other hydrologic factors - can impact mapping for risk of floods, especially

under climate change projections, and develops a precipitation disaggregation model.

The assessment of temporal distribution variation with climate shows that current temporal distributions being used may result in under- or over-design based on the location of interest and climate condition used, either current climate or future climate projections. It highlights the importance of using the appropriate temporal distribution to justify the conservative design. The temporal distributions identified are taken a step further to determine their interplay with hydrologic loss methods and their impact on mapping for the risk of floods. The outcome shows that the extent of a flooded area is highly sensitive to the temporal distribution and loss method used. A precipitation disaggregation model is also developed by coupling a method-of-fragments model with a crossover operator and applied to meteorological stations at Ruby Line, St. John's and Corner Brook to generate hourly data from daily data. These stations were chosen to mainly draw attention to the lack of precipitation data across most locations in the province. The results show that the model can generate hourly data statistics similar to that observed.

Acknowledgements

First and foremost, I thank God for His grace and favor throughout this doctorate program.

Next, my heartfelt gratitude goes to my supervisor, Dr. Joseph Anthony Daraio, for his patience and guidance in the program. I have benefited immensely from your wealth of knowledge and friendship. To you, I say a very big thank you for always making yourself available to answer my questions and to steer me in the right directions. I would also like to thank my supervisory committee members, Dr. Joel Finnis and Dr. Ali Khan for their guidance throughout my program.

I would like to thank my father Mr. Amponsah Tawiah, whose invaluable support made it possible for me to climb this far up the educational ladder.

I like to thank the School of Graduate Studies, Faculty of Engineering and Applied Science, Memorial University and the Town of Pouch Cove for providing graduate student funding and the conducive environment to carry out this research.

I would like to thank the City of St. John's Planning, Engineering and Regulatory Services staff for providing precipitation data to test our developed model.

Finally, I would like to acknowledge the moral and emotional support of my husband, Kwasi Aboagye Tenkorang throughout the period of this program. Thank you all!!!

Table of Contents

List of Tables

List of Figures

List of Abbreviations

IDF	Intensity-Duration-Frequency
GA-MOF	Genetic Algorithm-based Method of Fragments
MoF	Method of Fragments
I-MOF	Interval-based sampling Method of Fragments
HEC-HMS	Hydrologic Engineering Center's Hydrologic Modeling System
HEC-RAS	Hydrologic Engineering Center's River Analysis System
RCP	Regional Concentration Pathway
OC	Onepoint Crossover
TC	Twopoint Crossover
UC	Uniformpoint Crossover
RCM	Regional Climate Model
GCM	Global Climate Model
CMIP5	Coupled Model Intercomparison Project Phase 5
SoF	Set of Fragments
KNN	K-Nearest Neighbor
GEV	Generalized Extreme Value
SIC	Schwarz Information Criterion
AIC	Akaike Information Criterion
BIC	Bayesian Information Criterion
AEP	Annual Exceedance Probability
NA-CORDEX	North American Coordinated Regional Downscaling Experiment
PCIC	Pacific Climate Impacts Consortium
ASCE	American Society of Civil Engineers

Co-authorship Statement

For each manuscript and the thesis as a whole, I took the lead in the problem identification, but particularly for chapter 2, Dr. Khan led the problem identification, design of the research methods, performed data analysis and model setups and prepared the original manuscripts Drs. Daraio and Khan reviewed and contributed ideas and interpretation to the manuscript for chapter 2; Drs. Daraio, Khan and Finnis reviewed and contributed ideas and interpretation to the manuscript for chapter 3. Drs. Finnis and Li reviewed and contributed ideas and interpretation to the manuscript for chapter 4. All manuscripts were reviewed and subsequently revised based on the feedback from the co-authors and the peer reviewers throughout the peer-review processes before submission to journals/conferences for publication.

Chapter 1

Introduction

1.1 Background

Information about rainfall events and their characteristics is fundamental in designing drainage infrastructure systems intended to convey runoff from these events and minimize adverse impacts on society, reducing flood vulnerability by preventing road washouts and destroying public property (Yilmaz et al., 2020; Ngene et al., 2020; Kimoto et al., 2011; Silva & Simonovic, 2020; Adamowski et al., 2010; Zhou et al., 2019). This is of utmost importance in urban areas as flooding remains an inevitable natural phenomenon, and such adverse impacts can be very costly. Effective drainage systems can be achieved when the correct runoff information is available. This information is drawn from design storms in combination with Intensity-Duration-Frequency (IDF) curves (Ngene et al., 2020).

This thesis also examines aspects of climate change's impact on design storms and possible approaches to improving local data use. Accurate estimates of these changes will lead to better storm system designs. There have been many reviews into better storm system designs, with a recent one by E. Watt and Marsalek (2013) which pointed out that the sensitivity of design storms to climate change is unknown. Watt and Marsalek's review also

discussed the importance of using local or regional information to develop design storms. Many countries use design storms not developed from their local climatic conditions. An example Watt and Marsalek give is the need to develop design hyetographs based on Canadian rainfall data. This research aims to fill this gap by designing for a previously neglected region, specifically Newfoundland and Labrador, Canada.

IDF curves are based on a stationary assumption where the climate is assumed to remain stable over a period. Recent climate trends indicate a shortening of this stability period (Knutson et al., 2021; Deser, 2020; Bănăduc et al., 2020; Hussain et al., 2020), consequently posing substantial risks in this century (Vicente et al., 2019; Pripoaie et al., 2019; Bai et al., 2021; Vu et al., 2018; Al Mamoon et al., 2019; V. Nguyen & Nguyen, 2019). One such risk would be continuing to design drainage systems using IDF curves based on the stationarity assumption as this would result in poor handling of runoff and inaccurate demarcation of flood risk zones (Silva et al., 2021; Al Saji et al., 2015; Nwaogazie & Sam, 2020; Srivastav et al., 2014; Einfalt et al., 1998; AghaKouchak et al., 2018; Ayyub et al., 2018). For the engineering community, it is necessary to develop mechanisms to deal with these risks (Wasko et al., 2021; Nasr et al., 2021; Manous & Stakhiv, 2021)

In addition to the shortening of the stable period comes many possible future trajectories of the climate, which creates uncertainty for engineering professionals concerning the design of structures. One of the goals of this dissertation is to help advance a simplified way for engineers to incorporate uncertainties from climate projections in engineering design by way of design parameters choice based on the acceptable level of risk for the project in question.

1.2 Intensity-Duration-Frequency Curves and Design Storms

Four parameters are required to generate input into hydrologic models for an event simulation: i) the amount of precipitation (depth) that ii) occurs in a time period (duration), iii) with a chosen likelihood of being met or exceeded (frequency; usually measured as a return period); and finally, iv) how this amount is distributed within the duration (temporal distribution). Intensity-Duration-Frequency (IDF) curves provide the first three parameters. Coupling these with the fourth parameter, a critical component in stormwater design, provides a 'design storm' that is an idealized and scalable representative rainfall 'event' informed by local observations and easily incorporated into infrastructure planning.

1.2.1 Intensity-Duration-Frequency Curves

Intensity-Duration-Frequency (IDF) curves comprise precipitation event duration and return period associated with average intensity (Sun et al., 2019). IDF curves are constructed from annual maximum precipitation values for durations ranging from 5 minutes to 24 hours (Simonovic et al., 2016). Due to their simple and practical nature, IDF curves are used to obtain design criteria for water infrastructure systems.

Over the years, there have been several techniques employed to develop IDF curves (Yan et al., 2021). The monotone ranking system was one of the earliest methods (Kumar & Kumar, 1989). This method involves ranking rainfall values in descending order and estimating the return periods using the Weibull formula (Selaman et al., 2007). The purpose of adopting the annual maximum series was to reduce data processing time (Hasan & Wai Chung, 2010). The use of an extreme value distribution fitted to annual maximum values followed this (Madsen, Rasmussen, & Rosbjerg, 1997). The 2-parameter Gumbel distribution is most commonly used (Hatch, 2008; Carlier & El Khattabi, 2016). The disadvantage of this method is that the annual maximum values may not always fit the distri-

bution correctly, and another distribution may be a better fit for the data set (Koutsoyiannis, 2003a, 2004). However, this conclusion also depends on the goodness-of-fit statistic used. For example, according to the Kolmogorov-Smirnov test, the Gumbel distribution was a good fit for the 15-minute rainfall data from Wabush Lake Airport. However, it was rejected by the Chi-Square test (Office of Climate Change & Energy Efficiency, 2015).

With the increase in computational power and the availability of new statistical methods, IDFs from partial duration series were developed (Madsen, Rasmussen, & Rosbjerg, 1997). This provides an alternative to using only annual maximum values where either the "n" largest values in a year or the values exceeding a set threshold fit with the Gumbel distribution (Madsen, Pearson, & Rosbjerg, 1997). Chin (2013) stated that while estimates of the average period between values of a particular magnitude are obtained using the partial duration series, the annual maximum series provides estimates of the average period between years when a particular value is exceeded. Despite the processing time and work involved in obtaining the partial duration series for IDFs, Flanders, Belgium, has adopted this method for everyday use (Flanders Environment Agency, 1996).

The use of IDFs does present some challenges. For example, the use of annual maximum for IDF construction has been proven, both theoretically (Demarée, 1985) and practically (Willems, 1998; Vaes et al., 1994), to lead to underestimating rainfall intensities or overestimating return periods. Other concerns include mismatch of durations used relative to durations of actual storms; and average intensities that do not represent actual historic rainfall (Bedient et al., 2012; Al-Areeq et al., 2021). Further, IDF curves require a great deal of data to give reliable estimates of extreme events (Hailegeorgis & Alfredsen, 2017; Mélèse et al., 2018). A minimum of ten years of data with durations from 5 minutes to 24 hours is required to develop these curves, ideally much longer. Such data length and fine-scale temporal resolution are difficult to obtain, especially in data-scarce regions.

In many temperate regions, snow is an inevitable consequence of cold weather. While

snowfall amounts are often converted to water equivalents and treated as individual events to predict annual precipitation events (Brown et al., 2018), snowfall from multiple events may accumulate over time, thus storing potential runoff volumes. This storage may be released gradually over time in the form of snowmelt, or it may be rapidly converted to runoff by rain-on-snow events (Cohen et al., 2015). Gradual melting can cause problems since the runoff may fill or saturate stormwater systems before an actual design event occurs and consequently can produce wet soil conditions, leading to more runoff (Beniston & Stoffel, 2016; Freudiger et al., 2014). Refreezing during cold evenings may exacerbate some of these problems. Many rules for sizing water quantity volumes are based on treating a rainfall event with a specified occurrence frequency, such as the 2-year, 24-hour rainfall event. A similar process has been proposed for rain-on-snow events (Brown et al., 2018). However, a data set must be developed for rainfall events that occurred only for months with snow on the ground rather than for all precipitation events. This data set should exclude snow and non-runoff producing events (< 0.1 inch of precipitation). Rain-on-snow could affect the flow when evaluating long-duration storms, especially in regions with high snowfall. Except for higher elevations with deeper snowpacks, a long-duration design storm should be assumed to result in the complete melting and runoff of the typical snowpack.

1.2.2 Design Storms

Design storms are synthetic precipitation events or natural ones that are based off the IDF. They are essentially patterns of precipitation used as inputs into hydrologic models to obtain the hydrograph from a watershed (Ball et al., 2016). These are used in delineating floodplains and sizing drainage systems (Kimoto et al., 2011) and are often presented as hyetographs or isohyetal maps (Koutsoyiannis, 1994). Design storms give the distribution of a rainfall event in time, with the depth of this distribution obtained from the IDF curves. The coupling of these two items is the basis for most design standards. The choice of depth

6

for designing a water infrastructure depends on the design life of that infrastructure. The design life informs the choice of the return period from the IDF curves. The choice of the duration hinges on the time concentration of the watershed in question, with urban watersheds having a shorter time of concentration. Wu et al. (2006) categorized methods for design storm development into five groups: a) by discretion, b) based on IDF curves, c) using rainfall mass curves,d) rainfall hyetograph ordinates ranking and e) using statistical moments.

Veneziano and Villani (1999) categorized designs storms based on generation from a single point on the IDF curve; use of the complete IDF curve; standardized profiles; or outputs from stochastic models. A study by Peyron et al. (2002) identified a deficit in most of the current methods. The methods were either able to capture the peak runoff but not the volume of the storm or vice versa. An important conclusion of the study was that the choice of design storm hyetograph was very much dependent on the climate in the region. The design storm used should be based on one that produces acceptable rainfall patterns for a region or country (Kimoto et al., 2011). Local variations in climate in a region are often not considered (Al-Rawas & Valeo, 2009; Guo & Hargadin, 2009). Studies of variation in rainfall over short distances, including in Newfoundland, showed that, even over distances as short as 10 km, there could be significant variations in rainfall climatology (Wadden, 2002; Doyle, 1952).

Despite the difference in climate gradients and the amount of literature suggesting that design storms should be tailored to suit different climates (Vieux & Vieux, 2010), Newfoundland and Labrador (NL) currently uses one synthetic type of design storm in all cities and towns. This could have severe implications for water infrastructure design where under-design may be occurring in some locations and over-design in others. Designing for the worst possible storm and the cost of damages from under-design are both very expensive. As a result, balance is struck to design a system that poses an acceptable level of risk for the

community (Deng et al., 2020). The definition of acceptable risk depends on the community in question. Improper design can lead to the loss of lives and property damage worth billions of dollars of taxpayers' money. Measures should be put in place to ensure that such losses are prevented and, where they cannot be prevented, that their impacts are minimized.

1.2.2.1 History of Design Storms

Design storms have evolved since their inception in 1957. The first design storm was the Chicago Model by Keifer and Chu (1957). As the name suggests, it was designed specifically for the city of Chicago. However, it has since been implemented in many other cities. This method takes the rainfall volume from the IDF curve and distributes it over an allocated period. Several studies have identified drawbacks associated with this method (James & Robinson, 1982; Waiesh, 1979; McPherson, 1977).One of these drawbacks is that synthetic storms obtained from IDFs encompass data from many different storms, ranging from convective to cyclonic. This is of great concern, especially when the IDF curve's region spans a climate gradient. Many researchers in the 1970s and 80s developed alternative methods to overcome these drawbacks.

Huff (1967) developed a design storm based on the temporal distribution of actual rainfall events. This method split the storm duration into fractions of the total duration and categorized each storm into four groups based on the quarter where the greatest depth occurred. This was followed by the design storm model of Pilgrim and Cordery (1975). The difference between Huff's model and that of Pilgrim and Cordery was that, while Huff's was based on all storm events, Pilgrim and Cordery's model was only based on severe storms.

Given the differences in climatic conditions across Canada as compared to conditions in the United States, Hogg (1980) used Huff's method to generate a design storm based on the climate in Canada. He studied the temporal distribution of 1- and 12-hour rainfall in many parts of the country and provided mass curves for 35 of these locations. W. Watt

et al. (1986) developed another model for 1-hour design storms using Canadian data. This model was characterized by a linear rise from the storm's beginning until the peak, followed by an exponential decay from the peak to the storm's end. The ASCE model (US Army Corps of Engineers, 2000) was built as an improvement to the original balanced design model (United States Soil Conservation Service Engineering Division, 1986). Its inclusion in the HEC-HMS program has resulted in its frequent use. With changes in the climate anticipated, there is a need to understand why these changes are occurring, how these changes affect the hydrologic system and, in turn, impact design considerations.

1.3 Climate Change and Design Consideration

Climate is a probabilistic summary of expectations and variability of weather in a region (*Canada's Changing Climate Report*, 2019). Unlike weather which varies on a day-to-day basis, the climate is often evaluated in 30-year periods since this duration is long enough to notice variability and detect changes (McMichael et al., 2004). Through this evaluation, changes in patterns of meteorological variables such as precipitation, temperature and wind can be identified. Identifying such changes is essential to allow humans to plan for the future. At present the primary driver of climate change is human activity; specifically increased concentrations of key trace gases ("greenhouse" gases) as a consequence of fossil fuel consumption. The sixth Intergovernmental Panel on Climate Change (IPCC) report confirms the dominant role of humans in the current rate of change through activities such as energy production, changes to land cover and industrial activities (Ting & Ying, 2021). The report indicates that global surface temperatures have increased and will continue to increase (Masson-Delmotte et al., 2021).

The rate at which the climate is changing is of great concern given recent trends, which increase demand consideration by design professionals. With the increase in global tem-

perature comes a change in global precipitation patterns (Scherer et al., 2019). Increasing the temperature of the earth's atmosphere increases its water-holding capacity potentially making more atmospheric moisture available, which is expected to increase precipitation frequency and intensity in key locations (e.g. humid climates; areas influenced by extratropical cyclones) (Masson-Delmotte et al., 2021; Mirhosseini et al., 2013). The increase in precipitation events is observed to be more significant for extremes than total annual precipitation (*Canada's Changing Climate Report*, 2019). In addition to the changes in precipitation patterns, global warming would also lead to early spring melt in temperate regions generating extra runoff that has to be conveyed promptly to prevent adverse impacts on society (Masson-Delmotte et al., 2021).

Climate models are used to analyze how increased global warming impacts various components in the atmosphere. Despite advances in scientific knowledge, climate model complexity, and massive data availability, significant uncertainty still exists in climate model predictions. Carslaw et al. (2018) argued that increased physical understanding of the earth's system should be accompanied by an enhanced understanding of climate models and their uncertainties. There are many sources of uncertainty in climate model predictions. While some can be reduced with technical solutions (e.g. model improvements), others may not; e.g. uncertainty related to future greenhouse gas concentrations (climate scenarios), which depends on a host of social, economic, and political factors that will influence actions taken by the global community.

It has been suggested that the issue of climate modelling uncertainty is the primary factor preventing engineers from incorporating climate change into their designs (Meyer et al., 2008; Hallegatte et al., 2012; Underwood et al., 2020; Park et al., 2013). Though uncertainty due to model choice or analysis methods is often equivalent to the uncertainty inherent in observed data, it seems to be perceived as a more significant concern. Regardless of the source, uncertainty provides an opportunity for scientists to demonstrate that

climate analyses based on traditional (observation-based) methods and forward-looking climate projections can simultaneously be flawed and valuable.

1.3.1 Climate Downscaling

Scaling can also pose a challenge to using climate predictions. Engineers often design for infrastructure at a scale much smaller than that on which climate predictions are made. The General Circulation Models (GCMs) and Earth System Models (ESMs), the basis for studies of climate dynamics, sensitivity, and response to anthropogenic warming (Ahmed et al., 2019), are by necessity, run at relatively low spatial and temporal resolutions; projections are consequently too coarse for planning and design purposes. Although it is theoretically possible to address mismatched scales by running higher resolution GCM simulations, this solution is rarely feasible given the computational effort required (Allen et al., 2014; Haarsma et al., 2016; Liang-Liang et al., 2022). Consequently, other solutions have been sought in the form of 'climate downscaling.' Downscaling techniques evolved in a process by which regional and local climate variables are related to large-scale atmospheric conditions (e.g. from GCMs) (Friedrichs-Manthey et al., 2020). Figure 1.1 shows the relationship between GCM scales and hydrologic scales, which downscaling is meant to address. The two general categories of downscaling are dynamic and statistical downscaling.

1.3.1.1 Dynamic Downscaling

The first downscaling approach simply runs a higher resolution model, usually covering a smaller area to reduce computation costs. This is typically accomplished by forcing a Regional Climate Model (RCM) with boundary conditions extracted from GCM output (S. Li et al., 2021; Adachi & Tomita, 2020). The enhancement in spatial resolution changes from a large to a regional scale, e.g., from 2500km to 25km. The temporal resolution of the model output is also enhanced, enabling daily instead of monthly projections. These
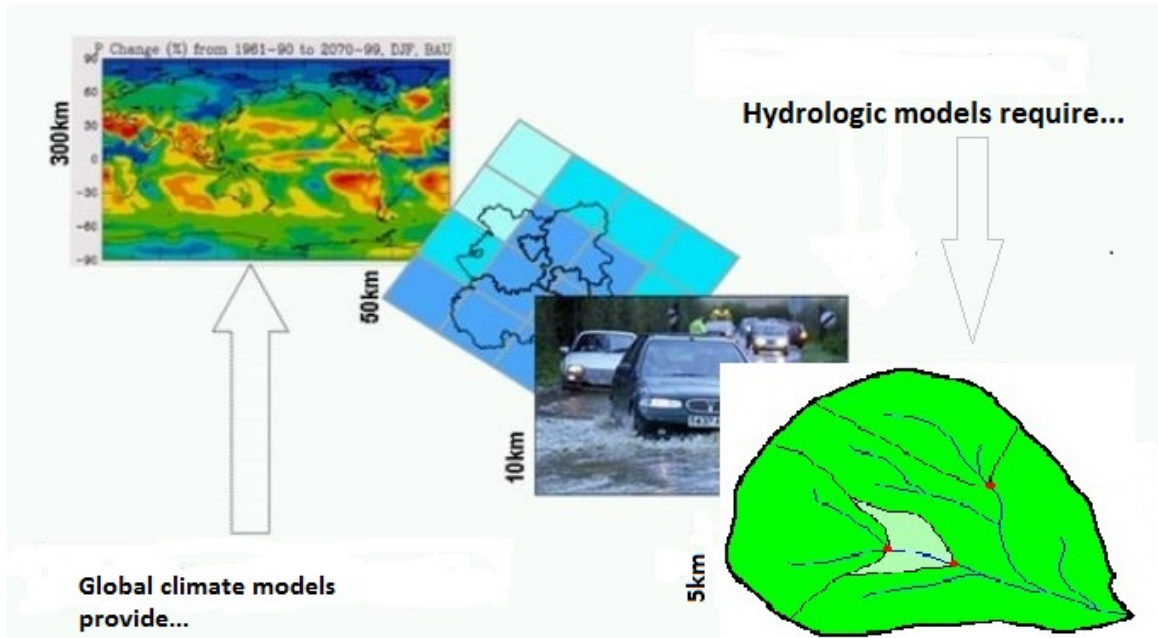
Figure 1.1: Relationship between General Circulation Model and hydrologic scales

enhanced outputs greatly improve inputs in hydrological models. A schematic illustration of this method is presented in Figure 1.2. One of the advantages of dynamic downscaling is that its basis in atmospheric physics can provide meteorologically consistent downscaled variables; however, it is computationally expensive.

There are RCMs available through international collaborations covering most geographical locations on earth. This dissertation uses RCM simulations from the North American Coordinated Regional Downscaling Experiment (NACORDEX), a database of regionally downscaled climate data to improve climate change impact assessments across North America. A major advantage of RCMs is their better representation of local climate variability and, more importantly, extremes compared to GCMs (Seenu & Jayakumar, 2020). RCMs are also known to improve the estimation of climate variables such as precipitation which is essential in engineering design for quantifying runoff (Tegegne & Melesse, 2021). A major influencing factor of RCM data is their GCM forcing. Researchers are working to improve on these GCMs, with the most recent being the development of the Coupled Model
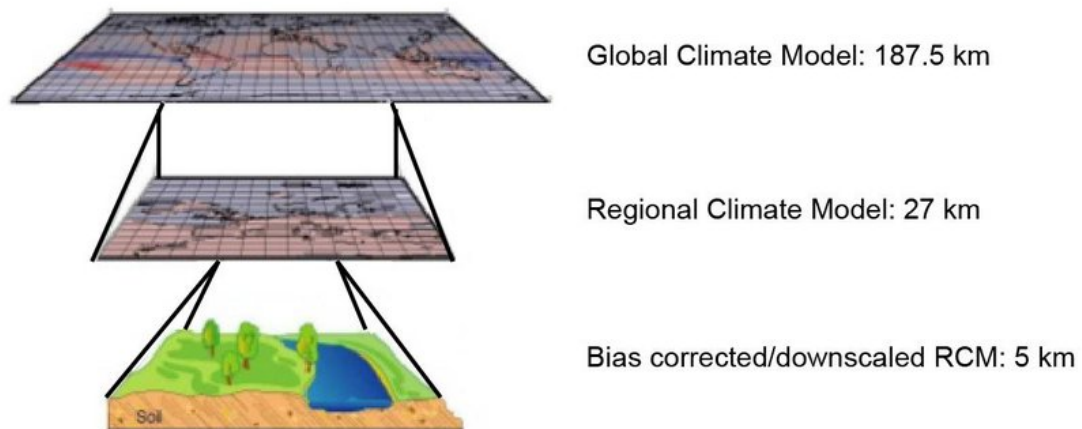
Figure 1.2: Dynamical downscaling scheme. (Fernandez & Golubiewski, 2019)

Intercomparison Project Phase 6 (CMIP6) with a spatial resolution of 0.1 degrees (Xin et al., 2021).

1.3.1.2 Statistical Downscaling

Statistical downscaling uses empirical methods and local observations to establish a statistical relationship between the large-scale physical model and local variables of interest with the assumption that this statistical relationship is stationary despite changes in the climate (Wilby et al., 2004; Schmidli et al., 2006; Ali et al., 2019; Baghanam et al., 2020; Maraun et al., 2019; Gutmann et al., 2014). In the statistical relationship, the variables to be downscaled at the local scale are designated as *predictands* while variables obtained from the GCM outputs are designated as *predictors* (Sachindra & Perera, 2016; Teegavarapu & Goly, 2018; Yang et al., 2017). These can be similar to the predictands, or they can vary. Any variable can be used as a predictor, provided a correlation exists between the predictand and the predictors.

The statistical relationship can be established in several ways. One way is through statistical regression methods, where a transfer function relating the predictors to the predictand

is obtained. Another method is through conditional probability-based methods where "the probability distribution of the predictand is conditionally based on the predictors" (Baguis et al., 2008). Another means is re-sampling (also known as weather typing), which entails searching historical data and matching the findings to similar conditions in the future. There are many advantages to statistical techniques: they are computationally inexpensive and can provide information at higher spatial and temporal resolutions if observational data is available, among others (Manzanas, 2016; Gutmann et al., 2014; Al Mamoon et al., 2019). Despite all these advantages, disadvantages also exist (Sunyer et al., 2015; Duan & Mei, 2014). A notable challenge of this method is that it does not provide uniform coverage. Similar to the international efforts which make RCM data freely available, statistically downscaled data are also available but usually on a regional basis. The Pacific Climate Impacts Consortium (PCIC), a regional climate center, provides statistically downscaled projections to support hydrologic impact assessment under climate change in the Yukon and Pacific regions. Table 1.1 provides a summary of the outputs, requirements, advantages, disadvantages and some applications of these methods.

1.3.1.3   Uncertainty

Because GCMs are models representing atmospheric interactions, imperfections are inevitable. These imperfections manifest as biases and uncertainties in the model output. Several studies (H. Li et al., 2010; Teutschbein & Seibert, 2012; Lafon et al., 2013) have developed methods to address different biases, such as bias correction via constructed analogues quantile mapping (Werner & Cannon, 2015). An overview of research findings on climate change impacts on IDF curves and design storms in provided in the next section.

Table 1.1: Advantages and Disadvantages of Dynamic and Statistical Downscaling

Dynamic	Statistical
Provides	
• ~11 km grid cell information, though it can be higher or lower than this value • Information at sites with no observational data	• Any scale, down to station-level information where observational data is available • Time series
Requires	
• High computational resources and expertise • Reliable GCM simulations	• Medium/low computational resources • Sufficient amount of good quality observational data • Reliable GCM simulations variables
Advantages	
• Based on consistent physical mechanisms	• Computationally inexpensive and efficient, which allows for many different emissions scenarios and GCM pairings
• Resolves atmospheric and surface processes occurring at sub-GCM grid scale	• Methods range from simple to elaborate and are flexible enough to tailor for specific purposes
• Not constrained by historical records so novel scenarios can be obtained	• The same method can be applied across regions or even the entire globe, which facilitates comparison across different case studies
• An ensemble of RCMs are available for uncertainty analysis	• Relies on the observed climate as a basis for driving future projections
	• Can provide point-scale climatic variables from GCM-scale output
	• Tools are freely available and easy to implement and interpret; some methods can capture extreme events

Dynamic	Statistical
Disadvantages	
• Computationally intensive	• High quality observed data may be unavailable for many areas or variables
• Limited number of RCMs available and model results are not available for all locations globally	• Assumes that relationships between large and local-scale processes will remain the same in the future (stationarity assumption)
• May require further downscaling and bias correction of RCM outputs	• The simplest methods may only provide projections at a monthly resolution variable
• Results depend on RCM assumptions, different RCMS will give different results	
• Affected by bias of driving GCM	
Applications	
• Country or regional level assessments with significant government support and resources	• Weather generators in widespread use for crop-yield, water and other natural resources modeling and management
• Future planning by government agencies across multiple sectors	• Delta or change factor method can be applied for most adaptation activities
• Impact studies that involve various geographic areas	

1.4 Impacts of Climate Change on IDF curves and Design Storms

As stated previously, ongoing changes to the climate from anthropogenic forces have motivated research into the consequences of these changes and how to better prepare for them (Simonovic, 2017; V.-T.-V. Nguyen, 2020). Major floods are likely to increase in frequency and severity (Kundzewicz et al., 2014; Arnell & Gosling, 2016; Tabari, 2020), as warming of the earth's atmosphere may intensify the hydrologic cycle (Siler et al., 2018; Fildier et al., 2021). Consequently, there will be an increase in both mean and extreme precipitation in some areas around the globe (Nazif et al., 2017). Together, these will impact runoff rates and discharge into rivers at timescales that vary from sub-daily to annual peak flows (Sorribas et al., 2016; Donnelly et al., 2017; Kay et al., 2021; Gudmundsson et al., 2021). In addition to the intensity of the precipitation, its temporal distribution and inter-event dry

spells impact the risk of flooding (Sridhar et al., 2019; Oppel & Fischer, 2020). Increased urbanization coupled with an expected increase in the frequency of significant storms due to climate change has sparked an interest in efforts to minimize vulnerabilities of cities to flooding through improved stormwater infrastructure design and estimation of design floods to guide the design of these infrastructures (Simonovic, 2017; V.-T.-V. Nguyen, 2020). Changes in precipitation mean changes to IDF curves.

The impact of climate change on IDF curves has been well studied (Vu et al., 2018; Luo et al., 2018; Al Mamoon et al., 2019; V. Nguyen & Nguyen, 2019; V.-T.-V. Nguyen, 2020) and suggests that IDF curves based on historical data are no longer valid for use in design under the changing climate. A basic assumption behind the use of IDF curves for engineering design is the stationarity rule, i.e., there is no significant change in extremes over a given period (Mirhosseini et al., 2013). However, changing climatic conditions challenge the validity of this assumption and have prompted several studies to include non-stationarity in IDFs. Cheng and AghaKouchak (2014) found that not including non-stationarity resulted in current IDFs underestimating extreme precipitation by as much as 60%. Shephard et al. (2014) conducted a trend analysis on extreme precipitation across Canada. In contrast to Cheng and AghaKouchak, they concluded that the stationarity assumption still holds, as fewer than 5.6% of the stations they studied showed significant changes in trends. The conclusions from these studies vary greatly. Mailhot et al. (2007) reported that, in southern Quebec, the return periods associated with 2 and 6 hours will be halved by 2070, while the return period of longer durations (12 to 24 hours) will decrease by a third. Xu et al. (2012) also found that the 24-hour rainfall depth from the IDF curve for the Qiantang River Bain in East China may have a relative change ranging from -16% to 113% by 2099. While increases in rainfall have been the most expected effect of climate change in temperate regions (Forsee & Ahmad, 2011), the opposite is expected in tropical regions, i.e., they are forecasted to experience decreases in rainfall and increases in droughts. De Paola et al. (2014),

in a study of the effects of climate change on IDFs in three African countries, presented findings that indicate a decrease in rainfall intensity. To study the impact of climate change on IDF curves, we need to look at one of the significant challenges with the generation of these curves, i.e., the availability of long-term data at various durations, from minutes to hours.

1.5 Disaggregation Models

To adequately prepare for current and future floods, stormwater infrastructure is put in place. Engineering design parameters for these structures are obtained from IDF curves which require at least ten years of data to develop (Simonovic et al., 2016). This data length is not always available; when available, missing or usable data might be shorter than the total time required for IDF construction. However, in the latter case, methods are available to correct bad data and fill in missing data. Disaggregation techniques are one such method. Disaggregation models are methods that break down observations, at a lower resolution into higher ones. Applying such models helps generate usable data for hydrologic purposes ranging from stormwater infrastructure design to flood risk mapping.

A review by Koutsoyiannis (2003b) discussed rainfall disaggregation models used in the hydrology field from early 1900 until 2003. This review dealt with two of the major disaggregation methods in use: the models based on point process (a.k.a Bartlett-Lewis models) and those based on the cascade technique. More than a decade later, many more techniques and variations have been introduced (Ormsbee, 1989; Burian et al., 2000; Molnar & Burlando, 2005; Kossieris et al., 2015). There are two schools of precipitation disaggregation models: deterministic and stochastic. Deterministic models are developed such that there is no element of randomness included: a set of parameter values and initial conditions will always produce the same result. On the other hand, as the name implies, stochastic mod-

els include some inherent randomness: a set of parameters and initial conditions will yield different results in consequent applications.

1.5.1 Deterministic Models

The first disaggregation models were simple and easy-to-use deterministic models. Two examples of these are the linear model (Ormsbee, 1989) and the constant disaggregation model. The former uses simple linear interpolation to divide the rainfall at coarse-scale into fine-scale durations. Some assumptions are associated with this model, the most important being that geometric similarity exists between the inner and outer temporal patterns. Six temporal patterns (Ormsbee, 1989) are defined using a 3-hour moving window (V_{t-1}, V_t, V_{t+1}) with the target hour at the center. The rainfall intensity, V, for a coarse-scale duration to disaggregate, T, is:

$$g(t) = \frac{V_{t-1}}{V*_t} - \frac{(V - t - 1 - V_t)t}{V*_t} \text{ for } 0 \leq t \leq t* \tag{1.1}$$

$$g(t) = \frac{V_t}{V*_t} - \frac{(V - t - V_{t+1})(t - t*)}{V*_t (T - t*)} \text{ for } t* \leq t \leq T \tag{1.2}$$

where $V*_t$ is a normalisation factor and $t*$ is the critical time that determines the temporal pattern used. (See Ormsbee (1989) and Hingray and Haha (2005) for full details.)

The constant disaggregation model is a simple method of dividing precipitation at a wet coarse-scale duration equally into fine-scale durations. This model assumes constant or uniform rainfall distribution over the wet period, implying no rainfall variability. This sometimes generates unrealistic precipitation values (Hingray & Haha, 2005). The advantages of deterministic models are their simplicity and parameter-less nature. The major drawback of models in this category is that they cannot produce dry periods within a wet duration (e.g., when disaggregating 24-hour rainfall to hourly, there will be rainfall for ev-

ery hour). Generally, deterministic models do not have huge data requirements; however, their inability to produce realistic rainfall data makes them undesirable for precipitation disaggregation.

1.5.2   Stochastic Models

Stochastic models evolved to address the problem of deterministic models generating unrealistic precipitation. Many stochastic disaggregation models exist, and they can be broadly grouped into 3 classes:

1. Probability-dependent models which generate precipitation within a wet hour using a specified probability (Hassan, 2020; Kim & Onof, 2020; Park et al., 2021).

2. Weighted-cascade models,in which precipitation at coarse-scale is divided into fine-scale based on randomly generated weights (Müller & Haberlandt, 2018; Müller-Thomy, 2020).

3. Resampling models, in which, coarse-scale precipitation is disaggregated to fine-scale using a vector of fragments, representing the ratio of fine-scale to coarse-scale precipitation (Aguilar & Costa, 2020; Schepen et al., 2020).

Below are descriptions of models in these classes. Stochastic models, like deterministic ones, also have a major drawback- they often require large amounts of data to provide reasonably disaggregated values (X. Li et al., 2018). For instance, resampling models are typically used with at least 20 years of data available both at the coarse and desired fine-scale to allow for a large sample space when resampling the fragment vectors (Breinl et al., 2017; Pui et al., 2012). Another instance is with the probability-dependent models in which model parameter estimates use part of the available data (Koutsoyiannis & Onof, 2001). In such cases, small data sets will yield unreliable parameters.

1.5.2.1 Probability-Dependent Models

Models based on the Poisson cluster process use rectangular pulses to show how precipitation generation occurs (Park et al., 2021). In these models, the time between discrete events is known, while the exact timing of these events is random (Koutsoyiannis & Onof, 2001). Clusters are a simple way to characterize varying rainfall types and amounts. The two main models in this category, Bartlett-Lewis (Figure 1.3) and Neyman-Scott (Figure 1.4), have the same configuration, where a Poisson process describes the arrival of storms and the origin of a rain-cell (individual cells that come together to form a storm) within each storm (Kaczmarska et al., 2014). At the same time, exponential distributions determine the rain-cell arrival and duration in each storm (Kaczmarska et al., 2014). The models use simplified stochastic assumptions and few physical parameters (Park et al., 2021).

The difference between these models is in how the rain cell originates in a storm (Kim et al., 2016). In the Bartlett -Lewis model, the interval between successive rain cells is independent and identically distributed (IID) while in the Neyman-Scott models, the independent and identically distributed component describes the time interval between the rain cells and the start of the storm (Velghe et al., 1994; Cowpertwait et al., 2002). Variants of the Bartlett-Lewis model include Bartlett-Lewis Rectangular Pulse, both its modified type and a gamma version, and the Randomized Bartlett-Lewis model (Rodriguez-Iturbe et al., 1987; Glasbey et al., 1995; Koutsoyiannis & Onof, 2001; Pui et al., 2012). The model requires observed time series over long periods. For example, Koutsoyiannis and Onof (2001) used 36 years of data, while Pui et al. (2012) used 42 and 63 years of data. In each case, the model uses all the data to estimate the five to seven parameters (depending on the version of the model) and to calibrate to ensure that it reproduces observed historical statistics well. This raises questions about the validity of the approach in situations with limited data.
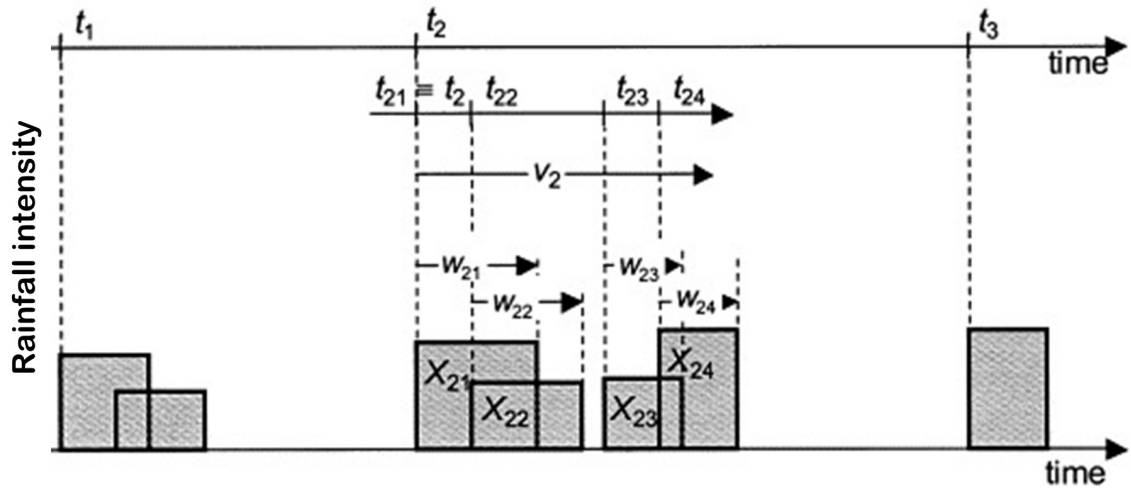
Figure 1.3: Visual Representation of the Bartlett-Lewis Rectangular Pulse Model Koutsoyiannis and Onof (2001))
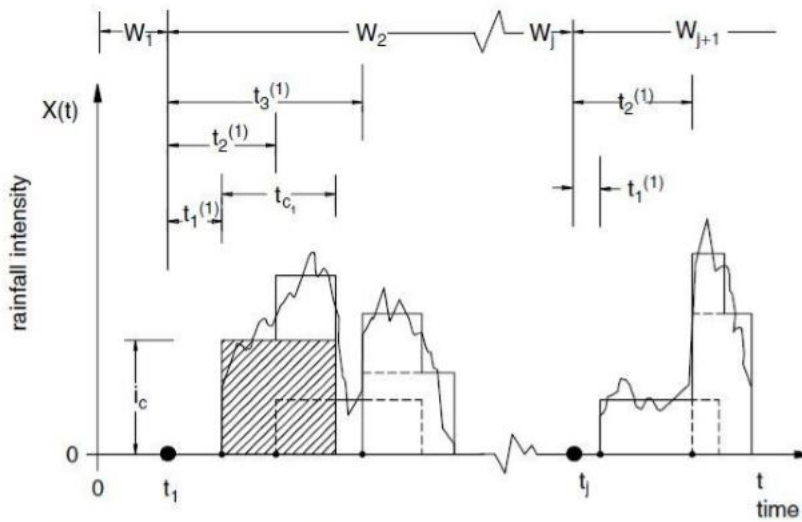
W_j = interarrival time of events (pulses)
$t_j^{(1)}$ = displacement of the j-th cell from the cluster center
t_{c_i} = duration of the i-th pulse
i_{c_i} = intensity of the i-th pulse

Figure 1.4: Visual representation of the Neyman-Scott Models Olsson and Burlando (2002)

1.5.2.2 Weighted-Cascade Models

Cascade models for rainfall disaggregation were first developed by Gupta and Waymire (1993). Güntner et al. (2001) and Molnar and Burlando (2005) further developed these models. Types of models in this class include the Canonical, Microcanonical, Continuous Universal Multifractal, and Random Multiplicative models(Pui et al., 2012; Müller & Haberlandt, 2018). To disaggregate rainfall intensity at a coarse-scale or cascade level $k-1$, rainfall intensity is multiplied by a set of weights, W, to obtain values at a fine-scale or cascade level, k. An important parameter in these models is the branching number, b, that determines how many subintervals rainfall at the coarse-scale will generate the fine-scale values. Rainfall intensity R for the jth subinterval at cascade level k is estimated using equation 1.3.

$$R_{j,k} = R_0 \Pi_{j=1}^{k} W_j(j) = A_{j,k} \lambda_k \text{for } i = 1, 2, ..., b^k; k > 0 \tag{1.3}$$

The shortcomings of the stochastic models described above include their need for distribution assumptions, long continuous rainfall data at fine-scale, and the estimation of numerous parameters. Developing stochastic non-parametric models addressed some of these shortcomings.

1.5.2.3 Resampling Models

Initially developed for stream data (Svanidze, 1980) and then applied to precipitation, the method of fragments (MoF) is a non-parametric disaggregation model. It entails three phases. The first phase involves dividing the fine-scale values by their corresponding coarse-scale values. The process produces sets of fragments. In the second phase, a set of fragments is chosen randomly (resampled) from the previous step. In the last phase, the disaggregated outcome is a product of the resampled set and the coarse-scale value to dis-

aggregate. This model is conceptually simple and has outperformed the probability-based and weighted- cascade models (Carreau et al., 2019).

1.6   Research Scope

1.6.1   Research questions

From the literature reviewed, three research questions emerged:

- Are temporal precipitation patterns for design storm development impacted by climate variations?

- What is the interaction between temporal precipitation patterns and hydrologic loss methods? How does this affect water resources planning and management, such as flood risk mapping?

- How can more data be made available to develop IDF curves and consequently design storms in data-scarce regions?

1.6.2   Thesis Contribution

In Chapter 2, temporal precipitation patterns are generated for design storm development for a region with climate variations using a Bayesian k-means algorithm. Identifying the temporal patterns is the first step towards identifying design storms considering local climate conditions. Some previous studies involved the development of IDF curves and temporal patterns. Most of the temporal precipitation pattern studies focused on the general climate condition, such as temperate or tropical, without incorporating the dependency of the general climate on the micro-climate, if present, within the region. The findings of this study serve to address this gap and show why local climate should be considered an essential factor when using or developing design storms.

The third chapter uses the temporal patterns identified in Chapter 2 to carry out one of many water resources planning tasks-flood risk mapping. The goal is to assess how current and future hydrographs are influenced by interaction between temporal precipitation patterns and the hydrologic loss method. These developed hydrographs are further used in hydraulic models to estimate the extent of flooding. The temporal patterns from the local climate are compared to a synthetic one. The research shows that the extent of the flood inundation boundary varies by temporal patterns based on the climate condition under study. Also, the type of hydrologic loss method used has a significant impact on the flood extent.

IDF curves are fundamental in engineering design and water resources management. The fourth chapter of this thesis develops a precipitation disaggregation model for regions where precipitation data is limited. It is common to find massive precipitation at daily duration, but not with short duration data. Many disaggregation models exist, but have the drawback of being data-intensive, making them inapplicable to data-scarce regions. Developing a disaggregation model that can be applied to data-scarce regions provides precipitation data at desired temporal resolutions for various uses ranging from water resources planning to irrigation studies.

Decision-making and planning of water resources should consider details from the research and findings in Chapters 2 and 3. The findings of Chapter 4 are especially relevant to water managers in data-scarce regions. However, they can also be useful for locations where data may be available but missing some portions.

This thesis is structured according to the order of the questions that emerged through research papers. By identifying the temporal precipitation patterns based on the climate gradient, the findings are used partly to address the question of temporal patterns' interplay with hydrologic loss methods. The disaggregation model development is discussed in the last section as it provides the second piece of information needed in combination with

design storms for any engineering design project. Altogether, these findings contribute to engineering design with climate change in the face of data scarcity.

References

Adachi, S., & Tomita, H. (2020). Methodology of the constraint condition in dynamical downscaling for regional climate evaluation: A review. *Journal of Geophysical Research: Atmospheres*, *125*(11), e2019JD032166.

Adamowski, J., Adamowski, K., & Bougadis, J. (2010). Influence of trend on short duration design storms. *Water Resources Management*, *24*(3), 401–413.

AghaKouchak, A., Ragno, E., Love, C., & Moftakhari, H. (2018). Projected changes in california's precipitation intensity-duration-frequency curves. *Energy Commision of Satet of California: Sacramento, CA, USA*.

Aguilar, M. G. d., & Costa, V. A. F. (2020). A regional similarity-based approach for sub-daily rainfall nonparametric generation. *RBRH*, *25*.

Ahmed, K., Shahid, S., Sachindra, D., Nawaz, N., & Chung, E.-S. (2019). Fidelity assessment of general circulation model simulated precipitation and temperature over pakistan using a feature selection method. *Journal of hydrology*, *573*, 281–298.

Al-Areeq, A., Al-Zahrani, M., & Chowdhury, S. (2021). Rainfall intensity–duration–frequency (idf) curves: Effects of uncertainty on flood protection and runoff quantification in southwestern saudi arabia. *Arabian Journal for Science and Engineering*, *46*(11), 10993–11007.

Ali, S., Eum, H.-I., Cho, J., Dan, L., Khan, F., Dairaku, K., . . . others (2019). Assessment of climate extremes in future projections downscaled by multiple statistical downscaling

methods over pakistan. *Atmospheric Research*, *222*, 114–133.

Allen, M. R., Barros, V. R., Broome, J., Cramer, W., Christ, R., Church, J. A., . . . others (2014). Ipcc fifth assessment synthesis report-climate change 2014 synthesis report. *Intergovernmental Panel on Climate Change: Geneva, Switzerland*.

Al Mamoon, A., Rahman, A., & Joergensen, N. E. (2019). Assessment of climate change impacts on idf curves in qatar using ensemble climate modeling approach. In *Hydrology in a changing world* (pp. 153–169). Springer.

Al-Rawas, G. A., & Valeo, C. (2009). Characteristics of rainstorm temporal distributions in arid mountainous and coastal regions. *Journal of hydrology*, *376*(1-2), 318–326.

Al Saji, M., O'Sullivan, J., & O'Connor, A. (2015). Design impact and significance of non-stationarity of variance in extreme rainfall. *Proceedings of the International Association of Hydrological Sciences*, *371*, 117–123.

Arnell, N. W., & Gosling, S. N. (2016). The impacts of climate change on river flood risk at the global scale. *Climatic Change*, *134*(3), 387–401.

Ayyub, B. M., Medina, M., Vinson, T., Walker, D., Wright, R., AghaKouchak, A., . . . others (2018). Climate-resilient infrastructure: Adaptive design and risk management. In *American society of civil engineers.*

Baghanam, A. H., Eslahi, M., Sheikhbabaei, A., & Seifi, A. J. (2020). Assessing the impact of climate change over the northwest of iran: an overview of statistical downscaling methods. *Theoretical and Applied Climatology*, *141*(3), 1135–1150.

Baguis, P., Boukhris, O., Ntegeka, V., Roulin, E., Willems, P., & Demarée, G. (2008). *Climate change impact on hydrological extremes along rivers and urban drainage systems. i. literature review, belgian science policy–ssd research programme* (Tech. Rep.). Technical report CCI-HYDR project by KU Leuven–Hydraulics & Royal . . . .

Bai, J. J., Chu, Y., Shen, C., & Wan, C. (2021). Managing climate change risks: Sea level rise and mergers and acquisitions. *Yongqiang and Shen, Chen and Wan, Chi,*

Managing Climate Change Risks: Sea Level Rise and Mergers and Acquisitions (May 11, 2021).

Ball, J., Babister, M., Nathan, R., Weeks, W., Weinmann, E., Retallick, M., & Testoni, I. (2016). Design rainfall. In *Australian rainfall and runoff: A guide to flood estimation.* Commonwealth of Australia (Geoscience Australia).

Bănăduc, D., Joy, M., Olosutean, H., Afanasyev, S., & Curtean-Bănăduc, A. (2020). Natural and anthropogenic driving forces as key elements in the lower danube basin–south-eastern carpathians–north-western black sea coast area lakes: a broken stepping stones for fish in a climatic change scenario? *Environmental Sciences Europe*, *32*(1), 1–14.

Bedient, P. B., Huber, W. C., & Vieux, B. E. (2012). *Hydrology and floodplain analysis. ed.* Pearson Upper Saddle River, NJ, USA.

Beniston, M., & Stoffel, M. (2016). Rain-on-snow events, floods and climate change in the alps: Events may increase with warming up to 4 c and decrease thereafter. *Science of the total environment*, *571*, 228–236.

Breinl, K., Strasser, U., Bates, P., & Kienberger, S. (2017). A joint modelling framework for daily extremes of river discharge and precipitation in urban areas. *Journal of Flood Risk Management*, *10*(1), 97–114.

Brown, R., Tapsoba, D., & Derksen, C. (2018). Evaluation of snow water equivalent datasets over the saint-maurice river basin region of southern québec. *Hydrological Processes*, *32*(17), 2748–2764.

Burian, S. J., Durrans, S. R., Tomić, S., Pimmel, R. L., & Wai, C. N. (2000). Rainfall disaggregation using artificial neural networks. *Journal of Hydrologic Engineering*, *5*(3), 299–307.

Canada's changing climate report. (2019). Retrieved from `https://www.nrcan.gc.ca/sites/www.nrcan.gc.ca/files/energy/Climate-change/pdf/`

`CCCR_FULLREPORT-EN-FINAL.pdf`

Carlier, E., & El Khattabi, J. (2016). Impact of global warming on intensity-duration-frequency (idf) relationship of precipitation: a case study of toronto, canada. *Open Journal of Modern Hydrology*, *6*(01), 62683.

Carreau, J., Mhenni, N. B., Huard, F., & Neppel, L. (2019). Exploiting the spatial pattern of daily precipitation in the analog method for regional temporal disaggregation. *Journal of Hydrology*, *568*, 780–791.

Carslaw, K., Lee, L., Regayre, L., & Johnson, J. (2018). Climate models are uncertain, but we can do something about it. *Eos*, *99*.

Cheng, L., & AghaKouchak, A. (2014). Nonstationary precipitation intensity-duration-frequency curves for infrastructure design in a changing climate. *Scientific reports*, *4*, 7093.

Chin, D. (2013). *Water resources engineering* (Vol. 12). Pearson Education, Inc. Upper Saddle River, NJ.

Cohen, J., Ye, H., & Jones, J. (2015). Trends and variability in rain-on-snow events. *Geophysical Research Letters*, *42*(17), 7115–7122.

Cowpertwait, P., Kilsby, C., & O'Connell, P. (2002). A space-time neyman-scott model of rainfall: Empirical analysis of extremes. *Water Resources Research*, *38*(8), 6–1.

Demarée, G. (1985). Intensity–duration–frequency relationship of point precipitation at uccle. reference period 1934–1983. *Belgium Royal Meteorological Institute*.

Deng, Y., Baeyens, J., Zhang, H., & Li, S. (2020). Challenges for design engineers in sustainable engineering. In *Iop conference series: Earth and environmental science* (Vol. 544, p. 012010).

De Paola, F., Giugni, M., Topa, M. E., & Bucchignani, E. (2014). Intensity-duration-frequency (idf) rainfall curves, for data series and climate projection in african cities. *SpringerPlus*, *3*(1), 1–18.

Deser, C. (2020). Certain uncertainty: The role of internal climate variability in projections of regional climate change and risk management. *Earth's Future*, *8*(12), e2020EF001854.

Donnelly, C., Greuell, W., Andersson, J., Gerten, D., Pisacane, G., Roudier, P., & Ludwig, F. (2017). Impacts of climate change on european hydrology at 1.5, 2 and 3 degrees mean global warming above preindustrial level. *Climatic Change*, *143*(1), 13–26.

Doyle, J. (1952). Local variations in rainfall. *The Forestry Chronicle*, *28*(3), 30–33.

Duan, K., & Mei, Y. (2014). A comparison study of three statistical downscaling methods and their model-averaging ensemble for precipitation downscaling in china. *Theoretical and applied climatology*, *116*(3), 707–719.

Einfalt, T., Arnbjerg-Nielsen, K., Fankhauser, R., Rauch, W., Schilling, W., Despotovic, J., et al. (1998). Use of historical rainfall series for hydrological modelling—workshop summary. *Water science and technology*, *37*(11), 1–6.

Fernandez, M. A., & Golubiewski, N. (2019). *An assessment of vulnerability to climate change in auckland*. Auckland Council, Te Kaunihera o Tāmaki Makaurau.

Fildier, B., Collins, W. D., & Muller, C. (2021). Distortions of the rain distribution with warming, with and without self-aggregation. *Journal of Advances in Modeling Earth Systems*, *13*(2), e2020MS002256.

Flanders Environment Agency, A. (1996). *Guidelines for an integrated policy on sewers in flanders.* Retrieved from `https://en.vmm.be/publications/vmm-an-introduction`

Forsee, W. J., & Ahmad, S. (2011). Evaluating urban storm-water infrastructure design in response to projected climate change. *Journal of Hydrologic Engineering*, *16*(11), 865–873.

Freudiger, D., Kohn, I., Stahl, K., & Weiler, M. (2014). Large-scale analysis of changing frequencies of rain-on-snow events with flood-generation potential. *Hydrology and*

Earth System Sciences, *18*(7), 2695–2709.

Friedrichs-Manthey, M., Langhans, S. D., Hein, T., Borgwardt, F., Kling, H., Jähnig, S. C., & Domisch, S. (2020). From topography to hydrology—the modifiable area unit problem impacts freshwater species distribution models. *Ecology and evolution*, *10*(6), 2956–2968.

Glasbey, C., Cooper, G., & McGechan, M. (1995). Disaggregation of daily rainfall by conditional simulation from a point-process model. *Journal of Hydrology*, *165*(1-4), 1–9.

Gudmundsson, L., Boulange, J., Do, H. X., Gosling, S. N., Grillakis, M. G., Koutroulis, A. G., ... others (2021). Globally observed trends in mean and extreme river flow attributed to climate change. *Science*, *371*(6534), 1159–1162.

Güntner, A., Olsson, J., Calver, A., & Gannon, B. (2001). Cascade-based disaggregation of continuous rainfall time series: the influence of climate. *Hydrology and Earth System Sciences Discussions*, *5*(2), 145–164.

Guo, J. C., & Hargadin, K. (2009). Conservative design rainfall distribution. *Journal of Hydrologic Engineering*, *14*(5), 528–530.

Gupta, V. K., & Waymire, E. C. (1993). A statistical analysis of mesoscale rainfall as a random cascade. *Journal of Applied Meteorology*, *32*(2), 251–267.

Gutmann, E., Pruitt, T., Clark, M. P., Brekke, L., Arnold, J. R., Raff, D. A., & Rasmussen, R. M. (2014). An intercomparison of statistical downscaling methods used for water resource assessments in the u nited s tates. *Water Resources Research*, *50*(9), 7167–7186.

Haarsma, R. J., Roberts, M. J., Vidale, P. L., Senior, C. A., Bellucci, A., Bao, Q., ... others (2016). High resolution model intercomparison project (highresmip v1. 0) for cmip6. *Geoscientific Model Development*, *9*(11), 4185–4208.

Hailegeorgis, T. T., & Alfredsen, K. (2017). Analyses of extreme precipitation and runoff

events including uncertainties and reliability in design and management of urban water infrastructure. *Journal of Hydrology*, *544*, 290–305.

Hallegatte, S., Shah, A., Brown, C., Lempert, R., & Gill, S. (2012). Investment decision making under deep uncertainty–application to climate change. *World Bank Policy Research Working Paper*(6193).

Hasan, H., & Wai Chung, Y. (2010). Extreme value modeling and prediction of extreme rainfall: A case study of penang. In *Aip conference proceedings* (Vol. 1309, pp. 372–393).

Hassan, Z. (2020). An integration based optimization approach (abc and pso) for parameter estimation in blrp model for disaggregating daily rainfall. *Pertanika Journal of Science & Technology*, *28*(1).

Hatch. (2008, January). *The Lower Churchill Project: PMF and Construction Design Flood Study* (Technical report Nos. GI1140, 2008). Author. Retrieved from `https://muskratfalls.nalcorenergy.com/wp-content/uploads/2013/03/Muskrat-Falls-PMF-and-Construction-Design-Flood-Study_Dec2007.pdf`

Hingray, B., & Haha, M. B. (2005). Statistical performances of various deterministic and stochastic models for rainfall series disaggregation. *Atmospheric Research*, *77*(1-4), 152–175.

Hogg, W. (1980). Time distribution of short duration storm rainfall in canada. In *Proc. canadian hydrology symposium* (Vol. 80, pp. 53–63).

Huff, F. A. (1967). Time distribution of rainfall in heavy storms. *Water resources research*, *3*(4), 1007–1019.

Hussain, M., Butt, A. R., Uzma, F., Ahmed, R., Irshad, S., Rehman, A., & Yousaf, B. (2020). A comprehensive review of climate change impacts, adaptation, and mitigation on environmental and natural calamities in pakistan. *Environmental monitoring*

and assessment, *192*(1), 1–20.

James, W., & Robinson, M. (1982). Continuous models essential for detention design.

Kaczmarska, J., Isham, V., & Onof, C. (2014). Point process models for fine-resolution rainfall. *Hydrological Sciences Journal*, *59*(11), 1972–1991.

Kay, A., Griffin, A., Rudd, A., Chapman, R., Bell, V., & Arnell, N. (2021). Climate change effects on indicators of high and low river flow across great britain. *Advances in Water Resources*, *151*, 103909.

Keifer, C. J., & Chu, H. H. (1957). Synthetic storm pattern for drainage design. *Journal of the hydraulics division*, *83*(4), 1332–1.

Kim, D., Kwon, H.-H., Lee, S.-O., & Kim, S. (2016). Regionalization of the modified bartlett–lewis rectangular pulse stochastic rainfall model across the korean peninsula. *Journal of Hydro-environment Research*, *11*, 123–137.

Kim, D., & Onof, C. (2020). A stochastic rainfall model that can reproduce important rainfall properties across the timescales from several minutes to a decade. *Journal of Hydrology*, *589*, 125150.

Kimoto, A., Canfield, H. E., & Stewart, D. (2011). Comparison of synthetic design storms with observed storms in southern arizona. *Journal of Hydrologic Engineering*, *16*(11), 935–941.

Knutson, T. R., Chung, M. V., Vecchi, G., Sun, J., Hsieh, T.-L., & Smith, A. (2021). Climate change is probably increasing the intensity of tropical cyclones. In *Critical issues in climate change science.* ScienceBrief Review.

Kossieris, P., Efstratiadis, A., Tsoukalas, I., & Koutsoyiannis, D. (2015). Assessing the performance of bartlett-lewis model on the simulation of athens rainfall. *European Geosciences Union General Assembly*.

Koutsoyiannis, D. (1994). A stochastic disaggregation method for design storm and flood synthesis. *Journal of Hydrology*, *156*(1-4), 193–225.

Koutsoyiannis, D. (2003a). On the appropriateness of the gumbel distribution for modelling extreme rainfall. In *Proceedings of the esf lesc exploratory workshop held at bologna* (pp. 24–25).

Koutsoyiannis, D. (2003b). Rainfall disaggregation methods: Theory and applications. In *Workshop on statistical and mathematical methods for hydrological analysis, rome* (Vol. 5270, pp. 1–23).

Koutsoyiannis, D. (2004). Statistics of extremes and estimation of extreme rainfall: I. theoretical investigation/statistiques de valeurs extrêmes et estimation de précipitations extrêmes: I. recherche théorique. *Hydrological sciences journal*, *49*(4).

Koutsoyiannis, D., & Onof, C. (2001). Rainfall disaggregation using adjusting procedures on a poisson cluster model. *Journal of Hydrology*, *246*(1-4), 109–122.

Kumar, D., & Kumar, S. (1989). Rainfall distribution pattern using frequency analysis. *J. Agril. Engg*, *26*(1), 33–38.

Kundzewicz, Z. W., Kanae, S., Seneviratne, S. I., Handmer, J., Nicholls, N., Peduzzi, P., . . . others (2014). Flood risk and climate change: global and regional perspectives. *Hydrological Sciences Journal*, *59*(1), 1–28.

Lafon, T., Dadson, S., Buys, G., & Prudhomme, C. (2013). Bias correction of daily precipitation simulated by a regional climate model: a comparison of methods. *International Journal of Climatology*, *33*(6), 1367–1381.

Li, H., Sheffield, J., & Wood, E. F. (2010). Bias correction of monthly precipitation and temperature fields from intergovernmental panel on climate change ar4 models using equidistant quantile matching. *Journal of Geophysical Research: Atmospheres*, *115*(D10).

Li, S., Li, L., & Le Treut, H. (2021). An idealized protocol to assess the nesting procedure in regional climate modelling. *International Journal of Climatology*, *41*(2), 1246–1263.

Li, X., Meshgi, A., Wang, X., Zhang, J., Tay, S. H. X., Pijcke, G., ... Babovic, V. (2018). Three resampling approaches based on method of fragments for daily-to-subdaily precipitation disaggregation. *International Journal of Climatology*, *38*, e1119–e1138.

Liang-Liang, L., Jian, L., & Ru-Cong, Y. (2022). Evaluation of cmip6 highresmip models in simulating precipitation over central asia. *Advances in Climate Change Research*, *13*(1), 1–13.

Luo, P., He, B., Duan, W., Takara, K., & Nover, D. (2018). Impact assessment of rainfall scenarios and land-use change on hydrologic response using synthetic area idf curves. *Journal of Flood Risk Management*, *11*, S84–S97.

Madsen, H., Pearson, C. P., & Rosbjerg, D. (1997). Comparison of annual maximum series and partial duration series methods for modeling extreme hydrologic events: 2. regional modeling. *Water Resources Research*, *33*(4), 759–769.

Madsen, H., Rasmussen, P. F., & Rosbjerg, D. (1997). Comparison of annual maximum series and partial duration series methods for modeling extreme hydrologic events: 1. at-site modeling. *Water resources research*, *33*(4), 747–757.

Mailhot, A., Duchesne, S., Caya, D., & Talbot, G. (2007). Assessment of future change in intensity–duration–frequency (idf) curves for southern quebec using the canadian regional climate model (crcm). *Journal of hydrology*, *347*(1-2), 197–210.

Manous, J., & Stakhiv, E. Z. (2021). Climate risk-informed decision analysis (crida):'top-down'vs 'bottom-up'decision making for planning water resources infrastructure. *Water Policy*, *23*(S1), 54–76.

Manzanas, R. G. (2016). *Statistical downscaling of precipitation in seasonal forecasting: advantages and limitations of different approaches* (Unpublished doctoral dissertation). Universidad de Cantabria.

Maraun, D., Widmann, M., & Gutiérrez, J. M. (2019). Statistical downscaling skill under

present climate conditions: A synthesis of the value perfect predictor experiment. *International Journal of Climatology*, *39*(9), 3692–3703.

Masson-Delmotte, V., Zhai, P., Pirani, A., Connors, S., Péan, C., Berger, S., ... Zhou, B. (2021). Summary for policymakers. In *Climate change 2021: The physical science basis. contribution of working group i to the sixth assessment report of the intergovernmental panel on climate change.* In Press.

McMichael, A. J., Campbell-Lendrum, D., Kovats, S., Edwards, S., Wilkinson, P., Wilson, T., ... others (2004). Global climate change.

McPherson, M. B. (1977). Urban runoff control planning..

Mélèse, V., Blanchet, J., & Molinié, G. (2018). Uncertainty estimation of intensity–duration–frequency relationships: A regional analysis. *Journal of Hydrology*, *558*, 579–591.

Meyer, M. D., et al. (2008). Design standards for us transportation infrastructure: The implications of climate change.

Mirhosseini, G., Srivastava, P., & Stefanova, L. (2013). The impact of climate change on rainfall intensity–duration–frequency (idf) curves in alabama. *Regional Environmental Change*, *13*(1), 25–33.

Molnar, P., & Burlando, P. (2005). Preservation of rainfall properties in stochastic disaggregation by a simple random cascade model. *Atmospheric Research*, *77*(1-4), 137–151.

Müller, H., & Haberlandt, U. (2018). Temporal rainfall disaggregation using a multiplicative cascade model for spatial application in urban hydrology. *Journal of Hydrology*, *556*, 847–864.

Müller-Thomy, H. (2020). Temporal rainfall disaggregation using a micro-canonical cascade model: possibilities to improve the autocorrelation. *Hydrology and Earth System Sciences*, *24*(1), 169–188.

Nasr, A., Ivanov, O. L., Björnsson, I., Johansson, J., & Honfi, D. (2021). Towards a conceptual framework for built infrastructure design in an uncertain climate: Challenges and research needs. *Sustainability*, *13*(21), 11827.

Nazif, S., Tavakolifar, H., & Eslamian, S. (2017). Climate change impact on urban water deficit. *Handbook of Drought and Water Scarcity: Environmental Impacts and Analysis of Drought and Water Scarcity*, 81–106.

Ngene, B., Nwafor, C., & Bamigboye, G. (2020). Design runoff estimation using an efficient rainfall analysis model for low data available catchment. In *International journal of engineering research in africa* (Vol. 50, pp. 29–36).

Nguyen, V., & Nguyen, T. (2019). A decision support tool for assessing the climate change impacts on urban water infrastructure design. In *11th international workshop on precipitation in urban areas (urbanrain18).*

Nguyen, V.-T.-V. (2020). Development of new methods for updating idf curves in canada in the context of climate change. In *World environmental and water resources congress 2020: Groundwater, sustainability, hydro-climate/climate change, and environmental engineering* (pp. 186–200).

Nwaogazie, I. L., & Sam, M. (2020). A review study on stationary and non-stationary idf models used in rainfall data analysis around the world from 1951-2020. *International Journal of Environment and Climate Change*, 465–482.

Office of Climate Change & Energy Efficiency, E. (2015). *Intensity-duration-frequency curves update for newfoundland and labrador.*

Olsson, J., & Burlando, P. (2002). Reproduction of temporal scaling by a rectangular pulses rainfall model. *Hydrological Processes*, *16*(3), 611–630.

Oppel, H., & Fischer, S. (2020). A new unsupervised learning method to assess clusters of temporal distribution of rainfall and their coherence with flood types. *Water Resources Research*, *56*(5), e2019WR026511.

Ormsbee, L. E. (1989). Rainfall disaggregation model for continuous hydrologic modeling. *Journal of Hydraulic Engineering*, *115*(4), 507–525.

Park, J., Cross, D., Onof, C., Chen, Y., & Kim, D. (2021). A simple scheme to adjust poisson cluster rectangular pulse rainfall models for improved performance at sub-hourly timescales. *Journal of Hydrology*, *598*, 126296.

Park, J., Seager, T. P., Rao, P. S. C., Convertino, M., & Linkov, I. (2013). Integrating risk and resilience approaches to catastrophe management in engineering systems. *Risk analysis*, *33*(3), 356–367.

Peyron, N., Nguyen, V., & Rivard, G. (2002). An optimal design storm pattern for urban runoff estimation in southern québec. In *Proceedings, annual conference of the canadian society for civil engineering, montreal, quebec, june* (pp. 5–8).

Pilgrim, D. H., & Cordery, I. (1975). Rainfall temporal patterns for design floods. *Journal of the Hydraulics Division*, *101*(1), 81–95.

Pripoaie, R., et al. (2019). The impact of global climate change and global warming on public health and welfare cost from exposure to environmental risks. *Risk in Contemporary Economy*, 64–92.

Pui, A., Sharma, A., Mehrotra, R., Sivakumar, B., & Jeremiah, E. (2012). A comparison of alternatives for daily to sub-daily rainfall disaggregation. *Journal of hydrology*, *470*, 138–157.

Rodriguez-Iturbe, I., Cox, D. R., & Isham, V. (1987). Some models for rainfall based on stochastic point processes. *Proceedings of the Royal Society of London. A. Mathematical and Physical Sciences*, *410*(1839), 269–288.

Sachindra, D., & Perera, B. (2016). Statistical downscaling of general circulation model outputs to precipitation accounting for non-stationarities in predictor-predictand relationships. *PloS one*, *11*(12), e0168701.

Schepen, A., Everingham, Y., & Wang, Q. J. (2020). Coupling forecast calibration and

data-driven downscaling for generating reliable, high-resolution, multivariate seasonal climate forecast ensembles at multiple sites. *International Journal of Climatology*, *40*(4), 2479–2496.

Scherer, D., Ament, F., Emeis, S., Fehrenbach, U., Leitl, B., Scherber, K., ... Vogt, U. (2019). Three-dimensional observation of atmospheric processes in cities. *Meteorol. Z*, *28*(2), 121–138.

Schmidli, J., Frei, C., & Vidale, P. L. (2006). Downscaling from gcm precipitation: a benchmark for dynamical and statistical downscaling methods. *International Journal of Climatology: A Journal of the Royal Meteorological Society*, *26*(5), 679–689.

Seenu, P., & Jayakumar, K. (2020). Optimization of bias correction methods for rcm precipitation data and their effects on extremes. In *Numerical optimization in engineering and sciences* (pp. 83–91). Springer.

Selaman, O. S., Said, S., & Putuhena, F. (2007). Flood frequency analysis for sarawak using weibull, gringorten and l-moments formula. *J. Inst. Eng*, *68*, 43–52.

Shephard, M. W., Mekis, E., Morris, R. J., Feng, Y., Zhang, X., Kilcup, K., & Fleetwood, R. (2014). Trends in canadian short-duration extreme rainfall: Including an intensity–duration–frequency perspective. *Atmosphere-Ocean*, *52*(5), 398–417.

Siler, N., Roe, G. H., & Armour, K. C. (2018). Insights into the zonal-mean response of the hydrologic cycle to global warming from a diffusive energy balance model. *Journal of Climate*, *31*(18), 7481–7493.

Silva, D. F., & Simonovic, S. P. (2020). Water resources research report.

Silva, D. F., Simonovic, S. P., Schardong, A., & Goldenfum, J. A. (2021). Assessment of non-stationary idf curves under a changing climate: Case study of different climatic zones in canada. *Journal of Hydrology: Regional Studies*, *36*, 100870.

Simonovic, S. P. (2017). Bringing future climatic change into water resources management practice today. *Water Resources Management*, *31*(10), 2933–2950.

Simonovic, S. P., Schardong, A., Sandink, D., & Srivastav, R. (2016). A web-based tool for the development of intensity duration frequency curves under changing climate. *Environmental modelling & software*, *81*, 136–153.

Sorribas, M. V., Paiva, R. C., Melack, J. M., Bravo, J. M., Jones, C., Carvalho, L., . . . Costa, M. H. (2016). Projections of climate change effects on discharge and inundation in the amazon basin. *Climatic change*, *136*(3), 555–570.

Sridhar, V., Modi, P., Billah, M. M., Valayamkunnath, P., & Goodall, J. L. (2019). Precipitation extremes and flood frequency in a changing climate in southeastern virginia. *JAWRA Journal of the American Water Resources Association*, *55*(4), 780–799.

Srivastav, R. K., Schardong, A., & Simonovic, S. P. (2014). Equidistance quantile matching method for updating idfcurves under climate change. *Water resources management*, *28*(9), 2539–2562.

Sun, Y., Wendi, D., Kim, D. E., & Liong, S.-Y. (2019). Deriving intensity–duration–frequency (idf) curves using downscaled in situ rainfall assimilated with remote sensing data. *Geoscience Letters*, *6*(1), 1–12.

Sunyer, M. A., Hundecha, Y., Lawrence, D., Madsen, H., Willems, P., Martinkova, M., . . . others (2015). Inter-comparison of statistical downscaling methods for projection of extreme precipitation in europe. *Hydrology and Earth System Sciences*, *19*(4), 1827–1847.

Svanidze, G. G. (1980). Mathematical modeling of hydrologic series for hydroelectric and water resources computations.

Tabari, H. (2020). Climate change impact on flood and extreme precipitation increases with water availability. *Scientific reports*, *10*(1), 1–10.

Teegavarapu, R. S., & Goly, A. (2018). Optimal selection of predictor variables in statistical downscaling models of precipitation. *Water resources management*, *32*(6), 1969–1992.

Tegegne, G., & Melesse, A. M. (2021). Comparison of trend preserving statistical downscaling algorithms toward an improved precipitation extremes projection in the headwaters of blue nile river in ethiopia. *Environmental Processes*, *8*(1), 59–75.

Teutschbein, C., & Seibert, J. (2012). Bias correction of regional climate model simulations for hydrological climate-change impact studies: Review and evaluation of different methods. *Journal of hydrology*, *456*, 12–29.

Ting, H., & Ying, S. (2021). Interpretation of ipcc ar6 on human influence on the climate system. *Advances in Climate Change Research*, *17*(6), 644.

Underwood, B. S., Mascaro, G., Chester, M. V., Fraser, A., Lopez-Cantu, T., & Samaras, C. (2020). Past and present design practices and uncertainty in climate projections are challenges for designing infrastructure to future conditions. *Journal of Infrastructure Systems*, *26*(3), 04020026.

United States Soil Conservation Service Engineering Division, D. (1986). *Urban hydrology for small watersheds* (No. 55). Engineering Division, Soil Conservation Service, US Department of Agriculture.

US Army Corps of Engineers, U. (2000). Hydrologic modeling system hec-hms technical reference manual. *Hydrol. Eng. Cent*.

Vaes, G., Willems, P., & Berlamont, J. (1994). A critical view of idf relationships. *Water*, *79*, 229–236.

Velghe, T., Troch, P. A., De Troch, F., & Van de Velde, J. (1994). Evaluation of cluster-based rectangular pulses point process models for rainfall. *Water Resources Research*, *30*(10), 2847–2857.

Veneziano, D., & Villani, P. (1999). Best linear unbiased design hyetograph. *Water resources research*, *35*(9), 2725–2738.

Vicente, J. R., Vaz, A. S., Queiroz, A. I., Buchadas, A. R., Guisan, A., Kueffer, C., . . . others (2019). Alien plant species: Environmental risks in agricultural and agro-

forest landscapes under climate change. In *Climate change-resilient agriculture and agroforestry* (pp. 215–234). Springer.

Vieux, B. E., & Vieux, J. E. (2010). Development of regional design storms for sewer system modeling. *Proceedings of the Water Environment Federation*, *2010*(10), 6248–6263.

Vu, M., Raghavan, S., Liu, J., & Liong, S.-Y. (2018). Constructing short-duration idf curves using coupled dynamical–statistical approach to assess climate change impacts. *International Journal of Climatology*, *38*(6), 2662–2671.

Wadden, D. (2002). *Rainfall distribution in the city of st. john's: temporal distribution, spatial variation, frequency analysis, and tropical storm gabrielle* (Unpublished doctoral dissertation). Memorial University of Newfoundland.

Waiesh, S. (1979). Summary seminar on the design storm concept. In *Proceedings, stormwater management model (swtvim) users group meeting, epa* (Vol. 600, pp. 9–79).

Wasko, C., Westra, S., Nathan, R., Orr, H. G., Villarini, G., Villalobos Herrera, R., & Fowler, H. J. (2021). Incorporating climate change in flood estimation guidance. *Philosophical Transactions of the Royal Society A*, *379*(2195), 20190548.

Watt, E., & Marsalek, J. (2013). Critical review of the evolution of the design storm event concept. *Canadian Journal of Civil Engineering*, *40*(2), 105–113.

Watt, W., Chow, K., Hogg, W., & Lathem, K. (1986). A 1-h urban design storm for canada. *Canadian Journal of Civil Engineering*, *13*(3), 293–300.

Werner, A., & Cannon, A. (2015). Hydrologic extremes–an intercomparison of multiple gridded statistical downscaling methods. *Hydrology & Earth System Sciences Discussions*, *12*(6).

Wilby, R. L., Charles, S. P., Zorita, E., Timbal, B., Whetton, P., & Mearns, L. O. (2004). Guidelines for use of climate scenarios developed from statistical downscaling meth-

ods. *Supporting material of the Intergovernmental Panel on Climate Change, available from the DDC of IPCC TGCIA*, *27*.

Willems, P. (1998). Hydrological applications of extreme value analysis. *Hydrology in a changing environment*, 15–25.

Wu, S.-J., Yang, J.-C., & Tung, Y.-K. (2006). Identification and stochastic generation of representative rainfall temporal patterns in hong kong territory. *Stochastic environmental research and risk assessment*, *20*(3), 171–183.

Xin, X., Wu, T., Jie, W., & Zhang, J. (2021). Impact of higher resolution on precipitation over china in cmip6 highresmip models. *Atmosphere*, *12*(6), 762.

Xu, Y.-P., Zhang, X., & Tian, Y. (2012). Impact of climate change on 24-h design rainfall depth estimation in qiantang river basin, east china. *Hydrological Processes*, *26*(26), 4067–4077.

Yan, L., Xiong, L., Jiang, C., Zhang, M., Wang, D., & Xu, C.-Y. (2021). Updating intensity–duration–frequency curves for urban infrastructure design under a changing environment. *Wiley Interdisciplinary Reviews: Water*, *8*(3), e1519.

Yang, C., Wang, N., & Wang, S. (2017). A comparison of three predictor selection methods for statistical downscaling. *International Journal of Climatology*, *37*(3), 1238–1249.

Yilmaz, A. G., Shanableh, A., Merabtene, T., Atabay, S., & Kayemah, N. (2020). Rainfall trends and intensity-frequency-duration relationships in sharjah city, uae. *International Journal of Hydrology Science and Technology*, *10*(5), 487–503.

Zhou, Q., Leng, G., Su, J., & Ren, Y. (2019). Comparison of urbanization and climate change impacts on urban flood volumes: Importance of urban planning and drainage adaptation. *Science of the Total Environment*, *658*, 24–33.

Chapter 2

Implications of Climatic Variations in Temporal Precipitation Patterns for the Development of Design Storms in Newfoundland and Labrador

*

Preface

*A version of this manuscript was published in the **Canadian Journal of Civil Engineering, 46.12(2019):1128-1141**. I am the primary author, and I carried out most of the research, performed the literature reviews, simulation setups and analysis of the results. I also prepared the first drafts of the manuscripts and subsequently revised the final manuscripts*

Abstract

The distribution of precipitation in time is an important aspect for the development of design storms for storm water infrastructure design. The current set of mass curves used throughout the province of Newfoundland and Labrador (NL) may not be justified. In order to identify variation in mass curves across NL, and compare results with existing mass curves, hourly precipitation data from 10 stations were used. Bayesian k-means clustering was used to identify dimensionless mass curves to represent precipitation patterns. Eight distinct temporal patterns of precipitation were identified and further regrouped into four, useful for making recommendations on the choice of mass curve. Crosstabulation applied to the patterns were found to be significantly influenced by event duration, depth and climate zone. Results support the conclusion that climate was an important determinant of temporal distribution of precipitation, and it is important to determine which pattern is dominant in a given region.

Index Terms: Bayesian estimation, cluster analysis, mass curves, storm water

2.1 Introduction

For engineering design applications, precipitation is characterized by its return period, duration, depth, and variation in time. These four elements are used to develop a design storm that determines the hyetograph for the given design application. Chow et al. (1988) define

a design storm as "a precipitation pattern defined for use in a hydrologic system," which provides precipitation intensity as a function of time increment.

Design storms are generally obtained through one of two methods; as a synthetic event derived from statistics of precipitation data or from actual historical precipitation events. They are presented in the form of hyetographs, often as non-dimensional cumulative storm depth as a function of dimensionless cumulative time (Koutsoyiannis & Foufoula-Georgiou, 1993). Synthetic design storms are usually characterized by return period, precipitation depth, event duration, along with a key aspect which is the temporal and spatial distribution of precipitation (D. Chin, 2013). Durations are determined by choice of an appropriate time scale dependent upon the application. For instance, the time of concentration is often used in the design of storm for water drainage systems for small residential basins. Once a duration is obtained, estimates of total precipitation depth for the duration are obtained from Intensity-Duration-Frequency (IDF) curves for a chosen return period, and the temporal distribution is represented as a cumulative mass curve. An IDF relation for a given duration can be used to get an estimate of peak discharge and total runoff volume from small basins using simple methods, such as the Rational Method and Curve Numbers. However, the time distribution of precipitation can have significant effects on the runoff hydrograph in a basin, and peak flow estimates in particular (Dullo et al., 2017; Alfieri et al., 2008). This is important in small basins where runoff response is more sensitive to precipitation of high intensity and short duration (Yen & Chow, 1980). Therefore inclusion of a mass curve is often used in more advanced hydrologic models to estimate peak runoff, runoff volume, and a hydrograph.

There are a range of approaches used to develop design storms including those based on IDF curves, the use of rainfall mass curves, rainfall hyetograph ordinates ranking, and the use of statistical moments (Wu et al., 2006). (Refer to introduction for a review of the design storm concept and methods). Table 2.1 shows a list of some existing methods.

47

Table 2.1: Design storm models

Model	Developers
Chicago design model	Keifer and Chu (1957)
Huff curves	Huff (1967)
The Sifalda design storm	Sifalda (1973)
Pilgrim and Cordery method	Pilgrim and Cordery (1975)
The Desbordes design model	Desbordes (1978)
AES design method	Hogg (1980)
Yen and Chow design storm model	Yen and Chow (1980)
Packman and Kidd method	Packman and Kidd (1980)
The balanced design model	US Army Corps of Engineers (1982)
The Watt design model	W. Watt et al. (1986)
SCS/NRCS method	SCS (1986)
ASCE method	US Army Corps of Engineers (2000)

E. Watt and Marsalek (2013) indicated that there is a need for the development of design storms based on Canadian precipitation data. Additionally, since the design life of storm water infrastructure extends into an increasingly uncertain future, it is vital to use IDFs and design storms that include nonstationarity due to climate change (Buttle et al., 2016). However, the sensitivity of design storms to climate change is largely unknown (E. Watt & Marsalek, 2013). As part of the process of updating IDFs and developing design storms that account for climate change impacts on precipitation, it is important to quantify the variation in IDFs and design storms as a function of climate (Dolšak et al., 2016).

2.1.1   Climate Impacts on Design Storms

There have been relatively few reports on temporal distribution of precipitation in Canada, and few studies looking at variation of spatial precipitation patterns with climate in general (W. Watt et al., 1986; Loukas & Quick, 1995; V.-T.-V. Nguyen et al., 2010; Asong et al., 2015). While design storms are developed using local rainfall data from a region, they may not always reflect the temporal distribution at a location within that region. For example, design storms developed using only rainfall data from Ohio had characteristics that differed

from the NRCS storm used for design in that state (NRCS, 2004). A possible explanation for this difference is that the NRCS storm was developed from a total number of storms greater than the Ohio rainfall data. Often times standard design storms, such as Huff curves, are shown to be unsatisfactory representations of the temporal distribution of precipitation (Kimoto et al., 2011; T. A. Nguyen et al., 2016; Dullo et al., 2017; Pan et al., 2017).

For many engineering applications extreme precipitation is most important, and intense "bursts" of precipitation within storms are of particular importance (Pilgrim & Cordery, 1975). A key part of the development of design storms is to determine at what time during the event the most intense precipitation occurs. For instance, Huff (1967) separated storms into time quartiles, e.g. the first quartile is the first quarter of the total storm duration and determined the peak intensity within each quartile.

Interannual variability impacts the intensity and timing of such bursts with implications for design storms. For instance, Terranova and Iaquinta (2011) were able to differentiate between storm profiles on a seasonal basis, including storm duration, depth, and maximum intensity in Southern Italy. However, their study area was relatively small, so a climate signal was unlikely. Thus, seasonal and regional (e.g. orographic effects) differences impacted the temporal distribution of precipitation. Others have found regional differences over relatively small areas, such as Lin et al. (2005), who were able to identify regional differences in design storms over Taiwan. However, these differences were not likely due to climate variation, given the location and size of the island. Some recent work suggests that climate impacts the temporal distribution of precipitation within events on regional scales. Dolšak et al. (2016) found that in regions of Slovenia with lower annual precipitation, maximum intensities tend to fall in the first half of the precipitation event. They found a general pattern of rainfall profile across a climatological gradient of dry to wet with maximum rainfall intensities that occurred in the latter half of the event in wetter regions.

There is some evidence that precipitation is impacted by natural climate variability in

Canada. Asong et al. (2015) were able to identify climatic regions for precipitation extremes that were linked with large scale atmospheric variability, the Pacific Decadal Oscillation (PDO) and the Pacific North American (PNA) pattern in the Canadian Prairies. Zhang et al. (2001) found that decadal variation was strong enough to show a signal in its impact on precipitation over a 50 year time period for stations located across Canada. In their analysis, Zhang et al. (2001) found clusters of stations with similar characteristics for heavy precipitation events in Western Canada, the Prairie region, the northern territories, and the Maritimes, with mixed results over Newfoundland and Labrador. This indicates more variation within Newfoundland and Labrador in storms than is observed across most of Canada.

Precipitation in Newfoundland and Labrador requires careful consideration. Located near the climatological position of the North Atlantic storm track, the province (particularly the island) experiences frequent frontal precipitation during the cold season (Fall through Spring) due to the passage of extratropical cyclones (e.g. (Banfield & Jacobs, 1998)). During the Atlantic hurricane season, it also occasionally experiences severe winds and high precipitation as a consequence of post-tropical storms; i.e. tropical storms (including hurricanes) that are in the process of transitioning to extratropical cyclones, but retain some of their prior strength (Environment & Climate Change Canada, 2013). Convective precipitation is also relatively common in the interior of the island and Labrador during summer. The result is considerable seasonality in precipitation sources and intensity, complicating efforts to simplify design criteria and/or generate IDF curves.

The Government of NL has been proactive in its approach to updating IDFs to incorporate recent and future climate change for engineering design calculations (GNL, 2011). There is a variation in practice amongst water resources professionals in the province on what is used as the design storm. In its flood risk studies, the province uses the alternating block method to derive the design storm whereas some municipalities and consultants use

rainfall distributions from post-tropical storms as the design storm. There is the need to develop guidelines for selecting the appropriate mass curves to ensure appropriate infrastructure design in the province.

The objectives of this paper were (1) to identify variation in the temporal distribution of precipitation that can be attributed to climate variation across Newfoundland and Labrador, (2) to quantify the temporal distribution of precipitation through the development of dimensionless mass curves representing precipitation events for locations across NL, and (3) to compare the results with existing mass curves and make recommendations regarding the development of design storms in NL. Results of these analyses will be used in conjunction with IDF curves developed by Finnis and Daraio (2018) to develop design storms that incorporate projected climate change in NL through 2100.

2.2 Methods

2.2.1 Study Area

Newfoundland and Labrador is located in Atlantic Canada with an area of approximately 373,800 km^2 (Government of Canada, 2005). The province ranges from the Southern Avalon Peninsula on the island of Newfoundland (N 46° 36' 36") to just inside the Arctic Circle in Northern Labrador (N 60° 22' 48"), a distance of around 1700 km, and includes a wide range of climate types (Figure 2.1). The climate of NL is broadly classified as tundra, subarctic, and humid continental moving from north to south. However the climate also varies with proximity to the coast and local physiography. For example, the Labrador coast and the northern coast of Newfoundland are influenced by the Labrador current and sea ice (Finnis & Bell, 2015), the west coast of Newfoundland is affected by the Gulf of St. Lawrence, and the southeastern portion of the island has a strong marine influence from the Atlantic. McManus and Wood (1991) assessed the climate of the province and classified it

into seven climate zones, which were used as a guide in choosing stations for this analysis, with mean annual precipitation being a significant component of this classification. Table 2.2 summarizes the climate zones throughout the province used in this paper.

Table 2.2: Description of the climate zones of Newfoundland and Labrador (McManus & Wood, 1991)

Climate	Description
Labrador	
Tundra (T)	Characterized by extremely cool and short summers. Full tree growth impossible in this region. The topography tends to create locally variable weather conditions, especially in summer.
Interior Labrador (IL)	Very long cold winters with deep snow cover. However, the region has relatively more settled weather patterns in comparison to the other areas whose weather is unsettled by changes in the Labrador Sea.
Coastal Labrador (CL)	Unsettled and stormy weather conditions. Extreme of temperature occasionally occur during offshore wind directions in winter and summer.
Newfoundland	
West Coast (WC)	Influenced by marine conditions from the Gulf of St. Lawrence. Increased precipitation with reduced temperature extremes, especially during fall and early winter, when snow falls are most frequent. Subject to locally high wind speeds.
Western Mountains and Central Uplands (WMCU)	High elevations result in increased cloud cover, intense precipitation, stronger winds and lower temperatures. Snow accumulation tends to increase westward.
North Coast and Central Lowlands (NCCL)	Driest area on the island. Low winter temperatures occur in valleys. Generally warm, sunny summers even when sea ice can persist into May along the coast.
South Coast and Avalon (SCA)	Relatively mild winters with a significant difference in local snow cover. Heavy rainfalls can occur from October through December. Mild summers near the coast due to low sea surface temperatures.
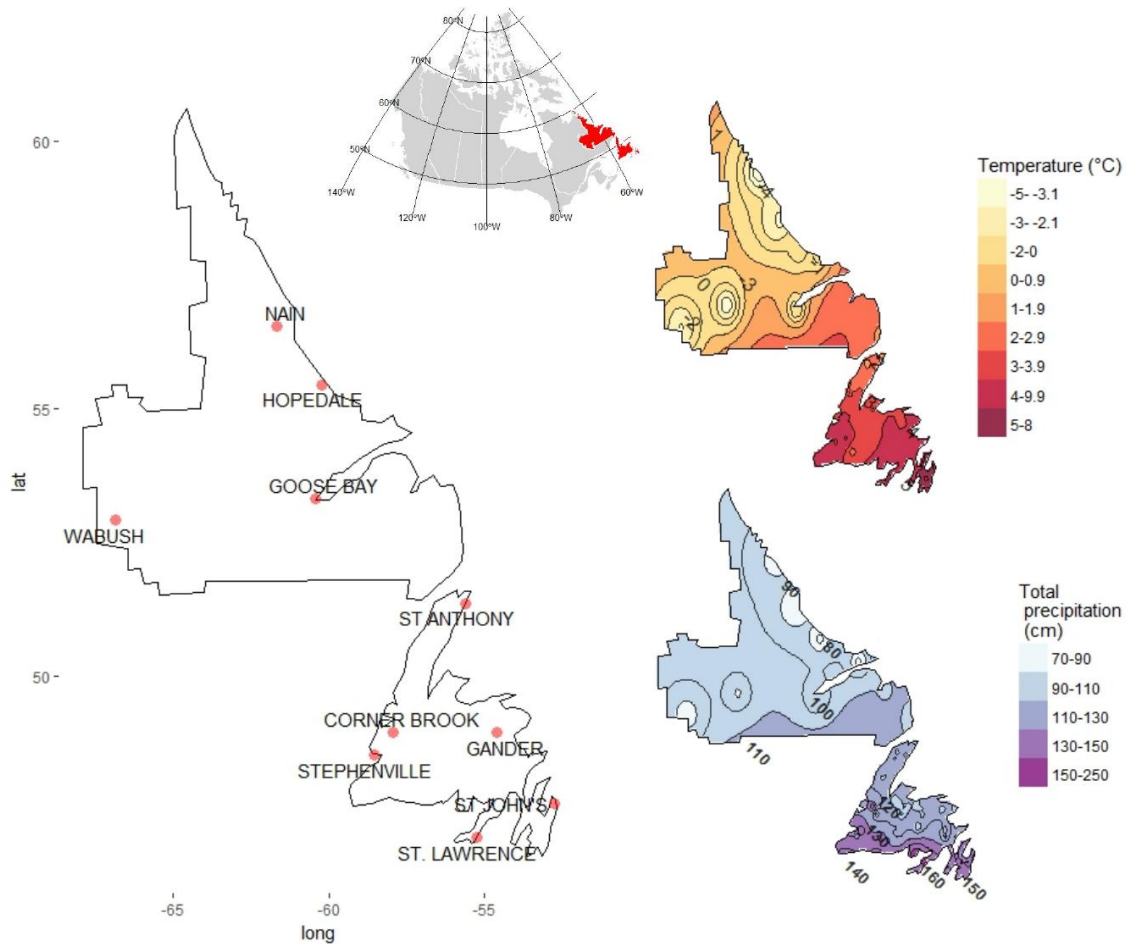
Figure 2.1: Map of the study area with stations used (left), mean annual temperature and total precipitation (top right and bottom right respectively). Inset is the study location in Canada

2.2.2 Data

Meteorological data from at least one station located within each climate zone in the province were used (Figure 2.1). Hourly precipitation data were obtained from Environment & Climate Change Canada (2013). Stations with a minimum of 50 events without consideration of time period were used in this analysis to allow for comparison across climate zones. While estimation of design storms most often utilizes short and intense rainfall events, due to the lack of data at these resolutions hourly data were used for this analysis, which represents a first step in continuing research. The longest continuous record of precipitation

53

(1960–2016) was from the station at Gander in Newfoundland while Hopedale, Corner Brook and St. Anthony stations had the shortest period of record (2004–2016; Table 2.3).

Table 2.3: List of stations in their respective climate zones used in the study.

ID	Location	Climate zone	Period of Record	Number of events
8502799	Nain	T	1993-2016	296
8501900	Goose-Bay	IL	1961- 2013	784
8504176	Wabush	IL	1973-2016	354
8502400	Hopedale	CL	2004-2016	177
8403800	Stephenville	WC	1967- 2016	1315
8401298	Corner Brook	WMCU	2004 -2016	297
8401700	Gander	NCCL	1960-2016	1316
8403400	St. Anthony	NCCL	2004-2016	248
8403501	St. John's	SCA	1961-1998	1026
8404201	St. Lawrence	SCA	1975-1996; 2006-2016	1415

2.2.2.1   Event Definition

Precipitation events were defined for use in this analysis based on both a minimum depth and a minimum inter-event time (MIT). The time of concentration of a basin is sometimes used to set an MIT (Branham & Behera, 2010; R. J. Chin et al., 2016), which can range from 5 minutes to 12 hours. The most commonly used MIT is 6 hours. The 6-hour duration is a compromise between being too strict (greater than 6 hours) or too lenient (less than 6 hours) in the separation criteria for precipitation events (Huff, 1967; Adams et al., 1986; Kauffman, 1987; Willems, 2000; Wadden, 2002; Powell et al., 2007; Asquith et al., 2006). A minimum depth was determined as a depth large enough to produce runoff. Runoff producing events were found by comparing rainfall records with observed hydrographs at nearby hydrometric stations. A single threshold value was used for consistency despite the spatial variation in this threshold value across watersheds in the study area. Based on this analysis, a precipitation event was defined to have a minimum depth of 10 mm

and an MIT of 6 hours. Additionally, events were defined with a minimum duration of 2 hours to allow for adequate temporal variation to be identified in the hyetograph without imposing unnecessary fine detail on the precipitation pattern. A total of 7228 events were identified, which represents 31.5% of the number of events using only the MIT criteria with the minimum depth being the biggest excluding factor for most events. The number of events at each station is shown in Table 2.3.

2.2.3   Characterization of Temporal Precipitation Patterns

The identified events in the previous section were converted into dimensionless mass curves. Dimensionless mass curves were produced using a cumulative distribution function (CDF) for the identified events. Empirical CDFs were fit using a non-parametric distribution. A non-parametric CDF was chosen because of the limitations of parametric methods that fail to differentiate between information and noise due to a smoothing effect (Fang, 1996). Additionally, using a non-parametric method avoids the need for prior assumptions about the underlying distribution of the temporal patterns of precipitation. The duration and depth of each event are divided into ten quantiles in the dimensionless mass curves. Interpolation was used to fit events with durations longer or shorter than the number of chosen time ordinates (Wu et al., 2006). Statistical cluster analysis is applied to the dimensionless precipitation mass curves to obtain the temporal patterns of precipitation.

2.2.3.1   Cluster Analysis

A commonly used method for cluster analysis is the k-means algorithm (Hartigan & Wong, 1979), which is relatively easy to apply and can identify natural groupings in a dataset. However, a number of drawbacks associated with this technique have been identified. In particular, the choice of the number of clusters is often subjective, and the algorithm performs poorly when the data are not spherically distributed (Raykov et al., 2016). To avoid

these problems, the Bayesian k-means technique (Welling & Kurihara, 2006) was used in this study. This method was able to identify the optimum number of clusters with fewer assumptions, find a small set of cluster centroids that was representative of the data, and assign each data point to a unique cluster.

A measure of similarity between the cluster groups was defined to find the centroid of a cluster. The Euclidean distance function, which employs the sum of squares of the difference between observations in a group, was used to minimize the *within-cluster dissimilarity* among vectors. This function is given by:

$$Z(K) = \sum_{i=1}^{K} \sum_{C(t)=i} \sum_{C(t')=i} d(u_t, u_{t'}) \tag{2.1}$$

where K is the number of clusters and $C(t)$ and $C(t')$ are assignment functions based on the Expectation-Maximization algorithm (see Hastie et al. (2009) for full details of the algorithm). The algorithm employed in equation 2.1 allows for a reduction in the number of clusters but fails to aid in choosing the optimal number of clusters. The function $Z(K)$ decreases to 0 if the number of clusters is equal to the number of observations in the data.

The Bayesian Information Criteria (BIC) was used to determine the optimal number of clusters using equation 2.1 with the goal of obtaining the smallest number of clusters that well represent the data. The BIC is a criterion that penalizes excessive clusters used that do not help explain the variance within the dataset and tends to prefer solutions with lesser clusters. Let y represent the data that are to be evaluated within the different clusters by model R_j. The vector of parameters associated with model R_j are denoted by p_j. Selection of a model using the Bayesian approach was achieved by maximizing the posterior probability of the model given the data, $P(R_j|y)$. i.e.

$$P(R_j|y) = \frac{P(y|R_j)P(R_j)}{P(y)} \tag{2.2}$$

56

where $P(y|R_j)$ is the marginal likelihood of the model R_j given the data. Maximizing the posterior probability of the model given the data is equivalent to maximizing the marginal likelihood.

$$P(y|R_j) = \int L(p_j|y)m_j(p_j)dp_j \qquad (2.3)$$

where $L(p_j|y)$ is the likelihood of y given the model being evaluated, $m_j(p_j)$ is the prior density of the parameters. This prior can be said to be uninformative and thus set to 1 (Neath & Cavanaugh, 2012). Applying the Laplace method for approximating an integral and employing the Fisher information matrix, while assuming that N (number of observations in a cluster) is large, the "weak law of large numbers" is invoked and this results in

$$\log\left[P(y|R_j)\right] = \log\left[L(\hat{p}_j|y)\right] - \frac{|p_j|}{2}\log[N] \qquad (2.4)$$

where $\hat{p}_j$ is the maximum likelihood estimation of p_j that maximizes $L(p_j|y)$. The right hand side of equation 2.4 provides the BIC estimate for the model R_j. The full derivation of BIC can be found in Bhat and Kumar (2010). This computation is carried out for all the models and the model with the lowest BIC is selected.

The maximum likelihood estimation (MLE) of the variance of clusters was estimated using

$$\sigma^2 = \frac{1}{N-K}Z(K) \qquad (2.5)$$

where N = number of observations in a cluster and σ^2 = single variance in a cluster. An MLE of variance is possible because the within-cluster distance is equal to the total sum of squared residuals from each cluster centroid (Tibshirani et al., 2001), which is equivalent to the maximum likelihood estimator of the variance. The log-likelihood, $L(K)$ was calculated using:

$$L(K) = \sum_{i=1}^{K}\left[-\frac{N_K}{2}\log(2\pi) - \frac{RN_K}{2}\log(\sigma^2) - \frac{N_K-K}{2} + N_K\log(N_K) - N_K\log(N)\right] \qquad (2.6)$$

where R = fitted cluster model, and N_K = number of observations assigned to cluster k.

A number of random initial clusters were tested because the initial choice of clusters tends to affect the outcome of the Bayesian k-means solution. After the calculations, the cluster centroids with the lowest value of $Z(K)$ were selected. All cluster analyses were performed using the "ClusterR" package (Mouselimis, 2018) in R (Team et al., 2018).

2.2.3.2 Crosstabulation

The frequency of precipitation clusters (temporal patterns) was evaluated based on determinants of event duration, depth and climate zone following Wu et al. (2006) and Nojumuddin et al. (2015). Crosstabulation was done to assess the effect of each determinant on temporal patterns of precipitation. Determinants were further broken into categories as follows. Storm depth, y, was divided into four categories of events: $10 \leq y < 20$ mm, $20 \leq y < 40$ mm, $40 \leq y < 100$ mm and $y > 100$ mm. Storm duration, x, was divided into five categories of events: $3 \leq x \leq 10$ h, $11 \leq x \leq 17$ h, $18 \leq x \leq 24$ h, $25 \leq x \leq 48$ h and $x \geq 100$ h. Climate was divided into the categories listed in Table 2.2.

A crosstabulation provides a joint distribution of a variable based on two or more categorizations (depth, duration, and climate zone) of that variable. The variable in this case was $P_{N_{i,p}}$, the proportion of the total number of events in each determinant category for a given pattern with respect to the total number of events.

$$P_{N_{i,p}} = \frac{N_{i,p}}{N} \tag{2.7}$$

where $N_{p,i}$ is the number of events that occurred in determinant category i for storm pattern p, and N is the total number of events (7228). The cross-tabulation was carried out in two ways: by using all eight temporal patterns, and by grouping the eight patterns into four broader patterns. A χ-square test was performed at a $p = 0.05$ significance level with

the null hypothesis that the clusters of temporal patterns occurrence were independent of the determinant under consideration. The alternate hypothesis that temporal patterns were dependent upon the determinant was accepted if the *p*-value was less than the significance level. Therefore, if $p < 0.05$ the interpretation was that the occurrence of the patterns were dependent on the category.

2.2.3.3   Regression Analysis and ANOVA

Neither total storm depth nor duration followed a normal distribution. These data were transformed using a Johnson transformation (Chou et al., 1998) that was done using the "jtrans" package (Wang, 2015) in R. Linear regression analysis and analysis of deviance was done using transformed data to check for potential effects of climate zone and storm pattern on relationships between total storm duration and depth using a multiple regression model given by

$$y_i = \alpha + \beta_1 x_{1i} + \beta_2 x_{2i} + \epsilon \tag{2.8}$$

where y_i is the total rainfall depth for event i, x_i is the total event duration for event i, β_1 and β_2 are the estimated slope parameter for determinant climate zone and pattern, respectively, $\alpha = 0$ since depth and duration $= 0$ at the same time, and ϵ is the model error. Analysis of deviance was used to test for interactions between determinants for the multiple linear regression analysis in equation 2.8, and χ-squared tests were used to test for significance. Analysis of deviance uses the generalized likelihood ratio test to determine if there was a significant difference in deviance when comparing models with each term in the regression equation (Fox & Weisberg, 2011). Analysis were done using the "car" package (Fox & Weisberg, 2011) in R.

Analysis of variance (ANOVA) was done on transformed data to assess the variation in storm depth and storm duration that can be attributed to climate zone and storm pattern, and to test for interactions between these groups (or determinants) (Gelman & Hill, 2007), and

F-tests were used to test for significance. The R package "arm" (Gelman et al., 2018) was used to assess ANOVA for interactions between determinants.

2.2.4 Comparison with Existing Design Storms

There are municipal, provincial, and national standards for choice of return periods, storm duration, and IDF curves that are used in practice in NL. However there are no required standards for choice of temporal distribution of design storms, except for the City of St. John's. A qualitative comparison of the temporal distribution of design storms was done using a review of the several design storm applications across the province. Many reports indicated use of guidelines from the City of St. John's Subdivision Design Manual (unpublished, obtained from the City of St. John's Department of Planning, Development, & Engineering), for example BAE Newplan Group Limited (2013) used the St. John's Design Manual to develop a storm water master plan in Paradise, which is a suburban area just outside of the City of St. John's. The city has recently updated some of its design criteria (City of St. John's, 2017). Design applications outside of St. John's often use NRCS design storms (SNC Lavalin Inc., 2015) that were developed for use in the United States. Other criteria have be used for the estimation of the probable maximum flood using the probable maximum precipitation (PMP) (Hatch, 2008).

2.3 Results

2.3.1 Precipitation Patterns

Eight distinct temporal patterns of precipitation were identified as being representative of precipitation in NL. The BIC decreased as the number of clusters increased from 1 through 8, and then began to increase with 9 or more clusters (Figure 2.2). The eight clusters were

categorized into two major patterns (Figure 2.3). (1) More than half of the total precipitation occurred in the first half of the precipitation event (advanced patterns; AP), and (2) less than half the total precipitation occurred in the first half of the precipitation event (delayed patterns; DP). Within these categories, there were two other patterns that stood out (Figure 2.3); an AP that had a more uniform distribution (AP-U), and a DP that had two peaks in the hyetograph (DP-2P). The eight patterns were identified as AP1, AP2, AP3, AP-U, DP1, DP2, DP3, and DP-2P.
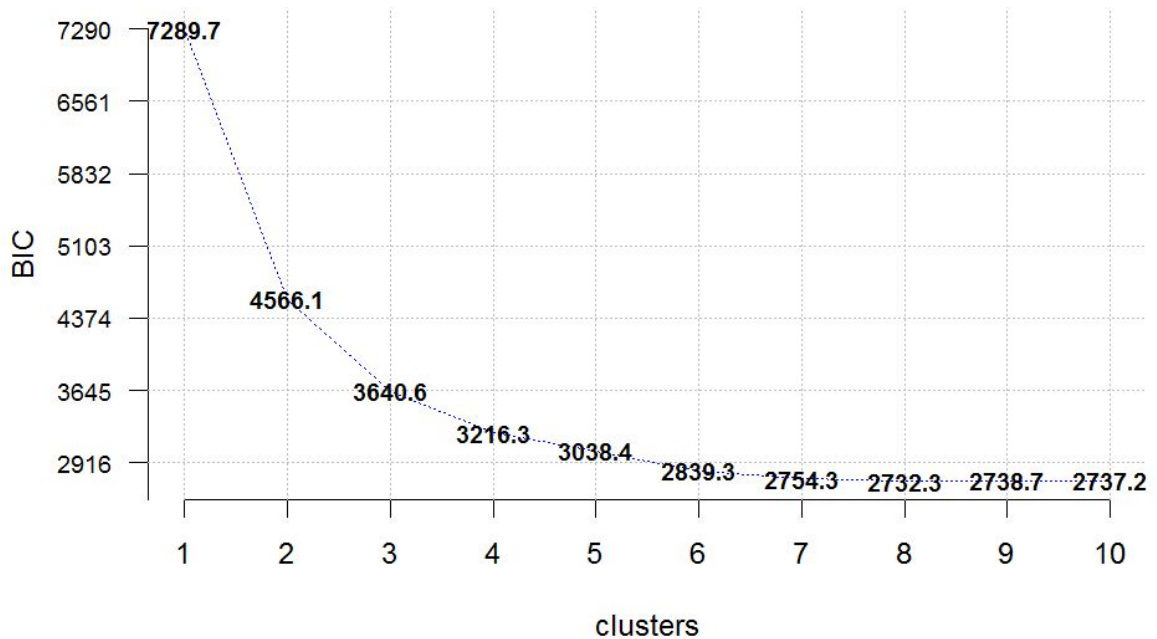
Figure 2.2: Outcome of the optimal cluster number selection through Bayesian k-means. The vertical axis is the BIC score used to penalize increasing cluster number with number of clusters on the horizontal axis.

Chi-squared tests from the crosstabulation indicated that precipitation depth, precipitation duration, and climate zone were each statistically significant ($p < 0.05$) determinants of the eight precipitation patterns (Table 2.4). The proportion of events falling into each determinant category indicates the relative influence the determinant had on the design storm pattern. Out of a total of 7228 events, 56% were events with 10-20 mm of precipitation, 33% of events had 20-40 mm of precipitation, 10% had 40-100 mm, and < 1% had depths
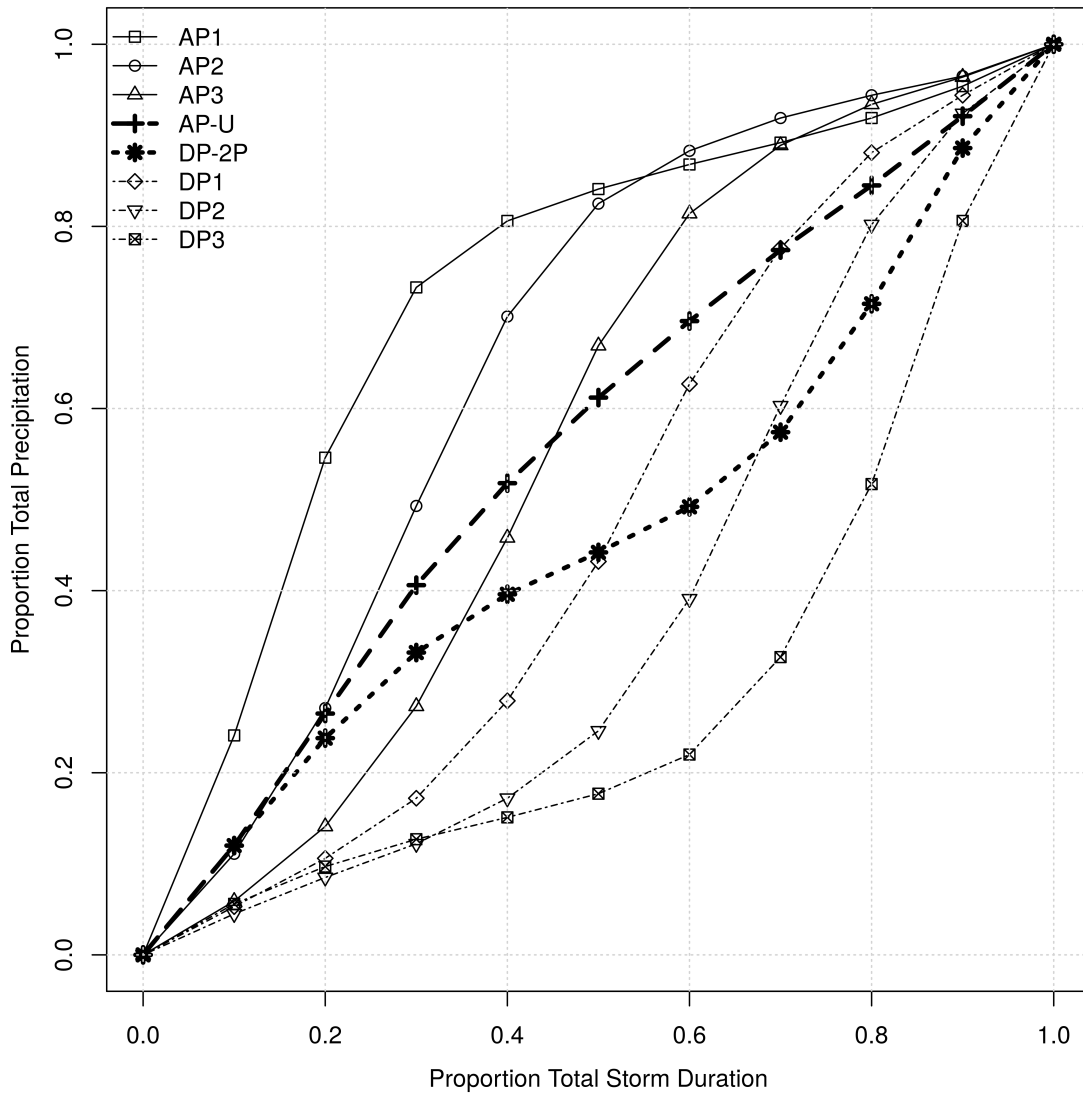
Figure 2.3: The eight temporal precipitation patterns for NL identified by cluster analysis. Patterns are grouped into advanced (AP), and delayed categories (DP). Patterns AP-U and DP-U represent an AP event with a more uniform distribution and a DP event with two peaks in the hyetograph, respectively.

greater than 100 mm. This indicates that more than half of the events that influenced the design storm for depth of precipitation were smaller events.

Event durations were more evenly distributed over the 8 identified patterns; 30% of events had durations between 3–10, 31% of events had 11–17 hour durations, 19% of events

Table 2.4: Crosstabulation of the eight precipitation patterns identified by the cluster analysis and its determinants. Bottom number in each row gives the percentage of events categorized in the pattern with respect to the total number of events in each determinant category. Patterns: Advanced patterns (AP), Delayed Patterns (DP), Uniform patterns (AP-U), 2-Peaked Delayed Patterns (DP-2P)

Determinant	Patterns								Total
	AP1	AP2	AP3	AP-U	DP-2P	DP1	DP2	DP3	
Precipitation depth (mm)									
10 - 20	395	596	668	501	321	773	562	254	4070
	9.7%	14.6%	16.4%	12.3%	7.9%	19.0%	13.8%	6.2%	56.3%
20-40	182	336	449	265	160	530	320	149	2391
	7.6%	14.1%	18.8%	11.1%	6.7%	22.2%	13.4%	6.2%	33.1%
40 - 100	42	97	123	89	49	141	121	44	706
	5.9%	13.7%	17.4%	12.6%	6.9%	20.0%	17.1%	6.2%	9.8%
>100	5	3	11	7	3	13	10	9	61
	8.2%	4.9%	18.0%	11.5%	4.9%	21.3%	16.4%	14.8%	0.8%
	$\chi^2 = 49.81$; DF = 21 ; $p \ll 0.05$								
Precipitation duration (h)									
3-10	172	310	425	200	98	531	309	121	2166
	7.9%	14.3%	19.6%	9.2%	4.5%	24.5%	14.3%	5.6%	30.0%
11-17	186	346	389	215	171	447	347	162	2263
	8.2%	15.3%	17.2%	9.5%	7.6%	19.8%	15.3%	7.2%	31.3%
18-24	149	169	211	189	123	230	166	98	1335
	11.2%	12.7%	15.8%	14.2%	9.2%	17.2%	12.4%	7.3%	18.5%
25-48	107	188	192	225	127	219	174	70	1302
	8.2%	14.4%	14.7%	17.3%	9.8%	16.8%	13.4%	5.4%	18.0%
48	10	19	34	33	14	30	17	5	162
	6.2%	11.7%	21.0%	20.4%	8.6%	18.5%	10.5%	3.1%	2.2%
	$\chi^2 = 195.64$; DF = 28 ; $p \ll 0.05$								
Climate Zone									
Tundra	20	54	59	37	14	67	34	11	296
	6.8%	18.2%	19.9%	12.5%	4.7%	22.6%	11.5%	3.7%	4.1%
Interior Labrador	102	159	182	179	104	201	153	58	1138
	9.0%	14.0%	16.0%	15.7%	9.1%	17.7%	13.4%	5.1%	15.7%
Coastal Labrador	14	21	33	28	15	29	19	18	177
	7.9%	11.9%	18.6%	15.8%	8.5%	16.4%	10.7%	10.2%	2.4%
West Coast	128	196	208	140	117	257	185	84	1315
	9.7%	14.9%	15.8%	10.6%	8.9%	19.5%	14.1%	6.4%	18.2%
Western Mountain	25	53	42	45	26	49	40	17	297
	8.4%	17.8%	14.1%	15.2%	8.8%	16.5%	13.5%	5.7%	4.1%
North Coast	159	214	279	183	122	297	221	89	1564
	10.2%	13.7%	17.8%	11.7%	7.8%	19.0%	14.1%	5.7%	21.6%
South Coast and Avalon	176	335	448	250	135	557	361	179	2441
	7.2%	13.7%	18.4%	10.2%	5.5%	22.8%	14.8%	7.3%	33.8%
	$\chi^2 = 116.61$; DF = 42 ; $p \ll 0.05$								
* Total	624	1032	1251	862	533	1457	1013	456	7228
	8.6%	14.3%	17.3%	11.9%	7.4%	20.1%	14.0%	6.3%	

had 18–24 hour durations, and 18% of events had 25–48 hour durations. However, 80% of storms that influence design storm patterns had sub-daily durations. Events with durations greater than 48 hours only influenced 2% of the identified precipitation patterns.

The proportion of events from each climate zone that influenced the determination of precipitation patterns provides an indication of the sample size from each zone. Therefore it is more useful to look at the proportion of storms in each climate zone that contributed to pattern determination. For instance, the proportion of storms that fell into an AP1 was similar across all climate zones (7–10%; Table 2.4), and 23% of storms in both Tundra and South Coast zones were DP1 while only 16% were of this type in Coastal Labrador. However, there were too many types of patterns to make any generalizations, therefore further analyses were done by grouping the clusters into a total of four patterns (Table 2.5).

2.3.1.1 Four Pattern Analysis

Four groupings were analyzed with 3 storm types falling in AP category (AP1, AP2, and AP3), 3 storm types falling in the DP category (DP1, DP2, and DP3), and the other two storm types (AP-U and DP-2P) each considered as separate categories. Crosstabulation analysis and the results of χ-square tests (Table 2.5) indicated that event duration and climate zone were each significant factors in the determination of these groupings ($p < 0.05$), however total storm depth was not a significant determinant for these groupings ($p > 0.05$). Overall, an equal proportion of AP and DP storms occurred (40% each) which accounted for 80% of all storms; 12% of storms were AP-U and 7% were DP-2P (Table 2.5). Most climate zones had an equal or higher proportion of AP storms relative to DP storms except for the South Coast and Avalon (SCA) zone of Newfoundland, which had a greater proportion of DP storms. Interior Labrador had the greatest proportion of DP-2P storms (9%) compared to other climate zones.

Table 2.5: Crosstabulation of sub-groups of precipitation patterns identified by the cluster analysis and its determinants.

Determinant	Patterns				Total
	AP	AP-U	DP	DP-2P	
Precipitation depth (mm)					
0 - 20	1659	501	1589	319	4068
	40.8%	12.3%	39.1%	7.8%	56.3%
20-40	967	265	999	160	2391
	40.4%	11.1%	41.8%	6.7%	33.1%
40 - 100	262	89	306	49	706
	37.1%	12.6%	43.3%	6.9%	9.8%
>100	19	7	32	5	63
	30.2%	11.1%	50.8%	7.9%	0.9%
	$\chi^2 = 14.91$; DF = 9 ; p-value = 0.09				
Precipitation duration (h)					
3-10	907	200	961	98	2166
	41.9%	9.2%	44.4%	4.5%	30.0%
11-17	921	215	956	171	2263
	40.7%	9.5%	42.2%	7.6%	31.3%
18-24	529	189	494	123	1335
	39.6%	14.2%	37.0%	9.2%	18.5%
25-48	487	225	463	127	1302
	37.4%	17.3%	35.6%	9.8%	18.0%
>48	63	33	52	14	162
	38.9%	20.4%	32.1%	8.6%	2.2%
	$\chi^2 = 140.1$; DF = 12 ; $p \ll 0.05$				
Climate zone					
Tundra	133	37	112	14	296
	44.9%	12.5%	37.8%	4.7%	4.1%
Interior Labrador	443	179	412	104	1138
	38.9%	15.7%	36.2%	9.1%	15.7%
Coastal Labrador	68	28	66	15	177
	38.4%	15.8%	37.3%	8.5%	2.4%
West Coast	532	140	526	117	1315
	40.5%	10.6%	40.0%	8.9%	18.2%
Western Moun-tain	120	45	106	26	297
	40.4%	15.2%	35.7%	8.8%	4.1%
North Coast	652	183	607	122	1564
	41.7%	11.7%	38.8%	7.8%	21.6%
South Coast and Avalon	959	250	1097	135	2441
	39.3%	10.2%	44.9%	5.5%	33.8%
	$\chi^2 = 75.14$; DF = 18 ; $p \ll 0.05$				
Total	2907	862	2926	533	7228
	40.2%	11.9%	40.5%	7.4%	

2.3.1.2 Regression and ANOVA

There was a significant linear relationship between total storm duration and total storm depth for all events combined, as was expected, and the strength of this relationship varied

by climate zone and pattern type (Figure 2.4). Analysis of deviance from multiple linear regression model results (likelihood ratios) indicated that the model fit for the relationship between depth and duration was significantly improved ($p < 0.001$) when climate zone and storm pattern groupings were included, and indicated that there were not significant interactions between duration and storm patterns. However there was significant improvement in the model when including an interaction between duration and climate zones. That is, climate zone did have effects on the relationship between event depth and event duration. There was no effect of interaction between pattern and climate zone on the relationship between duration and depth.

The ANOVA for the effects of climate zone and pattern, and their interaction, on variance of event depth and duration showed that climate zone had a stronger effect on variance of event depth ($F = 16$, $p < 0.0001$) than storm pattern ($F = 5.6$, $p < 0.001$), and that there was no significant interaction between pattern and climate with effects on depth ($F = 0.5$). The ANOVA for storm duration showed the same result, but with a stronger indication that climate and pattern had significant effects on variation in event duration ($F = 27$ and $F = 27$, respectively, $p < 0.0001$). Additionally, there was an interaction between climate zone and pattern for event duration, though it was not statistically significant ($F = 1.2$, $p = 0.25$). This is evident in plots showing mean storm duration (hours) and variance in storm duration by storm pattern indicate relatively little intersection across climate zones (Figure 2.5).

Both mean storm depth and duration were highest in the Tundra climate zone for APU patterns. The South Coast and Avalon (SCA) zone had the second highest depth for AP patterns and highest depth for DP patterns. By contrast, the SCA had consistently lower mean and variance for duration than most climate zones when grouped by storm pattern. There are 38 APU events with storm depths ranging from 11mm to 109.8 mm for the Tundra region, with an average of 31.34mm. Though the DP2P has the smallest number of
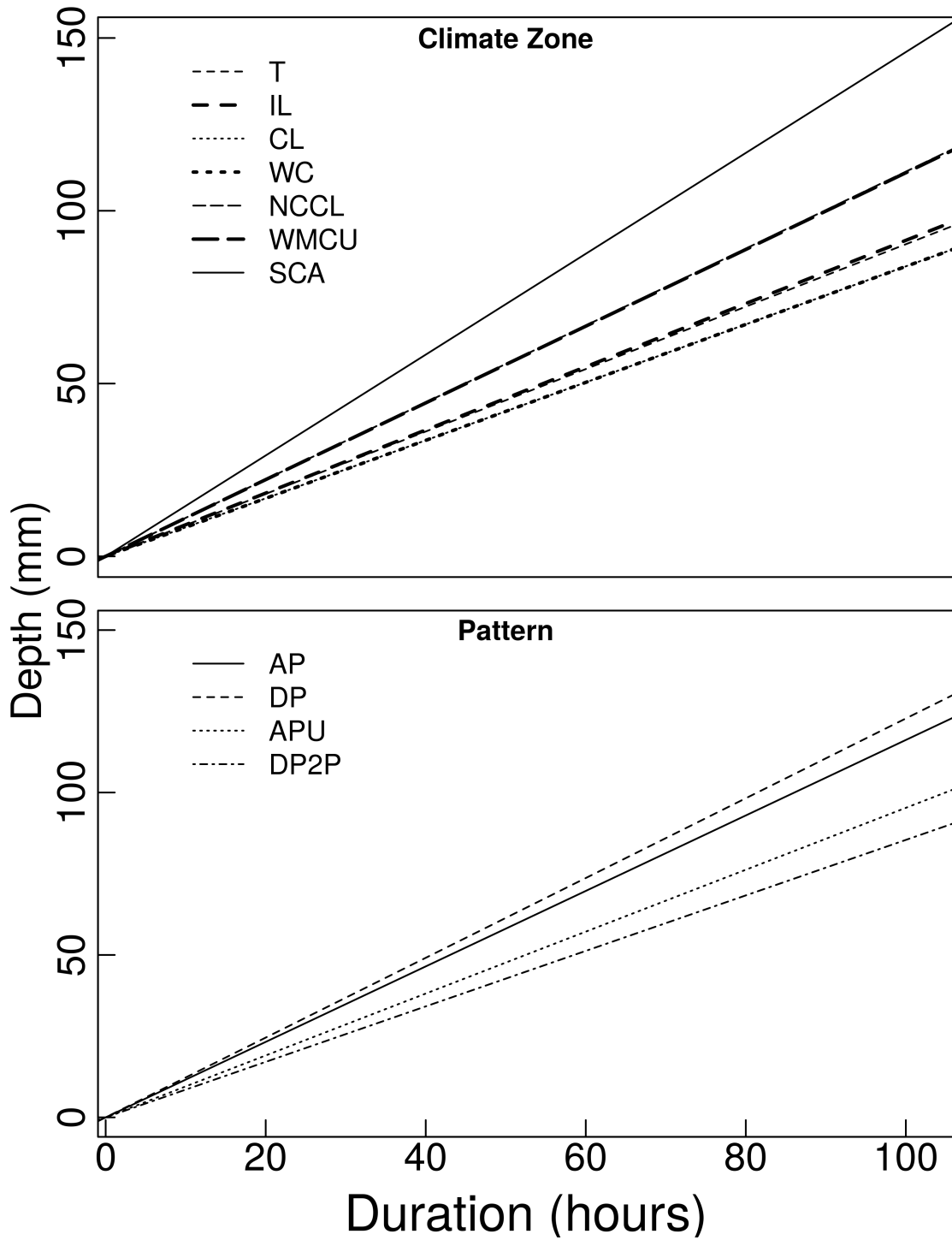
Figure 2.4: Linear regression lines for the relationship between total storm depth as a function of total storm duration.
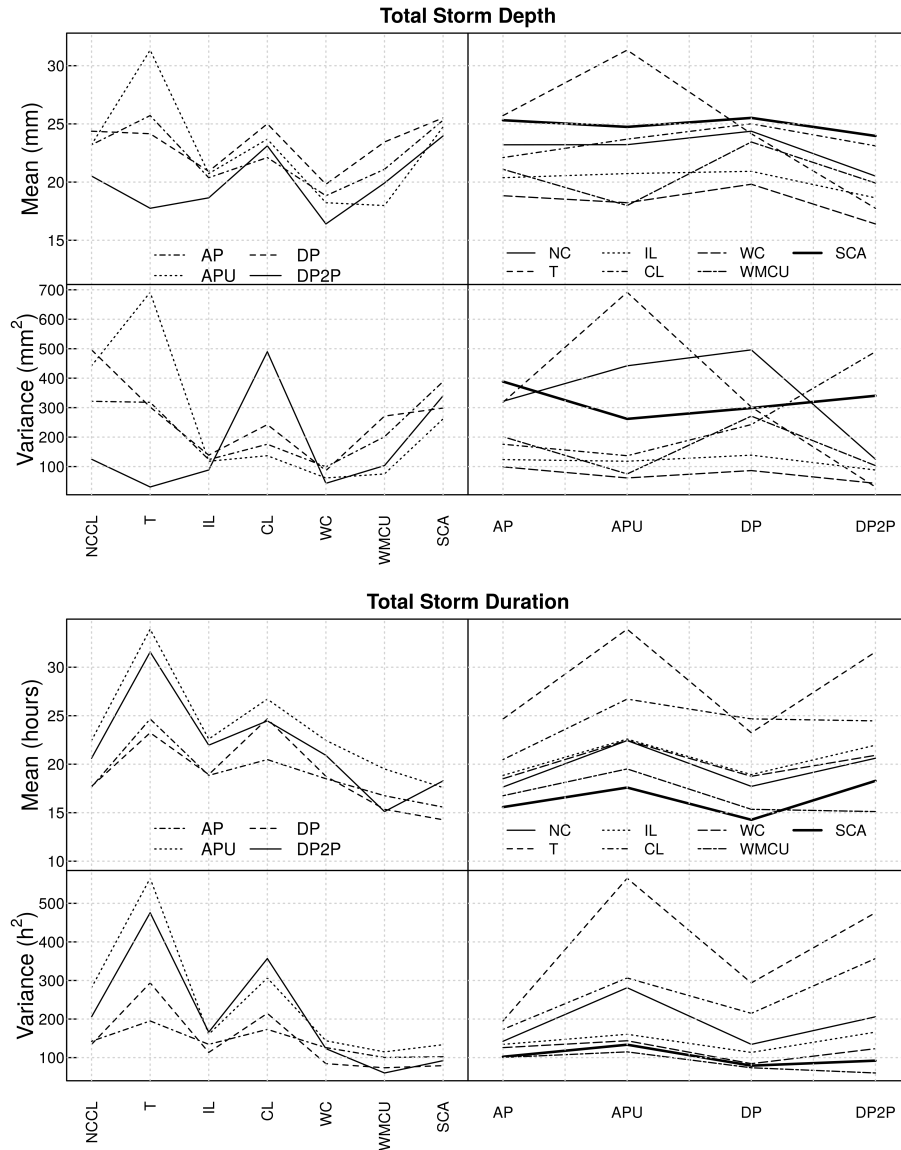
Figure 2.5: Interaction plots showing the mean and variation of storm depth and storm duration for events grouped by climate zone and storm pattern as indicated.

events (14), its range of values was much smaller (10.4mm to 28mm), resulting in a mean of 17.75mm. For the NCCL region, there are 182 APU events with storm depths between 10.2mm and 117.2mm, giving a mean of 22.18mm. The results in Figure 2.5 (top row) are mean values; hence for a wide range of values, if the total number of elements in the denominator is small, as was the case for the Tundra, the resulting mean value will be greater

compared to the NCCL region, there the total number of elements in the denominator is large, hence the smaller mean value.

In the Tundra region, storm durations ranged from 4 to 118 hours (for 297 events) with a mean of 25.6 hours. The greatest duration was also associated with the largest storm depth, which had the characteristics of an APU event. Compared to the WMCU region, the number of events was also small (296), but durations ranged from 3 hours to 63 hours, averaging 16.52 hours. In this case, the denominator in estimating the mean value was similar, but the numerator had significant differences, which explains the large difference in mean values. Tundra is a cool climate, and hence high storm depths are rare. A possible explanation for this result is the MIT used for event characterization, which could have resulted in smaller events being grouped into one significant event with a high storm depth and duration. Additionally, the variance of storm duration grouped by storm pattern was greatest for all storm patterns in the Tundra (Figure 2.5). This seems more apparent when looking at plots of event depth as a function of duration (Figure 2.6). Stations in Tundra and Interior Labrador tended to have more extended duration events and relatively few events with shorter, more intense precipitation. In contrast, Coastal Labrador had more extended duration events along with some short, intense events (Table 2.6). Gander, which is off the coast in central Newfoundland (Figure 2.1), also had longer duration events. Mountain and coastal climates had more frequent events with intense bursts of precipitation.

2.3.1.3   Station Correlations

Correlations between depths of precipitation events at stations were computed to assess overall support for the analyses (Figure 2.7), i.e. nearby stations that are highly correlated will tend to underestimate p-values used to assess significance of climate zones on results since these data would not be independent. The only stations with a relatively high significant correlation ($\rho \approx 0.7$) were in the South Coast and Avalon climate zone (St. John's and
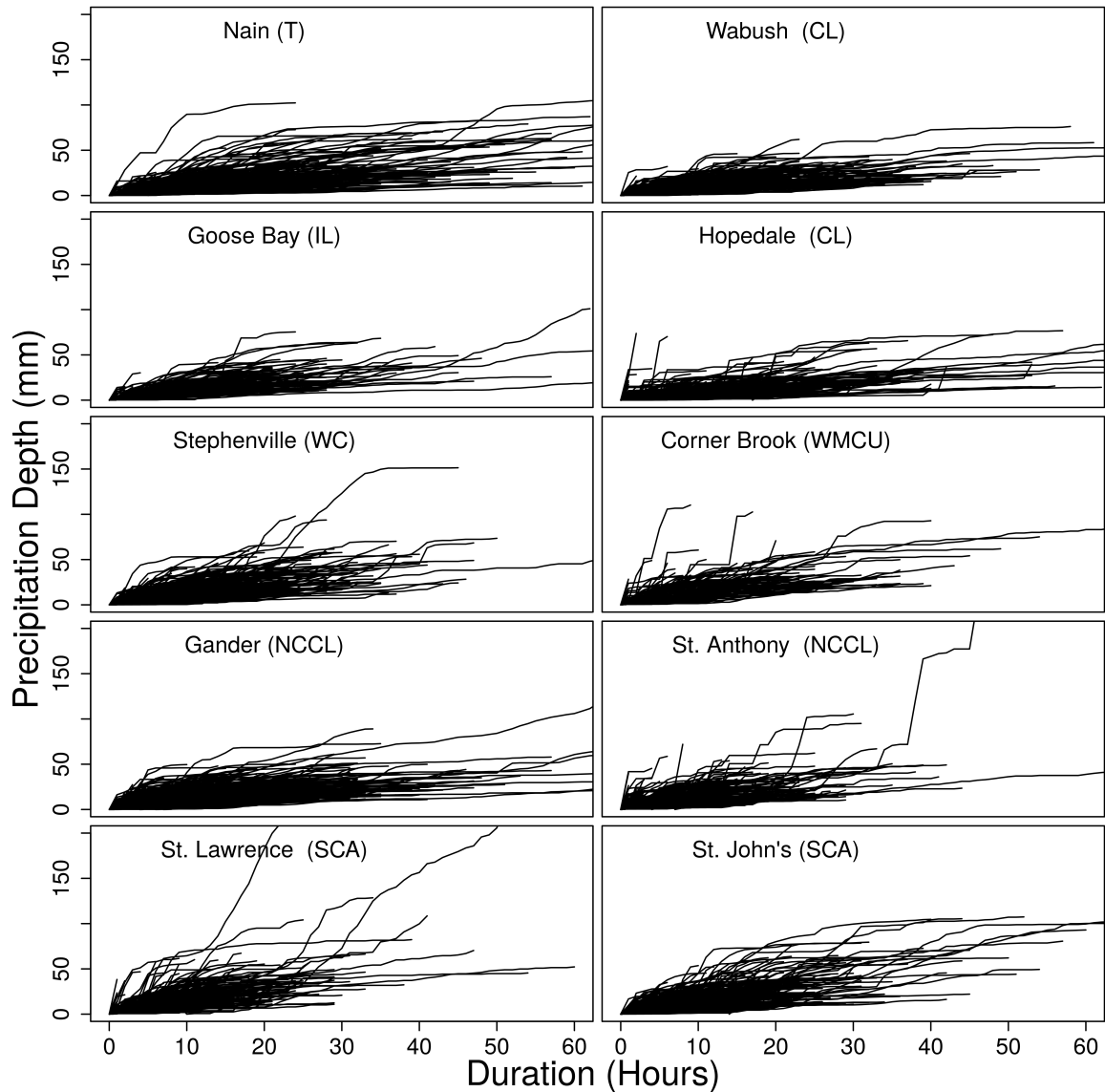
Figure 2.6: Cumulative precipitation depth for each event in relation to event duration for events at each station used in the cluster analysis. Note that there were two events with greater than 200 mm of precipitation at St. Lawrence and one event with greater than 200 mm of precipitation at St. Anthony.

St. Lawrence). The above crosstabulation analyses were repeated with only the St. John's station representing SCA climate zone and with only the St. Lawrence station representing SCA climate zone. The inclusion of both stations did lower the *p*-value in each analysis but did not change the significance of the results. Correlations between stations within

Table 2.6: Total number of events that the precipitation intensity was > 10 mm/h at least once in any one hour time increment.

Station	Climate zone	Events
Nain	T	14
Wabush	IL	19
Goose Bay	IL	13
Hopedale	CL	33
Stephenville	WC	34
Corner Brook	WMCU	37
Gander	NCCL	28
St. Anthony	NCCL	80
St. Lawrence	SCA	81
St. John's	SCA	39

other climate zones was not expected to have a major impact on results, including Interior Labrador and the North Coast and Central Lowlands.

2.3.2 Design Storms for NL

The mass curves identified by the cluster analysis did not fit well with design storms used most frequently in the province (Figure 2.8). The City of St. John's uses mass curves that fall within an AP type of event, however the majority of storms on the Avalon were determined to be DP events. The mass curve used to develop a design storm for the PMP in Labrador provides a good approximation of the DP that was identified for the region (Figure 2.8).

2.4 Discussion

Eight patterns for the temporal distribution of precipitation (mass curves) were identified as being representative of the precipitation in Newfoundland and Labrador (NL). These consisted broadly of advanced patterns (AP) and delayed patterns(DP), where at least half of the event total depth of precipitation fell in the first and second half of an event, re-
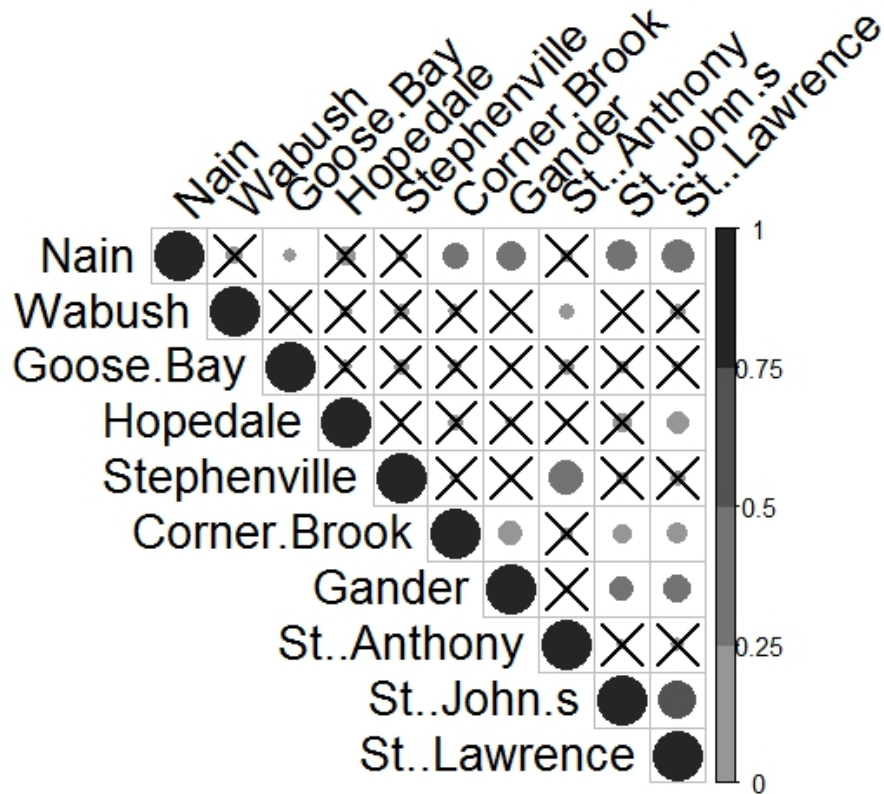
Figure 2.7: Correlation of precipitation depth between stations. X indicates that station correlations are not significant ($p > 0.05$). The size of the circles reflect the amount of correlation between the stations

spectively. Grouping these patterns into four more distinct patterns; AP, AP-U, DP, and DP-2P (see above for descriptions of these patterns) was more useful towards interpretation of the results. There appears to be an effect of climate on mass curves through the interaction with storm duration in addition to mean annual precipitation, which was one of the criteria that determines climate zones in NL (McManus & Wood, 1991). It seems
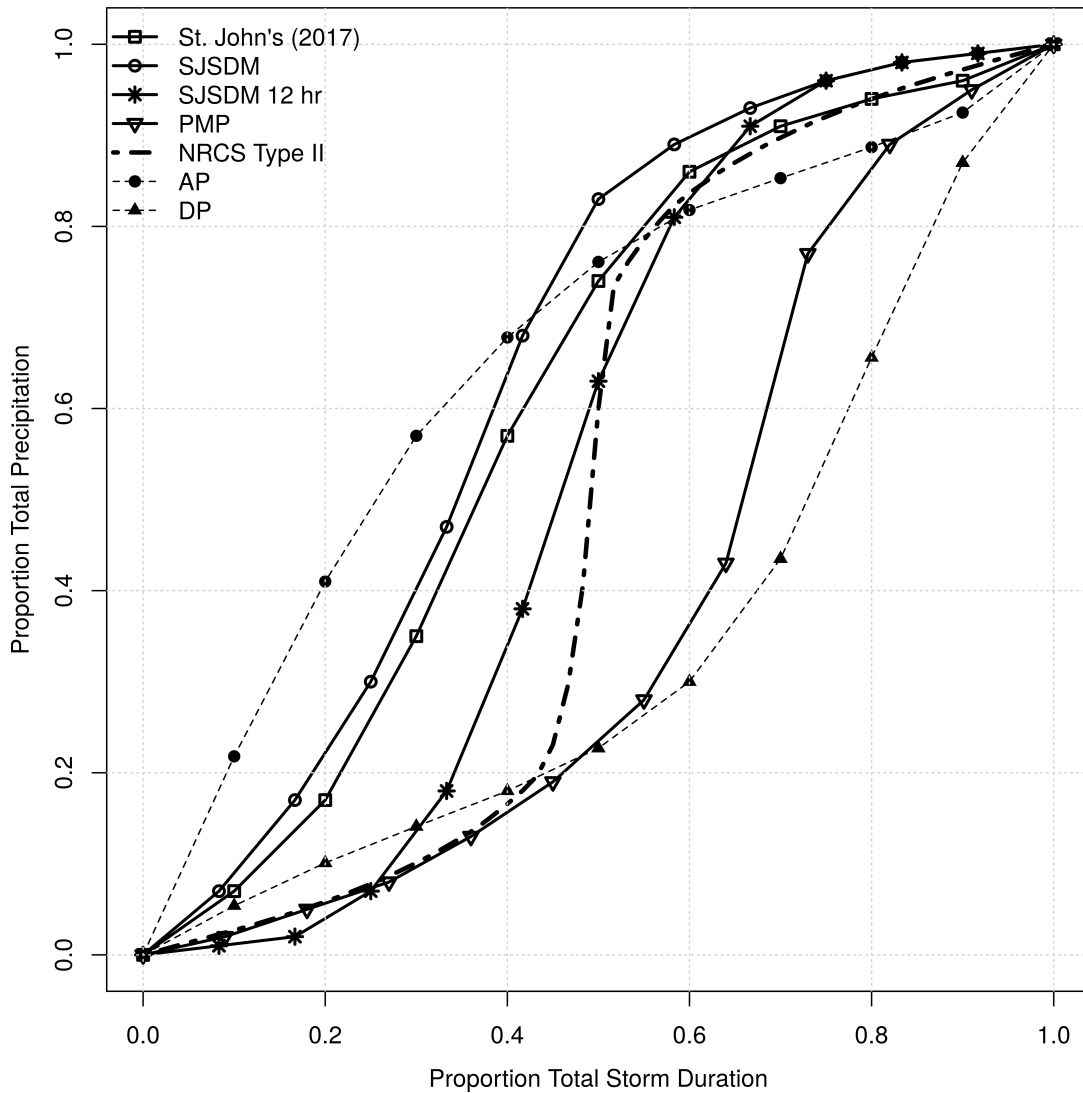
Figure 2.8: Temporal distribution of rainfall used for the determination of design storms from the City of St. John's Subdivision Design Manual (SJSDM), the St. John's 2017 updated storm, the storm used in Labrador to determine probable maximum precipitation (PMP) for dam design, the NRCS Type II storm, and AP and DP type of events determined from the cluster analysis.

most likely that climate affects the mass curve through its impact on event duration in a region, and the occurrence of intense bursts within a given event. It is likely that there is also an interaction between incremental rainfall intensity and event duration (Koutsoyiannis & Foufoula-Georgiou, 1993) that could be dependent upon climate. This is not a surprising

result given the current level of understanding of precipitation and the fact that an important aspect to identifying climate zones is through identification of differences in types of precipitation.

Overall, the proportion of events, out of all events used in the analysis, falling into AP and DP event categories was approximately equal at 0.4, but the proportions varied by climate zone. The highest proportion of AP events occurred in the Tundra (45%) and the highest proportion of DP events occurred along the South Coast and Avalon (45%). While this type of variation in occurrence of the four patterns across climate zones was not statistically significant, there may still be some implications for choice of design storms.

While the slopes of linear regressions for the relationship of depth with duration varied between events grouped by climate zone and events grouped by pattern, there was no evidence that either grouping had effects on this relationship. However, the mean and variation of event depth and duration within each of the four groupings of patterns suggests a climate impact on both storm depth and duration. That is, variation in storm depth can be explained in part by storm pattern and climate zone independently, and there were climate zone effects on the mean and variance in storm depth that did not depend on storm pattern. Additionally, the results suggest that climate zone and pattern both impact mean and variance in storm duration.

Taken together, the results seem to indicate that climate impacts the mass curve primarily through its impact on event duration. For instance, locations in Labrador (T and IL) had longer duration events with fewer short intense bursts. The occurrence of short bursts of intense precipitation was much less frequent in northern and interior Labrador than Newfoundland. This tends to change along the coast of Labrador where more intense precipitation bursts have been observed in Hopedale. Orographic effects are known to impact temporal distribution in Canada (Loukas & Quick, 1995), and this is likely to play a role in the short intense bursts observed at Corner Brook. The differences in the number

of bursts between stations in the same climate zones, along the North Coast of Newfoundland (St. Anthony and Gander) and the South Coast and Avalon (St. Lawrence and St. John's), points to the existence of more local impacts that can have strong implications for the choice of design storms. The impacts of post-tropical systems are apparent at St. Lawrence which is most likely to be impacted by these systems that drop large volumes of rainfall over longer durations.

2.4.1 Implications for Design Storm Choice

The impact of post-tropical events has been the rationale for the practice of using these as design events in NL, as recent events have caused significant damage to infrastructure in many parts of the island (Federation of Canadian Municipalities, 2017; Turn Back The Tide, 2011). However, the variation in event patterns across the island found in this analysis suggests a mass curve based on a single large event may not be applicable in all regions and for all applications. Additionally, use of these recent events have been taken as method of incorporating recent climate change into design of storm water infrastructure. This is questionable given the results of this analysis, and for other reasons that are beyond the scope of this paper to discuss (see Adams et al. (1986)). Moreover, it is not clear how climate change will affect the occurrence of such storms.

Smaller events (< 40 mm depth) likely had the most impact on temporal patterns of precipitation based on results here, in particular for DP-2P events. The DP-2P type of precipitation events were classified by a mass curve with a two-peaked hyetograph, though not all events so classified had two peaks in intensity. It is not clear what the impact of this type of event might have on flood frequencies or stormwater controls, these types of events were primarily for events with depths < 40 mm and durations > 10 hours. However it is not likely that these types of storms are of importance for storm water infrastructure design applications, nor for larger scale flooding or dam design applications. Moreover, given that

the significance of event depth as a determinant was lost when grouping the eight patterns into four groups, it seems event depth may not provide an accurate means of determining the choice of mass curve for development of a design storm.

A focus on the two dominant groups of events, AP and DP, seems to be the best way to proceed in order to choose a mass curve for design storms. The proportion of AP and DP storms was about equal in all climate zones. It may seem reasonable to use DP mass curves as these will tend to lead to more runoff, and hence, designs that can handle larger events. However, it is also possible that use of a DP mass curve may lead to over design and higher unnecessary costs. Since there is an interaction of duration with climate zone, the inclusion of longer duration events may be required for development of design storms. While it has been found that there are significant trends for events of all durations with observed climate change (Adamowski et al., 2010), evidence indicates that precipitation is increasing at a greater rate for longer duration events in Canada (Burn & Taleghani, 2013), which further supports this contention.

Given the variation in mass curves across the province and at a single station, choice of mass curve for a design storm seems best to be done depending upon the particular application. The probable maximum flood for design of parts of the hydraulic structures for Muskrat Falls (Hatch, 2008) was developed using a design storm with a DP mass curve that matches well with the DP types of mass curves identified in this analysis. Used in simulations, the DP mass curves allow for soil wetting and saturation to occur before most of the precipitation occurs in the event. For other applications, such as runoff estimation from areas with a high percentage of impervious area, AP mass curves may be more appropriate. In cases where it may not be as clear which mass curve is best, a conservative approach may be best (Guo & Hargadin, 2009). The NRCS Type II distribution matches the first half of a DP event and the latter half of an AP event, so a type II curve may be a more justifiable choice of distribution than those currently used by St. John's. However, this is more

difficult to justify from an empirical perspective since the type II events were developed to represent high intensity thunderstorms (Froehlich, 2009), which are rare events in NL.

A key limitation of this analysis was that hourly precipitation data were used and durations were ≥ 3 hours, while many engineering applications require precipitation at sub-hourly time scales. Therefore it is not possible to make any direct recommendations regarding choice of mass curve for design applications that require sub-hourly precipitation. The authors' work is ongoing to include sub-hourly precipitation and more extreme precipitation events in analysis of mass curves and the development of design storms. However results of this analysis support the contention that a standard mass curve may be difficult to apply for all design applications. For instance, the mass curve, and hence design storm, for a multi-modal non-linear system with highly varying response times of large drainage areas (such as a combined sewer system) would likely differ from that required for a simple more linear system (Vaes et al., 2004), such as culvert design (Vaes et al., 2002), for applications in NL. Smaller scale and more complex applications require more detailed analysis at the sub-hourly time scale that also include the potential impacts of climate change.

2.5 Conclusion

Eight patterns for the temporal distribution of precipitation were identified as representative for NL. Four groups of these eight patterns were identified as distinct patterns; AP, AP-U, DP, and DP-2P were useful towards making recommendations for choice of mass curve for design storms. Results support the conclusion that climate was an important determinant of temporal distribution of precipitation, and it is important to determine which pattern is dominant in a given region. Therefore it is not recommended that mass curves developed from storms from a particular region be directly applied to another region without justification. The choice of mass curve may be best made based on region (climate zone) and

77

design application, and a more conservative and justifiable choice may be to use a mass curve that represents a trade-off between AP and DP mass curves, such as the NRCS Type II mass curve. Finally, the results suggests the importance of incorporating the impacts of climate and climate change on the temporal distribution of rainfall. It is possible that mass curves or the dominant type of mass curve may change with a changing climate, so it is recommended that the potential impacts of climate change on temporal distribution of rainfall be assessed for the development of design storms. The authors are continuing this work to assess the potential impacts of climate change on mass curves and design storms.

Acknowledgements

References

Adamowski, J., Adamowski, K., & Bougadis, J. (2010). Influence of trend on short duration design storms. *Water Resources Management*, *24*(3), 401–413.

Adams, B. J., Fraser, H. G., Howard, C. D., & Sami Hanafy, M. (1986). Meteorological data analysis for drainage system design. *Journal of environmental Engineering*, *112*(5), 827–848.

Alfieri, L., Laio, F., & Claps, P. (2008). A simulation experiment for optimal design hyetograph selection. *Hydrological Processes: An International Journal*, *22*(6), 813–820.

Asong, Z., Khaliq, M., & Wheater, H. (2015). Regionalization of precipitation characteristics in the canadian prairie provinces using large-scale atmospheric covariates and geophysical attributes. *Stochastic Environmental Research and Risk Assessment*, *29*(3), 875–892.

Asquith, W. H., Roussel, M. C., Cleveland, T. G., Fang, X., & Thompson, D. B. (2006). Statistical characteristics of storm interevent time, depth, and duration for eastern new mexico, oklahoma, and texas. *US Geological Survey professional paper*(1725), 1–299.

BAE Newplan Group Limited, G. (2013, May). *Paradise storm water master plan, town of paradise, technical report, 2013*. Retrieved 2014-07-12, from `http://www.paradise.ca/en/town-hall/resources/Storm-Water-Report.pdf`

Banfield, C. E., & Jacobs, J. D. (1998). Regional patterns of temperature and precipitation for newfoundland and labrador during the past century. *Canadian Geographer/Le Géographe canadien*, *42*(4), 354–364.

Bhat, H. S., & Kumar, N. (2010). On the derivation of the bayesian information criterion. *School of Natural Sciences, University of California*, *99*.

Branham, T., & Behera, P. (2010). Development of a rainfall statistical analysis tool for analytical probabilistic models for urban stormwater management analysis. In *World environmental and water resources congress 2010: Challenges of change* (pp. 3281–3290).

Burn, D. H., & Taleghani, A. (2013). Estimates of changes in design rainfall values for canada. *Hydrological Processes*, *27*(11), 1590–1599.

Buttle, J. M., Allen, D. M., Caissie, D., Davison, B., Hayashi, M., Peters, D. L., ... Whitfield, P. H. (2016). Flood processes in canada: Regional and special aspects. *Canadian Water Resources Journal/Revue canadienne des ressources hydriques*, *41*(1-2), 7–30.

Chin, D. (2013). *Water resources engineering* (Vol. 12). Pearson Education, Inc. Upper Saddle River, NJ.

Chin, R. J., Lai, S. H., Chang, K. B., Jaafar, W. Z. W., & Othman, F. (2016). Relationship between minimum inter-event time and the number of rainfall events in peninsular malaysia. *Weather*, *71*(9), 213–218.

Chou, Y.-M., Polansky, A. M., & Mason, R. L. (1998). Transforming non-normal data to normality in statistical process control. *Journal of Quality Technology*, *30*(2), 133–141.

Chow, V., Maidment, D., & Mays, L. (1988). Applied hydrology mcgraw-hill international editions. *New York, USA*.

City of St. John's, G. (2017). City of st. john's 2017 rainfall design hyetographs for climate

change.

Desbordes, M. (1978). Urban runoff and design storm modelling. In *Proceedings of the international conference on urban storm drainage, held at the university of southampton.*

Dolšak, D., Bezak, N., & Šraj, M. (2016). Temporal characteristics of rainfall events under three climate types in slovenia. *Journal of Hydrology*, *541*, 1395–1405.

Dullo, T. T., Kalyanapu, A. J., & Teegavarapu, R. S. (2017). Evaluation of changing characteristics of temporal rainfall distribution within 24-hour duration storms and their influences on peak discharges: case study of asheville, north carolina. *Journal of Hydrologic Engineering*, *22*(11), 05017022.

Environment & Climate Change Canada, G. (2013, May). *Environment and Climate Change Canada - Weather and Meteorology - Home.* Retrieved 2017-07-12, from `https://www.ec.gc.ca/ouragans-hurricanes/default.asp?lang=EnandC8A7AA0-1`

Fang, T. (1996). Analysis of wyoming extreme precipitation patterns and their uncertainty for safety evaluation of hydraulic.

Federation of Canadian Municipalities, G. (2017). *The cost of climate adaptation - insurance bureau of canada.* Retrieved from `http://assets.ibc.ca/Documents/Disaster/The-Cost-of-Climate-Adaptation-infographic-EN.pdf`

Finnis, J., & Bell, T. (2015). An analysis of recent observed climate trends and variability in labrador. *The Canadian Geographer/Le Géographe canadien*, *59*(2), 151–166.

Finnis, J., & Daraio, J. (2018, January). *Projected impacts of climate change for the province of newfoundland & labrador: 2018 update* (Tech. Rep.). Government of Newfoundland and Labrador. Retrieved 2017-07-12, from `https://www.exec.gov.nl.ca/exec/occ/publications/Final_Report_2018.pdf`

Fox, J., & Weisberg, S. (2011). *An r companion to applied regression.* Sage publications.

Froehlich, D. C. (2009). Mathematical formulations of nrcs 24-hour design storms. *Journal of irrigation and drainage engineering*, *135*(2), 241–247.

Gelman, A., & Hill, J. (2007). *Data analysis using regression and multilevel/hierarchical models*. Cambridge university press.

Gelman, A., Su, Y., Masanao, Y., Zheng, T., & Dorie, V. (2018). *arm: Data analysis using regression and multilevel/hierarchical models, version 1.10-1.*

GNL. (2011, January). *Charting our course: Climate change action plan 2011* (Tech. Rep.). Government of Newfoundland and Labrador. Retrieved 2018-01-13, from `http://www.exec.gov.nl.ca/exec/occ/publications/climate_change.pdf`

Government of Canada, S. C. (2005, September). *Population estimates on July 1st, by age and sex.* Retrieved from `https://www150.statcan.gc.ca/t1/tbl1/en/tv.action?pid=1710000501`

Guo, J. C., & Hargadin, K. (2009). Conservative design rainfall distribution. *Journal of Hydrologic Engineering*, *14*(5), 528–530.

Hartigan, J. A., & Wong, M. A. (1979). Algorithm as 136: A k-means clustering algorithm. *Journal of the royal statistical society. series c (applied statistics)*, *28*(1), 100–108.

Hastie, T., Tibshirani, R., & Friedman, J. (2009). The elements of statistical learnin. *Cited on*, 33.

Hatch. (2008, January). *The Lower Churchill Project: PMF and Construction Design Flood Study* (Technical report Nos. GI1140, 2008). Author. Retrieved from `https://muskratfalls.nalcorenergy.com/wp-content/uploads/2013/03/Muskrat-Falls-PMF-and-Construction-Design-Flood-Study_Dec2007.pdf`

Hogg, W. (1980). Time distribution of short duration storm rainfall in canada. In *Proc. canadian hydrology symposium* (Vol. 80, pp. 53–63).

Huff, F. A. (1967). Time distribution of rainfall in heavy storms. *Water resources research*, *3*(4), 1007–1019.

Kauffman, G. (1987). A comparison for analytical and simulation models for drainage system design. *MASc. thesis, Dept. of Civil Engineering, Univ. of Toronto, Toronto*.

Keifer, C. J., & Chu, H. H. (1957). Synthetic storm pattern for drainage design. *Journal of the hydraulics division*, *83*(4), 1332–1.

Kimoto, A., Canfield, H. E., & Stewart, D. (2011). Comparison of synthetic design storms with observed storms in southern arizona. *Journal of Hydrologic Engineering*, *16*(11), 935–941.

Koutsoyiannis, D., & Foufoula-Georgiou, E. (1993). A scaling model of a storm hyetograph. *Water Resources Research*, *29*(7), 2345–2361.

Lin, G.-F., Chen, L.-H., & Kao, S.-C. (2005). Development of regional design hyetographs. *Hydrological Processes: An International Journal*, *19*(4), 937–946.

Loukas, A., & Quick, M. C. (1995). 24-h design storm for coastal british columbia. *Journal of Hydraulic Engineering*, *121*(12), 889–899.

McManus, G. E., & Wood, C. H. (1991). Atlas of newfoundland & labrador//review. *Cartographica*, *30*(4), 84.

Mouselimis, L. (2018). *Clusterr: Gaussian mixture models, k-means, mini-batch-kmeans and k-medoids clustering. r package version 1.1. 1*.

Neath, A. A., & Cavanaugh, J. E. (2012). The bayesian information criterion: background, derivation, and applications. *Wiley Interdisciplinary Reviews: Computational Statistics*, *4*(2), 199–203.

Nguyen, T. A., Grossi, G., & Ranzi, R. (2016). Design storm for mixed urban and agricultural drainage systems in the northern delta in vietnam. *Journal of Irrigation and Drainage Engineering*, *142*(2), 04015051.

Nguyen, V.-T.-V., Desramaut, N., & Nguyen, T.-D. (2010). Optimal rainfall temporal

patterns for urban drainage design in the context of climate change. *Water Science and Technology*, *62*(5), 1170–1176.

Nojumuddin, N. S., Yusof, F., & Yusop, Z. (2015). Identification of rainfall patterns in johor. *Applied Mathematical Sciences*, *9*(38), 1869–1888.

NRCS, U. (2004). National engineering handbook: part 630—hydrology. *USDA Soil Conservation Service: Washington, DC, USA*.

Packman, J., & Kidd, C. (1980). A logical approach to the design storm concept. *Water Resources Research*, *16*(6), 994–1000.

Pan, C., Wang, X., Liu, L., Huang, H., & Wang, D. (2017). Improvement to the huff curve for design storms and urban flooding simulations in guangzhou, china. *Water*, *9*(6), 411.

Pilgrim, D. H., & Cordery, I. (1975). Rainfall temporal patterns for design floods. *Journal of the Hydraulics Division*, *101*(1), 81–95.

Powell, D. N., Khan, A. A., Aziz, N. M., & Raiford, J. P. (2007). Dimensionless rainfall patterns for south carolina. *Journal of Hydrologic Engineering*, *12*(1), 130–133.

Raykov, Y. P., Boukouvalas, A., Baig, F., & Little, M. A. (2016). What to do when k-means clustering fails: a simple yet principled alternative algorithm. *PloS one*, *11*(9), e0162259.

SCS, U. (1986). *Urban hydrology for small watershed (technical release 55)* (Tech. Rep.). Washington, DC: US Department of Agriculture. Retrieved from `https://www.nrcs.usda.gov/Internet/FSE_DOCUMENTS/stelprdb1044171.pdf`

Sifalda, V. (1973). Development of a computational rain for the design of sewer networks. *GWF-Water sewage*, *114*(H9), 435–440.

SNC Lavalin Inc., G. (2015, January). *Little Cobb's Pond Hydrological/Hydrogeo-logical Study* (Technical Report). Town of Gander. Retrieved from `http://www.gandercanada.com/images/stories/pdfs/LittleCobbsStudy.pdf`

Team, R. C., et al. (2018). *R: A language and environment for statistical computing; 2018.*

Terranova, O., & Iaquinta, P. (2011). Temporal properties of rainfall events in calabria (southern italy). *Natural hazards and earth system sciences*, *11*(3), 751–757.

Tibshirani, R., Walther, G., & Hastie, T. (2001). Estimating the number of clusters in a data set via the gap statistic. *Journal of the Royal Statistical Society: Series B (Statistical Methodology)*, *63*(2), 411–423.

Turn Back The Tide, G. (2011). *Infrastructure.* Retrieved from `https://www.turnbackthetide.ca/impacts-of-climate-change/ iiew-infrastructure.shtml`

US Army Corps of Engineers, U. (1982). *HEC-5 simulation of flood control and conservation systems, user's manual.* Hydrologic Engineering Center, Davis.

US Army Corps of Engineers, U. (2000). Hydrologic modeling system hec-hms technical reference manual. *Hydrol. Eng. Cent*.

Vaes, G., Clemens, F., Willems, P., & Berlamont, J. (2002). Design rainfall for combined sewer system calculations: comparison between flanders and the netherlands. In *Global solutions for urban drainage* (pp. 1–16).

Vaes, G., Willems, P., Berlamont, J., et al. (2004). The use of design rainfall in the new flemish urban drainage guidelines. *Hydrology: Science & Practice for the 21st Century, II0 (March 2015)*, 346–353.

Wadden, D. (2002). *Rainfall distribution in the city of st. john's: temporal distribution, spatial variation, frequency analysis, and tropical storm gabrielle* (Unpublished doctoral dissertation). Memorial University of Newfoundland.

Wang, Y. (2015). jtrans: Johnson transformation for normality. *R package version*, *1*(0).

Watt, E., & Marsalek, J. (2013). Critical review of the evolution of the design storm event concept. *Canadian Journal of Civil Engineering*, *40*(2), 105–113.

Watt, W., Chow, K., Hogg, W., & Lathem, K. (1986). A 1-h urban design storm for canada.

Canadian Journal of Civil Engineering, *13*(3), 293–300.

Welling, M., & Kurihara, K. (2006). Bayesian k-means as a "maximization-expectation" algorithm. In *Proceedings of the 2006 siam international conference on data mining* (pp. 474–478).

Willems, P. (2000). Compound intensity/duration/frequency-relationships of extreme precipitation for two seasons and two storm types. *Journal of Hydrology*, *233*(1-4), 189–205.

Wu, S.-J., Yang, J.-C., & Tung, Y.-K. (2006). Identification and stochastic generation of representative rainfall temporal patterns in hong kong territory. *Stochastic environmental research and risk assessment*, *20*(3), 171–183.

Yen, B. C., & Chow, V. T. (1980). Design hyetographs for small drainage structures. *Journal of the Hydraulics Division*, *106*(6), 1055–1076.

Zhang, X., Hogg, W., & Mekis, É. (2001). Spatial and temporal characteristics of heavy precipitation events over canada. *Journal of Climate*, *14*(9), 1923–1936.

Chapter 3

Effects of Infiltration Method and Temporal Distribution of Precipitation on Peak Discharge Estimates in a Changing Climate

*

Preface

I am the primary author, and I carried out most of the research, performed the literature reviews, simulation setups, and analysis of the results. I also prepared the first drafts of the manuscripts and subsequently revised the final manuscripts based on feedback from the co-authors and the peer-review process. Dr. J.A. Daraio, supervised the research,

---

*This chapter is a modified version of "Effects of infiltration method and Temporal Distribution of Precipitation on Peak Discharge Estimates in a Changing Climate" which is currently under review with the Journal of Water and Climate

Abstract

Design parameters for stormwater infrastructure and flood risk mapping will be impacted by climate change. Projections are available for rainfall intensity, duration and frequency (IDF). However, it is not known if/how this will interact with other climate responses and hydrologic factors impacting flood risks in a changing climate. The objectives of this study are to examine the effects of different approaches to distributing heavy rainfall, specifically, varying temporal distributions and infiltration methods and considering their influence on peak stormwater discharge under climate change. Peak discharge was simulated with rainfall depths from the historical climate and two future time slices under two emission scenarios using HEC-HMS for watersheds on the island of Newfoundland. Flood extents from peak discharges were estimated using HEC-RAS. Peak discharge increased by over 100% and 200% from the historical climate peak discharges for increases in event rainfall and infiltration methods for the 20-year and 100-year return periods, respectively, under the climate change projections. Flood extents varied with temporal distribution and return period. The flood extents increased by approximately 8% for the 20-year return period and 15% for the 100-year return period. For some locations, the temporal distribution producing the greatest flood extent under the historical climate differed from that under the climate projections. These interactions should be analyzed when designing stormwater infrastructure under climate change.

Index Terms: Flood risk, temporal distribution, HEC-HMS, HEC-RAS

3.1 Introduction

A design storm is a statistical assessment indicating a rainfall intensity with a specified duration. Its purpose is to approximate the expected storm for a given duration and frequency. The statistical assessment of these storms is based on historical events or statistics of simulated ones. Design storms are composed of four key elements: (i) the rainfall amount (depth), (ii) the rainfall event's time span (duration), (iii) the rate of occurrence of the event (frequency; often indicated as return period) and distribution of the rainfall amount over the event's time span (temporal distribution). Design storms are developed using several methods, including, using historic rainfall to develop standardized mass curves, which are curves indicating the fraction of rainfall amount that would have occurred within a certain duration of the rainfall event, assuming a specified geometric shape (e.g. triangle or rectangle) to a point on the IDF curve, use of stochastic models to simulate a distribution and use of alternating block method, Where rainfall depths from an event are split into blocks and the block with the largest depth is placed at the center of the storm Veneziano and Villani (1999) and

IDF curves are a means of representing rainfall statistics constructed from observed extremes, and explicitly address the first three parameters of a design storm. Impact of climate change on IDF curves has been well studied (Vu et al., 2018; Luo et al., 2018; Al Mamoon et al., 2019; Nguyen & Nguyen, 2019) and results suggest that IDF curves based on historical data are no longer valid for use in design under the changing climate. IDF curves, while providing most of the parameters for a design storm, fail to provide a key component which is critical in stormwater design, temporal distribution; to date, the impacts of climate change on the validity of temporal distributions have received limited research attention.

Temporal distribution refers to a representation of the fraction of a precipitation depth

that occurs within a section of the event duration. Examples of the empirical distributions include triangular distribution, alternating block distribution and rectangular distribution (Gao et al., 2012; Gong et al., 2016; Umakhanthan & Ball, 2002). The temporal distribution dictates the timing of the maximum rainfall volume within a specified event duration, which can significantly impact generated runoff. For instance, if all factors are held constant in a hydrologic simulation, the runoff generated from the Natural Resources Conservation Service (NRCS) Type II storm would vary from the Type I storm. The difference in generated runoff is because the maximum rainfall volume occurs at the center of the event duration in the Type II storm. In contrast, the maximum rainfall volume occurs in the first half of the event duration for a Type I storm. The climate in a region governs the temporal distribution of precipitation events, e.g., rainfall events in tropical regions differ from temperate regions (Winstanley, 1973), and patterns of the temporal distribution of precipitation can vary across climate gradients within a region (Amponsah et al., 2019). Different design applications require different temporal distributions. In designing major hydraulic structures such as emergency spillways, a temporal distribution with the largest rainfall volume occurring during saturated watershed conditions is preferred. This setup, similar to the probable maximum precipitation, presumably generates the most runoff, and thus the structure must be designed to accommodate this. For smaller structures like culverts, a temporal distribution which results in the peak runoff rate occurring in the shortest time is ideal. Identifying the unique temporal distributions best suited to a location and purpose will guide engineers better than the "one-size-fits-all" approach where temporal distributions identified for one region are applied to another region, regardless of its fit to the climate.

Although it is unlikely that climate change will require the development of new temporal distribution models, it is very likely that shifts in climate regimes will alter the suitability of a given temporal distribution in a particular region, impacting their relevance for the development of design storms at any given location (Watt & Marsalek, 2013). With expected

changes to the climate, it is necessary for engineers and planners to know how current temporal distributions adopted for design storm formulation will change. Modifications to the temporal distributions will most likely have a direct impact on peak runoff rates and runoff volumes and consequently on design parameters.

Besides rainfall depth and temporal distribution, infiltration methods are another critical component in the design of hydraulic structures. Infiltration methods determine what proportion of rainfall does not contribute to the runoff generation process. Hence, it is inferred that the choice of infiltration method will directly impact runoff generation and consequently, design parameters. Infiltration methods are often the most dominant among rainfall abstractions. It is governed primarily by properties of the soil and its surface cover.

Many infiltration methods exist, and different design projects use different methods. The most popular of these in the engineering community is the NRCS (formerly Soil Conservation Services) Curve number (CN) (Boughton, 1989) method mainly because of its ease of application. This method was developed to estimate rainfall excess as a function of the land surface cover and the underlying hydrologic soil. Green and Ampt (G&A) (Green & Ampt, 1911) is another infiltration method used for design. This method is physically based and considered as one of the most realistic infiltration models in engineering (Chin, 2013). Other infiltration methods include the Horton model (Horton, 1940) and Initial and Constant (IC) loss model. Unlike IDF curves which rely directly on an atmospheric variable, infiltration methods, at the event scale, will be impacted by climate change through its impact on soil characteristics, vegetation, and climate forcing from the surface - all of which influence soil moisture and, consequently, the ability to attenuate flooding (Sharma et al., 2018). It can be hypothesized that peak discharges from different temporal distributions are directly dependent on rainfall intensity when the IC or CN infiltration method is used. This is because abstractions from these methods do not vary in time but are rather constant. With G&A on the other hand, the importance of temporal distributions become

91

significant due to the time varying saturation of soils.

Peak runoff rate estimation is an interplay between rainfall depth from a return period with specified duration, temporal distribution from the climate zone and infiltration method. An in-depth study of this interplay of factors has not been extensively conducted. Considering climate change and how it will impact this interplay has also not been studied at length. The objectives of this study were to: (1) to determine the relationships between precipitation intensity (return period), infiltration method, and temporal distribution of rainfall across climate zones; (2) to assess the potential impact of changes in intensity due to climate change on peak flows in these climate zones, and (3) to compare flood extents from the various temporal distributions.

3.2   Methods

Peak discharge was estimated for watersheds in two out of seven different climate zones using three different infiltration methods, three temporal distributions of precipitation, and rainfall depths from the current and projected IDF curves for two return periods. Climate change projections for IDFs were based on RCP4.5 (scenario where highest emissions occur by mid century and decline after) and RCP8.5 (scenario where emissions continue to increase until 2100) (Meinshausen et al., 2011) using two future time slices (2041-2070 and 2071-2100). The climate change projections used in this study were conducted by (Finnis & Daraio, 2018). A summary of the procedure used to obtain the climate projections is provided in subsequent sections.

3.2.1   Study Sites

Newfoundland and Labrador (NL) is about 373,800 km^2 and is located in eastern Canada between the longitudes of 52° 00' 00 "W and 68° 00' 00 "W and latitudes of 46° 36' 36"N

to 60° 22' 48"N (Figure 3.1). Newfoundland and Labrador experiences frequent passage of post-tropical cyclones due to its location within the climatological Atlantic storm track and this influences its weather and climate (Seiler & Zwiers, 2016). The province has varied weather and climate given that it spans roughly 14° of latitude. As many as seven climate zones have been identified for the province (McManus et al., 1991). A summary of the climate zone conditions is presented in 2 Table 2.2. The summer temperature averages about 16°C while winter averages -1°C in Newfoundland. There is high spatial variability in the precipitation of the region given that it features a range of climate zones, large spatial extent, extensive coastline, and varied topography.

Fourteen watersheds in three climate zones are used in this study (Figure 3.1 - 3.4). These watersheds were chosen because they have hydrologic models that are fully developed, calibrated and validated by engineering consultants based on the requirements of the Water Resources Division of the province (AMEC Environment & Infrastructure, 2013a, 2013b; Amec Foster Wheeler Environment & Infrastructure, 2015; CBCL LIMITED Consulting Engineers, 2012; HATCH, 2009, 2012). The analysis excludes Labrador, because there are few calibrated models available. For purposes of demonstration, it was decided to focus on climate zones with multiple calibrated models, rather than exploring the full range of NL climate variability. A summary of the watershed characteristics is presented in Table 3.1.

3.2.2 Runoff Model

Hydrologic Engineering Center's Hydrologic Modeling System (HEC-HMS), version 4.3 (Feldman, 2000) was used to estimate peak runoff rate. The HEC-HMS model has been extensively used in many hydrologic studies (Chu & Steinman, 2009; Koneti et al., 2018; Yuan et al., 2019; Joshi et al., 2019) and is required for the design of publicly funded infrastructure in Newfoundland and Labrador. While some of watershed models were calibrated
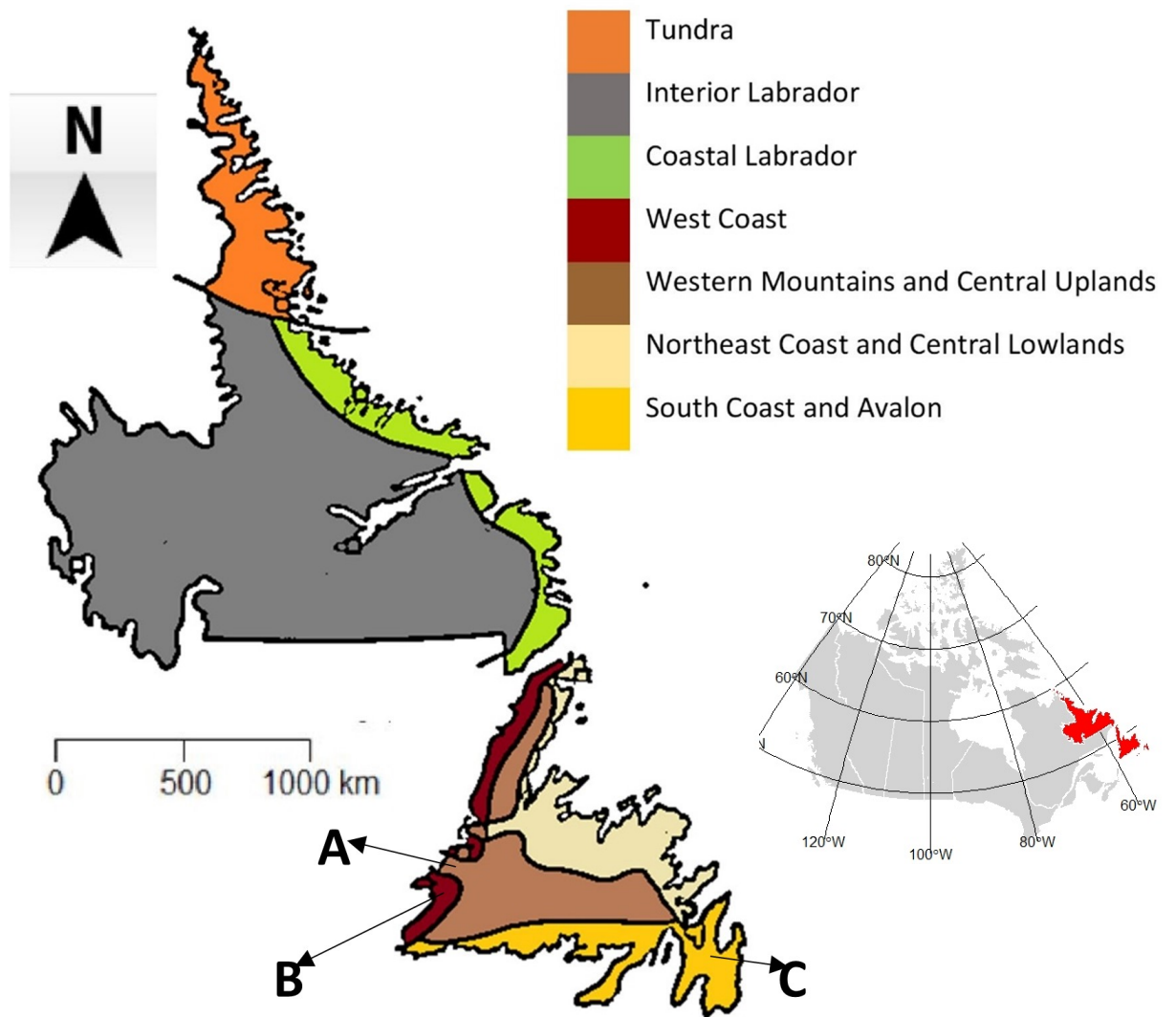
Figure 3.1: Map of study region with climate zones highlighted.Climate zones used in the study are marked by letters A, B, and C. (Inset is the study location in Canada)
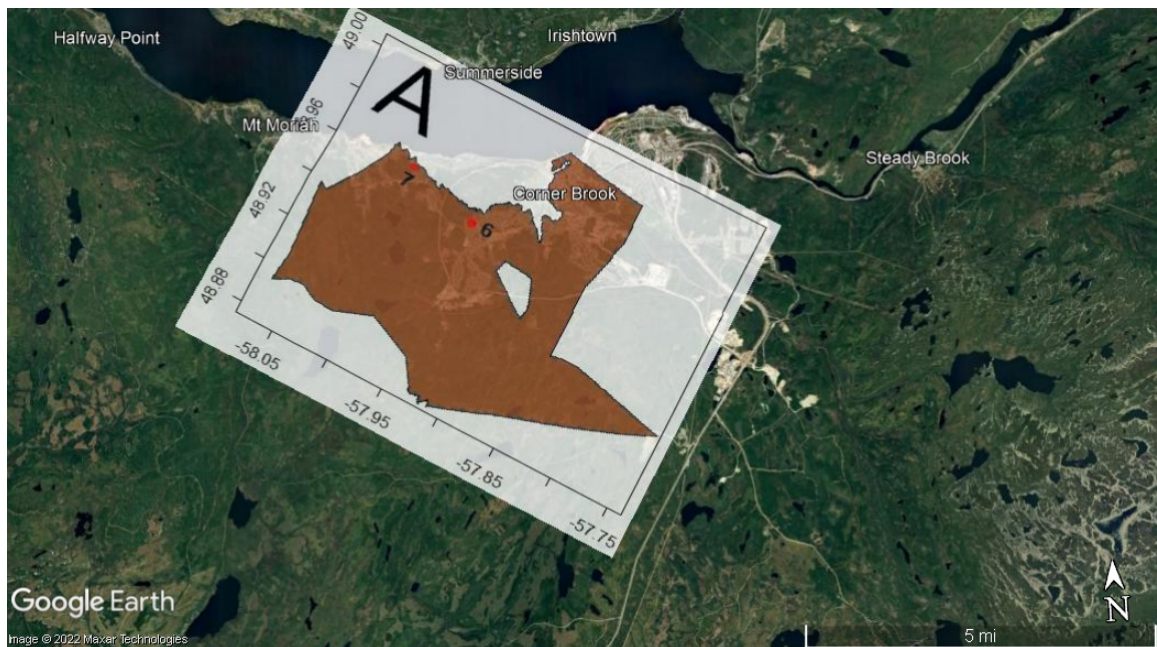
Figure 3.2: Locations of the watersheds in the Western Mountain and Central Uplands (A) climate zone used in the study
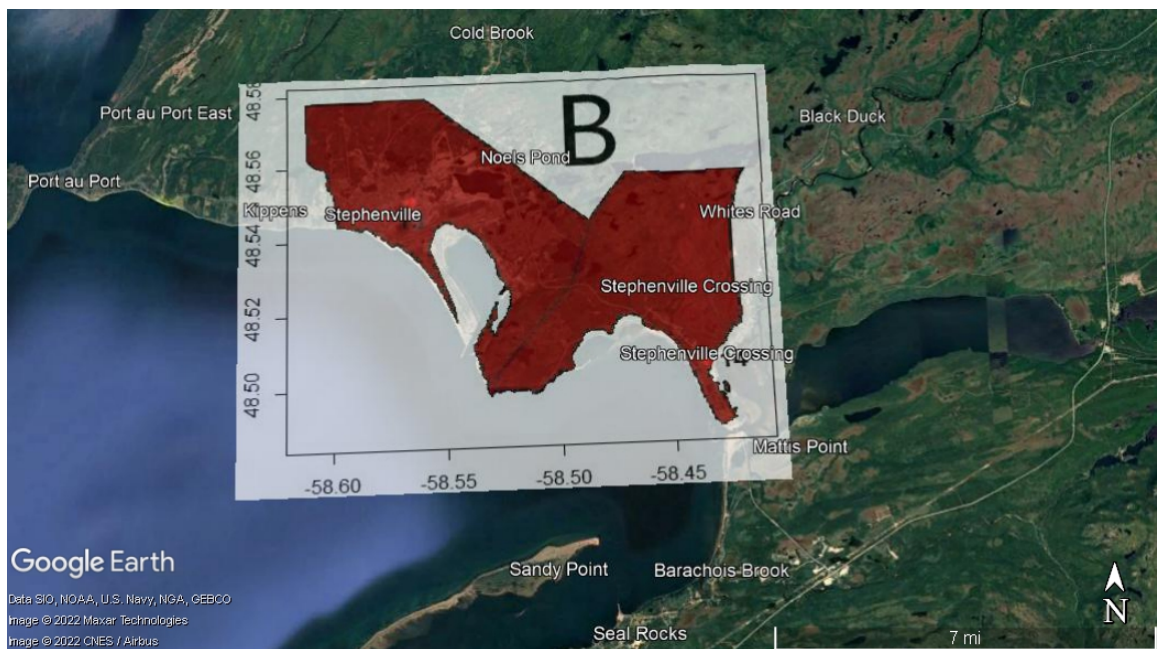
Figure 3.3: Locations of the watersheds in the West Coast (B) climate zone used in the study
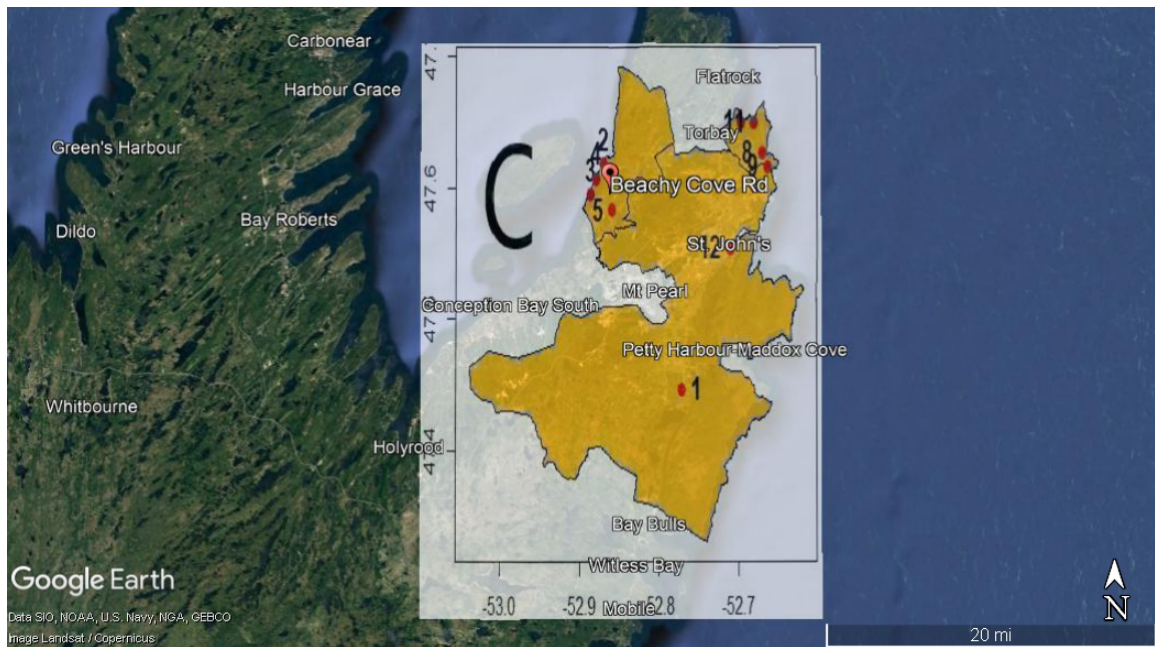
Figure 3.4: Locations of the watersheds in the South Coast and Avalon (C) climate zone used in the study

using observed flow data, others were calibrated using regional frequency analysis conducted for nearby hydrometric stations. The inputs needed for this model are a temporal distribution to define the hyetograph, rainfall depth, watershed area and infiltration model.

3.2.2.1 Model Calibration

Model calibration involves varying model parameters to minimize the difference between observed and simulated flows using an observed event(s). Often model parameters may be fixed or variable. Fixed model parameters are usually obtained from GIS analysis and, as such, are often not modified during the calibration process. The variable parameters, however, are typically event-based; hence these are changed during the calibration process. This type of calibration is only possible where flow data is available. This conventional calibration process could not be applied for some watersheds due to the non-existence or insufficiency of flow data. Instead, streamflow estimates were obtained using statistical

Table 3.1: Stations used in the study

Climate zone	Number	Watershed number	Area (km^2)	IDF station (period)
SCA	1	Goulds and Petty Harbour	134	St. John's Airport (1949-2015)
	2	Beachy Cove (PCSP)	8.6	St. John's Airport
	3	Broad Cove (PCSP)	39.1	St. John's Airport
	4	Goat Cove (PCSP)	2.6	St. John's Airport
	5	Main River (PCSP)	18	St. John's Airport
	8	Coaker's River (LB)	4.09	St. John's Airport
	9	Druken's River (LB)	1.81	St. John's Airport
	10	Kennedy's Brook (LB)	6.32	St. John's Airport
	11	Outer Cove Brook (LB)	12.32	St. John's Airport
	12	Waterford	66.36	St. John's Airport
WMCU	6	Corner Brook	158	Deer Lake (1966-2015)
	7	Petrie's Brook	6.2	Deer Lake
WC	13	Stephenville	123.7	Stephenville (1967-2015)
	14	Black Duck Siding	718.4	Stephenville

PSCP: Portugal Cove St. Philips
LB: Logy Bay

frequency analysis on neighbouring stream gauges.

Using Corner Brook as an example, a summary of the details involved in a typical calibration and validation process is outlined. At Corner Brook, two streamflow gauges located a few meters outside the watershed were used to provide flows to calibrate the model. Data at the two stations were 28 and 26 years in length. A third station was located within the Corner Brook stream watershed with only 16 years of data. This shorter data length would reduce confidence in estimating the 1 in 100-year AEP flows (Zervas et al., 2013).

Before carrying out any statistical frequency analysis, it is standard practice to test flows from these three stations for lack of trend, randomness, homogeneity, and independence. The original study used the Consolidated Frequency Analysis (CFA) package from Environment Canada to carry out the General Randomness, Mann-Whitney split sample homo-

geneity test and the Spearman independence and trend tests. The same tests were conducted using the Hyfran Plus program as a check, and similar results were obtained. Two of the gauges had missing instantaneous maximum flow for some years. The missing values were estimated using the peaking factor (PF) formula (Zhang et al., 2005) to address this gap where:

$$PF = \frac{\text{maximum flow}}{\text{average daily flow}} \tag{3.1}$$

Using an average PF for the years with available data, the maximum flow for missing years is computed as :

$$\text{Maximum flow} = \text{Average PF} \times \text{average daily flow} \tag{3.2}$$

During the test, outliers from each of the two stations with missing data were removed for the data to pass all four screening tests.

Once the data passed the tests, they were fitted with the 3-parameter Log-Normal (3PLN) distribution. This distribution was chosen because studies have found it best fits flood time series (Modarres, 2006; Sarhadi et al., 2012),de2021regional. Using the CFA program, the 1:20 and 1:100 AEP flows were obtained from the streamflow data. According to the orginial study, the CFA package does not provide confidence intervals on the estimated AEP flows. The confidence intervals were estimated using the Bulletin B17 method (Interagency Committee on Water Data, 2018 (revised and corrected)). For comparison purposes, the streamflow data were fitted with the 3PLN using the HyfranPlus program, which provides confidence intervals. The values obtained were similar to those from the Bulletin B17 method with slight variations (Table 3.2).

Like the Corner Brook flood risk mapping study, the confidence intervals on the 100-year AEP flows had a greater range than the 20-year ones. The estimated statistical flows

Table 3.2: Comparison of confidence limits from Bulletin B17 method and HyfranPlus

| | Bulletin B17 | | HyfranPlus | |
Station number	20-year	100-year	20-year	100-year
02YL004	110.2	194.8	98.7	199.3
02YL005	37.9	73.1	35.9	70.4
02YL011	26.1	64	25.6	65.1

were converted into flow per unit area. The statistical estimates for the Corner Brook stream were obtained by multiplying the average flow per unit area from the three stations by the watershed area.

3.2.3 Design Parameters

3.2.3.1 Temporal Distribution

Temporal distributions representing four of eight temporal precipitation patterns identified in Chapter 2 were used (Figure 2.3). The temporal distribution patterns, obtained using Bayesian k-means clustering, identified the natural grouping in rainfall patterns across a climate gradient. Two distributions- Advanced pattern (AP) and Delayed pattern (DP) - were used out of the four identified since these are the most dominant in the province. The temporal patterns from Amponsah et al. (2019) were developed as dimensionless cumulative curves that allowed them to apply to any duration and depth of interest. The province mandates using the alternating block pattern for flood risk mapping for consistency across the province; hence, this is added to this set of temporal distributions for comparison.

3.2.3.2 IDF curves for Rainfall Depth

This study used the 24hr rainfall depths for 25 and 100 year return periods from the most up-to-date IDF information available for current conditions as well as future ones for 2041-2070 and 2071-2100 for the Newfoundland and Labrador province. This information was

provided by the provincial government. The Newfoundland and Labrador (NL) province updated the IDFs to include climate change projections first in 2013 (Finnis, 2013) with subsequent updates in 2015 and 2018. (Conestoga-Rovers & Associates, 2015). The 2013 climate projections used an ensemble of 21st century Coupled Model Intercomparison Project Phase 3 (CMIP3) dynamically downscaled data from the North American Regional Climate Change Assessment Program (NARCCAP). The 2015 update coincided with Environment Canada's three-year regular updates of IDF curves which included data up to the end of 2013. During this round of updates, Conestoga-Rovers & Associates, a consulting firm contracted to update the IDF curves, updated thirteen inactive IDF stations in the province using precipitation from nearby precipitation recording stations. Updating the current IDF curves was necessary to prevent underestimation of precipitation due to climate change effects at these sites. A complete historic update of IDF curves was not done at some sites due to lack of data for certain durations.

The most recent update to the IDF projections was done in 2018 after an increase in the number of new climate data sets (Finnis & Daraio, 2018). The 2018 extrapolation project used two sets of data to represent the climate projections. The first was statistically downscaled projections from the Pacific Climate Impacts Consortium (PCIC) over North America. Statistical downscaling involves establishing a relationship between General Circulation Models (GCM) output and observed climate data, usually at a finer scale, statistically. PCIC uses the Bias Correction Constructed Analogues Quantile mapping (BCCAQ) methodology (Werner & Cannon, 2015). The second data set included dynamically downscaled projections from the North American Coordinated Regional Climate Downscaling Experiment (NA-CORDEX), produced with Regional Climate Models (RCM) driven with GCM outputs as boundary conditions. Both datasets used GCM simulations from CMIP5 for 2 RCPs (4.5 and 8.5) as base projections even though other RCPs were available.

Climate projections for the update were bias corrected using the Quantile Delta Map-

ping approach, ensuring results can be easily compared with existing IDFs derived from observation (specifically, daily station data from the Adjusted and Homogenized Canadian Climate Data (AHCCD) and the updated IDFs currently used in the province). The entire database included ten combinations of GCM/RCM from NA-CORDEX and twelve from PCIC for both RCPs in two time slices, 2041-2070 and 2071-2100. Climate projections in the database were available at daily time steps. To obtain the Gumbel distribution for the sub-daily time steps required for IDF construction, non-linear transfer functions were fitted between the observed annual maximum data and simulated annual maximum data from the climate models (Srivastav et al., 2014). The transfer functions were optimized using a differential evolution algorithm (Storn & Price, 1997) to minimize the differences between the observation and climate model outputs (Finnis & Daraio, 2018). This resulted in an ensemble of rainfall depths for all required durations. To develop the IDF curves from the projections, the data were fitted with parameters of the Gumbel distribution. (See Finnis and Daraio (2018) for full details of the report). Results reported the median rainfall from the projection ensemble, along with the 10th and 90th percentiles. Table3.1 shows the period of data used for the construction of the current IDF curves.

3.2.3.3   Infiltration Methods

Three infiltration models were used: Green and Ampt (G&A), SCS Curve Number (CN) and Initial & Constant (IC). These (G&A and CN) are the most commonly used infiltration methods for engineering design applications (Chin, 2013) due to their simplicity and represent the two major classes of infiltration models: physically based (G&A) and empirical (CN and IC). Green and Ampt's physical basis is dependent on soil texture classes and their properties such as the hydraulic conductivity, moisture content and wetting front. Curve number is a function of land cover, including soils and previous moisture content. The IC infiltration method estimates infiltration from an initial loss volume and a constant loss

thereafter and is a function of soil type. The calibrated hydrologic models were setup using CN as infiltration method. All values used in the study were obtained from the provincial website `https://www.gov.nl.ca/ecc/waterres/flooding/frm/`. The parameters for G&A and IC infiltration methods were obtained from the Canadian Soil Information Services where soil maps for the various watersheds were identified. Typically, the soil parameters are given as ranges. To be certain of which value to use, these infiltration methods were calibrated using the hydrograph from the calibrated CN model. The infiltration methods used, parameters and values of each method for a sub-basin in the Corner Brook basin is provided in Table 3.3 as an example. To ensure the hydrologic models' setup with the GA and IC loss methods produce good results, the flows from these models were checked against the statistically estimated flows and that from the hydrologic model with the CN loss method. Since the chnage in peak discharge was the focus of the study, calibration was done to minimize the percent error on the runoff volume. This was measured using the Nash–Sutcliffe efficiency (NSE) metric (Table 3.4).

Table 3.3: An example of infiltration methods, their parameters and values for a sub-basin in Corner Brook

Infiltration method	Parameters	Values
Initial and Constant	Initial abstraction (mm)	4.008
	Constant rate mm/hr)	2.000
SCS Curve Number	Initial abstraction (mm)	4.000
	Curve number	82.880
Green and Ampt	Initial content	0.296
	Saturated content	0.479
	Suction (mm)	292.200
	Hydraulic conductivity (mm/hr)	2.000

3.2.4 Simulations of Peak Discharges

Peak discharge rates (QP) from the simulations for each watershed were estimated using the rainfall depths from the current IDF curves for both return periods. To allow for com-

Table 3.4: NSE values for hydrologic models using different loss method

Watershed	CN	GA	IC
Corner Brook	0.85	0.67	0.75
Petries Brook	0.73	0.79	0.85
Goulds	0.81	0.78	0.73
Coaker's River	0.9	0.68	0.67
Druken's River	0.8	0.66	0.70
Kennedy's River	0.88	0.69	0.67
Outer Cove Brook	0.91	0.73	0.69
Beachy Cove	0.79	0.83	0.80
Broad Cove	0.84	0.76	0.74
Goat Cove	0.86	0.75	0.79
Main River	0.79	0.81	0.68
Stephenville	0.89	0.77	0.8
Black Duck Siding	0.84	0.88	0.89
Waterford	0.82	0.79	0.80

parisons within and across basins, a peak discharge ratio, QPR was estimated using

$$QPR_{i,j,k,l} = \frac{QP_{i,j,k,l}}{QP_{i,j,CN,ALT}} \tag{3.3}$$

where i is the watershed, j is the return period, k is the loss method and l is the temporal distribution. The normalizing $QP_{i,j,CN,ALT}$ in Equation 3.3 represents the runoff volume from the CN model in combination with the Alternating block temporal distribution. This is applied for each of the return periods. The choice of this combination as the baseline is because the CN model and the Alternating block temporal distribution are the loss method and temporal distribution used by the province to develop the calibrated models

3.2.4.1 Climate Projections

The QP obtained using rainfall depths from the two RCPs and time slices were converted to ratios using

$$QPR_{f,i,j,k,l} = \frac{QP_{f,i,j,k,l}}{QP_{i,j,k,l}} \tag{3.4}$$

where f indicated the projected peak ratio associated with a future RCP and time slice relative to QP from historical climate conditions. Equation 3.4 was applied to the median, 10th and 90th percentiles. The estimate of the uncertainty in projections uses the QPR from the percentiles. Under climate projection scenarios, all other factors were kept constant except for the projected rainfall depth. It is possible that population and development may change in the basins. However, knowledge of the direction of change, either increase or decrease, is uncertain. In a situation with an increase in population growth and commensurate development in a basin, there will be an increase in impervious surfaces, resulting in increased runoff independent of the increase in rainfall depth/intensity with climate change.

3.2.4.2 Uncertainty on Future Rainfall Depths

To estimate the uncertainty on the median rainfall depths, rainfall depths from the 10th and 90th percentiles of the projected IDF curves were used in the HMS model to estimate peak discharges. The peak discharges from both percentiles were converted to percentage change from the current peak discharge using

$$\%change = \frac{QP_{px} - QP_c}{QP_c} * 100 \tag{3.5}$$

where QP_{px} is the peak discharge from a percentile rainfall depth, QP_c is the peak discharge of rainfall depths from historical climate. The uncertainty was estimated from the range of the percent change in peak discharge based on equation 3.5

$$UC(\%) = QP_{p90}(\%) - QP_{p10}(\%) \tag{3.6}$$

where UC is the estimated range between QP_{p90} and QP_{p10}, which are the percentage changes from the 90th and 10th percentile rainfall depths, respectively.

3.2.4.3 Procedure for Model Setup

For each watershed, a total of 18 simulations (three temporal patterns, three infiltration methods and two return periods) were run to estimate *QPR* using Equation 3.3 representing current conditions, and 72 simulations (three temporal patterns, three loss methods, two return periods, two RCP scenarios, two future time slices) to estimate QPR_f from Equation 3.4. A flowchart of the model interactions, inputs and outputs is presented in Fig.3.5.
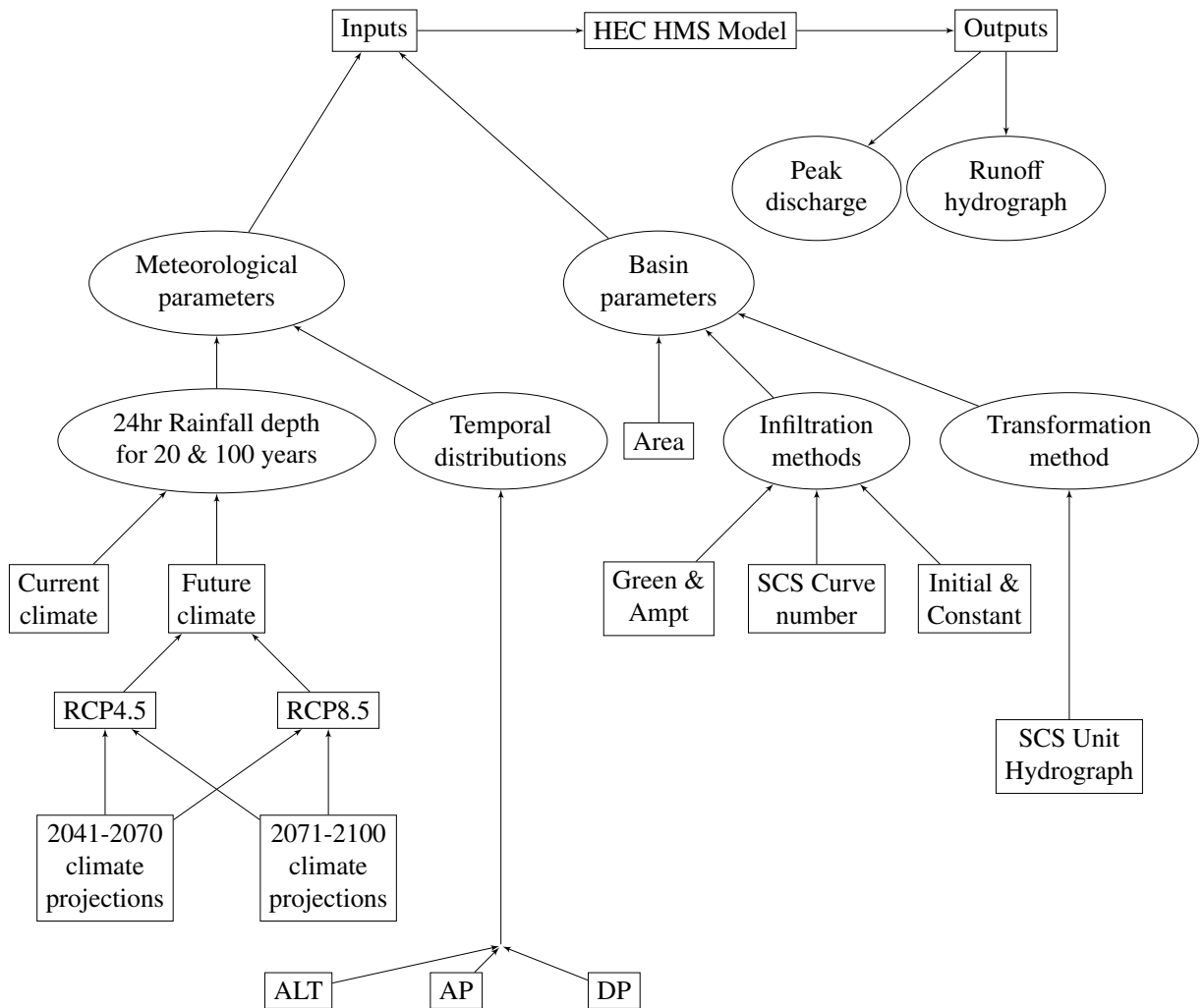
Figure 3.5: Schematic of HEC-HMS simulation setup for each watershed

3.2.5 Floodplain Mapping

Hydrologic Engineering Center's River Analysis System (HEC-RAS) version 5, combined with GIS data, was used to transform runoff from the hydrologic model into maps identifying the areal extent of flood inundation. HEC-RAS is a 1-dimensional hydraulic model that analyzes flows in both steady and unsteady states. The steady state was assumed and used for simulation as the flows within the channels in the study watersheds change gradually with time. In this state and at predefined cross-sections, the model computes velocity and water surface profiles by solving Manning's energy and continuity equations. Data requirements to set up the model include topographic data, the geometry of cross-sections in the channel under study, channel conveyance data and flow data, usually from a hydrologic model. The water surface elevations from the HEC-RAS model were transformed into flood inundation maps when combined with digital elevation data. Such maps were produced in this study using the hydrologic output from all three temporal distributions. Similar to the hydrologic models, the province developed the HEC-RAS models for the watersheds used in this study. Some of the reports indicate making manual edits to the flood inundation areas. However, no modifications were made for this study since the goal is more on the comparative side than setting the exact extents. Flood risk maps are developed for some of the watersheds within the study region as digital elevation models were not available for some of the watersheds. Full details of the HEC-RAS model setup and the models can be found on `https://www.gov.nl.ca/eccm/waterres/flooding/frm/`. Figure 3.6 shows the plan view of the Black Duck Siding HEC-RAS model. Plan views of all HEC-RAS models are presented in Appendix A.
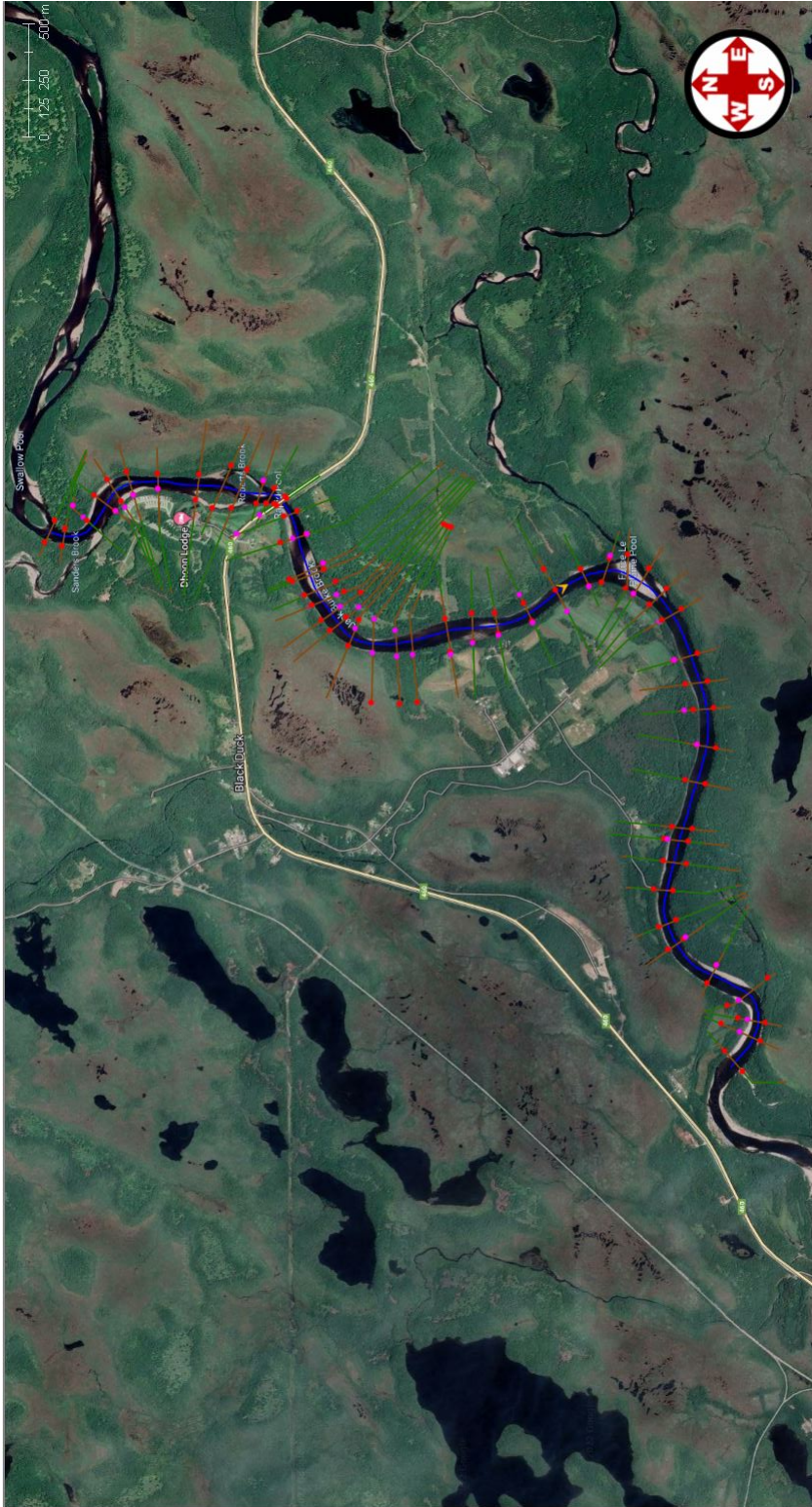
Figure 3.6: Plan View of Black Duck Siding HEC-RAS model with cross sections indicated by red lines

3.3 Results

Watersheds in the WMCU and WC climate zones displayed similar behaviours under all climate conditions. Applying the Alternating block pattern across different infiltration methods revealed vast differences in watersheds within the SCA climate zone. Though rainfall projections for the RCP4.5 2071-2100 time slice would decrease, this decrease is not commensurate with decreasing peak discharges across all climate zones.

3.3.1 Peak Discharges

3.3.1.1 Historical Climate Cata

Most watersheds produce peaks greater than the baseline with IC than GA under the Alternating block pattern for the smaller events (Figure 3.7). Under the Advanced pattern, most of the peaks are lesser than the baseline, with the most significant difference occurring under the G&A and the least under the CN infiltration methods. The anomaly in this trend occurred in the Logy Bay watersheds, where peak discharges were comparable to or greater than the baseline. Comparing different rainfall distributions under the same infiltration method (Figure 3.8), the Alternating block pattern tends to produce greater peaks than the baseline, irrespective of the infiltration method used. This is followed by the Delayed pattern and then the Advanced pattern. As mentioned earlier, the anomaly to this trend occurred in the Logy Bay watersheds and the Waterford watershed. As the return period increases, the direction of peak discharge for different infiltration methods under the same rainfall distribution (Figure 3.9) and for different rainfall distributions under the same infiltration method (Figure 3.10) was similar to that which occurred for the smaller events.
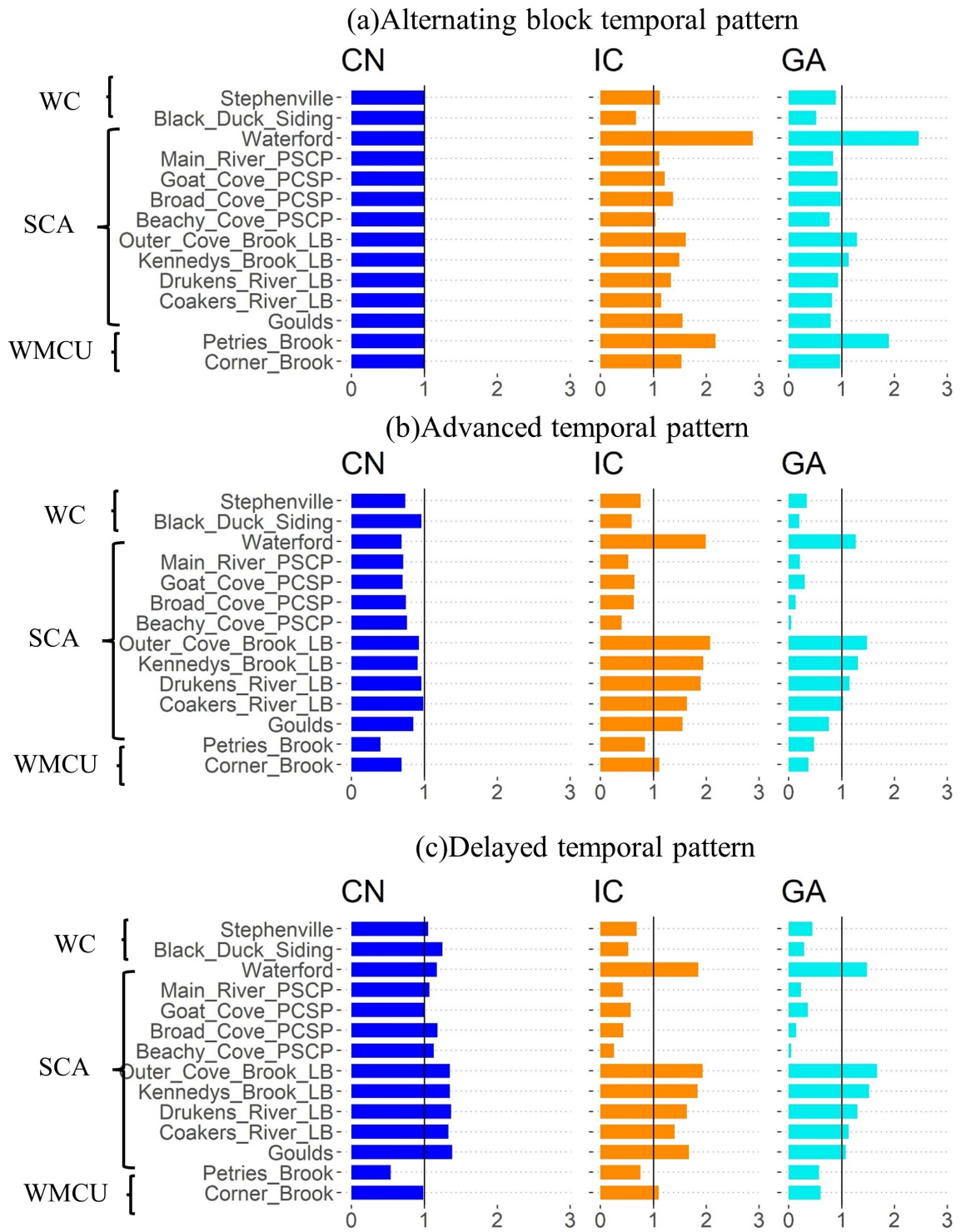
Figure 3.7: Ratio of peak discharge for Curve Number (CN), Initial & Constant (IC) and Green & Ampt (GA) infiltration methods under a rainfall distribution to the baseline (Alternating block temporal pattern and CN; vertical black line) under historical climate data for the 20-year return period [Climate zones: WC-West Coast; SCA-South Coast & Avalon; WMCU-Western Mountain & Central Uplands]
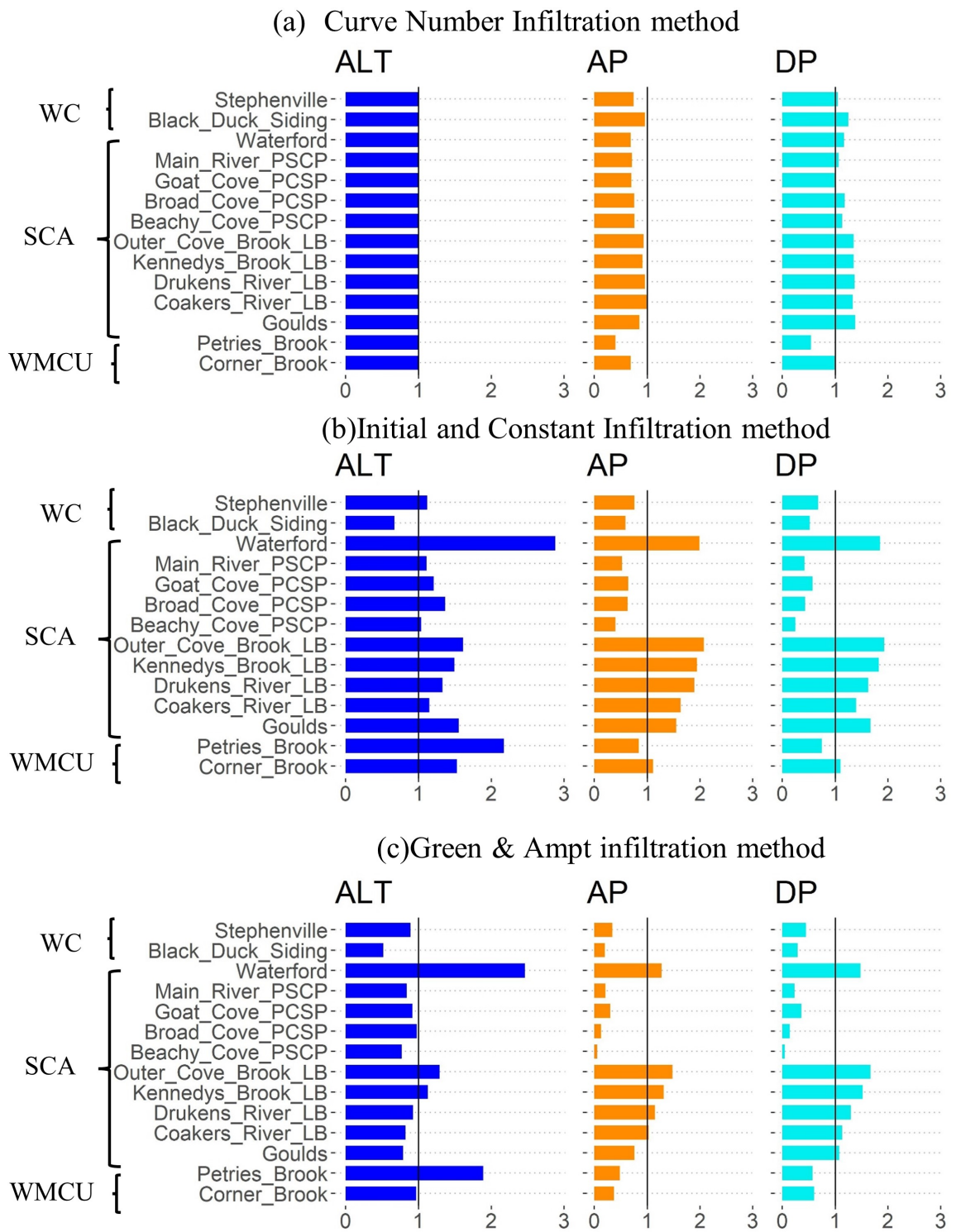
Figure 3.8: Ratio of peak discharge for Alternating block (ALT), Advanced (AP) and Delayed (DP) temporal patterns under an infiltration method to the baseline (Alternating block temporal pattern and CN; vertical black line) under historical climate data for the 20-year return period [Climate zones: WC-West Coast; SCA-South Coast & Avalon; WMCU-Western Mountain & Central Uplands]
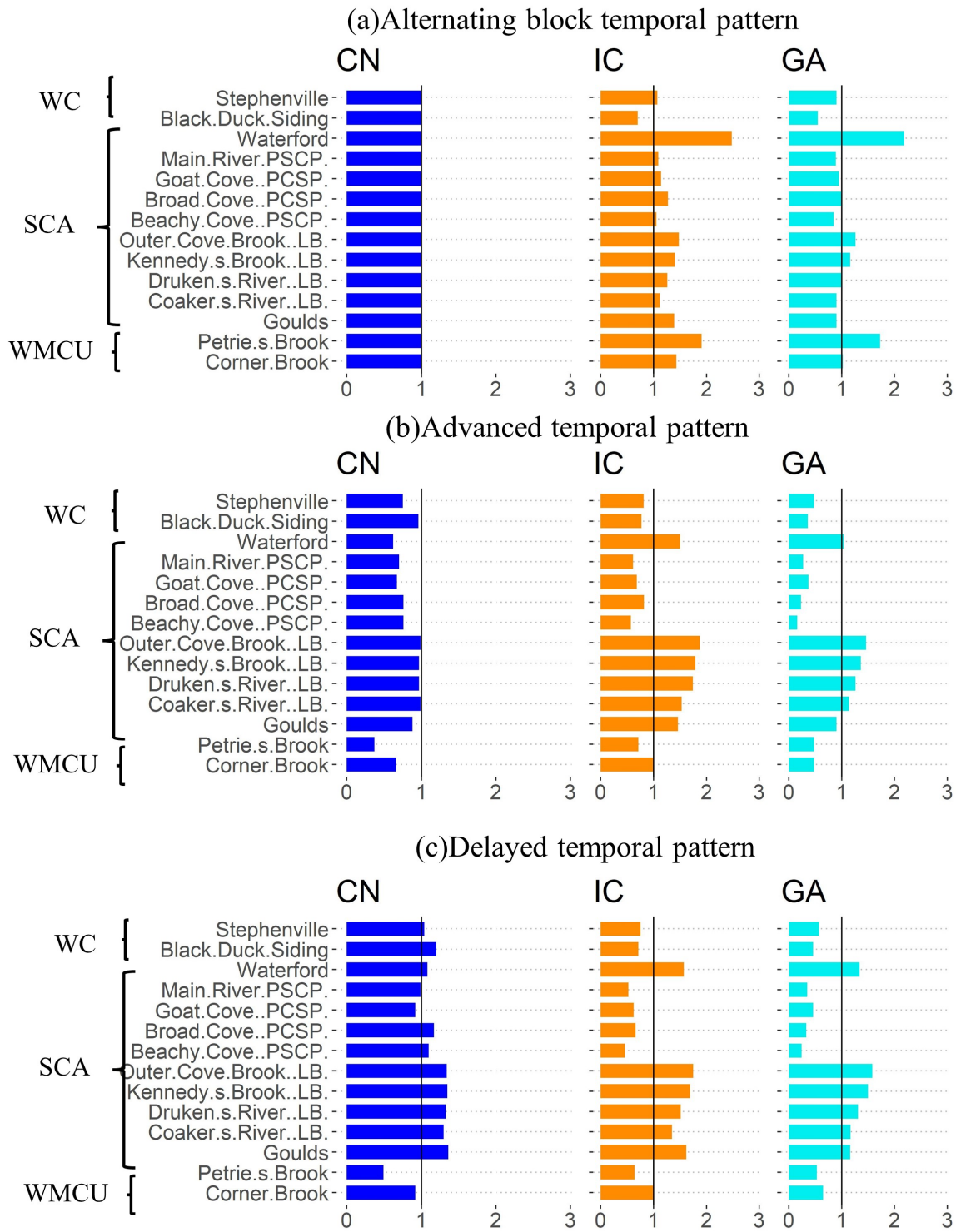
Figure 3.9: Ratio of peak discharge for Curve Number (CN), Initial & Constant (IC) and Green & Ampt (GA) infiltration methods under a rainfall distribution to the baseline (Alternating block temporal pattern and CN; vertical black line) under historical climate data for the 100-year return period [Climate zones: WC-West Coast; SCA-South Coast & Avalon; WMCU-Western Mountain & Central Uplands]
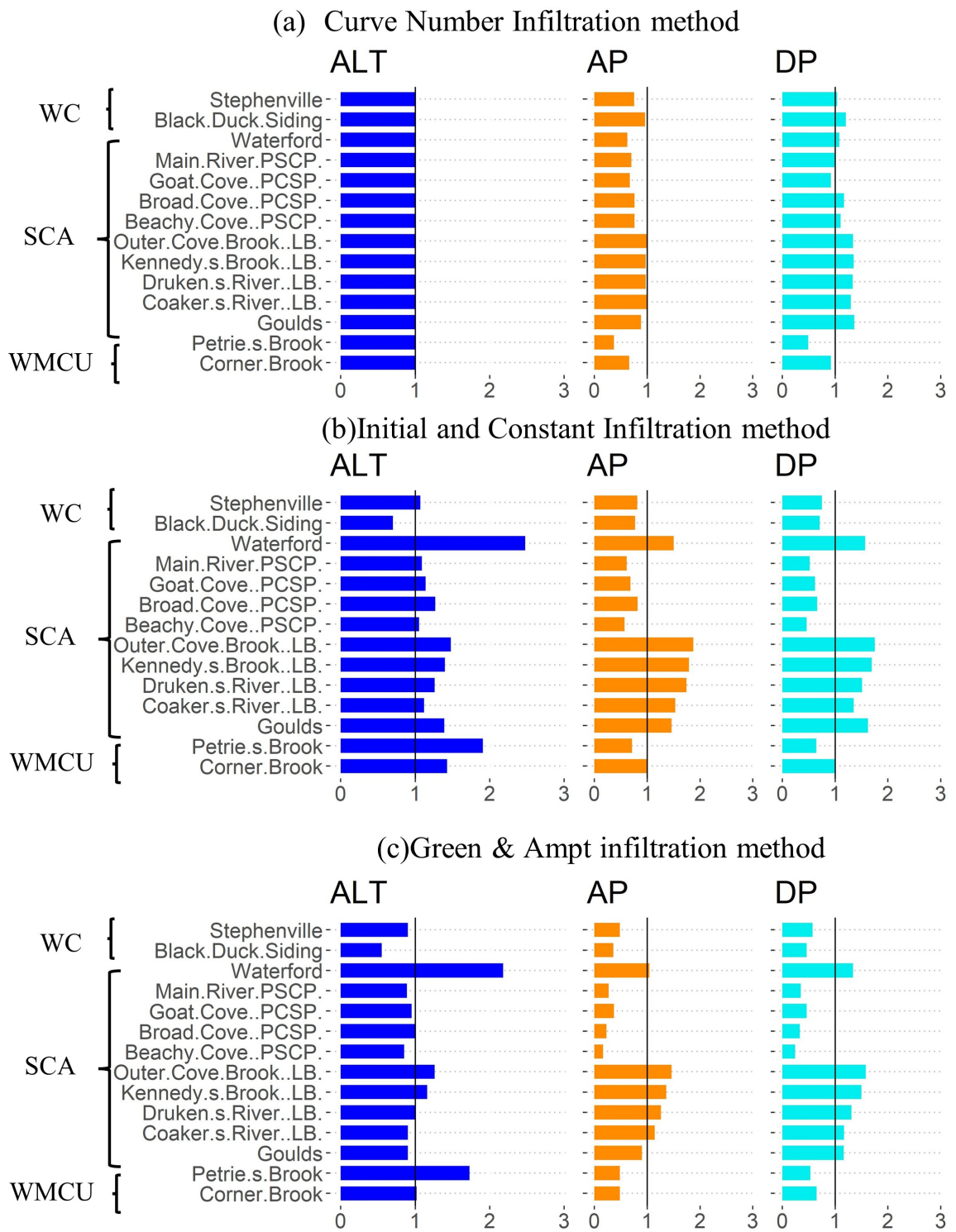
Figure 3.10: Ratio of peak discharge for Alternating block (ALT), Advanced (AP) and Delayed (DP) temporal patterns under an infiltration method to the baseline (Alternating block temporal pattern and CN; vertical black line) under historical climate data for the 100-year return period [Climate zones: WC-West Coast; SCA-South Coast & Avalon; WMCU-Western Mountain & Central Uplands]

112

3.3.1.2 Climate Change Projections

Peak discharges were projected to increase under both RCPs (Figs 3.11-3.22). These figures show a percentage change (equation 3.5) relative to the peak discharges from the historical climate and are not the actual discharge values. As expected, increases were greater for the 2071-2100 time slice than the 2041-2070 time slice, and increases were greater under RCP8.5 for the latter than RCP4.5.

An interesting trend emerges where watersheds in the Western Mountain and Central Uplands (WMCU) and West Coast (WC) climate zones show increases in peak discharge across all infiltration methods irrespective of the rainfall distribution used for the 2041-2070 and 2071-2100 time slices under RCP4.5 for the 20-year return period (Figure 3.11-3.13). Under the same conditions, all watersheds in the South Coast and Avalon (SCA) climate zone show increases in peak discharge for the 2041-2070 time slice and decreases for 2071-2100 relative to the 2041-2070 time slice. An exception occurs for the watersheds in the PCSP region, where all four behave contrary to the other SCA watersheds. These four watersheds show increases in peak discharge for the 2071-2100 time slice but only for the IC infiltration method and under the Alternating block pattern.

As the return period increases, this clear-cut trend is explicitly lost for the 2071-2100 time slice under the Alternating block pattern (Figure 3.14). Peak discharges for half of the watersheds in the WMCU and WC climate zone increased while the other half decreased. A mix of trends occurred in the SCA climate zone. 40% of the watersheds showed decreases, and 20% showed increases in peak discharge. For the remaining 40%, another trend emerges where increases in peak discharge occurred for the ic and G&A infiltration methods and decreases for the CN infiltration method. For the AP and DP, a more stable trend exists (Figures 3.15 and 3.16). Similar to the Alternating block pattern, half of the WMCU and WC climate zone watersheds showed increases in peak discharges while the other half showed decreases. Within the SCA climate zone, 80% of the watersheds showed

113

decreases, with the rest showing increases. Peak discharges within a watershed did not vary by infiltration methods, as was the case under the Alternating block pattern.
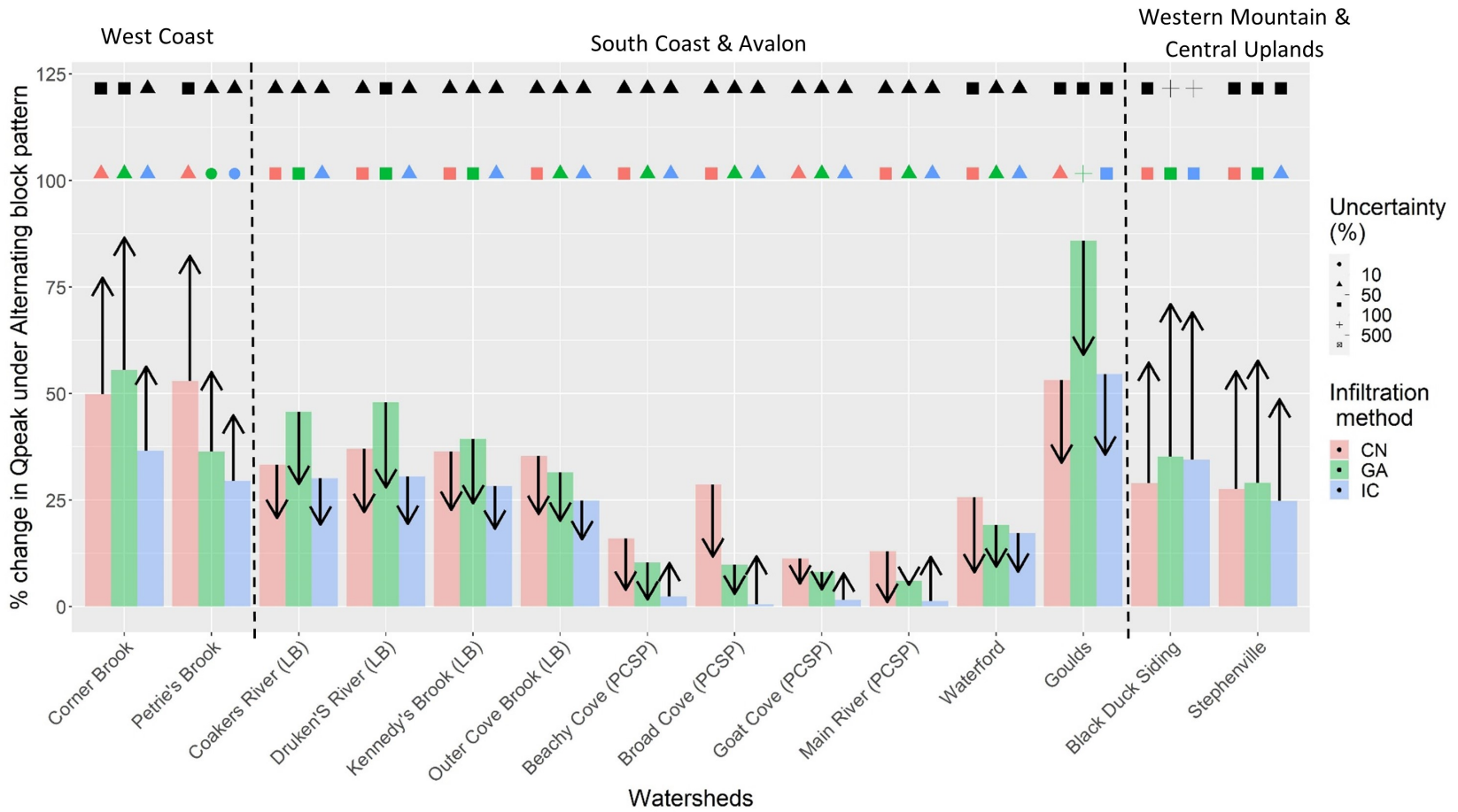
Figure 3.11: Percentage change in peak discharge (20-year) under RCP4.5 for different infiltration methods using the Alternating block temporal pattern. Colored bars represent change for the 2041-2070 time slice. Arrows represent change for the 2071-2100 time slice from the baseline. Colored and black shapes show uncertainty for 2041-2070 and 2071- 2100 time slices respectively.
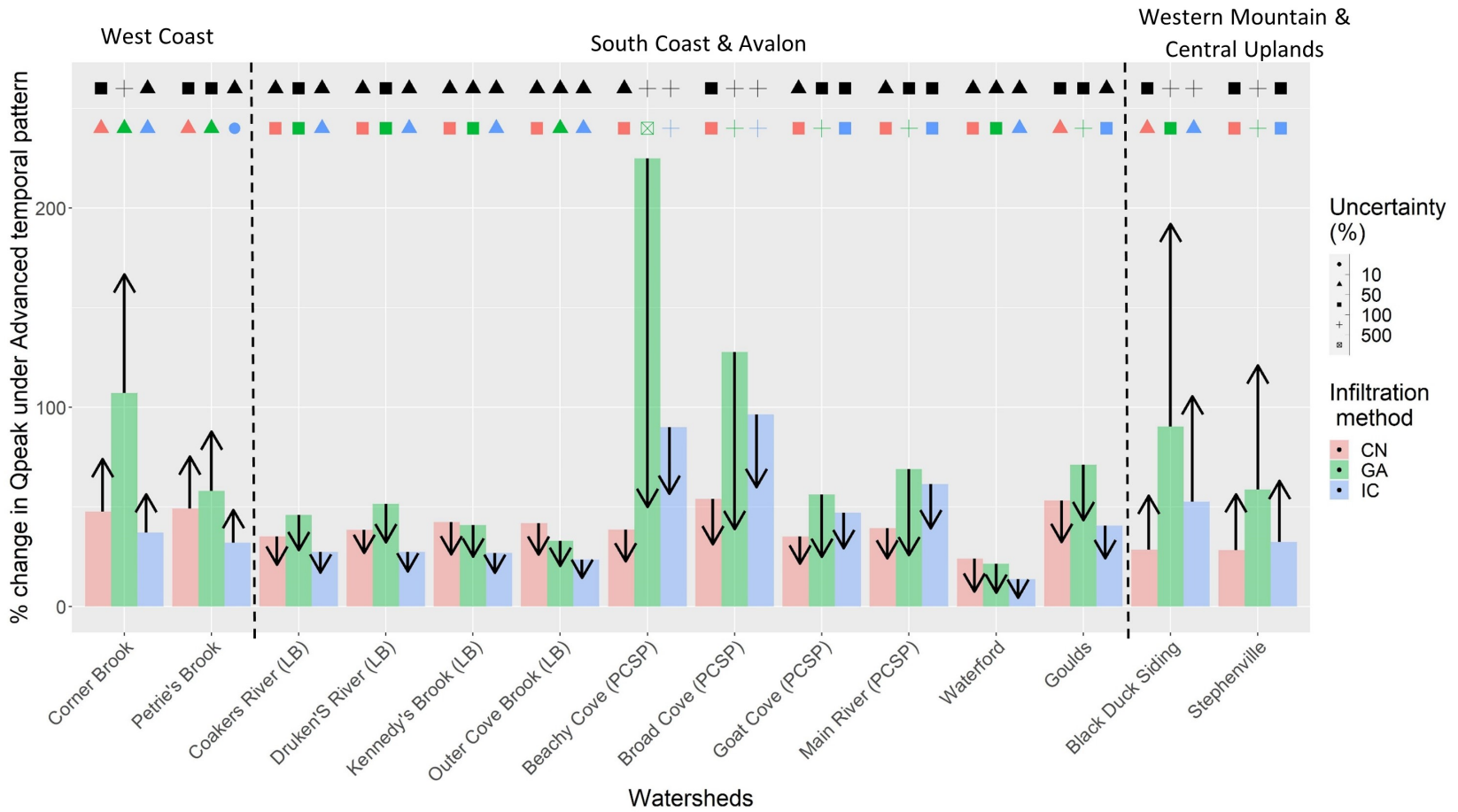
Figure 3.12: Percentage change in peak discharge (20-year) under RCP4.5 for different infiltration methods using the Advanced temporal pattern. Colored bars represent change for the 2041-2070 time slice. Arrows represent change for the 2071-2100 time slice from the baseline. Colored and black shapes show uncertainty for 2041-2070 and 2071- 2100 time slices respectively.
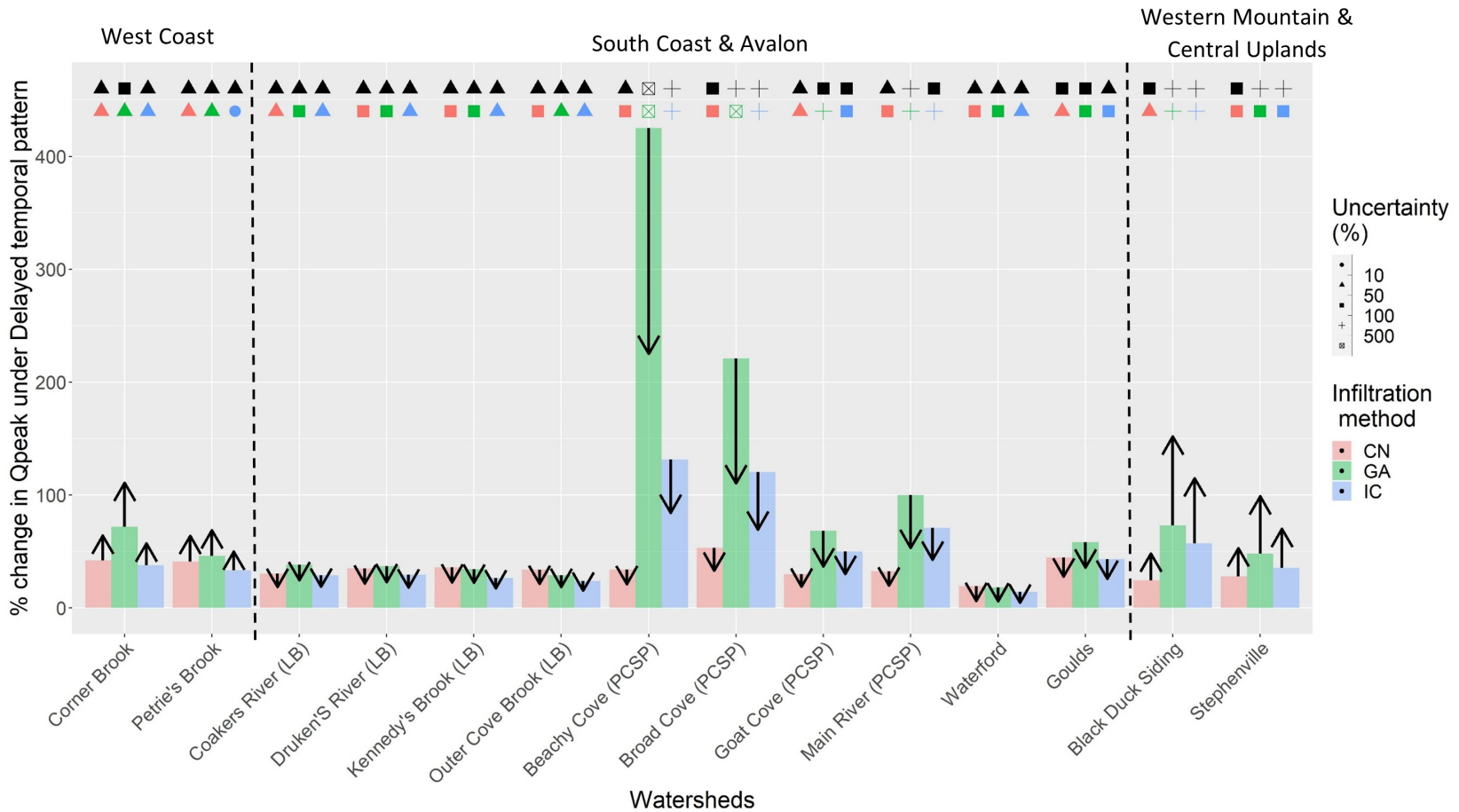
Figure 3.13: Percentage change in peak discharge (20-year) under RCP4.5 for different infiltration methods using the Delayed temporal pattern. Colored bars represent change for the 2041-2070 time slice. Arrows represent change for the 2071-2100 time slice from the baseline. Colored and black shapes show uncertainty for 2041-2070 and 2071- 2100 time slices respectively.
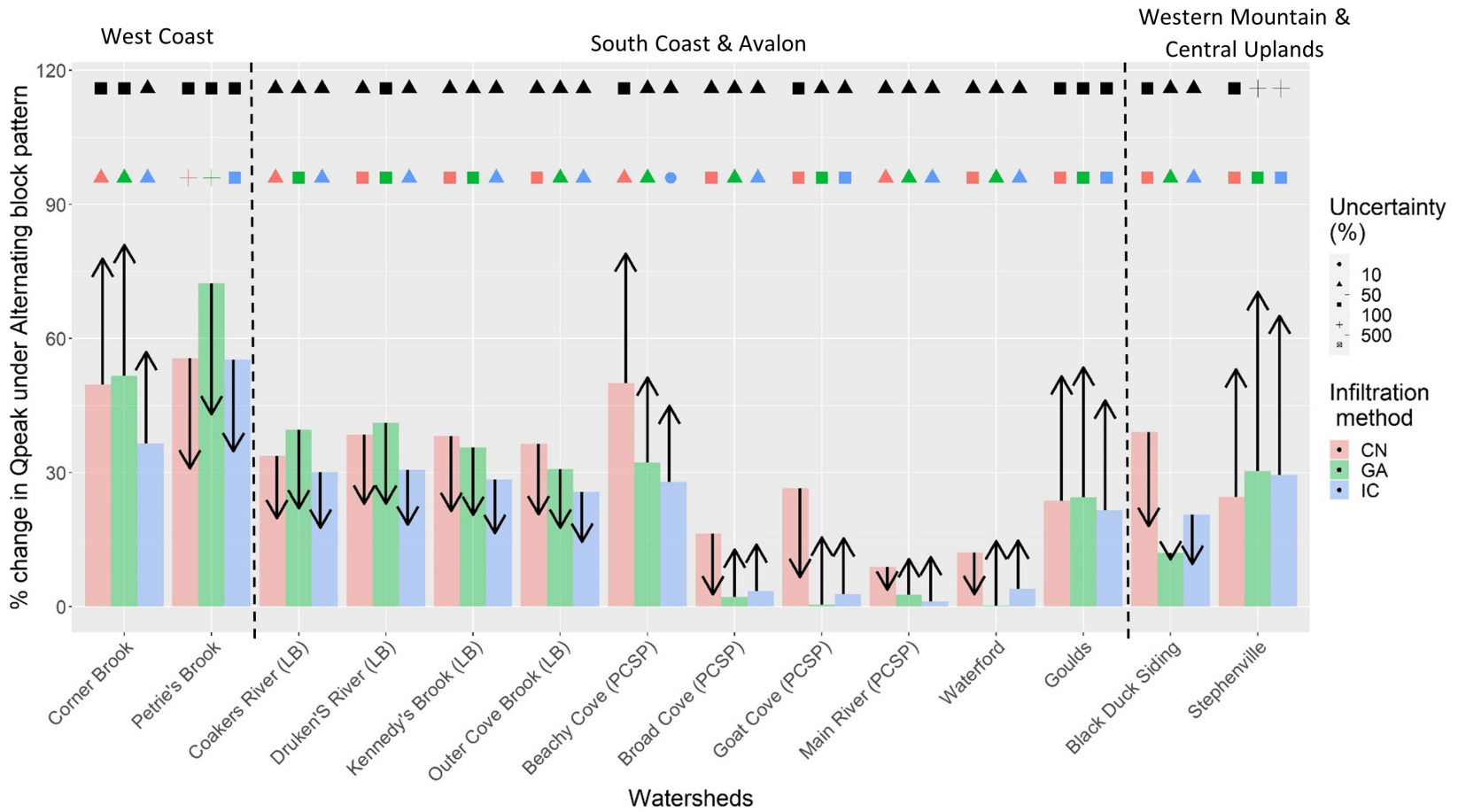
Figure 3.14: Percentage change in peak discharge (100-year) under RCP4.5 for different infiltration methods using the Alternating block temporal pattern. Colored bars represent change for the 2041-2070 time slice. Arrows represent change for the 2071-2100 time slice from the baseline. Colored and black shapes show uncertainty for 2041-2070 and 2071- 2100 time slices respectively.
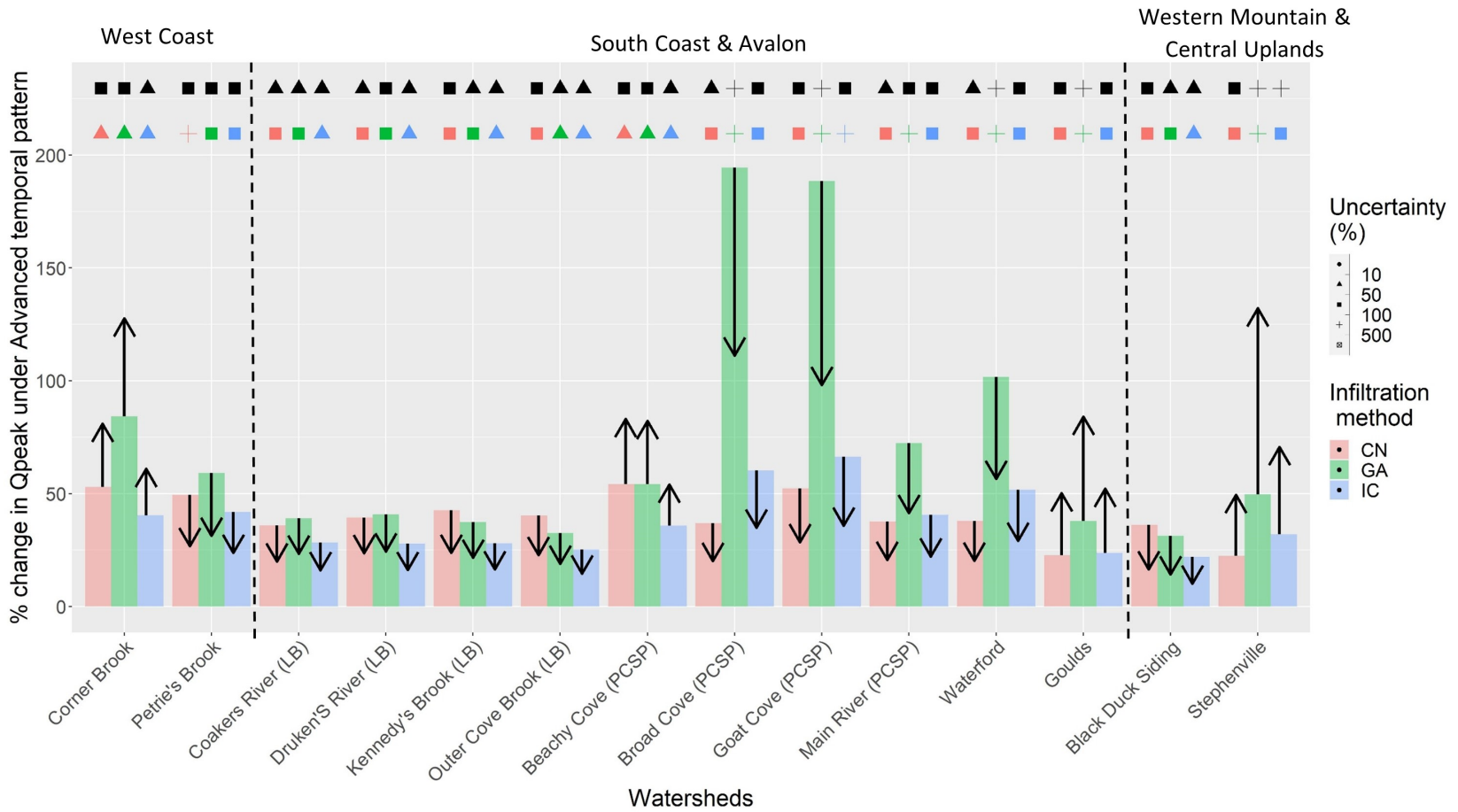
Figure 3.15: Percentage change in peak discharge (100-year) under RCP4.5 for different infiltration methods using the Advanced temporal pattern. Colored bars represent change for the 2041-2070 time slice. Arrows represent change for the 2071-2100 time slice from the baseline. Colored and black shapes show uncertainty for 2041-2070 and 2071- 2100 time slices respectively.
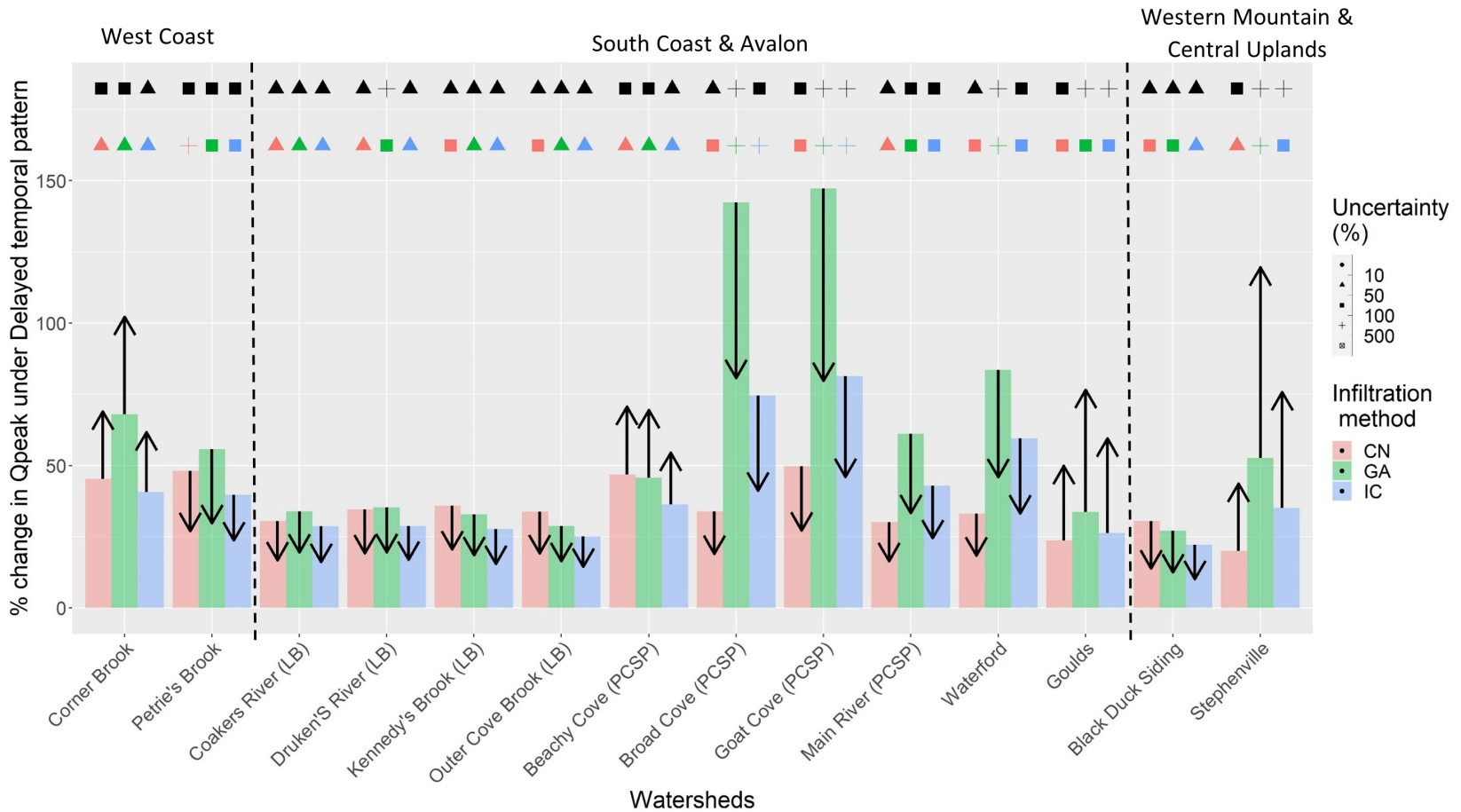
Figure 3.16: Percentage change in peak discharge (100-year) under RCP4.5 for different infiltration methods using the Delayed temporal pattern. Colored bars represent change for the 2041-2070 time slice. Arrows represent change for the 2071-2100 time slice from the baseline. Colored and black shapes show uncertainty for 2041-2070 and 2071- 2100 time slices respectively.

Under RCP8.5, there were increases in peak discharge observed in all climate zones for all infiltration methods and rainfall distributions for both time slices (2041-2070 and 2071-2100) and return periods (20-year and 100-year) (Figures 3.17-3.22). Watersheds in the PCSP region of the SCA climate zone displayed a step-like behaviour for the 20-year peak discharge where increases for CN were greatest, followed by G&A and IC under the Alternating block pattern. This behaviour was not replicated in the AP and DP, where the trend in the region was greatest for peak discharge under G&A, followed by IC and CN. The same behaviour is replicated under the 100-year peak discharges.

Uncertainty of the percentage increase in peak flows ranged from 8.5% to 550% under RCP4.5 and 12% to 475% under RCP8.5 (Figures 3.11-3.22). Simulations indicated that locations with greater ($\geq$75%) increase in peaks were associated with higher ($\geq$50%) uncertainties. Also, uncertainties in the 2071-2100 time slice were often greater than those in 2041-2070. For example, at Goulds, a percentage increase in peaks of 90% was associated with 56% and 87% uncertainty for the 2041-2070 and 2071-2100 periods under RCP8.5 with the IC infiltration method. Under RCP4.5, the uncertainty remained unchanged under the 2041-2070 time slice as 21% for CN, 9.5% for IC and 12% for G&A infiltration methods. For the 2071-2100 time slice, the unchanged uncertainties were 20% for CN, 2.3% for both IC and G&A infiltration methods. For RCP8.5, unchanged uncertainties percentages: 7% and 0% for CN, 23.8% and 11.9% for IC and 0% and 2.3% for G&A infiltration methods were identified for 2041-2070 and 2071-2100 time slices.
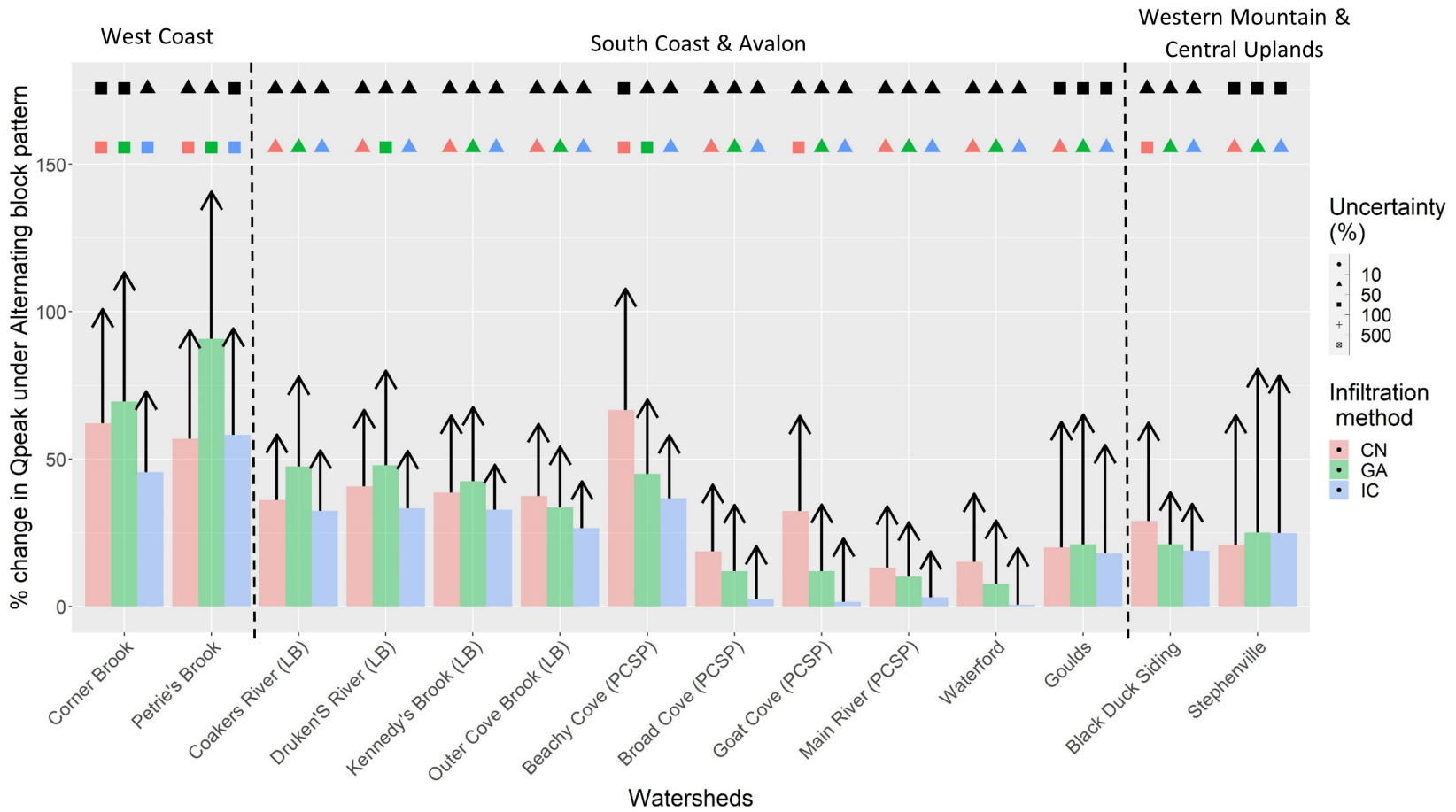
Figure 3.17: Percentage change in peak discharge (20-year) under RCP8.5 for different infiltration methods using the Alternating block temporal pattern. Colored bars represent change for the 2041-2070 time slice. Arrows represent change for the 2071-2100 time slice from the baseline. Colored and black shapes show uncertainty for 2041-2070 and 2071- 2100 time slices respectively.
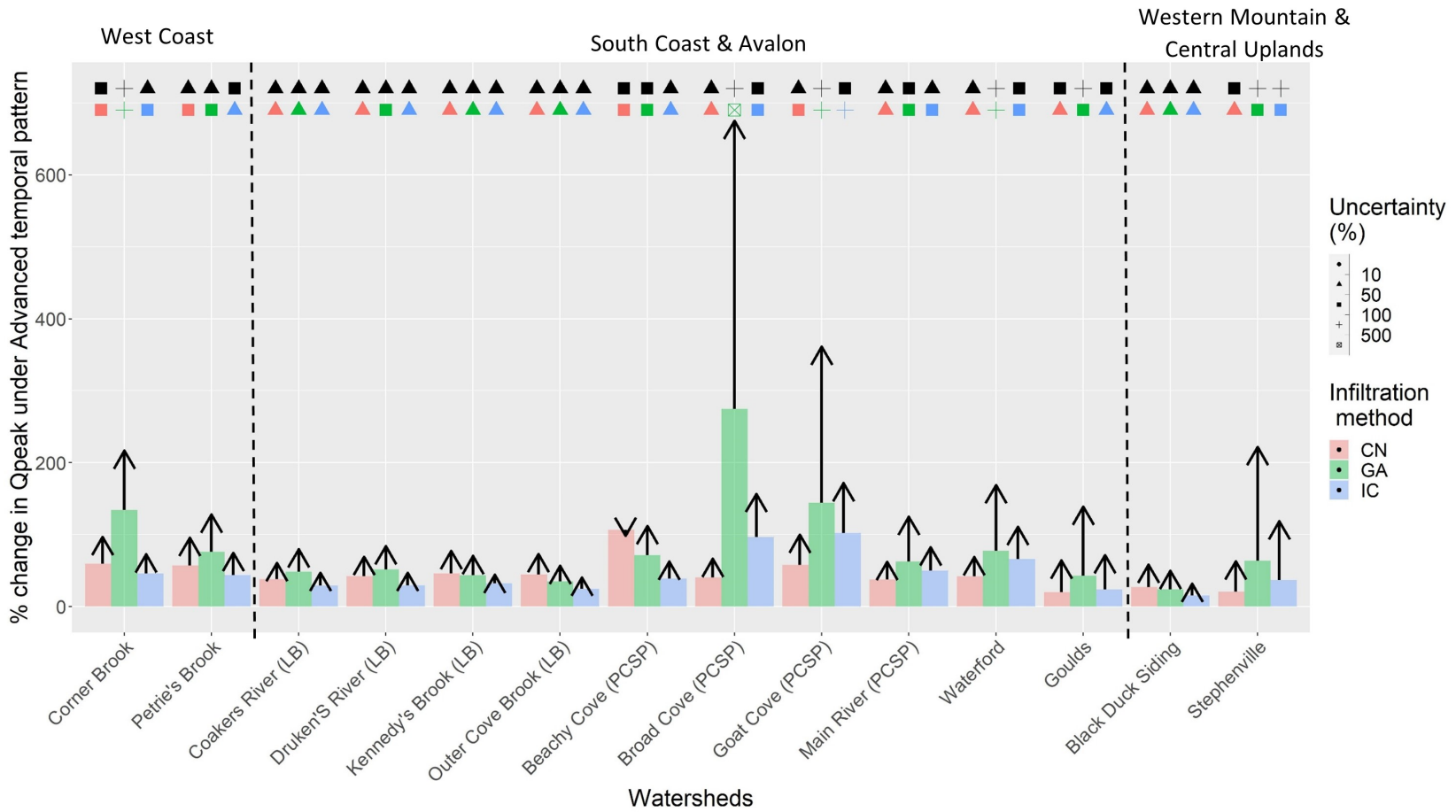
Figure 3.18: Percentage change in peak discharge (20-year) under RCP8.5 for different infiltration methods using the Advanced temporal pattern. Colored bars represent change for the 2041-2070 time slice. Arrows represent change for the 2071-2100 time slice from the baseline. Colored and black shapes show uncertainty for 2041-2070 and 2071- 2100 time slices respectively.
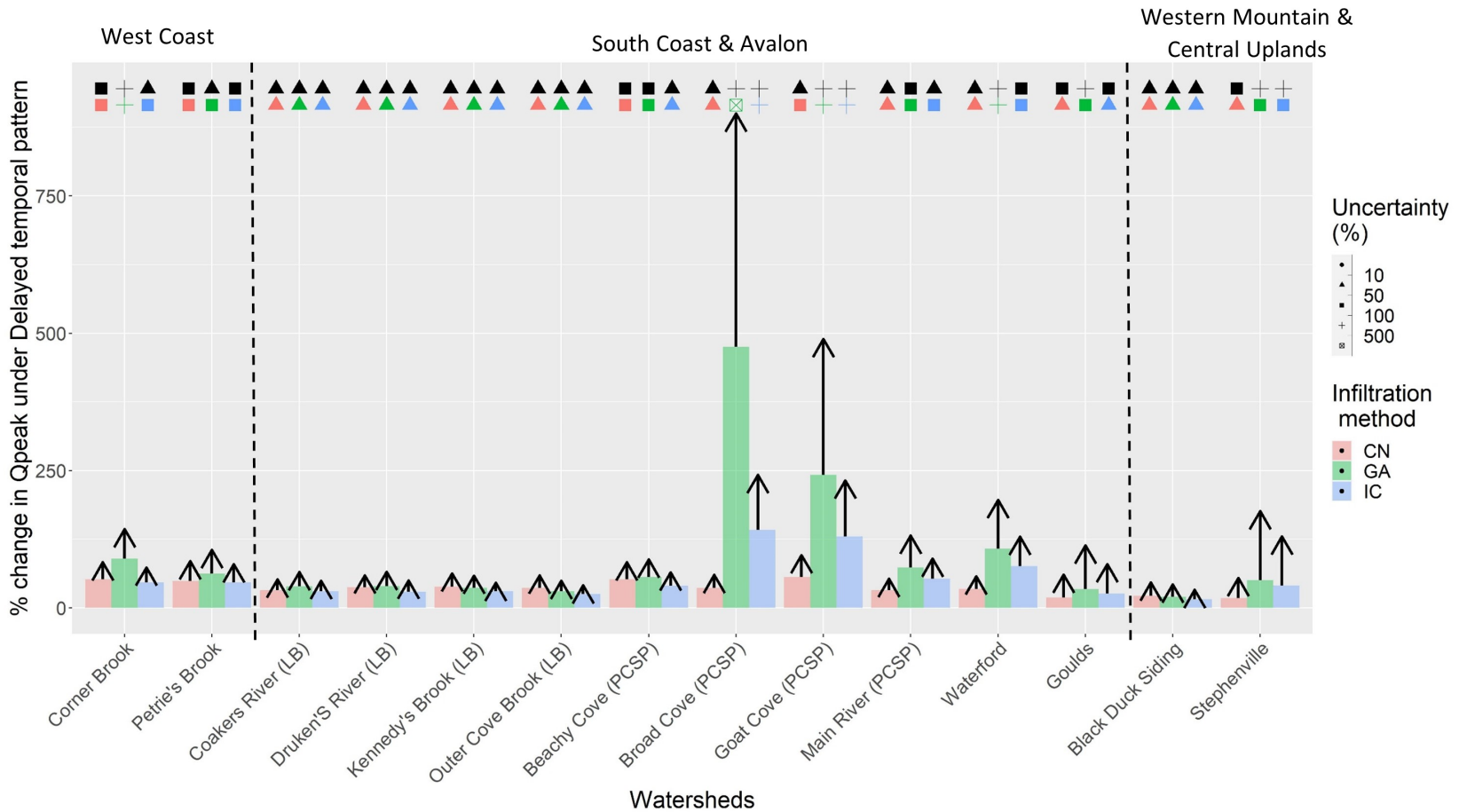
Figure 3.19: Percentage change in peak discharge (20-year) under RCP8.5 for different infiltration methods using the Delayed temporal pattern. Colored bars represent change for the 2041-2070 time slice. Arrows represent change for the 2071-2100 time slice from the baseline. Colored and black shapes show uncertainty for 2041-2070 and 2071- 2100 time slices respectively.
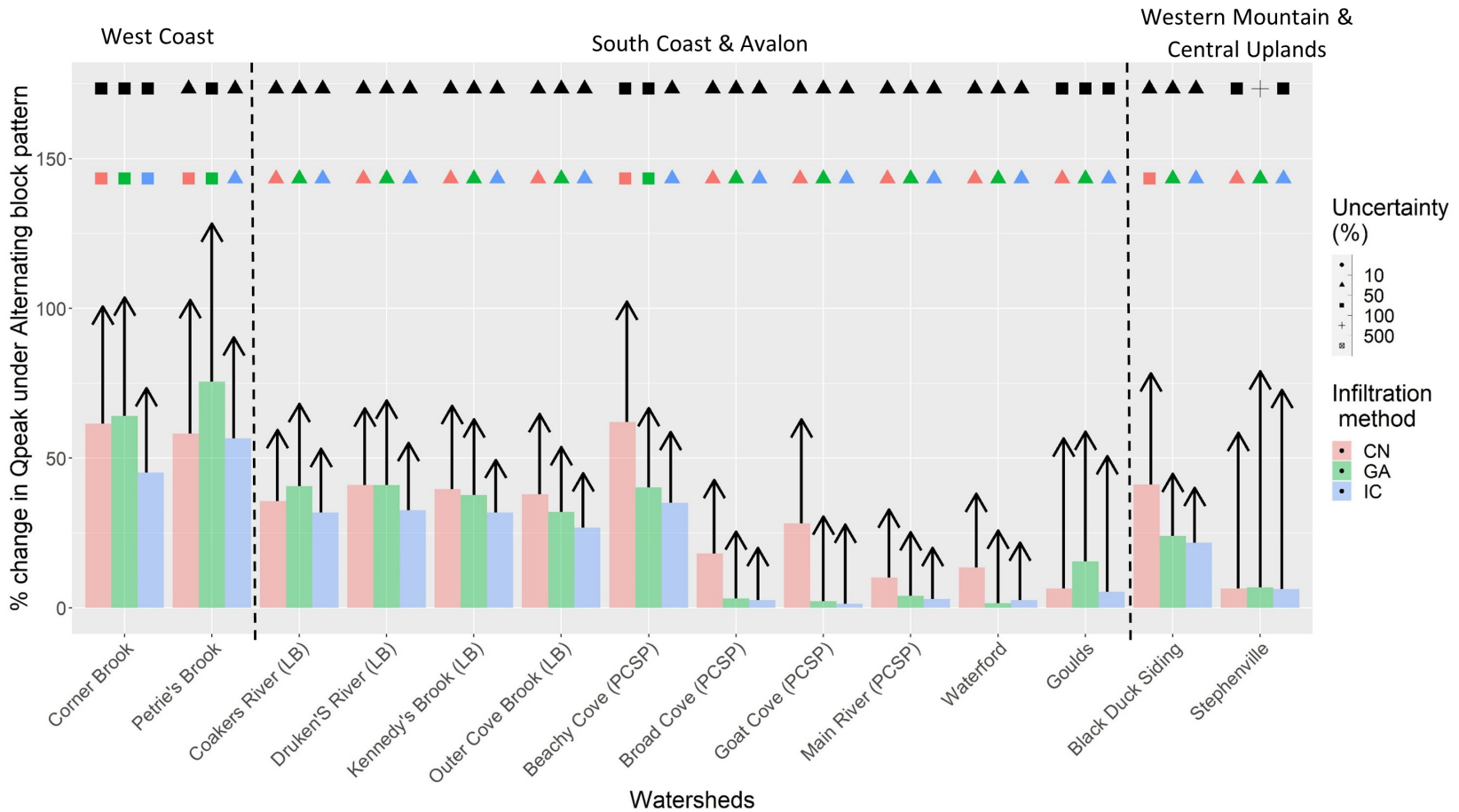
Figure 3.20: Percentage change in peak discharge (100-year) under RCP8.5 for different infiltration methods using the Alternating block temporal pattern. Colored bars represent change for the 2041-2070 time slice. Arrows represent change for the 2071-2100 time slice from the baseline. Colored and black shapes show uncertainty for 2041-2070 and 2071- 2100 time slices respectively.
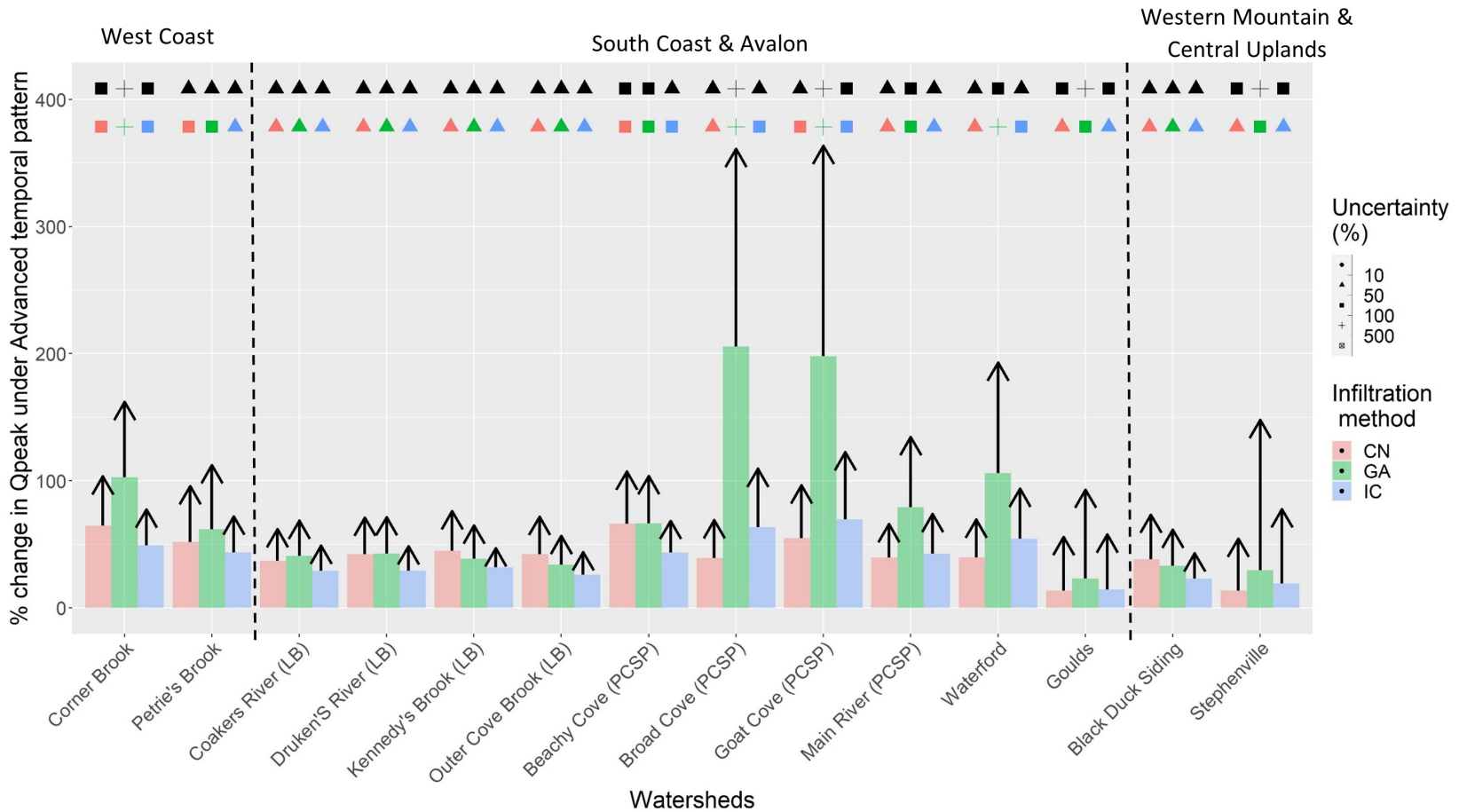
Figure 3.21: Percentage change in peak discharge (100-year) under RCP8.5 for different infiltration methods using the Advanced temporal pattern. Colored bars represent change for the 2041-2070 time slice. Arrows represent change for the 2071-2100 time slice from the baseline. Colored and black shapes show uncertainty for 2041-2070 and 2071- 2100 time slices respectively.
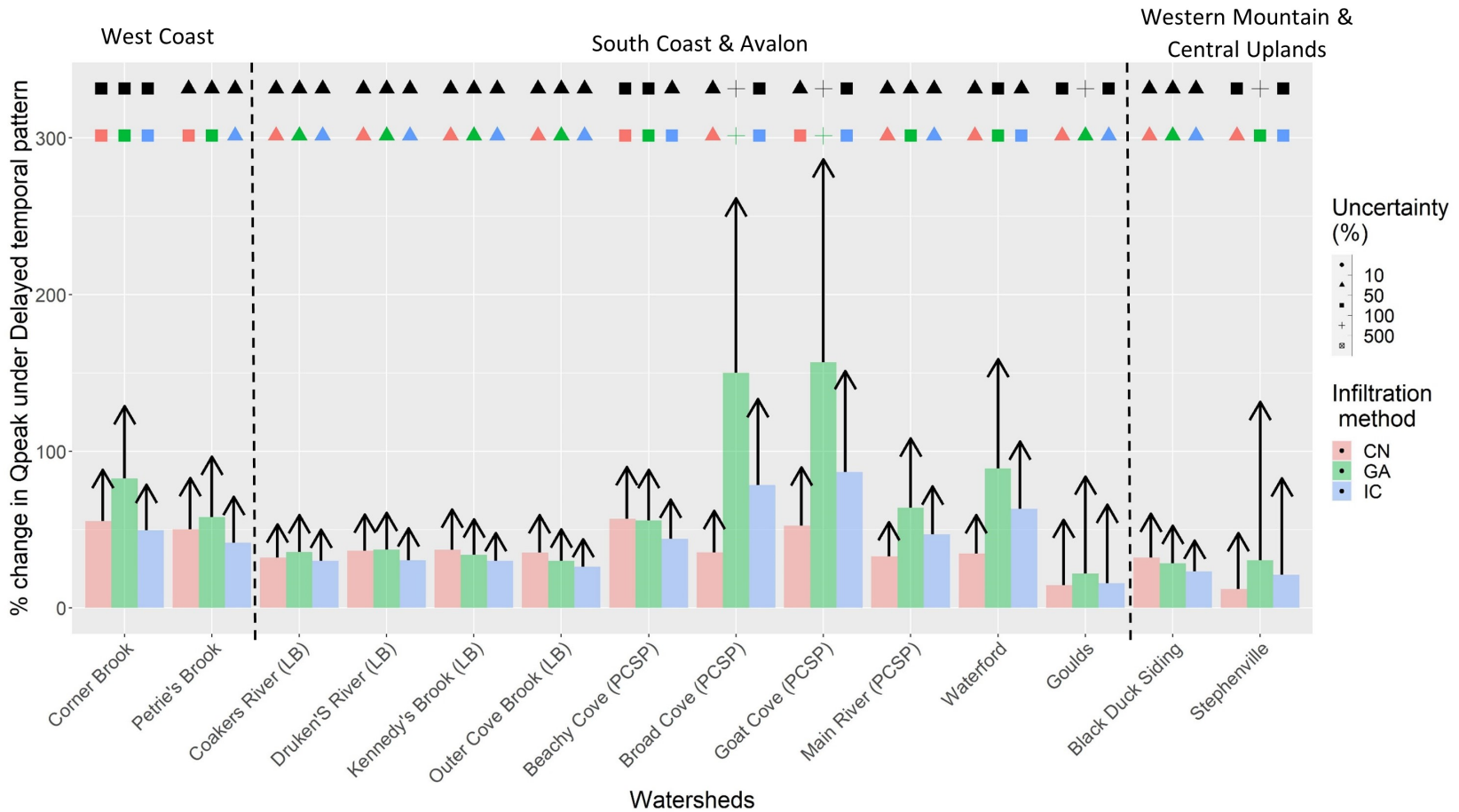
Figure 3.22: Percentage change in peak discharge (100-year) under RCP8.5 for different infiltration methods using the Delayed temporal pattern. Colored bars represent change for the 2041-2070 time slice. Arrows represent change for the 2071-2100 time slice from the baseline. Colored and black shapes show uncertainty for 2041-2070 and 2071- 2100 time slices respectively.

The rainfall amounts' uncertainty ranges were smaller than the uncertainties on the peak discharges (Figure 3.23). Rainfall amount uncertainties ranged from 7% to 56% for RCP4.5 and 15% to 44% for RCP8.5 There was a trend where locations with high uncertainty in peak discharges were associated with high uncertainty in rainfall amounts as well. For example, in Stephenville, a percentage change in peak charge with an associated uncertainty of 162% was also associated with a rainfall amount uncertainty of 56%. Uncertainty ranges on rainfall amounts were lower for the 20-year return period than the 100-year return period. The uncertainty of 1% on the rainfall amounts from the St. John's Airport station under the RCP4.5 2041-2070 time slice suggests that all the ensemble models used for IDF updates in the province tend to agree on the future direction of rainfall in this region.
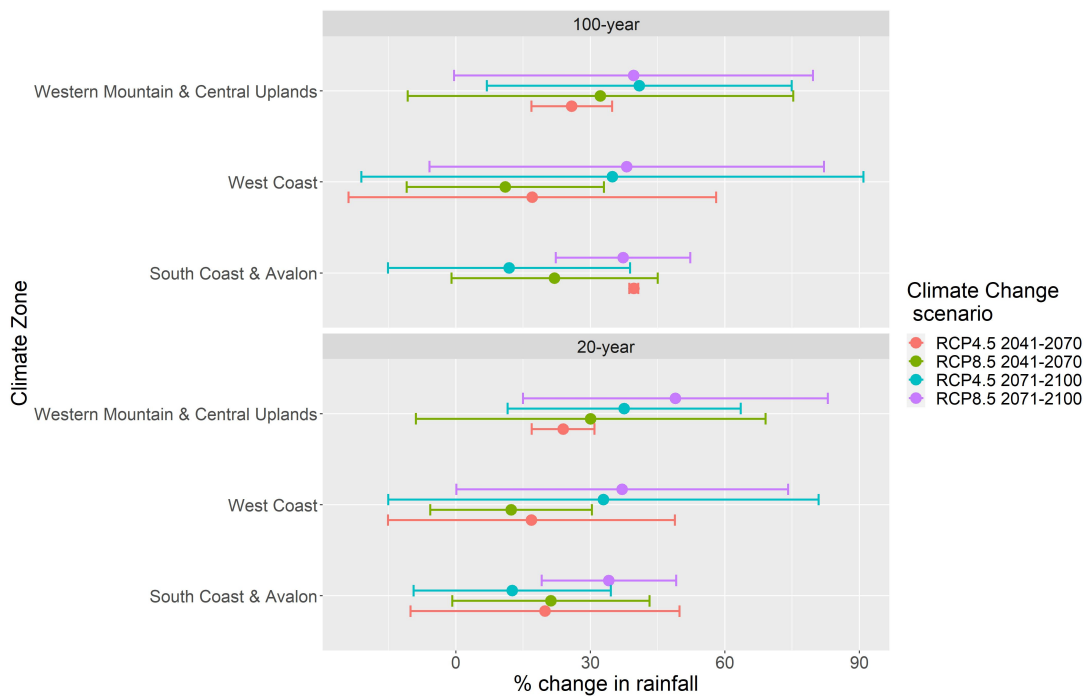
Figure 3.23: Percentage change in rainfall amounts under climate change by climate zones

3.3.2 Floodplain Mapping

Flood inundation boundaries for the watersheds showed variation by location, return period and climate conditions. As expected, the flood inundation extent was greater for the 100-year return period compared to the 20-year return period. For all watersheds, return periods and climate conditions, the AP temporal distribution produced the lowest flood inundation area except for the 100-year historical climate at Goulds, where the Alternating block pattern produced the lowest flood area. Under the historical climate, for short return periods, the Alternating block produced the largest flood inundation area at 43% of the locations, with the rest dominated by the Delayed temporal pattern. As the return levels increased, this trend reversed with the Alternating block producing the largest flood area at 71% of the locations. Under RCP4.5, the Delayed pattern produced the greatest (57.1%) flood area for the 2040 and 2070 time slice and under both return levels. The only exception was the 100-year return level under the 2040 time slice, where the Alternating block produced the largest inundation area. For RCP8.5, the results showed a trend, reverse that of RCP4.5, where the Alternating block generated the largest (57.1%) flood area for the 20 and 100-year return levels under both the 2040 and 2070 time slices except for the 20-year return period under the 2040 time slice where the Delayed pattern produced the largest flood area. Changes in flooded area relative to the flooded area under historical climate are presented in Figures 3.24 and 3.25. Actual flooded area for the watersheds under historical climate and the two time slices for RCP8.5 are presented in Appendix A. .

The flood inundation boundaries produced by the temporal distributions varied greatly. For instance, in Corner Brook, there were locations within the watershed flooded by the Alternating block but not the Advanced or Delayed patterns. Specific temporal patterns dominated watersheds located in a climate zone. For instance, in Corner Brook and Petries Brook, both located in the Western Mountains and Central Uplands climate zone, the most extensive flood inundation boundaries were produced by the alternating block irrespective
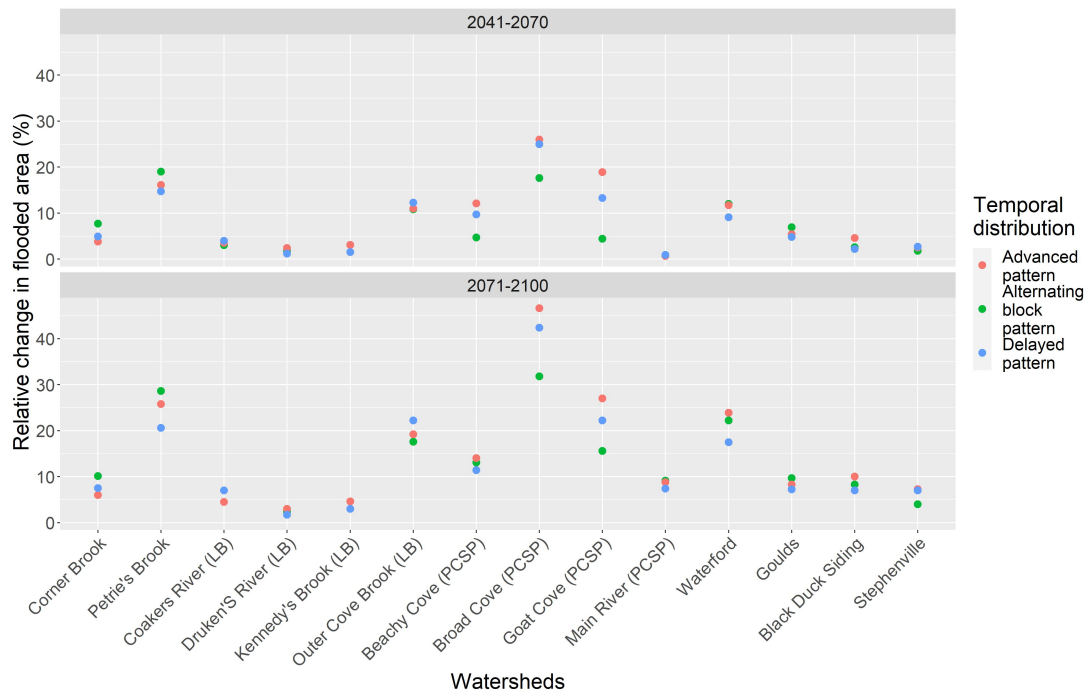
Figure 3.24: Change in flooded area (%) under RCP8.5 for the 20-year return period
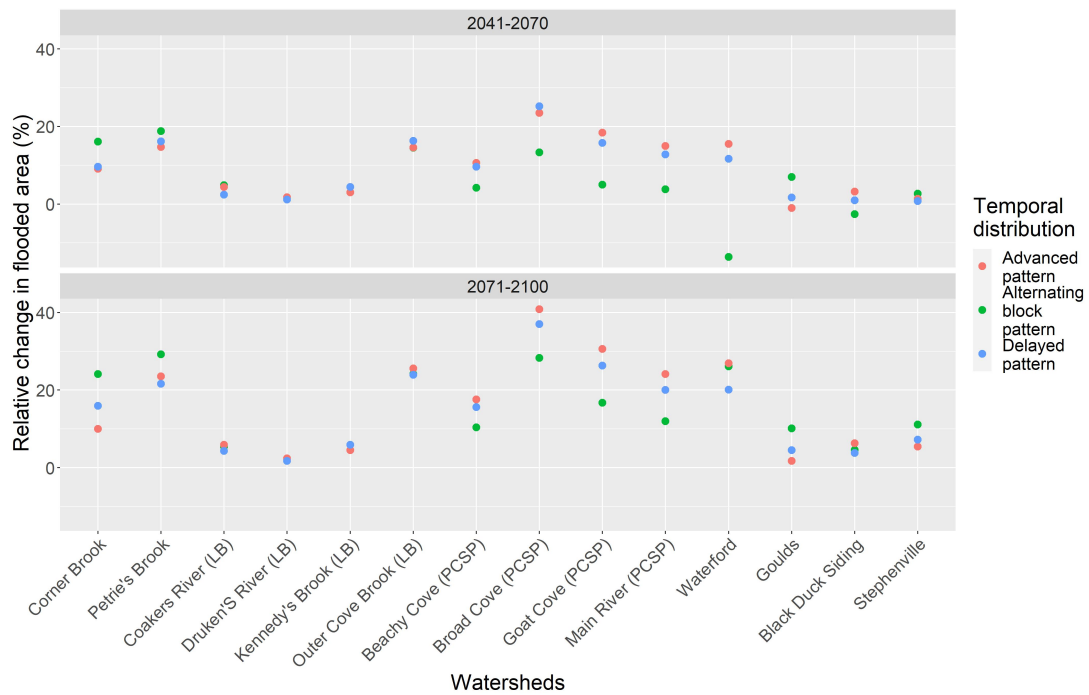
Figure 3.25: Change in flooded area (%) under RCP8.5 for the 100-year return period

of the return period or climate condition. This finding, however, was not uniform across all climate zones. In the South Coast and Avalon, some variations occur. For instance, there was no particular temporal distribution dominating the Portugal Cove-St.Philips region in the production of the most considerable flood extent. Under the historical climate, most of the extensive flood inundation boundaries were associated with the Delayed pattern, with a few associated with the Alternating block pattern.

3.4 Discussion

The overall results revealed how the choice of infiltration method greatly influences the peak flows in a hydrologic simulation. Under historical climate data, simulations using the IC had the most significant peak discharge, with the Alternating block storm type indicating the greatest peaks relative to the baseline. This occurrence appeared to occur irrespective of the climate zone or the size of the watershed. While some studies (Wang et al., 2022; Schoener & Stone, 2019; Ismail et al., 2022) agree with this finding, others have found GA to produce the highest peaks compared to CN and IC (Ficklin et al., 2012; Viji et al., 2015). The difference in results could be attributed to the rainfall distributions and watershed characteristics which primarily influence the parameters used in the model calibration and validation. This was evident in the varied watershed response across climate zones and some cases, within a region of a climate zone.

The similarity in peak discharge relative to the baseline for the AP and DP storm types could be attributed to their mirror-like difference in rainfall distribution. For AP, the highest intensity of the storm occurs in the first half of the event duration. The soils quickly become saturated with this intensity, resulting in runoff. As the event tapers off, the soil may begin to dry, thus reabsorbing some of the rainfall, causing the runoff to reduce. With DP, on the other, the highest storm intensity occurs in the latter half of the event duration. Rainfall

131

in the event's first half may not be enough to cause the soil to reach saturation, thus still allowing for a good amount of rainfall in the latter part of the event to be absorbed, reducing runoff. For ALT, the highest rainfall intensity is at the center of the event duration. The rainfall from the earlier part of the event may cause the soil to almost reach saturation, if not full saturation. During the portion of the rainfall event where the intensities are high, the soil will not hold any more water, which contributes to total runoff.

There is little to no variation in peak discharges when comparing the shorter and longer return period using historical climate data. The results are, however, different under climate change conditions. As total event rainfall increases with climate change for longer return periods, watersheds are more likely to become saturated, or the infiltration methods tend to indicate saturation. Hence, peak discharges become more directly correlated to the amount of rainfall. These results suggest a possible change from being dominated by Hortinian runoff to saturation excess in some locations as saturation of the basin becomes more likely during an event with climate change. Once the soil in the watershed becomes saturated, the propensity of an area to produce runoff is primarily independent of rainfall intensity; instead, the total rainfall amount and landscape attributes such as soil and local topography become important factors in determining the amount of runoff generated. Under these conditions, the saturated area increases during a rainfall event, thus increasing the area generating runoff. This is in contrast to the Hortonian runoff, which only depends on the soil type and the runoff generating area remains the same.

This potentially implies that the dominant hydrologic processes in a basin may change as climate changes. This change could explain the increases in peak discharge observed in the watersheds of the WMCU and WC, where increases were found for the 2071-2100 timeslice under RCP4.5 despite decreases in rainfall amounts. This could be because the model setup ceased to simulate the hydrologic processes accurately and would indicate that models calibrated using historical climate data may not be entirely valid for use with

climate change.

3.4.1 Climate Change Impacts in Newfoundland

Projections under both RCPs showed variable changes in the relationship between peak discharge and temporal pattern for different infiltration methods at various locations. On the island of Newfoundland, the IC infiltration method with DP events produced the greatest peaks with climate change. It seems likely that the choice of temporal distribution for a design storm used to estimate peak flow may change as the climate changes in some locations. Additionally, the choice of temporal distribution will likely need to be made in conjunction with the infiltration method used in the simulations to estimate design discharge. There were changes in peak discharge with the timing of rainfall projected to occur in the South Coast and Avalon and West Coast. No change in peak discharge with rainfall timing was projected for Western Mountains and Central Uplands. Compared to the other sites, Corner Brook and Petrie's watersheds' significant changes in peak discharge could be attributed to their location in the same climate zone, i.e. Western Mountain and Central Uplands. As described in 2 Table 2.2, high elevations in the area tend to cause increased cloud cover and precipitation. The climate zone effect is most likely picked up by the global climate models when representing atmospheric processes resulting in increased precipitation projected for these regions hence the increased discharge simulated. Given these interactions, design standards will need to be developed for different locations, similar to how different IDFs are used for each site.

The simulated magnitudes of peak discharge across the climate zones can be directly related to the total precipitation in these zones, and peak magnitudes increase accordingly with the return period and climate change. As expected, the percentage change in peak flows simulated under RCP8.5 was more significant than under RCP4.5. Projected precipitation depths estimated from RCP4.5 showed an increase in the first time slice (2041–2070)

and a slight decrease in the latter (2071-2100) since greenhouse gas emissions are projected to decline during this period under this emission scenario. Projected precipitation from RCP8.5, on the other hand, showed an increase for both future time slices, with increases in the second being more significant than that of the first.

The flood mapping process, in general, produces many outcomes such as the water's depth, velocity and surface elevations and these outcomes can be used in various ways, either individually or combined. This mapping aimed to indicate the possible hazard locations; hence maximum flood extent was sufficient. The maps showing the maximum extent of inundation for a given event provide a simple way to evaluate the future risk of inundation. The variation in the flooded areas indicated how much temporal patterns impact flood zones and draw attention to how flood management may vary even within a region. Few studies analyze the influence of temporal rainfall patterns on floods (Forestieri et al., 2016; Pedrozo-Acuña et al., 2017; Mu et al., 2020). In addition to topography, a significant input for flood mapping is flows from the hydrologic models. As mentioned earlier, if there is the possibility that hydrologic models calibrated with historical climate data may not capture the change in dominant hydrologic processes under climate change. This could mean there are implications for flood maps developed using these hydrologic inputs and questioning their reliability in demarcating potential flood zones.

The minor differences in inundation area produced by the Alternating block pattern and Delayed pattern point to similarities in the watershed response to these temporal patterns, even though they are different in terms of their development and the timing of peak rainfall. The Alternating block pattern is more of an arbitrary rainfall pattern where the goal is to have the maximum rainfall intensity at the storm's center. The Delayed pattern is developed from actual historic rain storms at the study sites, with the maximum rainfall depth occurring towards the end of the rainfall event. Hou et al. (2017) identified a link between the timing of rainfall peak in an event and urban flood extent in Xi'an, China. They concluded

that larger inundation areas correspond to earlier peak rainfall for short return levels.

Very often, the purpose of using the Alternating block pattern is to generate the maximum runoff, producing conservative results, which may be a good option in terms of flood risk mapping. Under climate change, one might argue that using the Alternating block pattern might be ideal, considering projections show increased rainfall in this region. However, considering the cost of flood-proofing communities, especially rural ones, adopting the flood lines from temporal distributions developed using local rainfall data may be a better alternative as the Alternating block pattern could lead to over-design in some communities.

A study by Mu et al. (2020) using temporal rainfall patterns similar to those used in this study showed the Alternating block pattern produces the maximum water depth but a lower inundation area. In contrast, the Advanced and Delayed patterns produce the largest inundation area. This study did not explore the maximum water depth hence a comparison cannot be made on that front. However, for the inundation area, the findings of this study differ from that of Mu et al. (2020). Variation in geographic and climate conditions could account for these differences. Based on the climatic conditions under consideration, the dominant flood extent varied across the climate zones identified in the study. Along the Western Mountains and Central Uplands, flood extents from the Advanced and Delayed patterns were lower than that from the Alternating block pattern.

In addition to the climate, another critical factor impacting the inundation area is topography. Across NL, there are significant variations in topography. Such variations should be considered in flood management since water is likely to pond in areas with lesser slopes. Using different temporal distributions to estimate inundation areas provides a good sense of uncertainty by providing a lower and upper limit of the potential flood areas.

The increases in the flooded area were not significant compared to the peak discharges, even under the climate change scenarios. However, it should be noted that the climate scenario flooded areas are obtained using the median projection. These areas could be

more significant if the 90th percentile were used instead. The slight increase in flooded area can also be attributed to the storm duration used for the study. Increases in precipitation intensity are projected to be highest at shorter duration storms (Hardwick Jones et al., 2010; Panthou et al., 2014; Oh & Sushama, 2020). Thus, using a shorter duration storm may result in a more significant flood area. Another factor contributing to the minor effect of increased storm intensity under climate change is the size of the catchment. In a smaller catchment, there is a high chance that a storm will cover the entire catchment, resulting in soil moisture saturation. As a result, more of the precipitation will contribute to the runoff. Do et al. (2017) show that smaller catchments are more susceptible to increased flood amounts. On the other hand, larger catchments are more likely to observe reduced flood peaks (Do et al., 2017) . This implies the dominance of scale in the determination of future flooding.

3.4.2   Designing and Floodplain Mapping with Climate Change

Design of stormwater drainage systems must be considered under conditions of non-stationarity (Vaze et al., 2010; Cheng & AghaKouchak, 2014), and climate change projections indicate with confidence that precipitation events will increase in intensity throughout NL. The direct proportionality between pipe diameters and peak runoff rate means that any increase in peak flow will require the design of larger systems. Results of simulations indicated that events with the most significant increases of peak discharge with climate change also had the highest levels of uncertainty. IDF projections estimated from an ensemble of climate models account for much of this uncertainty. A lack of skill in climate model simulations of precipitation formation in some regions around the world also contributes to the uncertainty (Chadwick et al., 2016; Seager et al., 2010). It is acknowledged that some GCMs are biased towards projecting drier or wetter conditions in particular areas. However, using large ensembles of GCMs, which would encompass both biases, allows for robust quantification of uncertainty in climate projections (Nolan & Flanagan, 2020; Coppola et al.,

2021). Uncertainty also enters through the downscaling methods used to estimate IDFs at point locations. Regardless of its source, high levels of uncertainty in design parameters present society and engineers with a dilemma of choosing between expensive design costs and an acceptable risk of failure. Increasing the capacity of these systems can reduce flood occurrence, which will have positive social and economic impacts, such as minimizing the disruption of businesses and cutting infrastructure damage caused by floods. However, under-design of drainage systems can lead to severe flooding and the failure of vital infrastructure, causing significant economic losses and potential loss of life.

For the design of infrastructure requiring a shorter event at most locations, uncertainty is low enough that the choice of design parameters should be relatively straightforward. There is enough confidence in climate projections using the CMIP5 multimodel ensemble in these cases because they can capture the most relevant processes (Shu et al., 2015). Infrastructure designed at these levels is not critical; however, uncertainty in peak flow estimation for higher return levels relevant to more critical infrastructure was greater. Uncertainty was also greater for projections for the last 30 years of the century, at a longer time horizon. For this reason, taking an adaptive approach to design is the recommendation to engineers (Parry et al., 2007; Connor et al., 2013). A complete discussion of methods to increase the adaptive capacity and resilience of infrastructure is beyond the scope of this paper. However, such an approach allows for flexible design with plans for adjustments to be made on a system as more information becomes available in the future.

Alternatively, climate change projections for IDF curves in a location can be used for design. As the results reported here indicate, other important considerations for choosing design parameters include the infiltration method and temporal pattern used in hydrologic simulations. It seems clear that the local climate and basin will determine the choice of both. Based on our results, the recommendation is to design a stormwater system or establish flood lines; the analysis should include using a range of infiltration methods and temporal

distributions, including percentile ranges in projected IDF curves. Such an approach will allow for estimates of design parameters that account for uncertainty and its sources and represents a relatively simple way to assess uncertainty and design with climate change. Ultimately the choice of design parameters will depend on overall costs weighed against the acceptable risk of failure. No matter what decision-making method is used, considering the uncertainties associated with climate change and hydrologic simulations, estimating design parameters based on the results presented here provides vital information from which to proceed.

3.4.3   Study Limitations

The flooded areas computed in this study were done using 1D hydrodynamic models; hence it does not simulate lateral diffusion of the flood wave, which impacts the timing and duration of the inundation areas and, consequently, the flood extents identified. Under future projections, this study did not consider changes in floodplain landscape or land use changes over time, which limits the extrapolation of specified results to other locations, especially ones where development may be at a high rate. While the uncertainty on the rainfall projections was propagated to the peak discharge, the same was not done for the flood extents. It is understood that these models are not going to provide definitive decisions. Still, engineers can draw on this information and consider them during a design project and also on how to communicate uncertainty when projects involve climate change analysis. As mentioned earlier, the estimation of flood area and peak discharges were limited to the island where climate zones had at least two watersheds with calibrated and validated hydrologic and hydraulic models. Efforts are underway by the NL province to provide these models for the Labrador region to enhance such studies.

3.5   Conclusion

The interaction between infiltration methods and temporal precipitation patterns and their impact on hydrographs under historical and future climates is assessed across a climate gradient. Developed hydrographs are further used to estimate flood inundation areas. Peak discharge increased in conjunction with increases in event rainfall intensity based on return period and climate change impacts on IDF curves. Under historical climate conditions, the greatest hydrographs are produced by the Initial and Constant infiltration methods and the Alternating block pattern at most study sites. Climate change projections, which provide changes in IDF curves, seem to change this relationship in many locations as peak discharges increase when most rainfall occurs later in the event (Delayed pattern) and is more pronounced with the Green and Ampt infiltration method. The occurrence of this switch in dominant temporal patterns and infiltration methods emphasizes that it is essential to consider these interactions when designing infrastructure or establishing flood lines. It also points to a possible change in the dominant hydrology in a watershed as rainfall volume increases under climate change conditions. The most significant uncertainties were associated with locations that show the most considerable potential change in peak discharge. It is recommended that in addition to changes in IDF curves with climate change, the variation in peak discharges with temporal distribution of rainfall and infiltration method be included in determining design parameters for stormwater infrastructure and flood risk mapping.

References

Al Mamoon, A., Rahman, A., & Joergensen, N. E. (2019). Assessment of climate change impacts on idf curves in qatar using ensemble climate modeling approach. In *Hydrology in a changing world* (pp. 153–169). Springer.

AMEC Environment & Infrastructure. (2013a). *Flood risk mapping project corner brook stream and petrie's brook* (Tech. Rep.). Government of Newfoundland and Labrador. Retrieved from `https://www.gov.nl.ca/ecc/files/waterres -flooding-corner-brook-stream-cornerbrook-report.pdf`

AMEC Environment & Infrastructure. (2013b). *Flood risk mapping project goulds and petty harbour area* (Tech. Rep.). Government of Newfoundland and Labrador. Retrieved from `https://www.gov.nl.ca/ecc/files/waterres -flooding-petty-harbour-goulds-goulds-pettyharbour-report.pdf`

Amec Foster Wheeler Environment & Infrastructure. (2015). *Flood-risk mapping project portugal cove – st. philip's* (Tech. Rep.). Government of Newfoundland and Labrador. Retrieved from `https://www.canal.gov.nl.ca/reports/frm/ FRM_PCSP_2015/Portugal_Cove_StPhilips_Flood_Final_25may2015_MAIN _REPORT.pdf`

Amponsah, A. O., Daraio, J. A., & Khan, A. A. (2019). Implications of climatic variations in temporal precipitation patterns for the development of design storms in newfoundland and labrador. *Canadian Journal of Civil Engineering*(ja).

Boughton, W. (1989). A review of the usda scs curve number method. *Soil Research*, *27*(3), 511–523.

CBCL LIMITED Consulting Engineers. (2012). *Town of logy bay – middle cove – outer cove flood risk mapping study* (Tech. Rep.). Government of Newfoundland and Labrador. Retrieved from `https://www.canal.gov.nl.ca/reports/frm/FRM_LBMCOC/FRM_LBMCOC_Final_Report_Volume1.pdf`

Chadwick, R., Good, P., Martin, G., & Rowell, D. P. (2016). Large rainfall changes consistently projected over substantial areas of tropical land. *Nature Climate Change*, *6*(2), 177.

Cheng, L., & AghaKouchak, A. (2014). Nonstationary precipitation intensity-duration-frequency curves for infrastructure design in a changing climate. *Scientific reports*, *4*, 7093.

Chin, D. (2013). *Water resources engineering* (Vol. 12). Pearson Education, Inc. Upper Saddle River, NJ.

Chu, X., & Steinman, A. (2009). Event and continuous hydrologic modeling with hec-hms. *Journal of Irrigation and Drainage Engineering*, *135*(1), 119–124.

Conestoga-Rovers & Associates. (2015). *Intensity-duration-frequency curve update for newfoundland and labrador.*

Connor, T., Niall, R., Cummings, P., & Papillo, M. (2013). Incorporating climate change adaptation into engineering design concepts and solutions. *Australian Journal of Structural Engineering*, *14*(2), 125-134. Retrieved from `http://www.tandfonline.com/doi/abs/10.7158/13287982.2013.11465127` doi: 10.7158/13287982.2013.11465127

Coppola, E., Nogherotto, R., Ciarlo', J. M., Giorgi, F., van Meijgaard, E., Kadygrov, N., ... others (2021). Assessment of the european climate projections as simulated by the large euro-cordex regional and global climate model ensemble. *Journal of*

Geophysical Research: Atmospheres, *126*(4), e2019JD032356.

Do, H. X., Westra, S., & Leonard, M. (2017). A global-scale investigation of trends in annual maximum streamflow. *Journal of Hydrology*, *552*, 28–43.

Feldman, A. D. (2000). *Hydrologic modeling system hec-hms: technical reference manual*. US Army Corps of Engineers, Hydrologic Engineering Center.

Ficklin, D., Zhang, M., et al. (2012). A comparison of the curve number and green-ampt models in an agricultural watershed. *Transactions of the ASABE*, *56*(1), 61–69.

Finnis, J. (2013). *Projected impacts of climate change for the province of newfoundland & labrador.*

Finnis, J., & Daraio, J. (2018). *Projected impacts of climate change for the province of newfoundland & labrador: 2018 update.* (Tech. Rep.). Government of Newfoundland and Labrador.

Forestieri, A., Caracciolo, D., Arnone, E., & Noto, L. (2016). Derivation of rainfall thresholds for flash flood warning in a sicilian basin using a hydrological model. *Procedia Engineering*, *154*, 818–825.

Gao, P., Carbone, G. J., Tufford, D. L., Patel, A., & Rouen, L. F. (2012). Assessing methods to disaggregate daily precipitation for hydrological simulation.

Gong, Y., Liang, X., Li, X., Li, J., Fang, X., & Song, R. (2016). Influence of rainfall characteristics on total suspended solids in urban runoff: A case study in beijing, china. *Water*, *8*(7), 278.

Green, W. H., & Ampt, G. (1911). Studies on soil phyics. *The Journal of Agricultural Science*, *4*(1), 1–24.

Hardwick Jones, R., Westra, S., & Sharma, A. (2010). Observed relationships between extreme sub-daily precipitation, surface temperature, and relative humidity. *Geophysical Research Letters*, *37*(22).

HATCH. (2009). *Hydrotechnical study of stephenville* (Tech. Rep.). Government of

Newfoundland and Labrador. Retrieved from `https://www.canal.gov.nl.ca/`
`reports/frm/FRM_Stephenville/2009/Final\%20Report\%20Volume\%201`
`.pdf`

HATCH. (2012). *Hydrotechnical study of stephenville crossing/black duck siding* (Tech. Rep.). Government of Newfoundland and Labrador. Retrieved from `https://www.canal.gov.nl.ca/reports/frm/FRM_Stephenville\` `%20Crossing_Black\%20Duck\%20Siding_1996/2012/FRM_Stephenville` `_Crossing_Black_Duck_Siding_2012_Volume1.pdf`

Horton, R. (1940). An approach towards the physical interpretation of infiltration capacity. *Am. Soil Sci. Soc. Proc*, *339*.

Hou, J., Guo, K., Wang, Z., Jing, H., & Li, D. (2017). Numerical simulation of design storm pattern effects on urban flood inundation. *Adv Water Sci*, *28*(6), 820–828.

Interagency Committee on Water Data. (2018 (revised and corrected)). *Guidelines for determining flood flow frequency: Bulletin 17-b* (Tech. Rep.). Hydrology Subcommittee.

Ismail, H., Kamal, M. R., Mojid, M. A., Abdullah, A. F. B., & Hin, L. S. (2022). Loss methods in hec-hms model for streamflow projection under climate change: a review. *International Journal of Hydrology Science and Technology*, *13*(1), 23–42.

Joshi, N., Bista, A., Pokhrel, I., Kalra, A., & Ahmad, S. (2019). Rainfall-runoff simulation in cache river basin, illinois, using hec-hms..

Koneti, S., Sunkara, S., & Roy, P. (2018). Hydrological modeling with respect to impact of land-use and land-cover change on the runoff dynamics in godavari river basin using the hec-hms model. *ISPRS International Journal of Geo-Information*, *7*(6), 206.

Luo, P., He, B., Duan, W., Takara, K., & Nover, D. (2018). Impact assessment of rainfall scenarios and land-use change on hydrologic response using synthetic area idf curves. *Journal of Flood Risk Management*, *11*, S84–S97.

McManus, G. E., Wood, C. H., Mercer, D. J., & Conway, C. M. (1991). *Atlas of newfoundland and labrador*. Breakwater Books.

Meinshausen, M., Smith, S. J., Calvin, K., Daniel, J. S., Kainuma, M. L. T., Lamarque, J., ... van Vuuren, D. P. P. (2011). The RCP greenhouse gas concentrations and their extensions from 1765 to 2300. *Climatic Change*, *109*(1), 213–241. doi: 10.1007/ s10584-011-0156-z

Modarres, R. (2006). Regional precipitation climates of iran. *Journal of Hydrology (New Zealand)*, *45*(1), 13–27.

Mu, D., Luo, P., Lyu, J., Zhou, M., Huo, A., Duan, W., ... Zhao, X. (2020). Impact of temporal rainfall patterns on flash floods in hue city, vietnam. *Journal of Flood Risk Management*, e12668.

Nguyen, V., & Nguyen, T. (2019). A decision support tool for assessing the climate change impacts on urban water infrastructure design. In *11th international workshop on precipitation in urban areas (urbanrain18)*.

Nolan, P., & Flanagan, J. (2020). High-resolution climate projections for ireland–a multi-model ensemble approach. *Environmental Protection Agency*.

Oh, S.-G., & Sushama, L. (2020). Short-duration precipitation extremes over canada in a warmer climate. *Climate Dynamics*, *54*(3), 2493–2509.

Panthou, G., Mailhot, A., Laurence, E., & Talbot, G. (2014). Relationship between surface temperature and extreme rainfalls: A multi-time-scale and event-based analysis. *Journal of hydrometeorology*, *15*(5), 1999–2011.

Parry, M., Canziani, O., Palutikof, J., van der Linden, P., & Hanson, C. (Eds.). (2007). *Contribution of working group ii to the fourth assessment report of the intergovernmental panel on climate change, 2007*. Cambridge University Press, Cambridge, United Kingdom and New York, NY, USA.

Pedrozo-Acuña, A., Moreno, G., Mejía-Estrada, P., Paredes-Victoria, P., Breña-Naranjo, J.,

& Meza, C. (2017). Integrated approach to determine highway flooding and critical points of drainage. *Transportation research part D: transport and environment*, *50*, 182–191.

Sarhadi, A., Soltani, S., & Modarres, R. (2012). Probabilistic flood inundation mapping of ungauged rivers: Linking gis techniques and frequency analysis. *Journal of Hydrology*, *458*, 68–86.

Schoener, G., & Stone, M. C. (2019). Impact of antecedent soil moisture on runoff from a semiarid catchment. *Journal of Hydrology*, *569*, 627–636.

Seager, R., Naik, N., & Vecchi, G. A. (2010). Thermodynamic and dynamic mechanisms for large-scale changes in the hydrological cycle in response to global warming. *Journal of Climate*, *23*(17), 4651–4668.

Seiler, C., & Zwiers, F. (2016). How well do cmip5 climate models reproduce explosive cyclones in the extratropics of the northern hemisphere? *Climate dynamics*, *46*(3-4), 1241–1256.

Sharma, A., Wasko, C., & Lettenmaier, D. P. (2018). If precipitation extremes are increasing, why aren't floods? *Water resources research*, *54*(11), 8545–8551.

Shu, Q., Song, Z., & Qiao, F. (2015). Assessment of sea ice simulations in the cmip5 models. *The Cryosphere*, *9*(1), 399–409.

Srivastav, R. K., Schardong, A., & Simonovic, S. P. (2014). Equidistance quantile matching method for updating idfcurves under climate change. *Water resources management*, *28*(9), 2539–2562.

Storn, R., & Price, K. (1997). Differential evolution–a simple and efficient heuristic for global optimization over continuous spaces. *Journal of global optimization*, *11*(4), 341–359.

Umakhanthan, K., & Ball, J. E. (2002). Estimation of rainfall heterogeneity across space and time scale. In *Global solutions for urban drainage* (pp. 1–16).

Vaze, J., Post, D., Chiew, F., Perraud, J.-M., Viney, N., & Teng, J. (2010). Climate non-stationarity–validity of calibrated rainfall–runoff models for use in climate change studies. *Journal of Hydrology*, *394*(3-4), 447–457.

Veneziano, D., & Villani, P. (1999). Best linear unbiased design hyetograph. *Water resources research*, *35*(9), 2725–2738.

Viji, R., Prasanna, P. R., & Ilangovan, R. (2015). Modified scs-cn and green-ampt methods in surface runoff modelling for the kundahpallam watershed, nilgiris, western ghats, india. *Aquatic Procedia*, *4*, 677–684.

Vu, M., Raghavan, S., Liu, J., & Liong, S.-Y. (2018). Constructing short-duration idf curves using coupled dynamical–statistical approach to assess climate change impacts. *International Journal of Climatology*, *38*(6), 2662–2671.

Wang, X., Zhao, L., Zhang, J., Zou, T., & Zhang, N. (2022). Applicability analysis of different runoff schemes of the gulang river basin in arid region of gansu province, china. In *E3s web of conferences* (Vol. 350, p. 01026).

Watt, E., & Marsalek, J. (2013). Critical review of the evolution of the design storm event concept. *Canadian Journal of Civil Engineering*, *40*(2), 105–113.

Werner, A., & Cannon, A. (2015). Hydrologic extremes–an intercomparison of multiple gridded statistical downscaling methods. *Hydrology & Earth System Sciences Discussions*, *12*(6).

Winstanley, D. (1973). Rainfall patterns and general atmospheric circulation. *Nature*, *245*(5422), 190–194.

Yuan, W., Liu, M., & Wan, F. (2019). Calculation of critical rainfall for small-watershed flash floods based on the hec-hms hydrological model. *Water Resources Management*, 1–21.

Zervas, C., Gill, S., & Sweet, W. (2013). Estimating vertical land motion from long-term tide gauge records.

146

Zhang, X., Buchberger, S. G., & van Zyl, J. E. (2005). A theoretical explanation for peaking factors. In *Impacts of global climate change* (pp. 1–12).

Chapter 4

An enhanced non-parametric precipitation disaggregation model based on method of fragments and crossover operators

*

Preface

I am the primary author, and I carried out most of the research, conceived the research ideas, performed the literature reviews and simulation setups, and analyzed the results. I also prepared the first drafts of the manuscripts and subsequently revised the final manuscripts based on feedback from the co-authors and the peer-review process. Dr. Xin Li contributed

---

*This chapter is a modified version of "An enhanced non-parametric precipitation disaggregation model based on method of fragments and crossover operation" which is currently under review with the International Journal of Climatology

Abstract

Stochastic simulation of sub-daily precipitation is essential for assessing the hydrological response of drainage basins across multiple scales. Disaggregation methods provide a means to obtain sub-daily and sub-hourly precipitation data for various applications, from planning urban drainage networks to designing real-time flood control systems. Non-parametric disaggregation methods are more widely used because they do not require assumptions about the underlying distribution of the precipitation data are required. However, the data-intensive nature of these methods is a significant disadvantage as it renders them inapplicable to data-scarce regions. This study proposes a modification to an existing non-parametric disaggregation model, making it suitable for use in data-scarce locations. This was achieved by coupling three different crossover mixing algorithms with an interval-based sampling method of fragments model to generate fragments that did not previously exist in the data. The model's performance was assessed by its ability to reproduce key statistics in the data, including mean, standard deviation, lag-1 auto-correlation and proportion of dryness, as well as inter-day connectivity, intra-day wet and dry spell characteristics, and extreme value analysis. The results show that statistics from the simulated data were within an acceptable range of the observed data. All crossover methods evaluated produced comparable results except for the dryness proportion, for which the two-point crossover produced the best outcome. The 5th and 95th percentile range of annual maximum values created using only one year of data encompassed the observed maximum values. The proposed modification allows for disaggregation of long-term coarse-scale precipitation data based on available short-term fine-scale data. This could serve as a means for intensity-

duration-frequency curve construction and long-term hydrologic simulation in data-scarce regions.

Index Terms: Disaggregation, genetic algorithm, method of fragments

4.1 Introduction

Precipitation disaggregation models exist to correct bad precipitation data or fill in missing observations. Applying such models helps generate usable data for purposes ranging from stormwater infrastructure design to flood risk mapping. This paper aims to propose a modification to an existing non-parametric disaggregation model for use in data-scarce locations Over the past few decades, research into disaggregation methods has increased (Burian et al., 2000; Molnar & Burlando, 2005; Westra et al., 2012; Kossieris et al., 2015; Arfa et al., 2021), and current approaches differ in model design, geographic factors, dataset resolution, measuring instruments and treatment of climate, all of which affect the performance of the models (Willems et al., 2012). There are two categories of precipitation disaggregation models: deterministic and stochastic. Deterministic models are developed such that there is no element of randomness; parameters, e.g. the critical time in the linear model and initial conditions, will always produce the same result. They are simple and easy to use, and include the linear model (Ormsbee, 1989) and the constant disaggregation model. The advantages of deterministic models are their simplicity and minimal parameter requirements. The major drawback of these models is that they cannot produce dry periods within a wet duration (i.e. disaggregation of daily precipitation records to hourly, results in hourly precipitation values for every hour). Generally, deterministic models do not have huge data requirements, but their inability to produce realistic precipitation data makes them undesirable for precipitation disaggregation.

On the other hand, as the name implies, stochastic models possess some inherent ran-

domness, a set of parameters and initial conditions will yield different results. These models evolved to address the significant drawback of deterministic models, generating synthetic precipitation, making them the most adopted ones in the current research community. Stochastic models can be broadly grouped into three classes: i) probability-dependent models, which generate precipitation within a wet hour using a specified probability (Koutsoyiannis & Onof, 2001; Pui et al., 2012; Hassan, 2020; Kim & Onof, 2020; Park et al., 2021); ii) weighted-cascade models, in which, precipitation at coarse-scale breaks up into fine-scale based on randomly generated weights (Müller & Haberlandt, 2015, 2018; Müller-Thomy, 2020); and iii) resampling models, where coarse-scale precipitation disaggregate to fine-scale using a vector of fragments, representing the ratio of fine-scale to coarse-scale precipitation (Aguilar & Costa, 2020; Schepen et al., 2020; Willkofer et al., 2020; Rafatnejad et al., 2021). The first two classes of stochastic models require some parameters, e.g. the original Bartlett-Lewis has five parameters (λ, β, γ, μ and η), representing the various Poisson- and Exponential-distributed precipitation event generation processes. Resampling models based on the method of fragments (MoF) do not require any parameters.

The MoF model has been shown to outperform all the other disaggregation models in terms of reproducing standard statistics and percentiles of extreme precipitation in a study by Pui et al. (2012) based on four locations spanning different climate regimes and data ranging from 42 to 63 years in Australia. In addition to its performance, the MoF model does not require any parameters or assumptions about the precipitation data's distribution. These advantages make it a preferred option for use in precipitation disaggregation. It has been extensively used for precipitation disaggregation in many studies from daily to sub-daily using data of varying lengths from across the globe. Despite its extensive usage and advancement, two major limitations have been identified from the literature.

First, the precipitation data over extended periods and of high frequency are required to use the MoF models. For instance, Wójcik and Buishand (2003) studied the performance

of two nearest neighbour schemes for simulating 6-hourly precipitation and temperature from a stochastic weather generator. With 42 years of daily and 6-hourly data, their study revealed that simulating daily data and further, disaggregating it into 6-hourly precipitation using MoF better represented second-order statistics than simulating the 6-hourly precipitation directly. Breinl et al. (2017) implemented the k-nearest neighbour (KNN) resampling technique in MoF to estimate river discharge and precipitation daily extreme in a study to locate regions at risk of pluvial floods. MoF has even been extended to allow for concurrent disaggregation of precipitation and temperature spatiotemporally for the Italian Alps and Sweden with 15 and 22 years of data. The length of data requirement makes the MoF model inapplicable in regions where such data is lacking.

Second, is the possibility of generating precipitation patterns that almost duplicate historical observations because of the resampling process. Sharif et al. (2007) attempted to overcome this limitation by applying the K-nearest neighbour resampling technique in MoF to stochastically generated and perturbed daily temperature and precipitation into hourly data for the Thames River Basin, Ontario. The advantage of this approach was the generation of unprecedented meteorological variables, which makes it applicable for climate change scenario analysis. However, this limitation inherent in MoF disaggregated data has not been extensively addressed. Lee et al. (2010) indicated that duplicating precipitation patterns is not a problem if doing so closely reproduces the historical statistics. However, in reality, precipitation patterns vary, which should be captured by stochastic models. Lee et al. (2010) proposed using genetic algorithms to overcome this limitation in a stream flow disaggregation model, but this technique has not been applied to precipitation data.

The intensive data prerequisites of MoF models make them inapplicable to regions with sparse precipitation data records. This study provides a means of circumventing this limitation. Most applications of MoF focus on disaggregation from daily to hourly, limiting the output of these models in situations that require sub-hourly data. These issues drive the

need to develop less data-intensive models or to use available techniques to produce more extended "virtual" data sets from the limited observational dataset for the data-intensive disaggregation models. This study proposes modifications to an existing MoF model to make it applicable to data-scarce locations. Applying this relatively simple model to such locations can serve as a means of obtaining hydrologic data which can then be used for water resources planning and management.

4.2 Methods

4.2.1 Interval-Based Method of Fragments

Initially developed for streamflow data (Svanidze, 1980) and then applied to precipitation, the MoF technique has three phases. The first phase divides the fine-scale values, x, by their corresponding coarse-scale values, X. The process produces sets of fragments (F). For example, in the case of daily values, the hourly values are divided by the corresponding daily value; as such, the sum of the 24 hourly fragments must add to one. In phase two, a set of fragments is chosen randomly (resampled) from the previous step. In the last phase, the disaggregated outcome is a product of the resampled set and the coarse-scale value to disaggregate. This model is conceptually simple, non-parametric and has outperformed other stochastic disaggregation models (Carreau et al., 2019). Li et al. (2018) proposed the interval-based MoF (I-MoF) to disaggregate daily precipitation to hourly. The steps of the model are as follows:

- Daily precipitation values D_k (coarse-scale values) and their corresponding hourly precipitation data d_k (fine-scale values) are converted to sets of fragments $F_{k,j}$ (equation 4.1) (SoFs) with each set containing 24 hourly precipitation values.

$$F_{k,j} = d_{k,j}/D_k \text{ where } D_k = \Sigma_{j=1}^{24} d_{k,j} \qquad (4.1)$$

153

where k denotes the k_{th} day and j the j_{th} hour (j=1,2,...,24)

- D_k are grouped into the following classes:

class 1: $0.1\text{mm} \leq D_k < 1\text{mm}$
class 2: $1\text{mm} \leq D_k < 5\text{mm}$
class 3: $5\text{mm} \leq D_k < 10\text{mm}$
.
.
.
class y: $5(\text{y-1})\text{mm} \leq D_k < 5\text{y mm}$

where y is the number of classes determined by the maximum daily precipitation.

- The class of a daily precipitation value to disaggregate, X_i, is identified to initiate the process. The SoFs for that class are then selected from the set of SoFs, whose corresponding coarse-scale values meet the inter-day connectivity constraint for wetness state, i.e., $I(X_{i-1}) = I(D_{t-1})$ and $I(X_{i+1}) = I(D_{t+1})$, where $I()$ is a binary indicator function defined as $I(X) = 1$ for a wet day (X>0) and $I(X) = 0$ for a dry day (X=0) (Li et al., 2018).

- Disaggregated results = Daily value to disaggregate * selected SoF

The interval-based MoF model of Li et al. (2018) was proposed mainly to address the problem of sampling incommensurate daily precipitation values (especially for the values on the upper tail of the distribution) when using the K-nearest-neighbor (KNN) algorithm.

4.2.2   Proposed I-MoF

However, this model depends on long-term continuous precipitation data, a condition that renders it unusable when such data are not readily available. Daily data are often readily available, but corresponding hourly or sub-hourly data are not. The following modifications are applied to the I-MoF for the sparse data needed by the data-intensive model.

First, the daily observed precipitation data are grouped into four classes: [0.1mm,1mm], [1.1mm,10mm], [10.1mm,25mm] and [25.1mm, ∞], instead of using the classes divided by 5mm interval in Li et al. (2018). The four class grouping is a format used in meteorological forecasts. In this format, precipitation is split into classes of zero or trace, followed by gradually increasing precipitation "bins" that reflect forecasting concerns (i.e., from drizzle to "wet days", increasing in severity to more extreme events). This modification is necessary because the maximum precipitation that determines the number of classes in the 5mm grouping method is unknown. Second, the fragments to sample from would not be available for daily precipitation values without corresponding sub-hourly data. In situations where the sub-hourly data covers a short year block, the number of fragments assigned to each class will be smaller, and resampling from this will result in repeated patterns. We employed a crossover method from the genetic algorithm scheme to introduce some variation in the precipitation patterns to eliminate these. Hereafter, this GA-based I-MoF will be referred to as GA-MoF.

1. Daily precipitation values D_k (coarse-scale values) and their corresponding hourly precipitation data d_k (fine-scale values) are converted to sets of fragments $F_{k,j}$ (equation 4.2) (SoFs) with each set containing 24 hourly precipitation values.

$$F_{k,j} = d_{k,j}/D_k \text{ where } D_k = \Sigma_{j=1}^{24} d_{k,j} \tag{4.2}$$

where k represents the k_{th} day and j, the j_{th} hour (j=1,2,...,24)

2. The daily precipitation data which has corresponding sub-hourly data are put into the four classes: [0.1mm,1mm], [1.1mm,10mm], [10.1mm,25mm] and [25.1mm, ∞].

The class of a daily precipitation value to disaggregate, X_i, is identified to initiate the process. The SoFs for that class are then selected from the set of SoFs, whose corre-

sponding coarse-scale values meet the inter-day connectivity constraint for wetness state, i.e., $I(X_{i-1}) = I(D_{t-1})$ and $I(X_{i+1}) = I(D_{t+1})$, where $I()$ is a binary indicator function defined as $I(X) = 1$ for a wet day (X>0) and $I(X) = 0$ for a dry day (X=0) (Li et al., 2018).

3. From this set of SoFs, if the number of SoFs is greater than or equal to two, the genetic algorithm selects two of them and generates two new SoFs from the chosen pair. The two new SoFs are added to the original set of SoFs, and one is sampled at random. Using the genetic algorithm to create new SoFs reduces the duplication of historical precipitation patterns in the disaggregated data. This becomes more likely as the available sub-hourly data shortens in length. Details of the genetic algorithm are provided in the next section.

4. If the number of SoFs in the set is one, it is selected without modification. This situation is most likely to occur for extreme precipitation patterns in the [25.1, ∞] class, as they have fewer data points. No modification is made since preserving the extreme precipitation pattern is needed.

5. If no SoFs are selected in steps 2 or 3, one is chosen randomly from those generated in step 1. The random selection of the SoF is to ensure that all the daily values are disaggregated.

6. Disaggregated results = Daily value to disaggregate * selected SoF

A flowchart of the proposed model is presented in Figure 4.1.

4.2.3   Genetic Algorithms

Genetic algorithms are used in genetic studies to simulate natural evolution while preserving population status (Holland, 1992). Genetic algorithms have been applied in the field
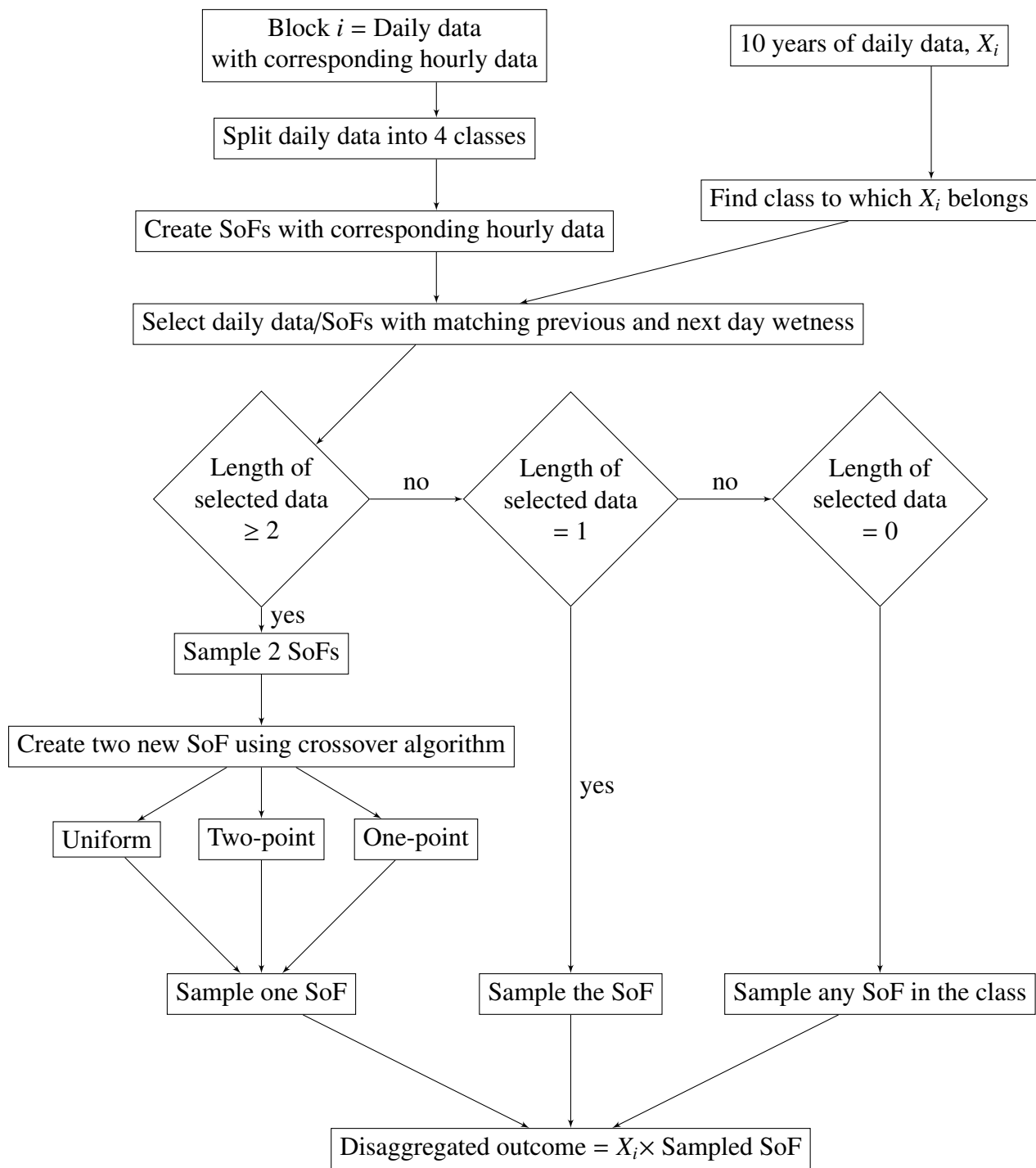
Figure 4.1: Flowchart of GA-MoF

of water resources for more than two decades with early works by Babović and Wu (1975) and Savic and Walters (1997). This indirectly ensures the maintenance of specific statistics within the population (Yang, 2002). The purpose of these algorithms in the proposed model is to create SoF that did not previously exist in the data. This helps to minimize generating repeated precipitation patterns. This has not yet been implemented in the MoF disaggregation models to the best of our knowledge. There are two ways of integrating insights and background knowledge into evolutionary algorithms: adaptation of operators (Keijzer et al., 2001; Zhang et al., 2007; Deep & Thakur, 2007; Sun et al., 2021) and use of objective functions which may be provided in the preferential or declarative form (Babovic, 2009; Mehr et al., 2018). Genetic algorithms involve three operations: reproduction, crossover and mutation. This study opted for only the crossover algorithms to minimize shifts in precipitation data distribution and not to affect month-to-month correlation by introducing a mutation algorithm (Goldberg, 1989; Lee et al., 2010). The crossover algorithm allows the creation of new SoF from current ones while preserving unity in the SoF. The algorithm implements the "mixing" within each class. The steps of the algorithm are as follows:

1. Within a class, randomly select two SoFs, f_1 and f_2. Create two new SoFs by choosing fragments from the two selected sets. There are several methods available for choosing the fragments. This study compared three methods: Two-point crossover, One-point crossover, and Uniform crossover (Yang & Abbass, 2003). In One-point crossover (Holland, 1992; Wang et al., 2014), a new SoF involves taking a part of f_1 from the beginning to a predetermined crossover point and the rest of the fragment set from f_2 using equation 4.3:

$$\text{new SoF } (S_{ij}) = \begin{cases} f_{1j} & \text{if j} \leq \text{r} \\ f_{2j} & \text{if j} > \text{r} \end{cases} \tag{4.3}$$

158

where r is a random integer sampled from a uniform distribution between 1 and t, with t being the dimensional of the search space. Two-point crossover (Eshelman et al., 1989; Bala & Sharma, 2015) is similar to One-point, with the only difference being the use of two predetermined crossover points instead of one, and that the new SoF builds by alternating between f_1 and f_2 using equation 4.4:

$$\text{new SoF } (S_{ij}) = \begin{cases} f_{1j} & \text{if } j \leq r_1 \\ f_{2j} & \text{if } j > r_1 \text{ and } j \leq r_2 \\ f_{1j} & \text{if } j > r_2 \end{cases} \tag{4.4}$$

where r_1 and r_2 are random integers sampled from a uniform distribution between 1 and t, with t being the dimensional of the search space and $r_2 \geq r_1$. For Uniform crossover (Syswerda et al., 1989; Wang et al., 2014), randomly sample the fragments from sets f_1 and f_2 until the desired length of the new SoF is achieved using equation 4.5 :(Figure 4.2).

$$\text{new SoF } (S_{ij}) = \begin{cases} f_{1j} & \text{if } r_j = 0 \\ f_{2j} & \text{if } r_j = 1 \end{cases} \tag{4.5}$$

where r_j is a random integer between 0 and 1 and is sampled at every index of the fragment.

2. To ensure the "mixing" does not violate the unity rule, normalize the new SoF.

The GA-based SoF is representative of the observed ones as these are generated from the existing precipitation patterns within an identified class. At the same time, the "mixing" process results in the creation of unobserved patterns.

159
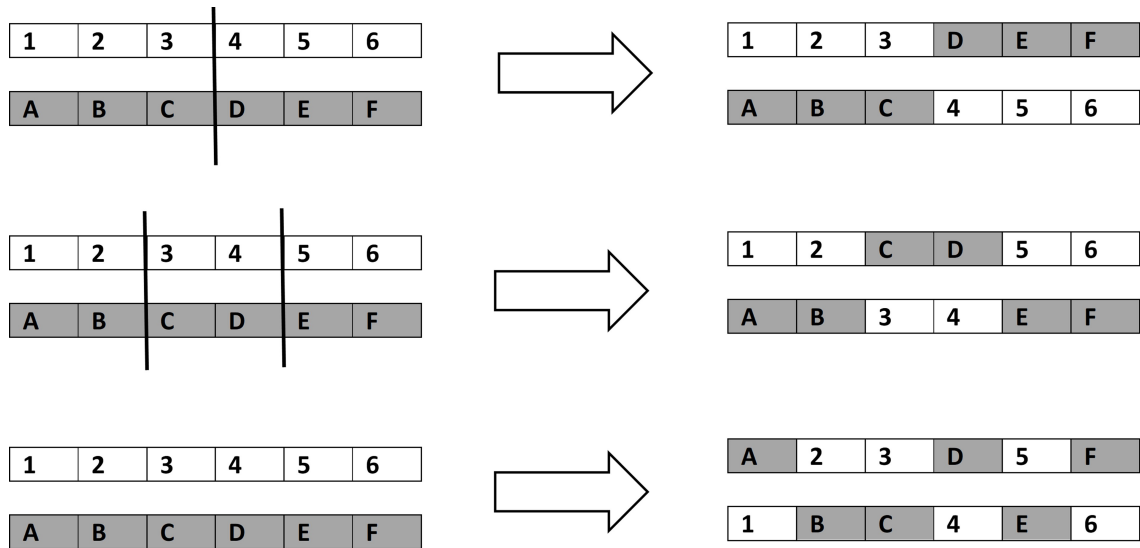
Figure 4.2: A simple schematic (not of precipitation data) showing how the crossover methods operate: One-point (top), Two-point (middle) and Uniform (bottom) crossover methods. 1-6 and A-F represent the fragments in the set. Source: Deb (2001)

4.3 Data Description, Application and Model Assessment

The performance of the proposed I-MoF was evaluated using hourly precipitation data from two locations on the island of Newfoundland and Labrador, Canada. The first station, Ruby Line, is located in the South Coast and Avalon climate zone. This climate zone is characterized by relatively mild winters, although snow cover differs locally (McManus et al., 1991). During the fall season, there is heavy precipitation, and the summers are typically warm (Price et al., 2013). Local physiography and proximity to the sea, affect the climate (Seiler & Zwiers, 2016). The precipitation data spanning ten years (2005-2014) was obtained from the City of St. John's Planning, Engineering and Regulatory Services. Missing data in this record was less than 4%; those days were not included in the analysis. The second station, Corner Brook, is located in the Western Mountains and Central Uplands climate zone. High elevations in this climate zone result in increased cloud cover, intense precipitation, stronger winds, and lower temperatures (McManus et al., 1991). There is also a tendency for more significant snow accumulation as one moves westward (Figure 4.3).

The precipitation record for Corner Brook was chosen to cover the same period as Ruby Line to allow for comparison. As was the case for Ruby Line, days with missing records, about 6%, were omitted from the analysis.

The observed data were divided into nine blocks in assessing the proposed model's sensitivity to available data. Each block represents the daily data with corresponding hourly data available. For the simulation, we used the observational data in each block to create sets of fragments, sample and disaggregate the ten years of daily data by generating an ensemble of 100 realizations of ten years each.

Block 1 =   randomly select 1 year of data
Block 2 =   randomly select 2 years of data
Block 3 =   randomly select 3 years data
.
.
.
Block 9 =   randomly select 9 years of data

The random selection was made without replacement, e.g., block two could not contain 2005 data twice. For stochastic models such as the GA-MOF, the performance measures focus on reproducing statistics instead of the one-to-one correspondence between the simulated and observed values; the model generates an ensemble of simulated values compared to one observation. The statistical metrics commonly used for disaggregation model assessment are mean, standard deviation, lag-1 auto-correlation, dryness and skewness (Pui et al., 2012; Li et al., 2018; Burian et al., 2000). These statistics are determined for each ensemble and presented as boxplots compared to the observed data.

Figure 4.3: Location of study sites in Newfoundland and Labrador

4.4 Results and Discussion

4.4.1 Statistics for Evaluating Disaggregation Models

The mean is the statistic best replicated by the simulated data. With just one year of data, the simulated mean's median is overestimated by 8% at Ruby Line station and 5% at the Corner Brook station. As the number of available block years used to generate the simulated data increases, the difference between the observed and simulated mean approaches zero for both stations (Figure 4.4). The ability of this model to reproduce this statistic may depend on the underlying MoF model. This model can preserve the mean when used for precipitation disaggregation (Pui et al., 2012; Li et al., 2018; Silva & Portela, 2012). Of the three crossover methods used, no one, in particular, outperformed the other in reproducing this statistic.

Similar to the mean, the simulated standard deviation is overestimated. With one year of available data, the simulated mean's median is overestimated by up to 60% for the Ruby Line and Corner Brook stations. This overestimation does not improve as the number of available years of data increases (Figure 4.5-top row). There is a significant reduction (~ 10%) in the overestimation of the simulated standard deviation median when the data are aggregated from the 1-hr timescale to the 12-hr timescale (Figure 4.5-bottom row). The uniform technique produces the least spread and the highest median for both stations in the crossover methods. The overestimation of the standard deviation could be a compounded effect of the previously overestimated simulated mean as well as the random sampling in the crossover methods causing the simulated precipitation values to be more spread out as it samples from within the specified class, which is an additional constraint (Breinl & Di Baldassarre, 2019).

KEY: A = Onepoint crossover; B = Twopoint crossover; C = Uniform crossover
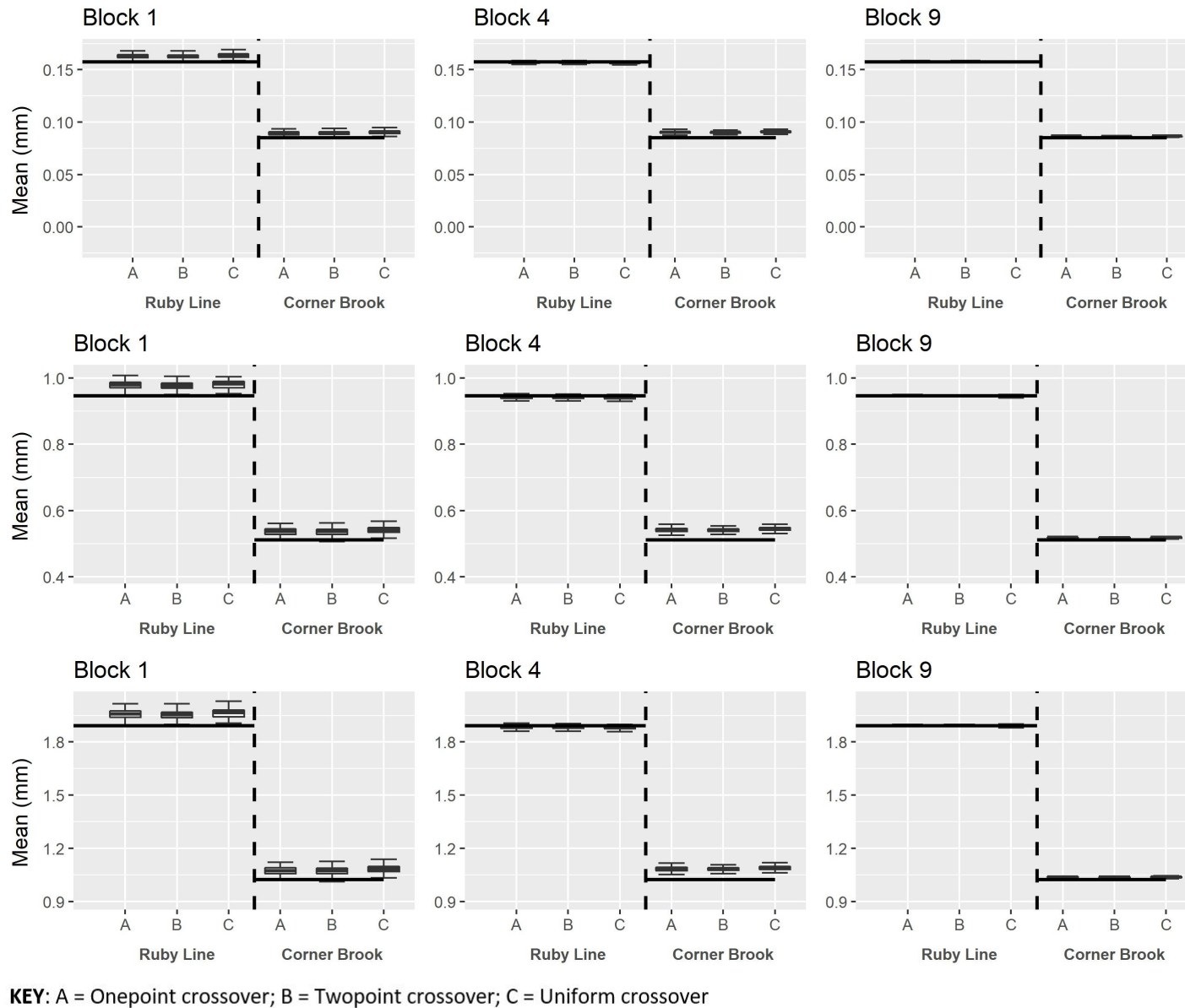
Figure 4.4: Mean of observed (solid line) and disaggregated data for 1 (top), 6 (middle) and 12 (bottom) hours for select blocks of available data (indicated at the top of the boxplot generated from 100 simulation runs). Station name is indicated below the plot
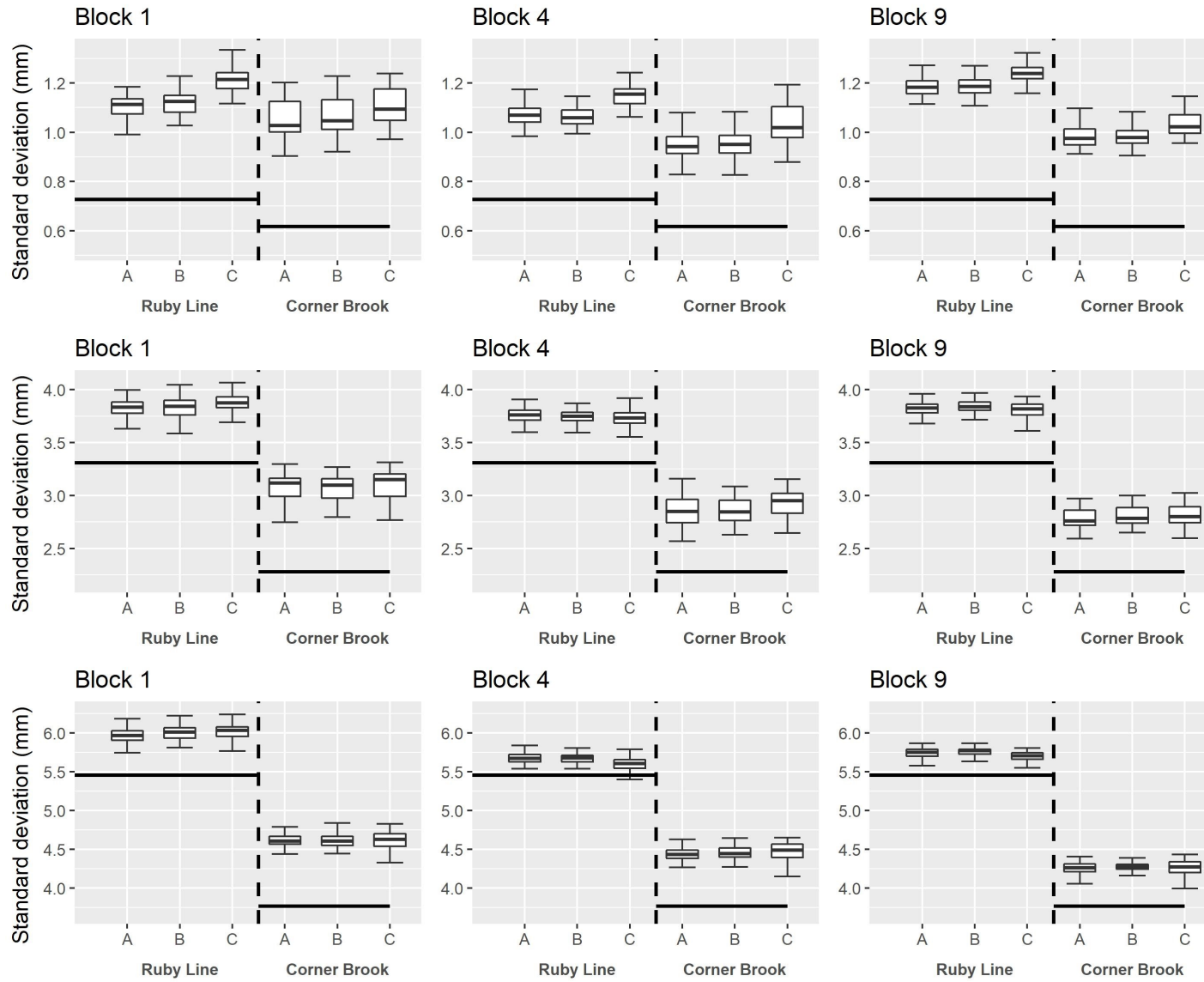
KEY: A = Onepoint crossover; B = Twopoint crossover; C = Uniform crossover

Figure 4.5: Standard deviation of observed (solid line) and disaggregated data for 1 (top), 6 (middle) and 12 (bottom) hours for select blocks of available data (indicated at the top of the boxplot generated from 100 simulation runs). Station name is indicated below the plot

Lag-1 auto-correlation reproduction in the simulated data shows an underestimation compared to the observed values (Figure 4.6). The underestimation is greater for the Ruby Line station than the Corner Brook location. Lag-1 autocorrelation is a statistic that is often difficult to reproduce in disaggregated precipitation (Li et al., 2018). In a study assessing seven disaggregation models' performance, five significantly underestimated the lag-1 autocorrelation, while the other two overestimated it (Hingray & Haha, 2005). Like the other statistics described, the spread in the simulated data decreases with an increase in the number of available years used for the simulation. The underestimation of the lag-1 autocorrelation significantly improves as coarser time steps are used (Figure 4.6-bottom row). The simulated median and observed lag-1 autocorrelation differences decrease by about 50% as one moves from the 1-hr timescale to the 12-hr timescale for the Ruby Line station. However, this improvement is not as significant for the Corner Brook station as the timescale increases from 1-hr to 12-hr (~16%). Similar decreases were found by Li et al. (2018) as timescales were aggregated from 1-hr to 12-hr. Following the mean's pattern, no specific crossover method performs better than the other.

Replication of skewness in the simulated data was also overestimated by about 30% and 10% at the Ruby Line and Corner Brook stations, respectively (Figure 4.7). Comparable with the standard deviation, the overestimation of the skewness does not improve as the number of available years increases. However, there is a significant improvement as the aggregation levels increase for the Ruby Line station (6%). The opposite effect occurs at the Corner Brook station, where the overestimation increases by 10% with an increase in aggregation level. The opposite effect occurs at the Corner Brook station, where the overestimation increases by 10% with an increase in aggregation level. A possible explanation for the overestimated skewness could be that the proposed model with its coupling features underestimates dry periods (Mezghani & Hingray, 2009; Paschalis et al., 2014).
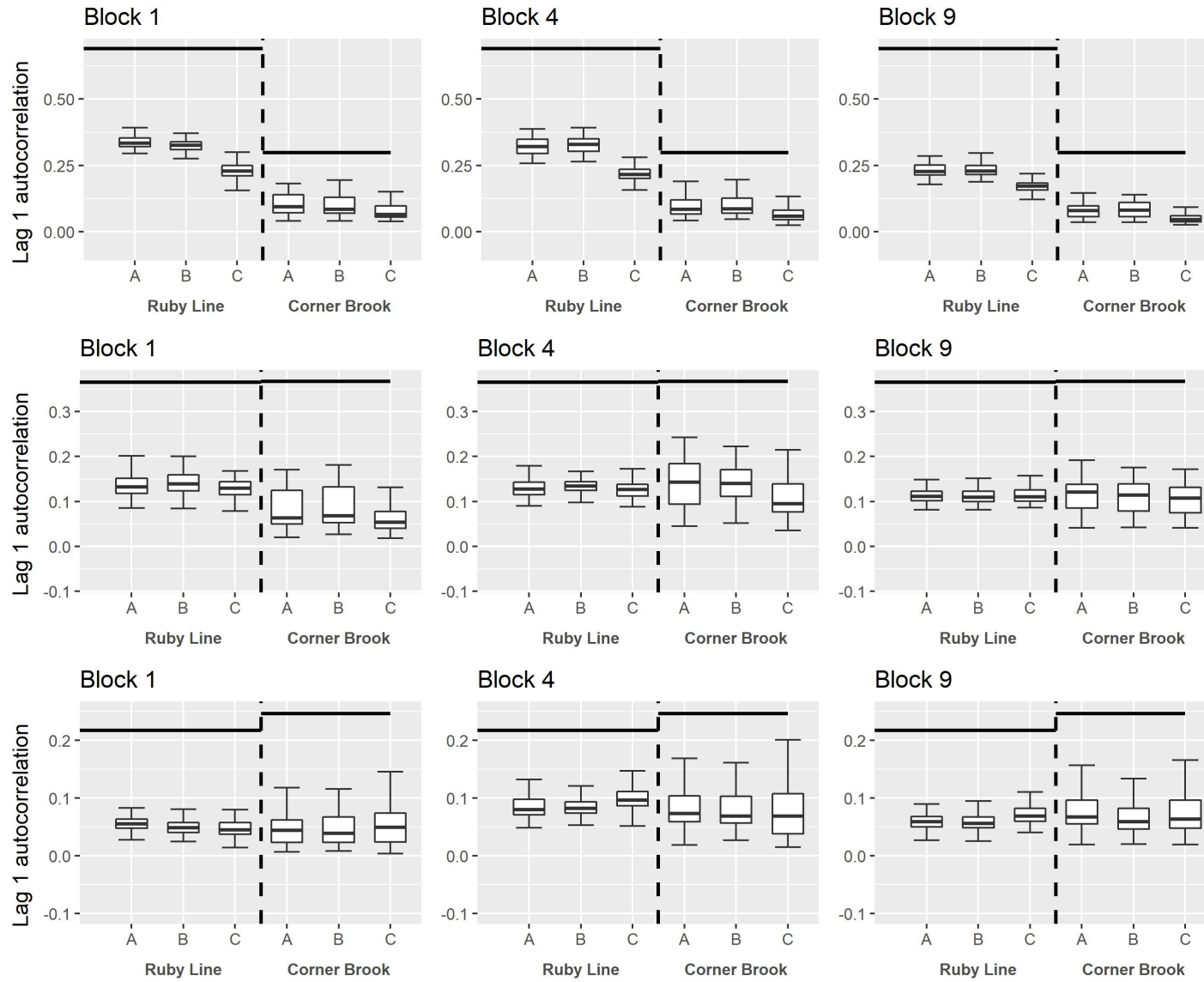
KEY: A = Onepoint crossover; B = Twopoint crossover; C = Uniform crossover

Figure 4.6: Lag-1 autocorrelation of observed (solid line) and disaggregated data for 1 (top), 6 (middle) and 12 (bottom) hours for select blocks of available data (indicated at the top of the boxplot generated from 100 simulation runs). Station name is indicated below the plot
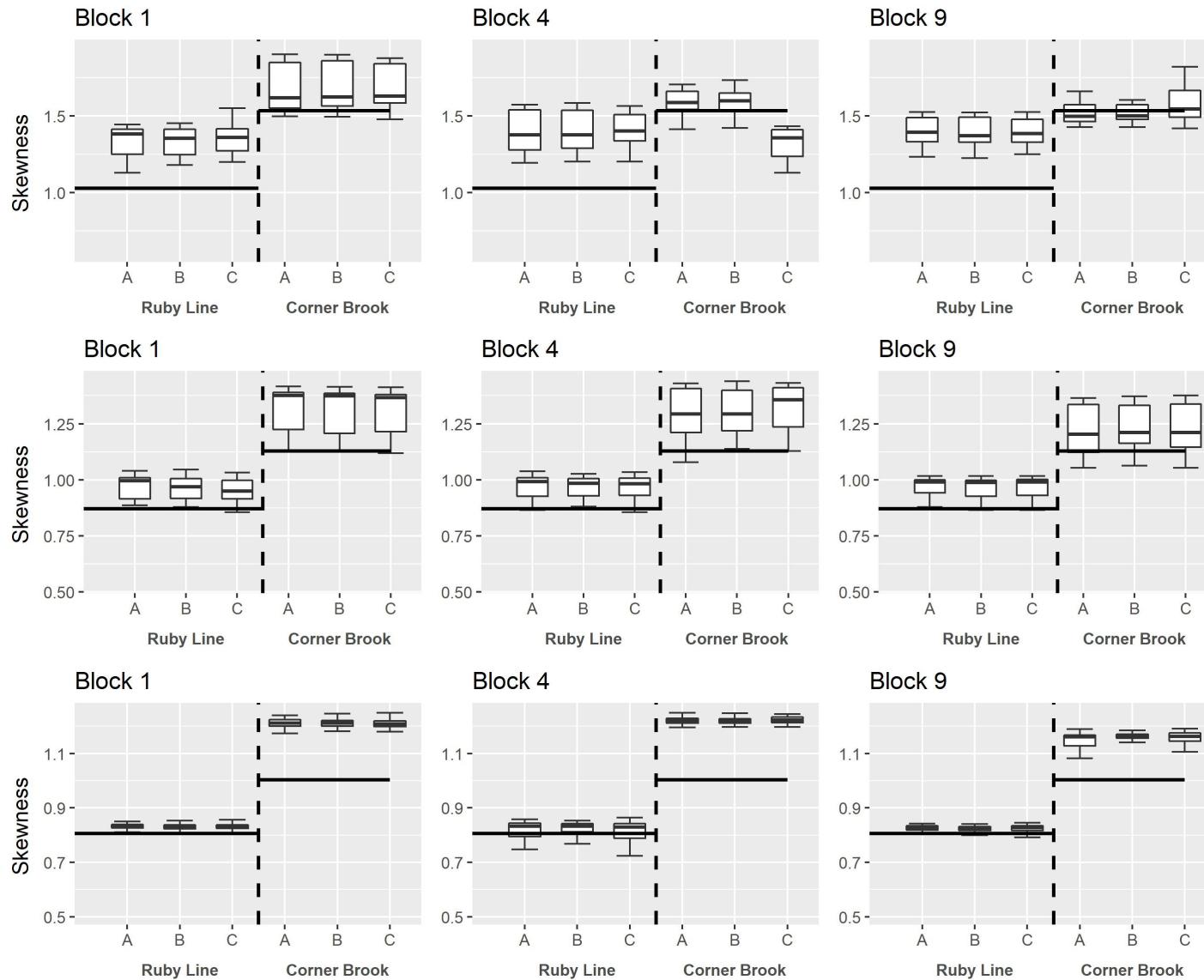
KEY: A = Onepoint crossover; B = Twopoint crossover; C = Uniform crossover

Figure 4.7: Skewness of observed (solid line) and disaggregated data for 1 (top), 6 (middle) and 12 (bottom) hours for select blocks of available data (indicated at the top of the boxplot generated from 100 simulation runs). Station name is indicated below the plot

Dryness proportion refers to periods with no precipitation. For the 1-hour time series, both stations underestimate the dryness proportion by about 40% for the one block of available data (Figure 4.8). This underestimation reduced to less than 5% as the number of available years used for the simulation increased. Increasing the aggregation levels also did improve the dryness proportion for both stations. The uniform crossover method produced the largest underestimations for dryness proportion across both the increasing number of available data and aggregation levels.

The simple random sampling from the uniform distribution in this proposed model may influence the reproduced statistics. Implementing more sophisticated sampling methods capable of maintaining the distribution within a dataset, such as the generalized extreme value distribution (GEV) with Schwartz Information Criterion (SIC), may improve the overall statistics (Arfa et al., 2021). The differences in the climate zones of the study stations appeared to have minimal impact on the model's performance. A statistic that was underestimated in Ruby Line, which is in the South Coast and Avalon climate zone, was also underestimated in Corner Brook, located in the Western Mountains and Central Uplands climate zone. The advantage of the GA-MoF over the MoF with the k-nearest neighbour is its applicability in regions where fine-scale data are limited to produce reasonable estimates of standard statistics.
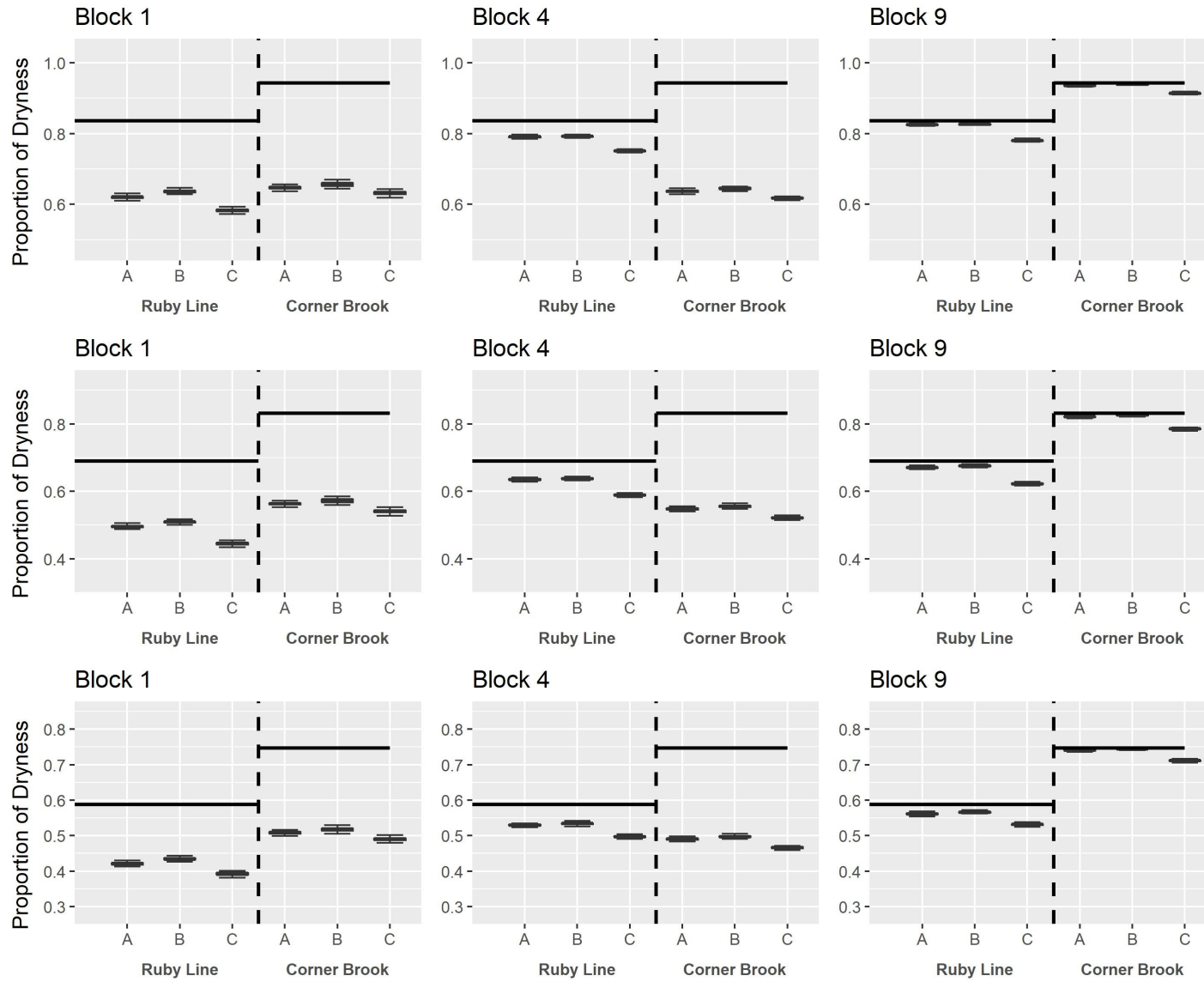
KEY: A = Onepoint crossover; B = Twopoint crossover; C = Uniform crossover

Figure 4.8: Dryness propoertion of observed (solid line) and disaggregated data for 1 (top), 6 (middle) and 12 (bottom) hours for select blocks of available data (indicated at the top of the boxplot generated from 100 simulation runs). Station name is indicated below the plot

4.4.2 Inter-Day Connectivity and Intra-Day Wet and Dry Spells

Another essential quality of precipitation disaggregation models is their ability to preserve inter-day dependence in the simulated data. To embed this trait in the GA-MoF models, the coarse-scale precipitation, whose fragments will be used to disaggregate the precipitation depth in question, needs to have the same previous and next-day wetness state also known as the state-based approach. The approach developed by Westra et al. (2012) and implemented by Li et al. (2018) enhances inter-day connectivity reproduction in the simulated data. Tables 4.1 and 4.2 show the ratios of inter-day connectivity for select data blocks for the Ruby Line and Corner Brook stations respectively. The joint probability is presented in the first four rows.

For the available 1-year data block, all three crossover methods overestimate the first two rows, with the highest overestimation occurring under the uniform crossover method for the Ruby Line station. The opposite trend is observed at the Corner Brook station. All three crossover methods underestimate the first two rows, with the highest underestimation occurring with the two-point crossover method. As the available data block years increase, one-point and two-point crossover GA-MoF models tend to underestimate the first two rows and overestimate the last two rows with the uniform crossover model. On the other hand, the values in the first four rows at Ruby Line station are approximated well. For the Corner Brook location, the underestimation persists in the one-point and two-point crossover methods for the first two rows and overestimation for the last two rows with the uniform crossover model reproducing the first four rows well.

The variation in the simulated ratios of inter-day connectivity could be due to the random process used in generating the new SoF. There is no rule restricting how the sampling process takes place and does not ensure the preservation of the inter-day connectivity. One way to address this would be to constrain the sampling process such that the new fragments created will need to ensure that the first and last hours remain wet if that day is wet. The

additional conditioning might help to improve these connections. However, increasing the

computational time of the model is a possibility. The last row of Tables 4.1 and 4.2 show the

joint probability where, given that day t and $t+1$ are wet, the last hour of day t and the first

hour of day $t+1$ are also wet. All three GA-MoF models appear to underestimate this joint

probability at both stations. Similar results were obtained by Li et al. (2018) and Westra

et al. (2012) where the use of the state-based approach did not maintain the connection

between the last hour of a day and the first hour of the next day.

Table 4.1: Ratios of inter-day connectivity for Ruby Line station

Joint Probability	Observed(%)	GA-MoF(%)		
		Onepoint crossover	Twopoint crossover	Uniform crossover
Block 1				
$P(X_{t,24} > 0, D_{t+1} > 0 \mid D_t > 0)$	19.03	20.9	20.68	25.85
$P(X_{t,24} > 0, D_{t+1} = 0 \mid D_t > 0)$	9.68	10.45	10.45	13.09
$P(X_{t,24} = 0, D_{t+1} > 0 \mid D_t > 0)$	47.30	35.75	36.30	30.91
$P(X_{t,24} = 0, D_{t_1} = 0 \mid D_t > 0)$	24.09	17.93	18.26	15.62
$P(X_{t,24} > 0, D_{t+1,1} > 0 \mid D_t > 0, D_{t+1} > 0)$	3	0.33	0.22	0.55
Block 5				
$P(X_{t,24} > 0, D_{t_1} > 0 \mid D_t > 0)$	19.03	14.63	14.63	19.03
$P(X_{t,24} > 0, D_{t_1} = 0 \mid D_t > 0)$	9.68	7.48	7.48	9.79
$P(X_{t,24} = 0, D_{t_1} > 0 \mid D_t > 0)$	47.30	49.28	49.39	45.10
$P(X_{t,24} = 0, D_{t_1} = 0 \mid D_t > 0)$	24.09	25.41	25.52	23.21
$P(X_{t,24} > 0, D_{t+1,1} > 0 \mid D_t > 0, D_{t+1} > 0)$	3	0.66	0.55	1.10
Block 9				
$P(X_{t,24} > 0, D_{t_1} > 0 \mid D_t > 0)$	19.03	14.74	14.85	19.14
$P(X_{t,24} > 0, D_{t_1} = 0 \mid D_t > 0)$	9.68	7.48	7.48	9.79
$P(X_{t,24} = 0, D_{t_1} > 0 \mid D_t > 0)$	47.30	51.26	51.15	46.64
$P(X_{t,24} = 0, D_{t_1} = 0 \mid D_t > 0)$	24.09	25.96	25.96	23.65
$P(X_{t,24} > 0, D_{t+1,1} > 0 \mid D_t > 0, D_{t+1} > 0)$	3	0.55	0.44	0.88

The joint probability, summing up to 100%, of the last hour of day t and the next day $t+1$
being dry (=0)/wet (>0) given that day t is wet is presented in the first four rows. The last
row shows the joint probability where given that day t and $t+1$ are wet, the last hour of day
t and the first hour of day $t+1$ are also wet.

A good disaggregation model will maintain the natural disruption inherent in precipi-

tation data. A within-day dry/wet spell is defined as continuous sub-daily durations of no

Table 4.2: Ratios of inter-day connectivity for the Corner Brook station

Joint Probability	Observed(%)	GA-MoF(%)		
		Onepoint crossover	Twopoint crossover	Uniform crossover
1-year data block				
$P(X_{t,24} > 0, D_{t+1} > 0\|D_t > 0)$	9.57	7.04	6.93	8.91
$P(X_{t,24} > 0, D_{t+1} = 0\|D_t > 0)$	5.61	3.96	3.85	4.95
$P(X_{t,24} = 0, D_{t+1} > 0\|D_t > 0)$	53.24	47.74	47.96	45.98
$P(X_{t,24} = 0, D_{t_1} = 0\|D_t > 0)$	31.57	26.84	26.95	25.85
$P(X_{t,24} > 0, D_{t+1,1} > 0\|D_t > 0, D_{t+1} > 0)$	1	0.11	0.00	0.11
5-years data block				
$P(X_{t,24} > 0, D_{t_1} > 0\|D_t > 0)$	9.57	8.80	8.80	12.43
$P(X_{t,24} > 0, D_{t_1} = 0\|D_t > 0)$	5.61	5.06	5.06	7.15
$P(X_{t,24} = 0, D_{t_1} > 0\|D_t > 0)$	53.24	52.03	52.03	48.62
$P(X_{t,24} = 0, D_{t_1} = 0\|D_t > 0)$	31.57	29.92	29.92	27.94
$P(X_{t,24} > 0, D_{t+1,1} > 0\|D_t > 0, D_{t+1} > 0)$	1	0.33	0.33	0.66
9-years data block				
$P(X_{t,24} > 0, D_{t_1} > 0\|D_t > 0)$	9.57	6.6	6.6	9.13
$P(X_{t,24} > 0, D_{t_1} = 0\|D_t > 0)$	5.61	3.96	3.96	5.39
$P(X_{t,24} = 0, D_{t_1} > 0\|D_t > 0)$	53.24	55.55	55.77	52.80
$P(X_{t,24} = 0, D_{t_1} = 0\|D_t > 0)$	31.57	33.11	33.22	31.46
$P(X_{t,24} > 0, D_{t+1,1} > 0\|D_t > 0, D_{t+1} > 0)$	1	0.33	0.22	0.33

The joint probability, summing up to 100%, of the last hour of day t and the next day $t+1$ being dry (=0)/wet (>0) given that day t is wet is presented in the first four rows. The last row shows the joint probability where given that day t and $t+1$ are wet, the last hour of day t and the first hour of day $t+1$ are also wet.

precipitation/precipitation within a dry/wet day. Tables 4.3 to 4.6 show the average length and number of monthly dry and wet spells for the two stations. All three GA-MoF models could reproduce the length of dry/wet spells of the observed precipitation, with underestimations and overestimations occurring for some months at both stations. There was no trend in the under and overestimations. The occurrence of overestimations and underestimations in the simulated data may be due to the imperfect reproduction of the proportion of dryness by the GA-MoF models. The GA-MoF models reproduced well the average number of dry and wet spells at the Ruby Line and Corner Brook stations.

Table 4.3: Average length of monthly dry and wet spells for Ruby Line station

Month	Observed (mm)	GA-MoF-OC 3yr (mm)	GA-MoF-TC 3yr (mm)	GA-MoF-UC 3yr (mm)	GA-MoF-OC 7yr (mm)	GA-MoF-TC 7yr (mm)	GA-MoF-UC 7yr (mm)
			Average length of dry spell				
Jan	13.6	12.3	12.5	11.5	12.3	12.3	11.5
Feb	14.2	13	13	12.6	13	13	12.6
Mar	13.8	14.2	14.5	13	12.9	13	11.6
Apr	13.6	12.6	12.7	11.9	12.1	12.3	11.5
May	14.1	14.8	15	13.1	13.1	13.2	11.7
Jun	13.7	13.5	13.5	12.5	13.3	13.4	12.7
Jul	14.2	11.7	11.7	10.5	11.6	11.7	10.7
Aug	13.7	13.1	13.1	11.8	14.7	14.7	13.4
Sep	12.6	14	14	12.3	15.2	15.2	13.5
Oct	11.6	9.6	9.7	8.9	10.1	10.1	9.5
Nov	11.6	5.9	6	7	6.7	6.7	6.7
Dec	12.5	12.1	12.2	12.1	10.1	10.1	10.1
			Average length of wet spell				
Jan	5.8	4.3	4.3	5	4.8	4.8	5.5
Feb	6	7.7	7.7	9	7.7	7.7	8.9
Mar	5.8	3.3	3.4	3.6	3	3.1	3.4
Apr	6.2	5.2	5.2	6	4.7	4.8	5.4
May	5.4	4.3	4.4	4.8	5	5	5.9
Jun	4.6	4.2	4.2	4.7	4.1	4.1	4.6
Jul	4.2	3.9	3.8	4	3.5	3.5	3.8
Aug	4.5	2.3	2.3	2.2	2.2	2.2	2.2
Sep	4.9	3	3	2.9	2.7	2.7	2.8
Oct	5.5	4.2	4.2	4.7	4.5	4.5	5.1
Nov	5.5	8	8.1	9.3	8	8	8
Dec	5.8	5.4	5.4	5.4	5.6	5.6	5.6

4.4.3 Extreme Values

The disaggregation method's ability to capture the annual maximum precipitation data distribution was evaluated for the 1, 6 and 12-hour aggregation levels. The annual exceedance probability (AEP) of these extreme values is estimated using the Weibull plotting position formula

$$AEP = \frac{m}{N + 1} \tag{4.6}$$

174

Table 4.4: Average length of monthly dry and wet spells for Corner Brook station

Month	Observed (mm)	GA-MoF-OC 3yr (mm)	GA-MoF-TC 3yr (mm)	GA-MoF-UC 3yr (mm)	GA-MoF-OC 7yr (mm)	GA-MoF-TC 7yr (mm)	GA-MoF-UC 7yr (mm)
			Average length of dry spell				
Jan	12.4	10.0	10.0	9.1	10.7	10.8	9.6
Feb	13.8	16.3	16.3	14.9	16.3	16.3	14.9
Mar	15.8	15.3	15.3	14.2	15.3	15.4	14.1
Apr	17.4	17.9	17.7	17.0	17.6	17.6	16.2
May	16.6	16.0	16.1	15.3	13.2	13.1	12.3
Jun	16.8	18.7	18.7	18.6	15.9	15.9	16.0
Jul	17.9	18.8	18.6	18.8	21.1	21.1	20.4
Aug	17.7	19.1	18.9	19.2	17.7	17.7	17.6
Sep	17.1	17.4	17.6	16.7	15.7	15.7	14.3
Oct	15.8	16.6	16.5	14.7	14.9	14.9	13.2
Nov	13.8	10.5	10.4	10.3	12.0	12.0	11.7
Dec	13.0	16.4	16.6	15.7	16.9	17	16.1
			Average length of wet spell				
Jan	3.8	2.5	2.5	2.7	2.8	2.8	2.8
Feb	3.6	2.3	2.3	2.4	2.5	2.5	2.4
Mar	3.6	2.3	2.3	2.4	2.3	2.3	2.4
Apr	4.2	2.3	2.1	2.6	2.3	2.2	2.7
May	3.5	4.6	4.2	4.3	2.0	2.0	2.1
Jun	3.6	5.2	5.3	5.3	4.6	4.5	4.5
Jul	3	2.6	2.6	2.7	2.5	2.5	2.4
Aug	3.4	2.9	3.0	3.1	3.0	3.1	3.0
Sep	3.8	3.8	3.8	3.9	2.8	2.8	2.8
Oct	3.3	2.3	2.3	2.3	2.5	2.5	2.6
Nov	4.5	5.1	5.1	5.8	5.4	5.4	6.1
Dec	4.1	2.0	2.0	2.0	2.0	2.0	2.0

where m is the rank of the extreme value sorted in descending order and N is the number of data years. Capturing the annual maximum precipitation distribution is essential to the engineering community as such information is used to develop IDF curves for engineering design. Generally, the distribution of the annual maximum values of the observed data lies between the 5th and 95th percentile values of the simulated annual maximum values for all three GA-MoF models at both stations. Similar findings were obtained for all aggregation

Table 4.5: Average number of monthly dry and wet spells for Ruby Line station

Month	Observed (mm)	GA-MoF-OC 3yr (mm)	GA-MoF-TC 3yr (mm)	GA-MoF-UC 3yr (mm)	GA-MoF-OC 7yr (mm)	GA-MoF-TC 7yr (mm)	GA-MoF-UC 7yr (mm)
			Average number of dry spell				
Jan	2.3	2.3	2.3	2.4	2.5	2.5	2.5
Feb	2.2	2.0	2	2	2	2	2
Mar	2.3	2.3	2.3	2.3	2.4	2.3	2.5
Apr	2.3	2.2	2.2	2.2	2.3	2.2	2.3
May	2.3	2	2	2	2.3	2.3	2.4
Jun	2.4	2.3	2.3	2.4	2.4	2.4	2.4
Jul	2.3	2.8	2.8	2.8	2.7	2.7	2.7
Aug	2.4	2.6	2.6	2.9	2.3	2.3	2.5
Sep	2.5	2.7	2.7	2.7	2.3	2.3	2.4
Oct	2.5	3	3	2.9	2.7	2.7	2.6
Nov	2.4	2.5	2.4	2.5	2.3	2.3	2.3
Dec	2.3	2.3	2.3	2.3	2.7	2.7	2.7
			Average number of wet spell				
Jan	2.2	2.3	2.2	2.4	2.2	2.1	2.3
Feb	2.1	2	2.2	2	2.1	2.1	2
Mar	2.3	2	2	2.1	2	2	2.2
Apr	2.3	2.3	2.4	2.5	2.4	2.4	2.6
May	2.1	2.1	2.1	2.2	2.1	2	2.2
Jun	2.3	2	2	2.1	2.2	2.3	2.5
Jul	2.3	2.1	2	2.5	2.5	2.5	2.7
Aug	2.4	2	2	2.1	2	2	2.1
Sep	2.4	2	2	2	2	2	2
Oct	2.3	2.2	2.2	2.4	2.3	2.3	2.5
Nov	2.4	2.2	2.1	2	2	2	2
Dec	2.3	2	2	2	2.6	2.6	2.6

levels, except for the 6-hour aggregation level where the observed annual maximum values tend to lie on the 5th percentile of the simulated annual maximum values (Figures 4.9-4.14). There appears to be a greater spread in the simulated maximum values at Ruby Line than at the Corner Brook location. This could be due to the difference in dominant rainfall patterns at the different locations. A study by Amponsah et al. (2019) showed that the dominant rainfall pattern in the South Coast and Avalon region tends to have more than half

Table 4.6: Average number of monthly dry and wet spells for Corner Brook station

Month	Observed (mm)	GA-MoF-OC 3yr (mm)	GA-MoF-TC 3yr (mm)	GA-MoF-UC 3yr (mm)	GA-MoF-OC 7yr (mm)	GA-MoF-TC 7yr (mm)	GA-MoF-UC 7yr (mm)
			Average number of dry spell				
Jan	2.7	3.4	3.5	3.6	3.3	3.3	3.4
Feb	2.5	2.0	2.0	2.3	2.0	2.0	2.3
Mar	2.5	2.6	2.5	2.7	2.6	2.5	2.7
Apr	2.3	2.4	2.4	2.4	2.3	2.3	2.5
May	2.4	2.5	2.4	2.6	3.2	3.3	3.5
Jun	2.4	2.0	2.1	2.0	4.0	4.0	4.0
Jul	2.4	2.4	2.4	2.4	2.0	2.0	2.0
Aug	2.4	2.2	2.2	2.2	2.0	2.0	2.0
Sep	2.3	2.2	2.2	2.2	2.6	2.6	2.9
Oct	2.5 2.3	2.3	2.7	2.7	2.7	3.1	
Nov	2.6	3.4	3.4	3.2	3.0	3.0	2.9
Dec	2.6	.0	2.0	2.2	2.0	2.0	2.1
			Average number of wet spell				
Jan	2.4	2.0	2.0	2.2	2.0	2.0	2.3
Feb	2.4	2.0	2.0	2.1	2.2	2.2	2.3
Mar	2	2.0	2.0	2.3	2.0	2.0	2.3
Apr	2	2.3	2.4	2.4	2.4	2.4	2.3
May	2.7	2.0	2.0	2.1	2.3	2.2	2.0
Jun	2.3	2.0	2.0	2.0	2.0	2.0	2.0
Jul	2.2	3.0	3.0	3.0	2.1	2.1	2.1
Aug	2.0	2.0	2.0	2.0 2.1	2.0	2.1	
Sep	2.2	2.3	2.3	2.4	2.5	2.5	2.0
Oct	2.5	2.3	2.3	2.0	2.2	2.2	2.0
Nov	2.1	2.0	2.0	2.1	2.0	2.0	2.1
Dec	2.1	2.0	2.0	2.1	2.0	2.0	2.1

of the total event depth occurring in the first half of the event's duration. At the same time, the reverse is true for rainfall patterns in the Western Mountains and Central Uplands.

4.5 Conclusion

This study proposed a new precipitation disaggregation model for data-scare regions. The model involves coupling a crossover method with an interval-based MoF model to generate long-term continuous synthetic precipitation data. The crossover method generates sets of fragments for resampling that did not previously exist in the data set. The fragment generation process was tested using three different methods: one-point, two-point and uniform crossover. The available data from which the sets of fragments were created ranged from one to nine years. The crossover methods reproduced statistics found in the observed data using data generated from the fragmentation process. The mean, standard deviation and skewness were typically overestimated, while lag-1 autocorrelation and dryness proportion were underestimated. Annual maximum exceedance probability curves developed from the simulated data's annual maximum precipitation were well within the range of the observed values. The outcome of this proposed modification makes it applicable to locations with as little as one year of data available to obtain an estimate of IDF curves for infrastructure development. Application of the technique to other time series such as streamflow can be explored and extension to multiple sites.
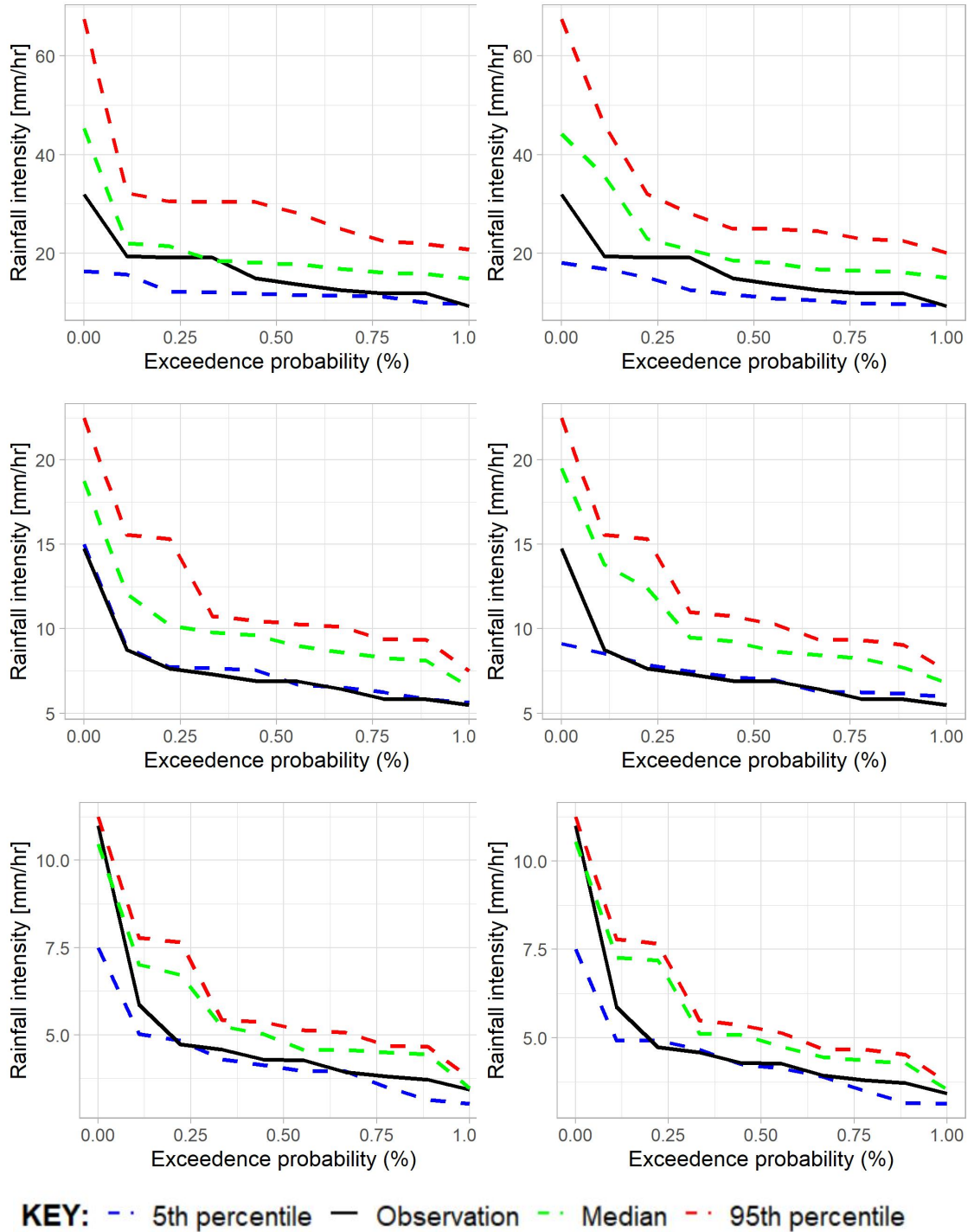
Figure 4.9: Intensities of annual maximum precipitation for 1 (top row), 6 (middle row) and 12-hr (bottom row) aggregation levels against exceedence probability using the GA-MoF Onepoint crossover disaggregation model for select blocks of data at the Ruby Line station.

179

Block 2   Block 8

KEY: -- 5th percentile —— Observation -- Median -- 95th percentile
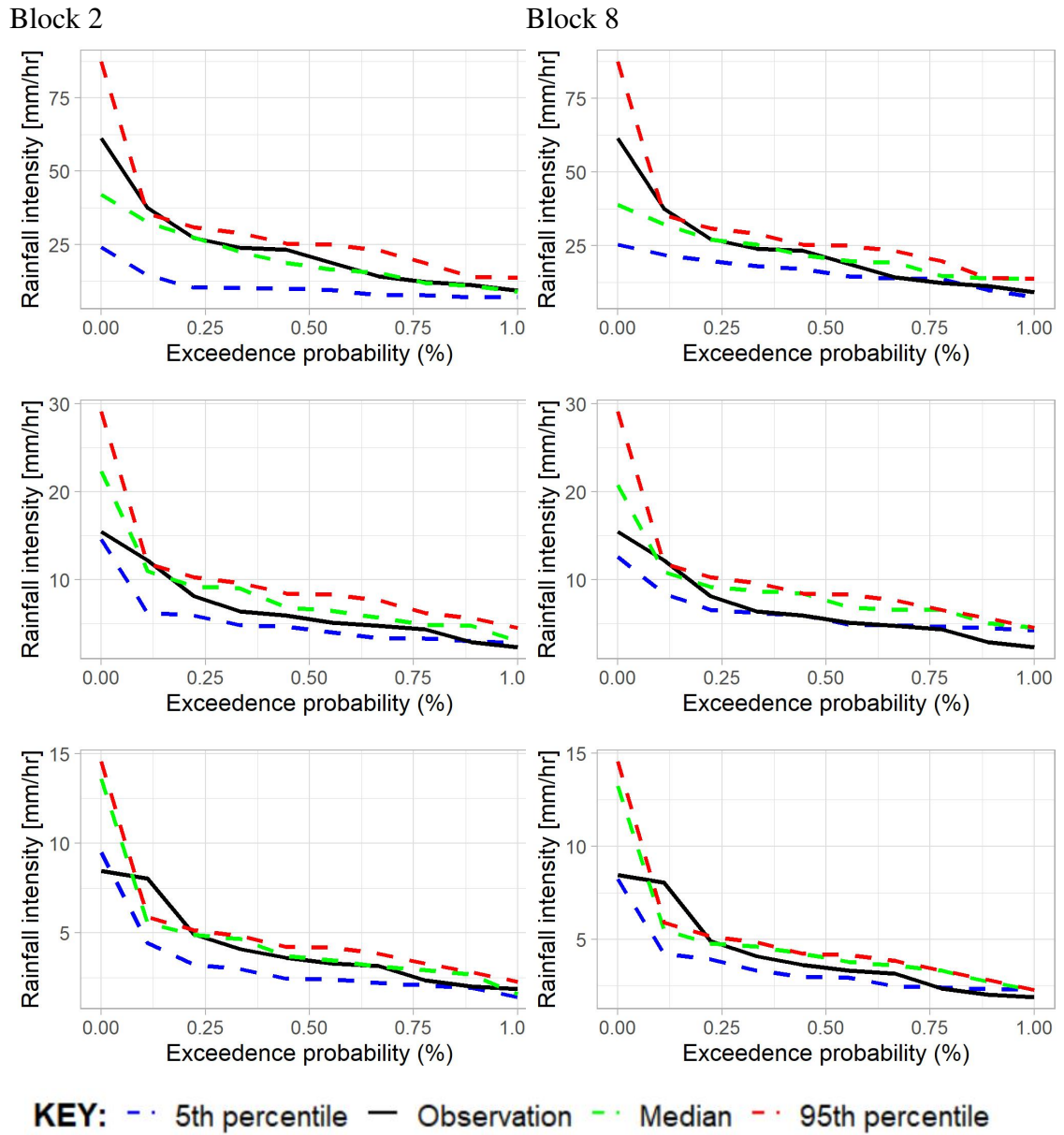
Figure 4.10: Intensities of annual maximum precipitation for 1 (top row), 6 (middle row) and 12-hr (bottom row) aggregation levels against exceedence probability using the GA-MoF Onepoint crossover disaggregation model for select blocks of data at the Corner Brook station.

Figure 4.11: Intensities of annual maximum precipitation for 1 (top row), 6 (middle row) and 12-hr (bottom row) aggregation levels against exceedence probability using the GA-MoF Twopoint crossover disaggregation model for select blocks of data at the Ruby Line station.

Block 2 Block 8
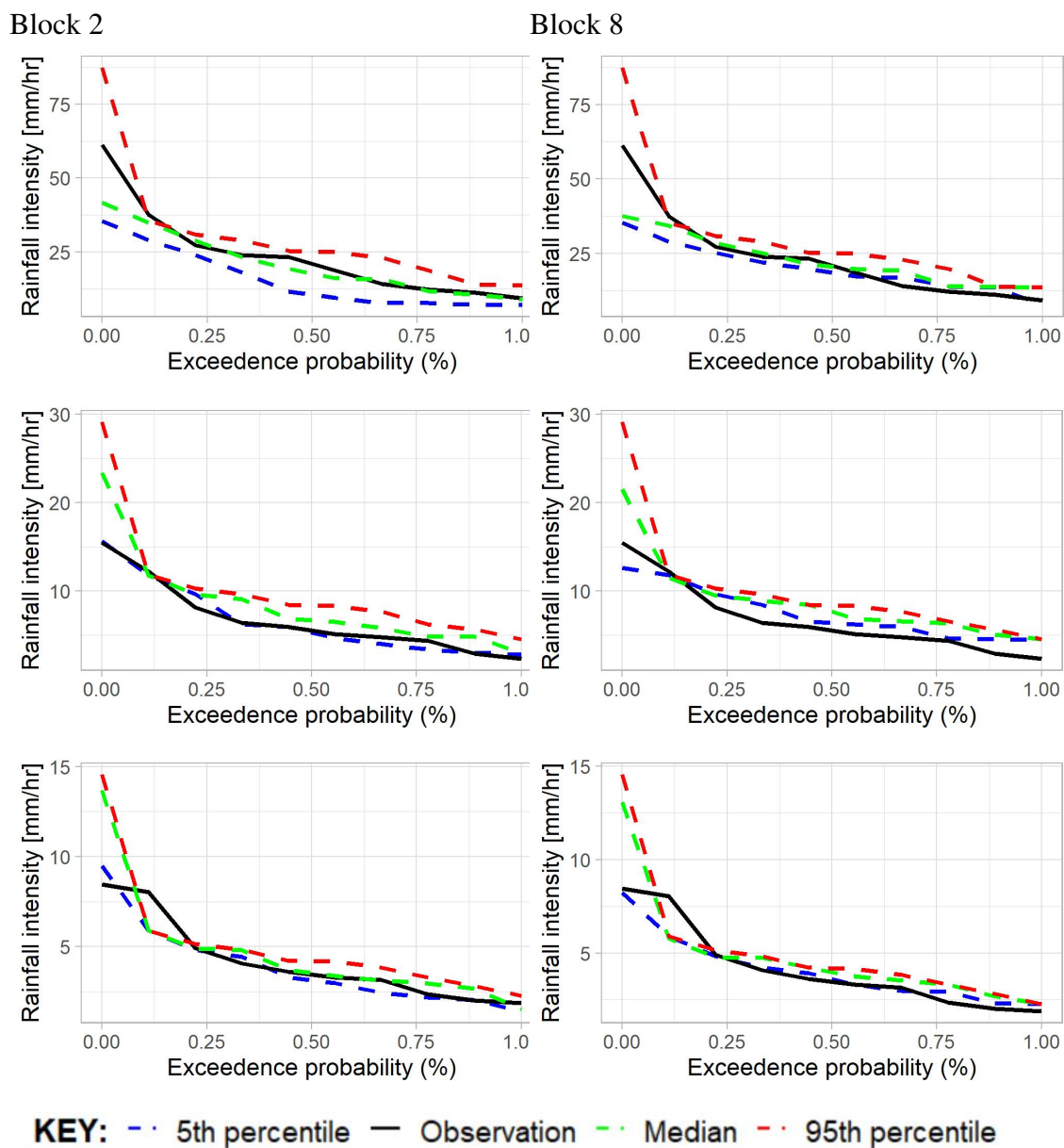
Figure 4.12: Intensities of annual maximum precipitation for 1 (top row), 6 (middle row) and 12-hr (bottom row) aggregation levels against exceedence probability using the GA-MoF Twopoint crossover disaggregation model for select blocks of data at the Corner Brook station.

Block 2

Block 8
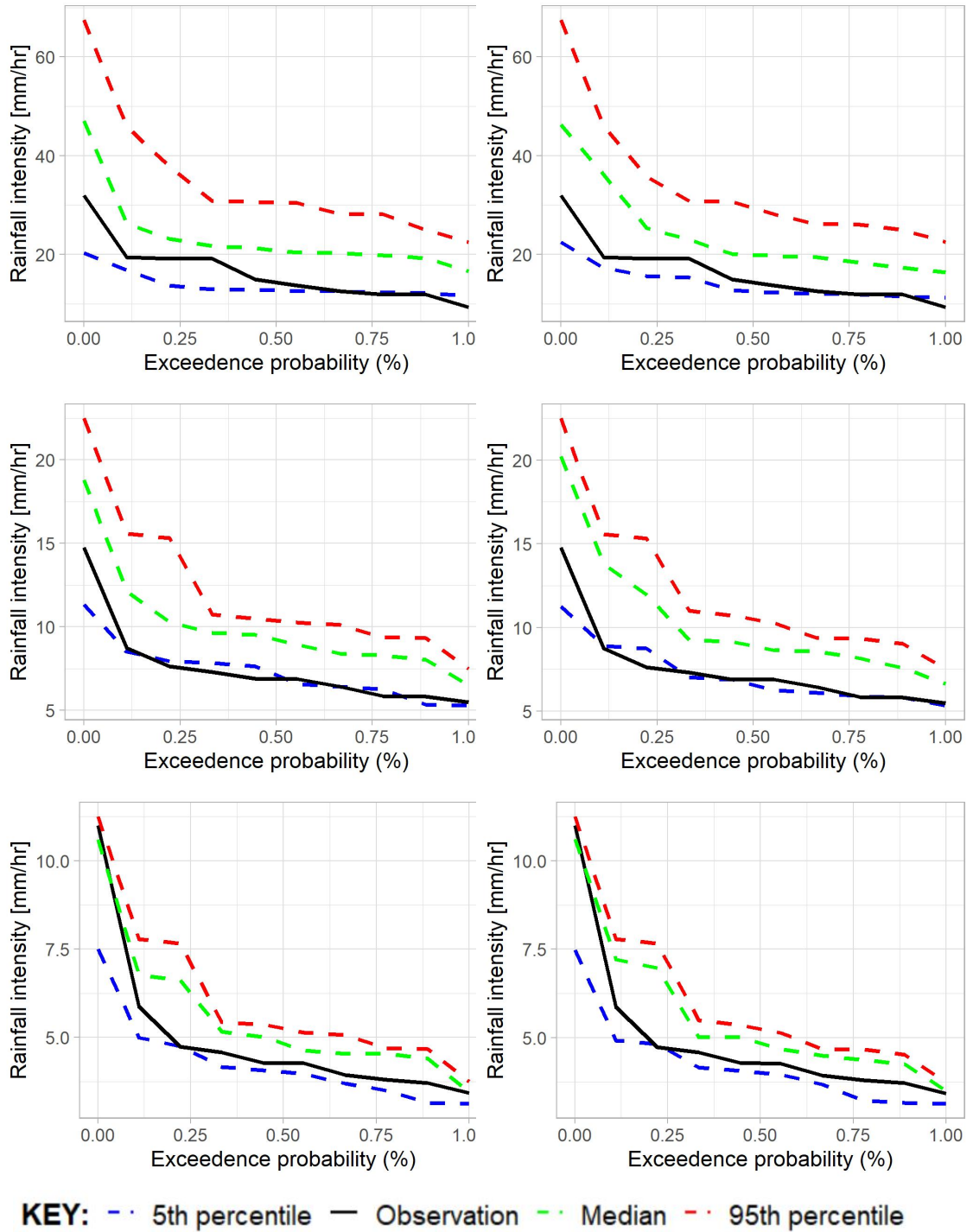
Figure 4.13: Intensities of annual maximum precipitation for 1 (top row), 6 (middle row) and 12-hr (bottom row) aggregation levels against exceedence probability using the GA-MoF Uniform crossover disaggregation model for select blocks of data at the Ruby Line station.

Block 2   Block 8
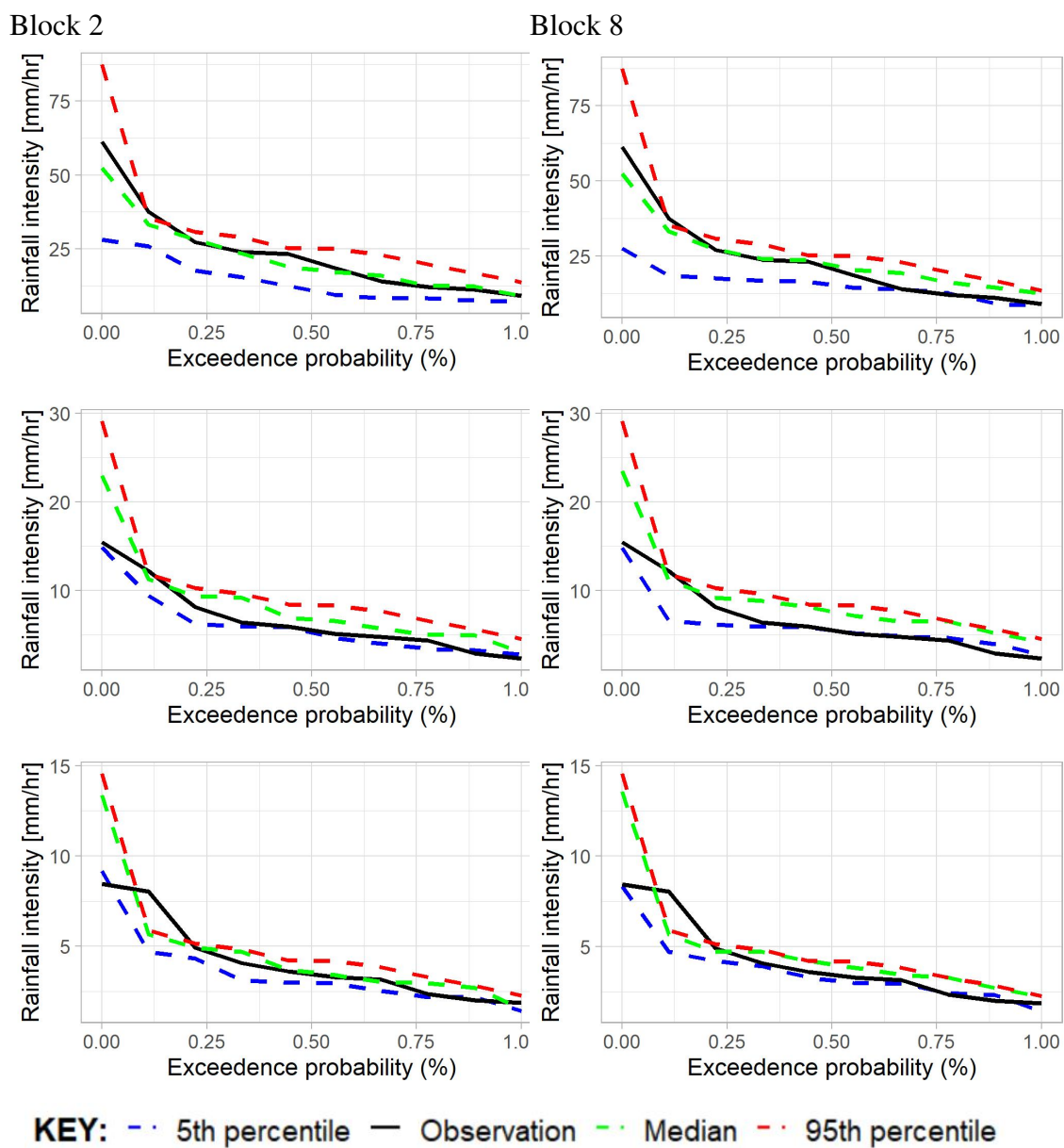
Figure 4.14: Intensities of annual maximum precipitation for 1 (top row), 6 (middle row) and 12-hr (bottom row) aggregation levels against exceedence probability using the GA-MoF Uniform crossover disaggregation model for select blocks of data at the Corner Brook station.

References

Aguilar, M. G. d., & Costa, V. A. F. (2020). A regional similarity-based approach for sub-daily rainfall nonparametric generation. *RBRH*, *25*.

Amponsah, A. O., Daraio, J. A., & Khan, A. A. (2019). Implications of climatic variations in temporal precipitation patterns for the development of design storms in newfoundland and labrador. *Canadian Journal of Civil Engineering*(ja).

Arfa, S., Nasseri, M., & Tavakol-Davani, H. (2021). Comparing the effects of different daily and sub-daily downscaling approaches on the response of urban stormwater collection systems. *Water Resources Management*, *35*(2), 505–533.

Babovic, V. (2009). Introducing knowledge into learning based on genetic programming. *Journal of Hydroinformatics*, *11*(3-4), 181–193.

Babović, V., & Wu, Z. (1975). Calibrating hydrodynamic models by means of simulated evolution. *Criterion*, *1*.

Bala, A., & Sharma, A. K. (2015). A comparative study of modified crossover operators. In *2015 third international conference on image information processing (iciip)* (pp. 281–284).

Breinl, K., & Di Baldassarre, G. (2019). Space-time disaggregation of precipitation and temperature across different climates and spatial scales. *Journal of Hydrology: Regional Studies*, *21*, 126–146.

Breinl, K., Strasser, U., Bates, P., & Kienberger, S. (2017). A joint modelling framework

for daily extremes of river discharge and precipitation in urban areas. *Journal of Flood Risk Management*, *10*(1), 97–114.

Burian, S. J., Durrans, S. R., Tomić, S., Pimmel, R. L., & Wai, C. N. (2000). Rainfall disaggregation using artificial neural networks. *Journal of Hydrologic Engineering*, *5*(3), 299–307.

Carreau, J., Mhenni, N. B., Huard, F., & Neppel, L. (2019). Exploiting the spatial pattern of daily precipitation in the analog method for regional temporal disaggregation. *Journal of Hydrology*, *568*, 780–791.

Deb, K. (2001). *Multi-objective optimization using evolutionary algorithms* (Vol. 16). John Wiley & Sons.

Deep, K., & Thakur, M. (2007). A new crossover operator for real coded genetic algorithms. *Applied mathematics and computation*, *188*(1), 895–911.

Eshelman, L. J., Caruana, R. A., & Schaffer, J. D. (1989). Biases in the crossover landscape. In *Proceedings of the third international conference on genetic algorithms* (pp. 10–19).

Goldberg, D. (1989). Genetic algorithms in search. optimization and machine learning. addism1—wesley. *Reading, MA*.

Hassan, Z. (2020). An integration based optimization approach (abc and pso) for parameter estimation in blrp model for disaggregating daily rainfall. *Pertanika Journal of Science & Technology*, *28*(1).

Hingray, B., & Haha, M. B. (2005). Statistical performances of various deterministic and stochastic models for rainfall series disaggregation. *Atmospheric Research*, *77*(1-4), 152–175.

Holland, J. H. (1992). Adaptation in natural and artificial systems. 1975. *Ann Arbor, MI: University of Michigan Press and*.

Keijzer, M., Ryan, C., O'Neill, M., Cattolico, M., & Babovic, V. (2001). Ripple crossover

in genetic programming. In *European conference on genetic programming* (pp. 74–86).

Kim, D., & Onof, C. (2020). A stochastic rainfall model that can reproduce important rainfall properties across the timescales from several minutes to a decade. *Journal of Hydrology*, *589*, 125150.

Kossieris, P., Efstratiadis, A., Tsoukalas, I., & Koutsoyiannis, D. (2015). Assessing the performance of bartlett-lewis model on the simulation of athens rainfall. *European Geosciences Union General Assembly*.

Koutsoyiannis, D., & Onof, C. (2001). Rainfall disaggregation using adjusting procedures on a poisson cluster model. *Journal of Hydrology*, *246*(1-4), 109–122.

Lee, T., Salas, J. D., & Prairie, J. (2010). An enhanced nonparametric streamflow disaggregation model with genetic algorithm. *Water Resources Research*, *46*(8).

Li, X., Meshgi, A., Wang, X., Zhang, J., Tay, S. H. X., Pijcke, G., . . . Babovic, V. (2018). Three resampling approaches based on method of fragments for daily-to-subdaily precipitation disaggregation. *International Journal of Climatology*, *38*, e1119–e1138.

McManus, G. E., Wood, C. H., Mercer, D. J., & Conway, C. M. (1991). *Atlas of newfoundland and labrador*. Breakwater Books.

Mehr, A. D., Nourani, V., Kahya, E., Hrnjica, B., Sattar, A. M., & Yaseen, Z. M. (2018). Genetic programming in water resources engineering: A state-of-the-art review. *Journal of hydrology*, *566*, 643–667.

Mezghani, A., & Hingray, B. (2009). A combined downscaling-disaggregation weather generator for stochastic generation of multisite hourly weather variables over complex terrain: Development and multi-scale validation for the upper rhone river basin. *Journal of Hydrology*, *377*(3-4), 245–260.

Molnar, P., & Burlando, P. (2005). Preservation of rainfall properties in stochastic dis-

aggregation by a simple random cascade model. *Atmospheric Research*, *77*(1-4), 137–151.

Müller, H., & Haberlandt, U. (2015). Temporal rainfall disaggregation with a cascade model: from single-station disaggregation to spatial rainfall. *Journal of Hydrologic Engineering*, *20*(11), 04015026.

Müller, H., & Haberlandt, U. (2018). Temporal rainfall disaggregation using a multiplicative cascade model for spatial application in urban hydrology. *Journal of Hydrology*, *556*, 847–864.

Müller-Thomy, H. (2020). Temporal rainfall disaggregation using a micro-canonical cascade model: possibilities to improve the autocorrelation. *Hydrology and Earth System Sciences*, *24*(1), 169–188.

Ormsbee, L. E. (1989). Rainfall disaggregation model for continuous hydrologic modeling. *Journal of Hydraulic Engineering*, *115*(4), 507–525.

Park, J., Cross, D., Onof, C., Chen, Y., & Kim, D. (2021). A simple scheme to adjust poisson cluster rectangular pulse rainfall models for improved performance at sub-hourly timescales. *Journal of Hydrology*, *598*, 126296.

Paschalis, A., Molnar, P., Fatichi, S., & Burlando, P. (2014). On temporal stochastic modeling of precipitation, nesting models across scales. *Advances in water resources*, *63*, 152–166.

Price, D. T., Alfaro, R., Brown, K., Flannigan, M., Fleming, R. A., Hogg, E., . . . others (2013). Anticipating the consequences of climate change for canada's boreal forest ecosystems. *Environmental Reviews*, *21*(4), 322–365.

Pui, A., Sharma, A., Mehrotra, R., Sivakumar, B., & Jeremiah, E. (2012). A comparison of alternatives for daily to sub-daily rainfall disaggregation. *Journal of hydrology*, *470*, 138–157.

Rafatnejad, A., Tavakolifar, H., & Nazif, S. (2021). Evaluation of the climate change

impact on the extreme rainfall amounts using modified method of fragments for sub-daily rainfall disaggregation. *International Journal of Climatology*.

Savic, D. A., & Walters, G. A. (1997). Genetic algorithms for least-cost design of water distribution networks. *Journal of water resources planning and management*, *123*(2), 67–77.

Schepen, A., Everingham, Y., & Wang, Q. J. (2020). Coupling forecast calibration and data-driven downscaling for generating reliable, high-resolution, multivariate seasonal climate forecast ensembles at multiple sites. *International Journal of Climatology*, *40*(4), 2479–2496.

Seiler, C., & Zwiers, F. (2016). How well do cmip5 climate models reproduce explosive cyclones in the extratropics of the northern hemisphere? *Climate dynamics*, *46*(3-4), 1241–1256.

Sharif, M., Burn, D. H., & Wey, K. M. (2007). Daily and hourly weather data generation using a k-nearest neighbour approach. In *Canadian hydrotechnical conference* (pp. 1–10).

Silva, A., & Portela, M. (2012). Disaggregation modelling of monthly streamflows using a new approach of the method of fragments. *Hydrological Sciences Journal*, *57*(5), 942–955.

Sun, X., Wang, Y., Kang, H., Shen, Y., Chen, Q., & Wang, D. (2021). Modified multi-crossover operator nsga-iii for solving low carbon flexible job shop scheduling problem. *Processes*, *9*(1), 62.

Svanidze, G. G. (1980). Mathematical modeling of hydrologic series for hydroelectric and water resources computations.

Syswerda, G., et al. (1989). Uniform crossover in genetic algorithms. In *Icga* (Vol. 3, pp. 2–9).

Wang, S., Gain, J., & Nitschke, G. (2014). Comparing crossover operators in neuro-

evolution with crowd simulations. In *2014 ieee congress on evolutionary computation (cec)* (pp. 2298–2305).

Westra, S., Mehrotra, R., Sharma, A., & Srikanthan, R. (2012). Continuous rainfall simulation: 1. a regionalized subdaily disaggregation approach. *Water Resources Research*, *48*(1).

Willems, P., Olsson, J., Arnbjerg-Nielsen, K., Beecham, S., Pathirana, A., Gregersen, I. B., ... others (2012). Modelling and analysis of rainfall extreme in a stationary context. In *Impacts of climate change on rainfall extremes and urban drainage systems* (pp. 7–26). IWA publishing.

Willkofer, F., Wood, R. R., von Trentini, F., Weismüller, J., Poschlod, B., & Ludwig, R. (2020). A holistic modelling approach for the estimation of return levels of peak flows in bavaria. *Water*, *12*(9), 2349.

Wójcik, R., & Buishand, T. A. (2003). Simulation of 6-hourly rainfall and temperature by two resampling schemes. *Journal of Hydrology*, *273*(1-4), 69–80.

Yang, S. (2002). Adaptive non-uniform crossover based on statistics for genetic algorithms. In *Proceedings of the 4th annual conference on genetic and evolutionary computation* (pp. 650–657).

Yang, S., & Abbass, B. (2003). Adaptive crossover in genetic algorithms using statistics mechanism. *Artificial Life*, *8*, 182–185.

Zhang, J., Chung, H. S.-H., & Lo, W.-L. (2007). Clustering-based adaptive crossover and mutation probabilities for genetic algorithms. *IEEE Transactions on Evolutionary Computation*, *11*(3), 326–335.

Chapter 5

Conclusions and Future Works

5.1 Summary

This thesis presented three stand-alone papers (Chapters 2 to 4), all contributing to the investigation of design storm formulation across Newfoundland and Labrador under climate change with scarce data. This investigation aimed to provide useful information to the Water Resources Division of the Government of Newfoundland and Labrador regarding design storms employed in flood risk mapping and provide a basis for conservative design under climate change in the province.

A literature review was conducted in Chapter 1, in addition to those found in Chapters 2 through 4, to shed light on the evolution of design storms and disaggregation methods in hydrology and provide context for this investigation.

There were three different methods used in this investigation across Newfoundland and Labrador. Chapter 2 used numerical methods to identify temporal precipitation patterns, one of four components that make up a design storm, across a climate gradient. Chapter 3 used hydrologic and hydraulic methods to support the analysis conducted in Chapter 2 and providing insight into the impacts of climate change on design parameters and flood

risk mapping. Chapter 4 uses an aspect of search-based optimization techniques to generate precipitation data which can provide information on the other three components, intensity, duration and frequency, needed for design storm formulation.

Environment Canada's and City of St. John's Planning, Engineering and Regulatory services precipitation data were all used at various stages of the research. Bias-corrected climate model output from NACORDEX and PCIC was used in this thesis's climate change analysis aspect.

To a large extent, each of these methods complements the other. Four major temporal precipitation patterns were identified in Chapter 2. Chapters 2 and 4 together provided the full range of information required to formulate a design storm where there is limited data available to construct an IDF curve using traditional methods. Both Chapters 2 and 3 found specific temporal precipitation patterns to dominate in each climate zone. 2 of the four temporal precipitation patterns and a standard precipitation pattern currently used by the province were evaluated and found to have varying dominance for watersheds across the province under climate change conditions in Chapter 3. It was also found in Chapter 3 that increases in precipitation amounts under climate change were not commensurate with increases in peak discharges.

In addition to the information requested by the Water Resources Division, each of the three chapters provide insight into the impact of design storm choice and applications for practicing engineers.

Overall, this thesis presented the potential impacts of design storm choice across a climate gradient under climate change in Newfoundland and Labrador while providing a means to generate other design storm formulation components in data-scarce regions. Although a combination of methods was used, climate change is generally expected to impact design storm choice when planning for the future. Though the dissertation's work was thorough, there is always room for further improvement in the methods and analysis. Sug-

gestions for future works are discussed in the next section.

5.2 Future Works

Based on the findings of the disaggregation model developed and the literature reviewed, it is suggested that the model developed should be applied to different climates to assess the robustness of its performance. The discussion section of Chapter 4 suggests that alternative sampling methods can be incorporated into the disaggregation model. This suggestion can serve as future work to further improve the statistical performance of the model. In addition, the work from Chapter 4 can be extended from the temporal scale to spatial or spatiotemporal.

The temporal precipitation patterns developed in Chapter 2 were based on hourly rainfall data as the amount of sub-hourly data available was limited. As more sub-hourly precipitation data becomes available, identification of the temporal patterns can be repeated across the province of Newfoundland and Labrador to identify any that may have been missed based on the resolution of the precipitation data used in this research. Another work can be undertaken by identifying temporal precipitation patterns using future climate projections. In cases where precipitation projections have durations greater than one hour, the developed disaggregation model can generate the required hourly data for the temporal precipitation patterns identification.

The findings of Chapter 2 which were used for the flood risk mapping study in Chapter 3 were only one of the many applications of temporal patterns. These temporal patterns can also be employed in flood forecasting and evaluating habitat restoration for aquatic organisms. These can serve as future implementations of identified precipitation patterns.

Appendix A

Supporting information for Chapter 3*

Plan View of HEC-RAS models used for flood inundation mapping

ADD HERE

Table to support flood inundation section
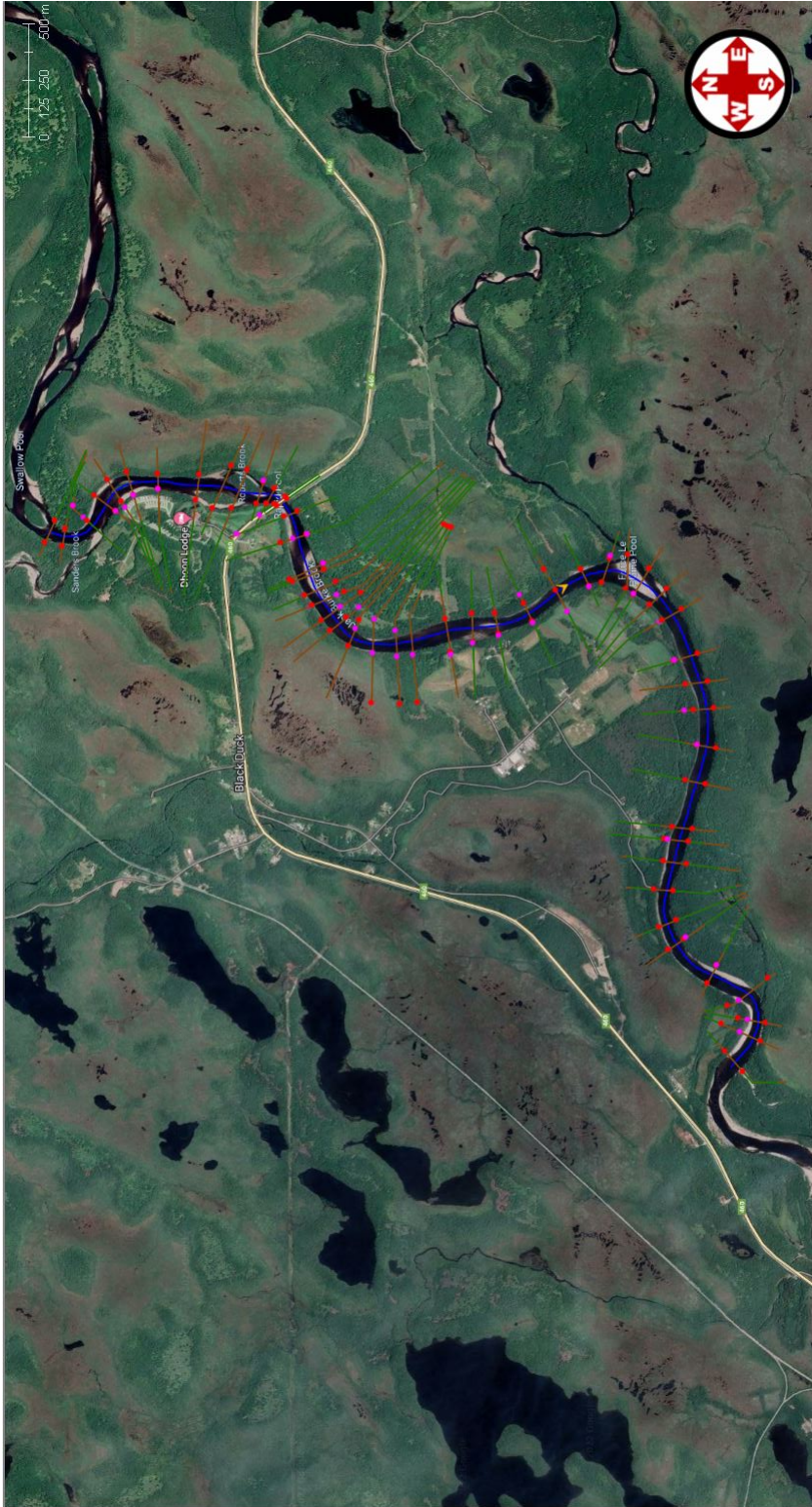
Figure A.1: Plan View of Black Duck Siding HEC-RAS model with cross sections indicated by red lines
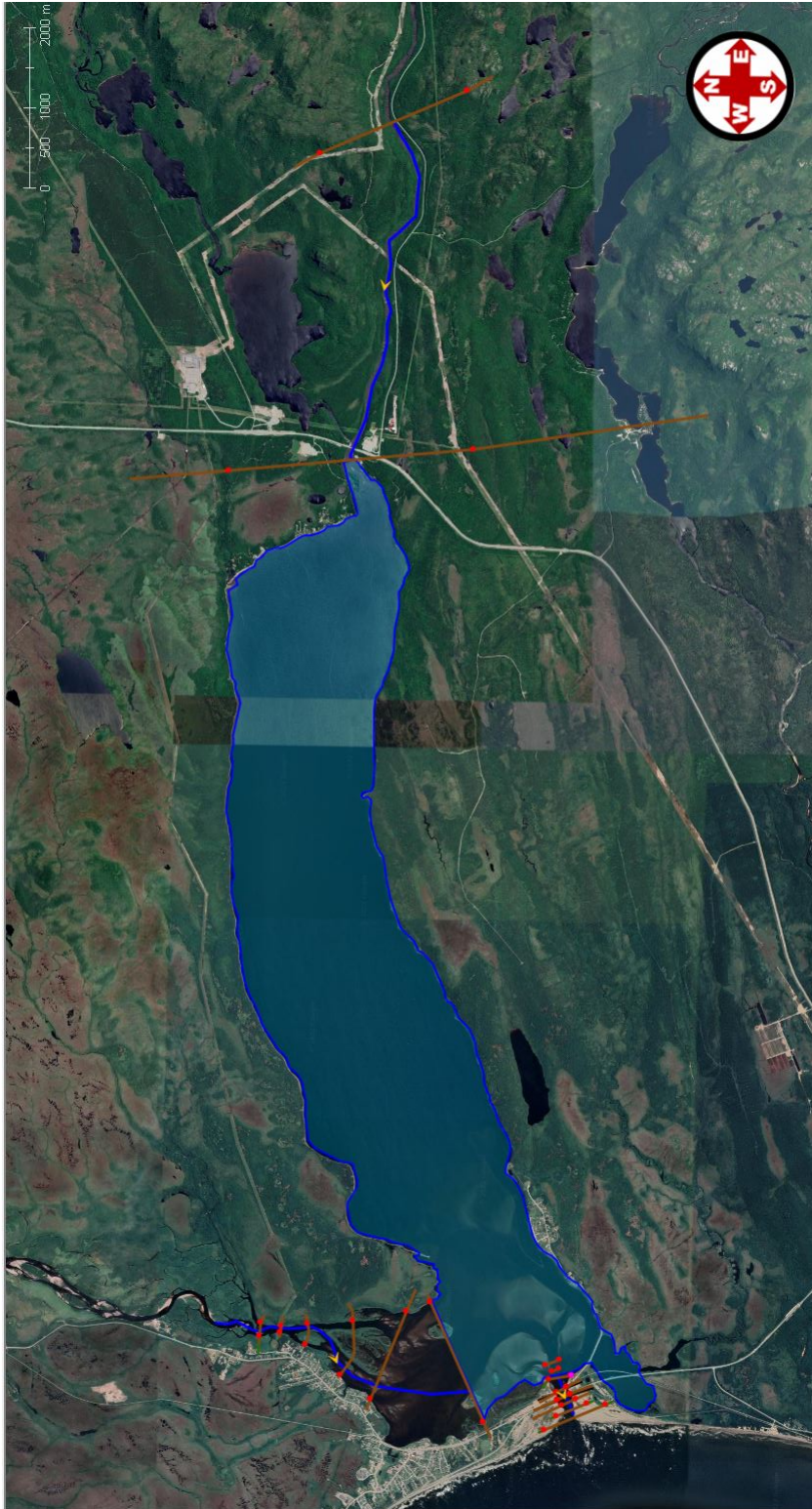
Figure A.2: Plan View of Stephenville HEC-RAS model with cross sections indicated by red lines
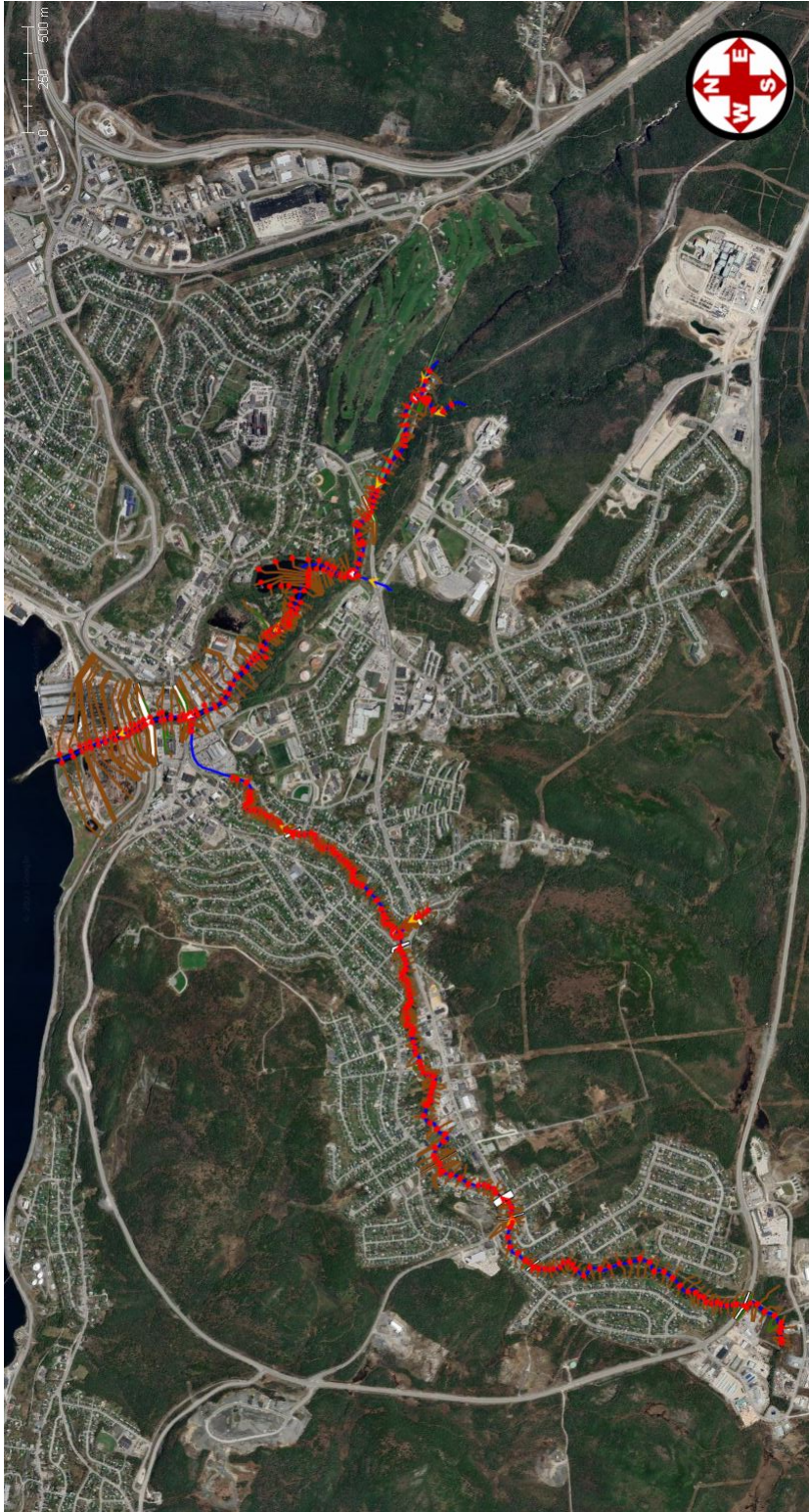
Figure A.3: Plan View of Corner Brook HEC-RAS model with cross sections indicated by red lines

Table A.1: Flood inundation areas (ha) of watersheds for historical climate and the 2041-2070 and 2071-2100 time slices under RCP8.5

| Watershed | Temporal distribution | 20-year | | | 100-year | | |
		Current	RCP8.5 2041-2070	RCP8.5 2071-2100	Current	RCP8.5 2041-2070	RCP8.5 2071-2100
Corner Brook	Alternating block	48.01	51.69	52.87	50.3	58.4	62.4
	Advanced pattern	44.88	46.60	47.57	46.2	50.4	50.8
	Delayed pattern	46.33	48.6	49.8	47.8	52.4	55.4
Petries Brook	Alternating block	4.2	5.0	5.4	4.8	5.7	6.2
	Advanced pattern	3.1	3.6	3.9	3.4	3.9	4.2
	Delayed pattern	3.4	3.9	4.1	3.7	4.3	4.5
Goulds	Alternating block	449.3	480.3	492.8	476.0	509.1	524.2
	Advanced pattern	429.6	453.0	465.4	484.4	479.5	492.8
	Delayed pattern	450.8	472.5	483.1	489.0	497.3	511.1
Beachy Cove (PCSP)	Alternating block	29.7	31.1	33.6	33.6	35.0	37.1
	Advanced pattern	26.4	29.6	30.1	30.1	33.3	35.4
	Delayed pattern	29.9	32.8	33.3	33.3	36.5	38.5
Broad Cove (PCSP)	Alternating block	8.5	10.0	11.2	11.3	12.8	14.5
	Advanced pattern	7.3	9.2	10.7	9.8	12.1	13.8
	Delayed pattern	9.2	11.5	13.1	11.9	14.9	16.3
Goat Cove (PCSP)	Alternating block	4.5	4.7	5.2	6.0	6.3	7.0
	Advanced pattern	3.7	4.4	4.7	4.9	5.8	6.4
	Delayed pattern	4.5	5.1	5.5	5.7	6.6	7.2
Main River (PCSP)	Alternating block	31.9	32.2	34.8	36.6	38.0	41.0
	Advanced pattern	28.4	28.6	30.9	29.4	33.8	36.5
	Delayed pattern	32.6	32.9	35.0	33.5	37.8	40.2

Watershed	Temporal distribution	20-year			100-year		
		Current	RCP8.5 2041-2070	RCP8.5 2071-2100	Current	RCP8.5 2041-2070	RCP8.5 2071-2100
Coaker's River (LB)	Alternating block	19.8	20.4	20.7	20.4	21.4	21.5
	Advanced pattern	19.8	20.5	20.7	20.5	21.4	21.7
	Delayed pattern	20.1	20.9	21.5	21.1	21.6	22.0
Druken's River (LB)	Alternating block	16.9	17.2	17.3	16.9	17.2	17.3
	Advanced pattern	16.8	17.2	17.3	16.9	17.2	17.3
	Delayed pattern	17.2	17.4	17.5	17.3	17.5	17.6
Kennedy's Brook (LB)	Alternating block	6.6	6.7	6.8	6.7	6.9	7.0
	Advanced pattern	6.5	6.7	6.8	6.7	6.9	7.0
	Delayed pattern	6.7	6.8	6.9	6.8	7.1	7.2
Outer Cove Brook (LB)	Alternating block	7.4	8.2	8.7	8.3	9.5	10.3
	Advanced pattern	7.3	8.1	8.7	8.2	9.4	10.3
	Delayed pattern	8.1	9.1	9.9	9.2	10.7	11.4
Stephenville	Alternating block	285.7	290.8	297.0	294.5	302.5	327.3
	Advanced pattern	271.2	278.1	291.0	288.2	292.2	303.7
	Delayed pattern	281.7	289.3	301.3	299.8	302.1	321.5
Black Duck Siding	Alternating block	166.5	170.8	180.4	178.6	174.0	186.8
	Advanced pattern	162.6	170.0	178.9	174.3	179.8	185.2
	Delayed pattern	170.6	174.3	182.6	181.3	183.1	188.2
Waterford	Alternating block	136.3	152.7	166.5	160.6	138.8	202.5
	Advanced pattern	110.2	123.1	136.5	130.4	150.6	165.5
	Delayed pattern	140.2	152.9	164.8	160.2	178.9	192.4
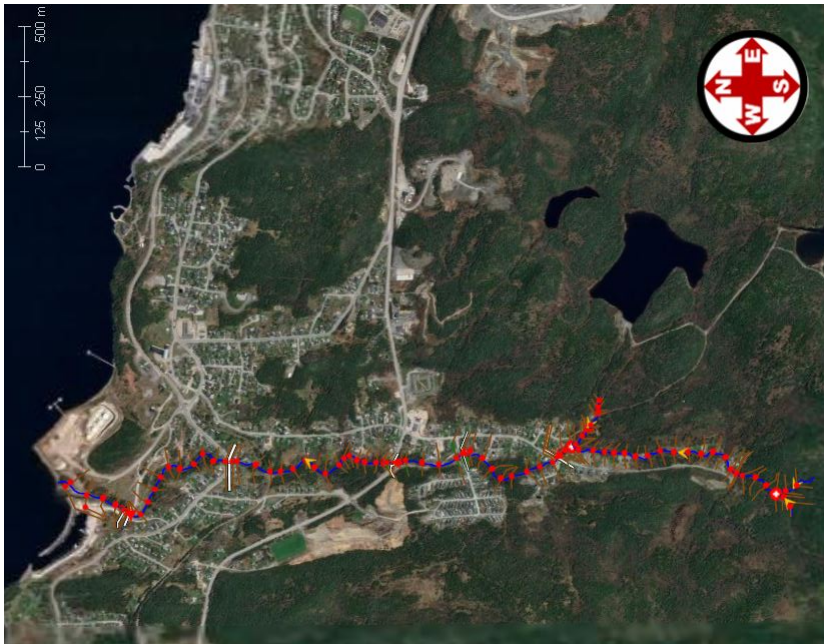
Figure A.4: Plan View of Petries Brook HEC-RAS model with cross sections indicated by red lines
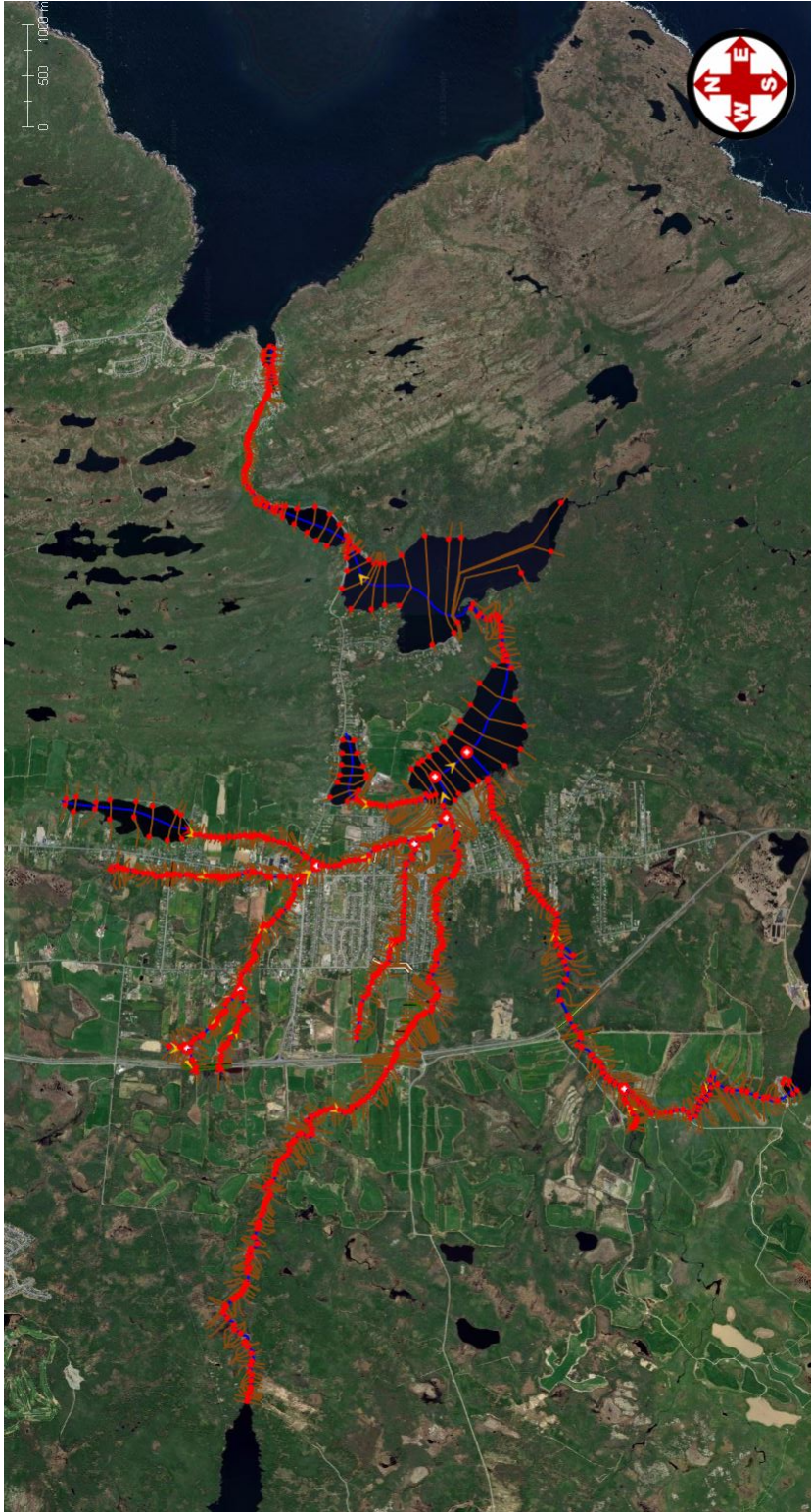
Figure A.5: Plan View of Goulds HEC-RAS model with cross sections indicated by red lines
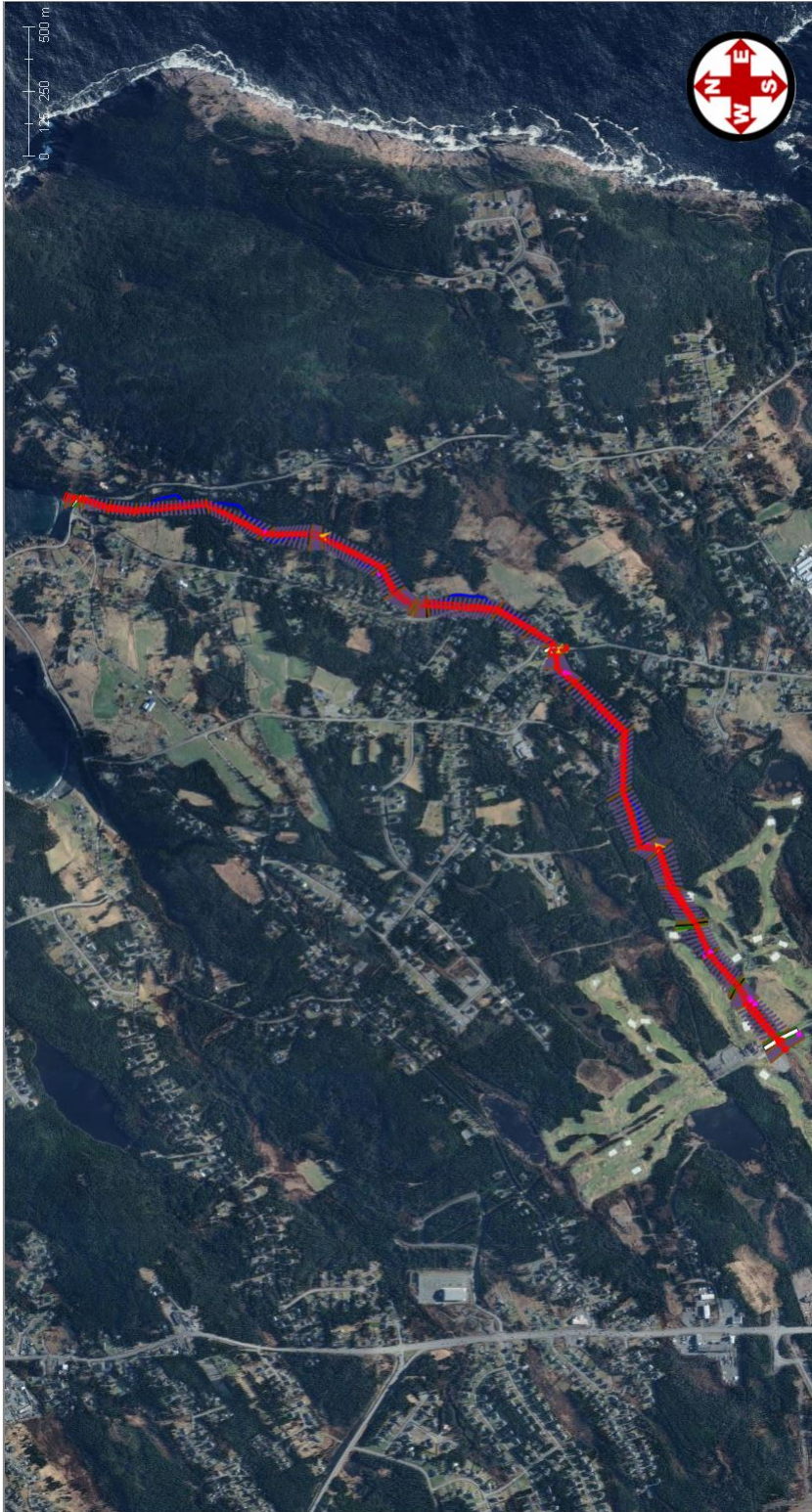
Figure A.6: Plan View of Outer Cove Brook HEC-RAS model with cross sections indicated by red lines

Figure A.7: Plan View of Kennedy's River HEC-RAS model with cross sections indicated by red lines

Figure A.8: Plan View of Main River HEC-RAS model with cross sections indicated by red lines

Figure A.9: Plan View of Coaker's River HEC-RAS model with cross sections indicated by red lines
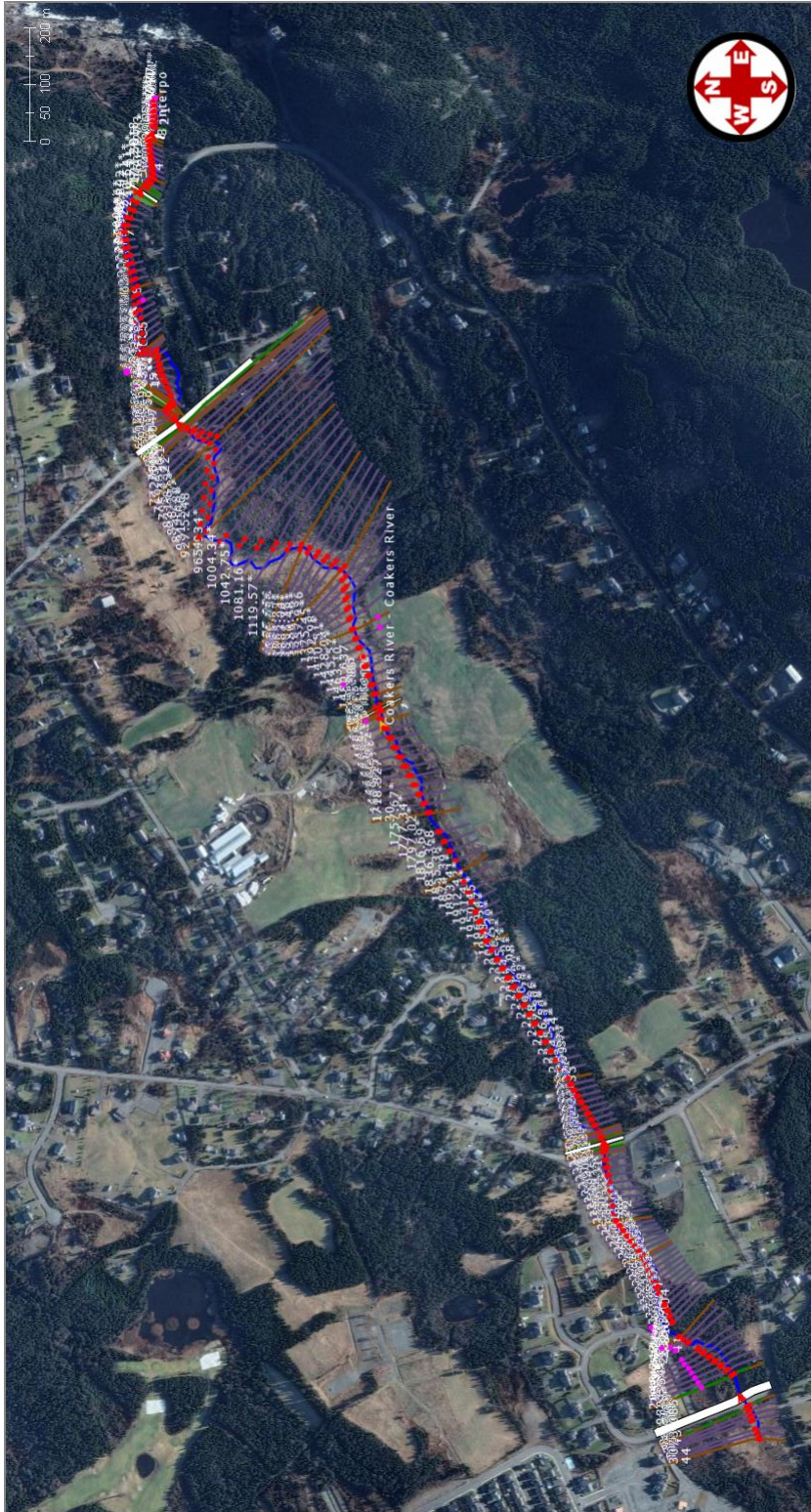
Figure A.10: Plan View of Goat River HEC-RAS model with cross sections indicated by red lines
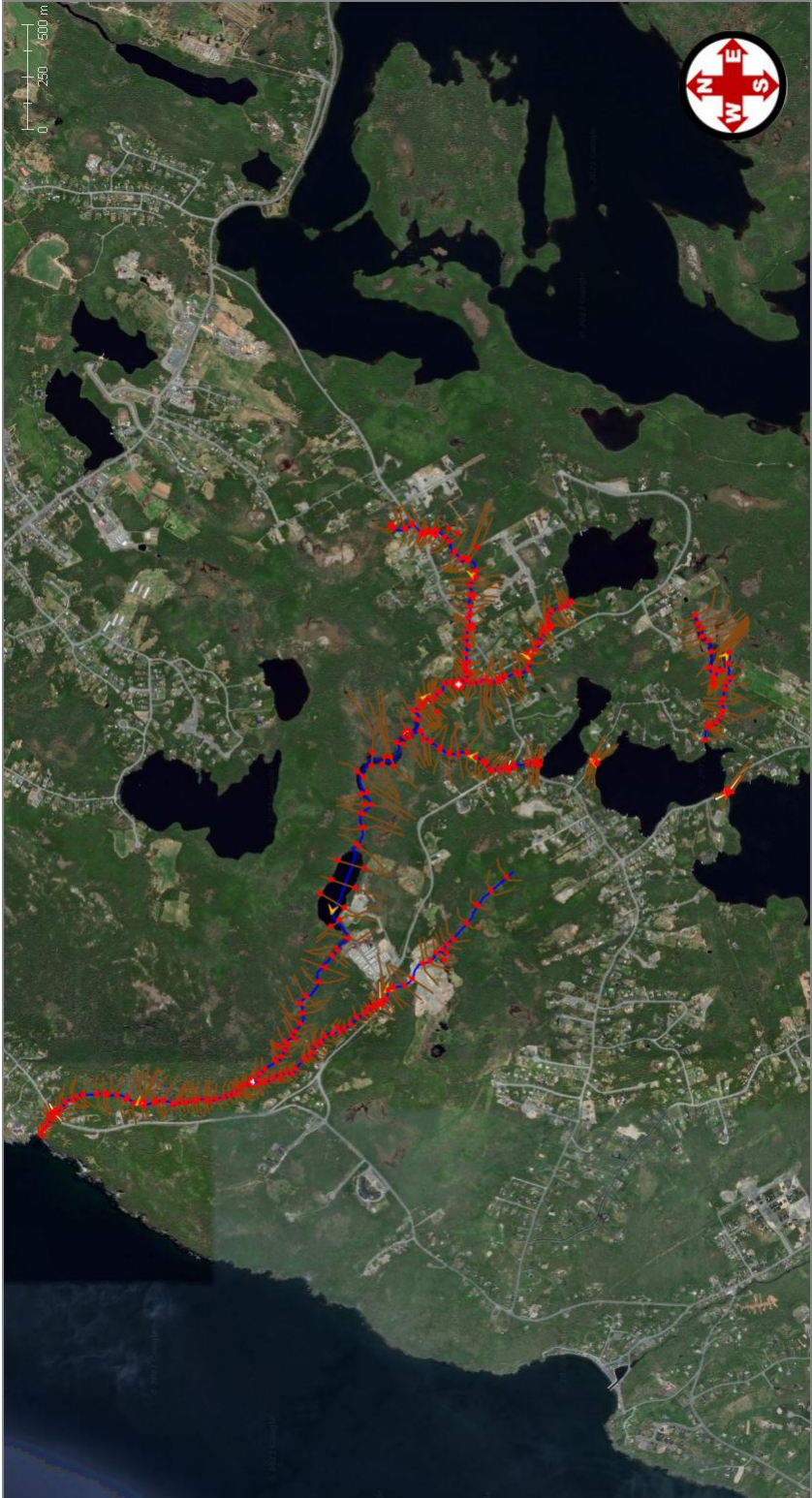
Figure A.11: Plan View of Beachy Cove HEC-RAS model with cross sections indicated by red lines
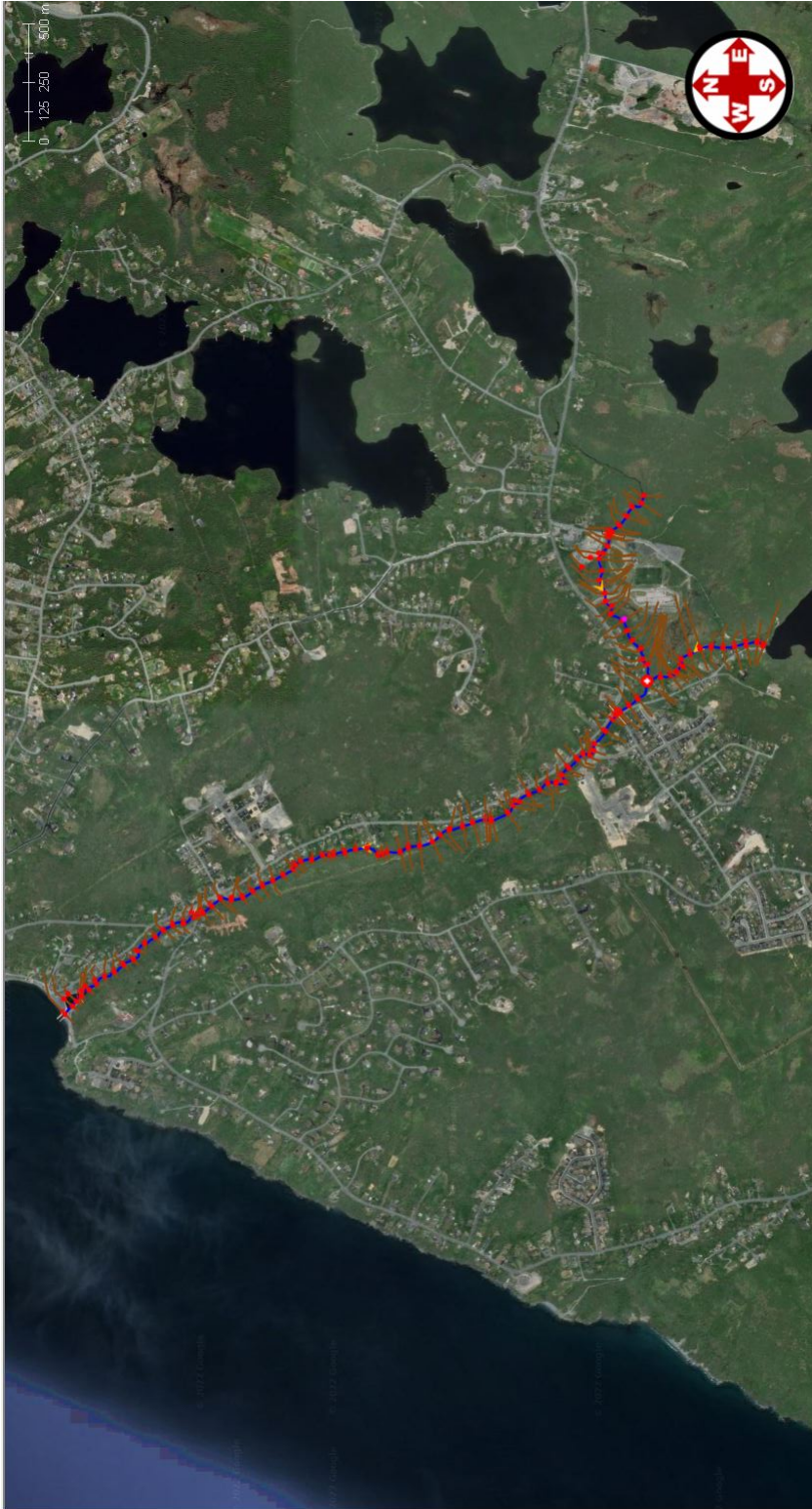
Figure A.12: Plan View of Broad Cove HEC-RAS model with cross sections indicated by red lines

Figure A.13: Plan View of Druken's River HEC-RAS model with cross sections indicated by red lines
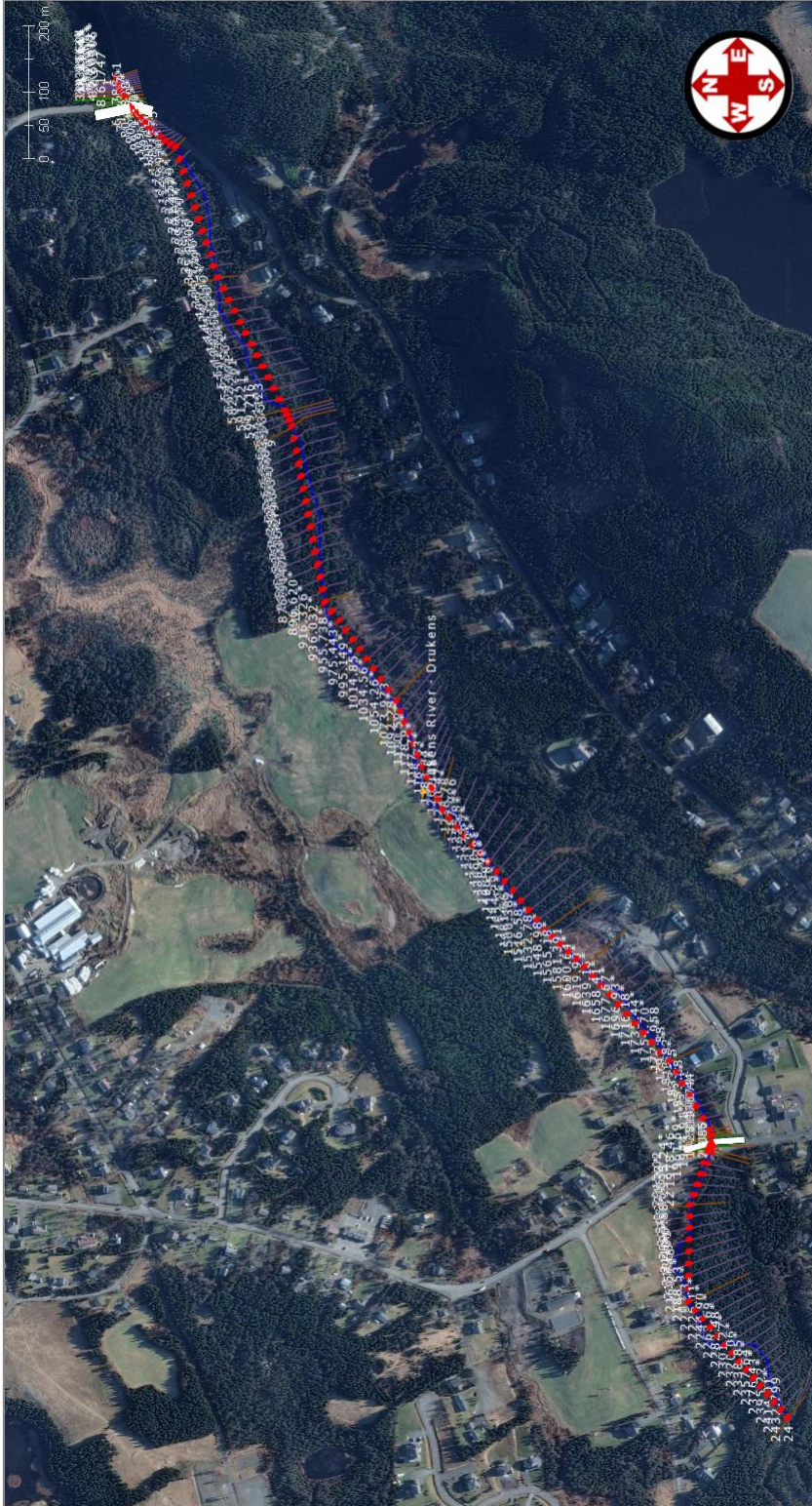
Appendix B

Supporting information for Chapter 4*

Results of disaggregated data in Chapter 4
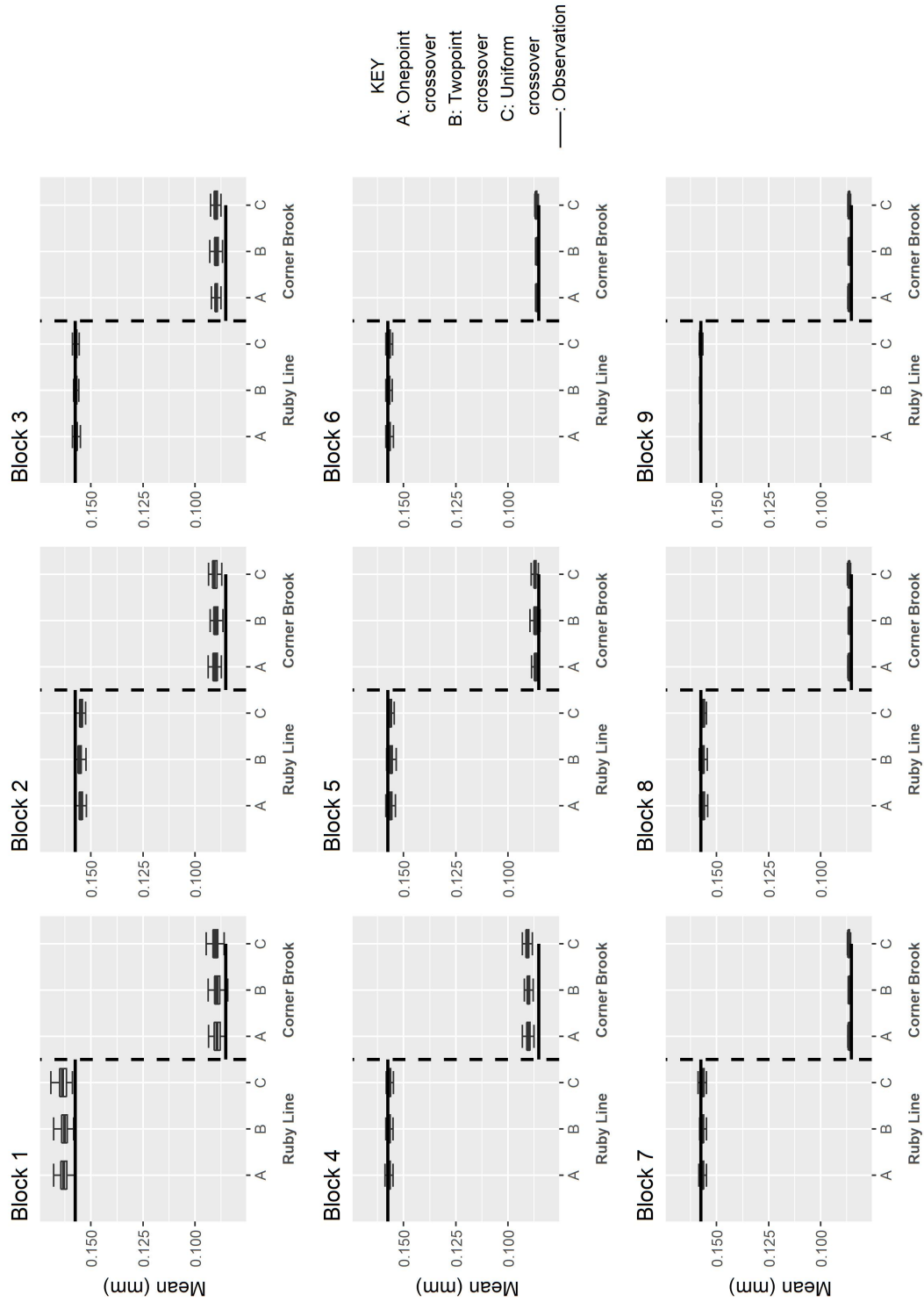
Figure A.1: Mean of observed and disaggregated data at 1hr for all blocks of available data (indicated at the top of the boxplot generated from 100 simulation runs). Station name indicated below the plot.

211

Figure A.2: Standard deviation of observed and disaggregated data at 1hr for all blocks of available data (indicated at the top of the boxplot generated from 100 simulation runs). Station name indicated below the plot.
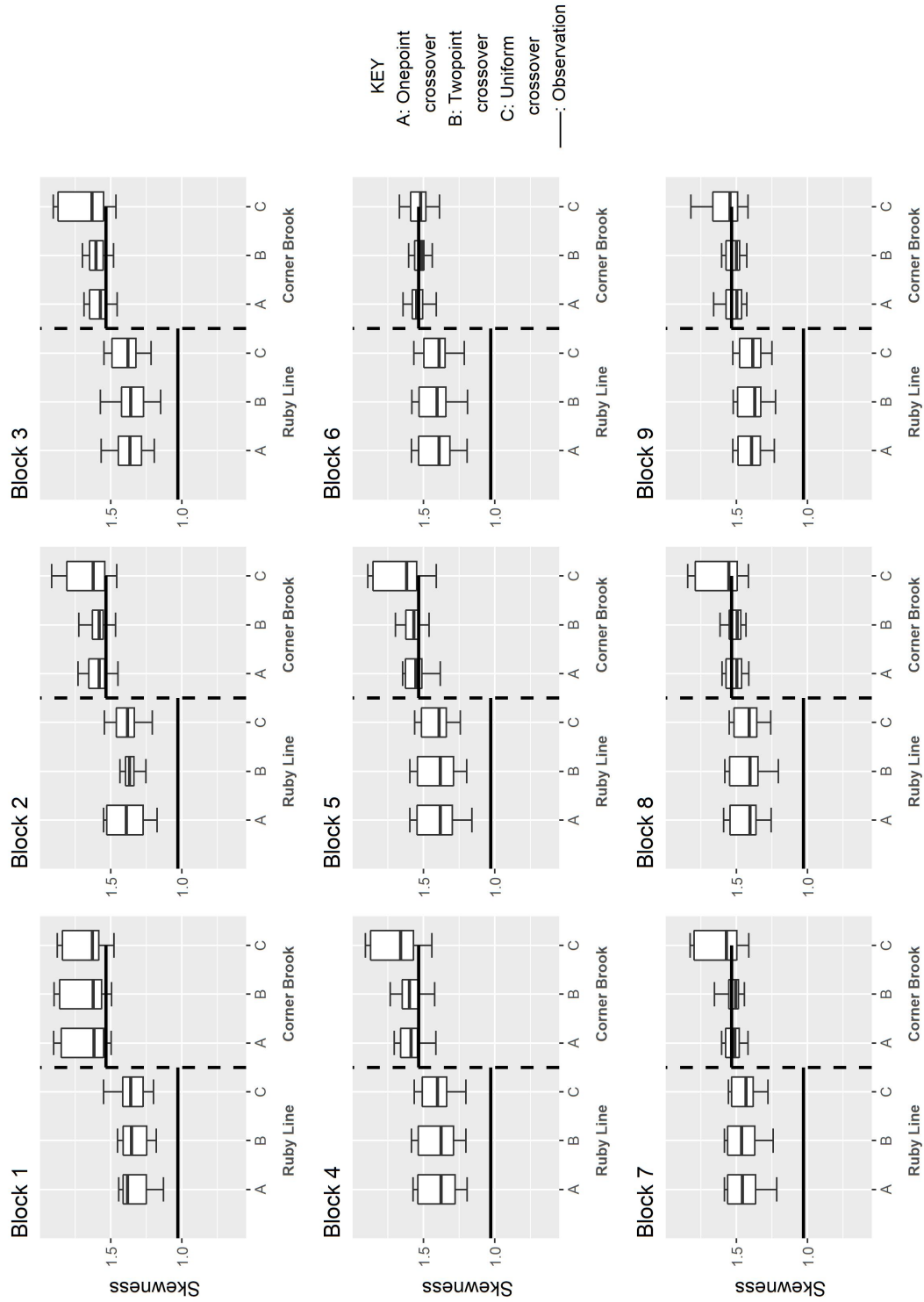
Figure A.3: Skewness of observed and disaggregated data at 1hr for all blocks of available data (indicated at the top of the boxplot generated from 100 simulation runs). Station name indicated below the plot.
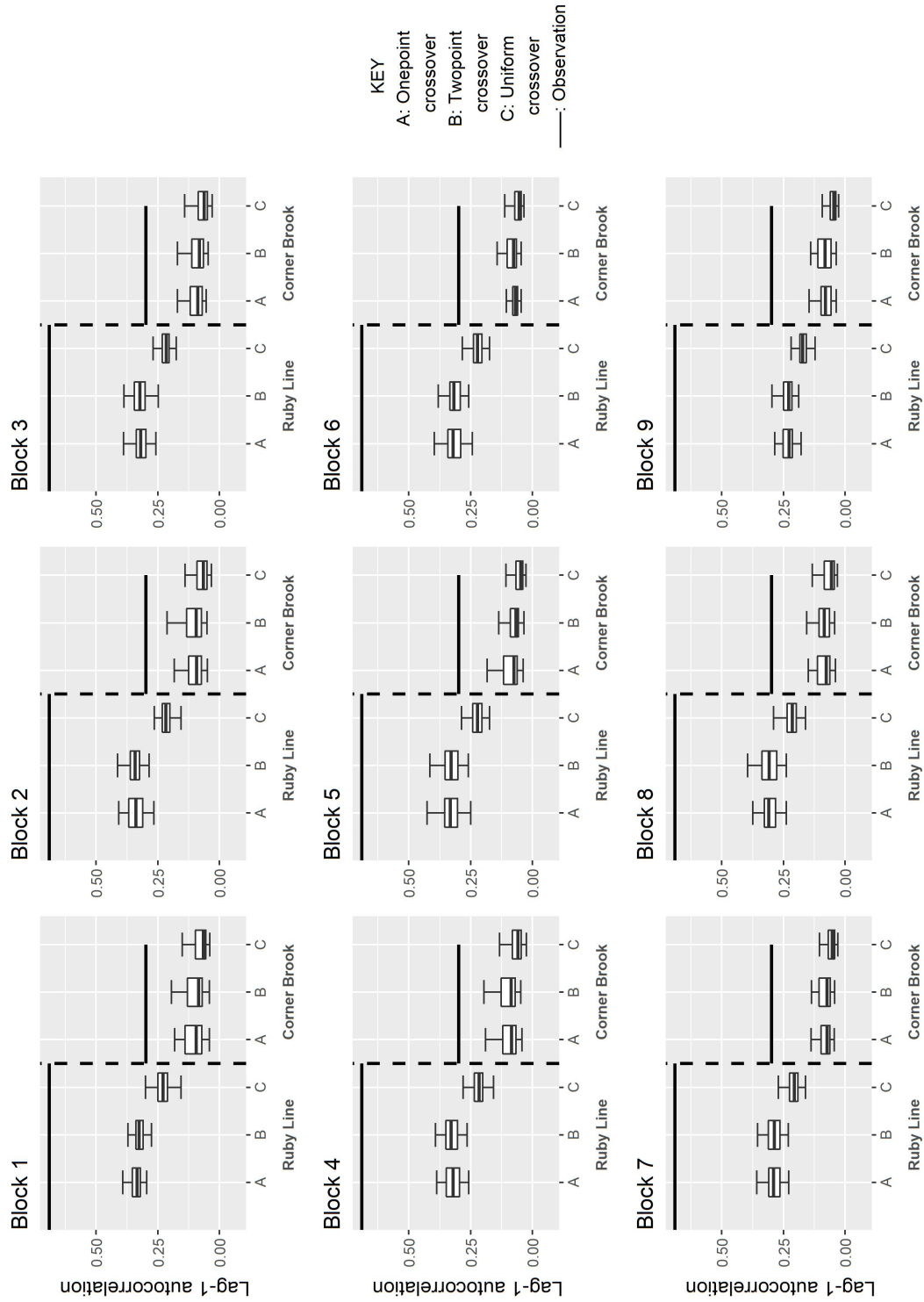
Figure A.4: Lag-1 autocorrelation of observed and disaggregated data at 1hr for all blocks of available data (indicated at the top of the boxplot generated from 100 simulation runs). Station name indicated below the plot.
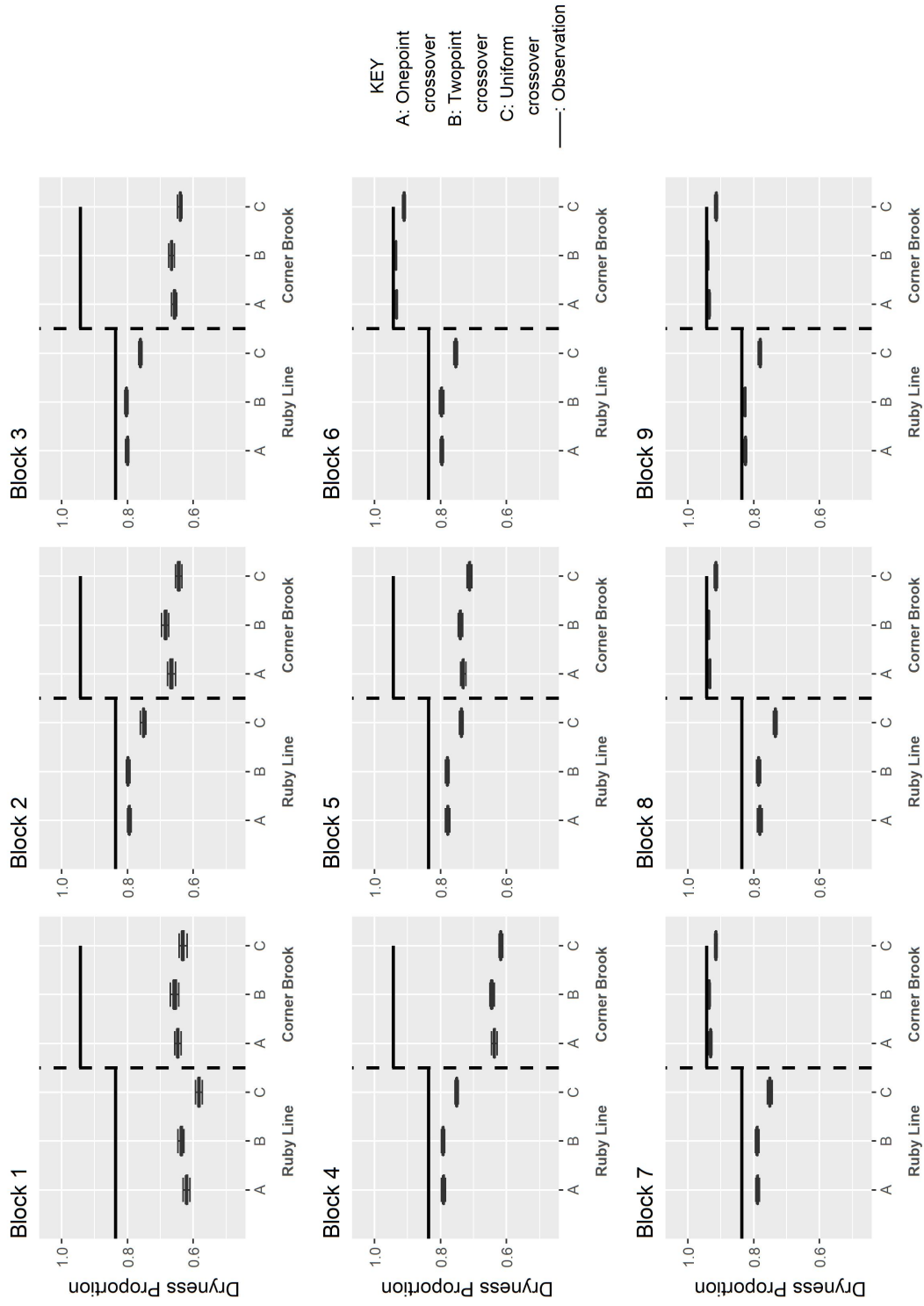
Figure A.5: Dryness proportion of observed and disaggregated data at 1hr for all blocks of available data (indicated at the top of the plot). Station name indicated below the plot.
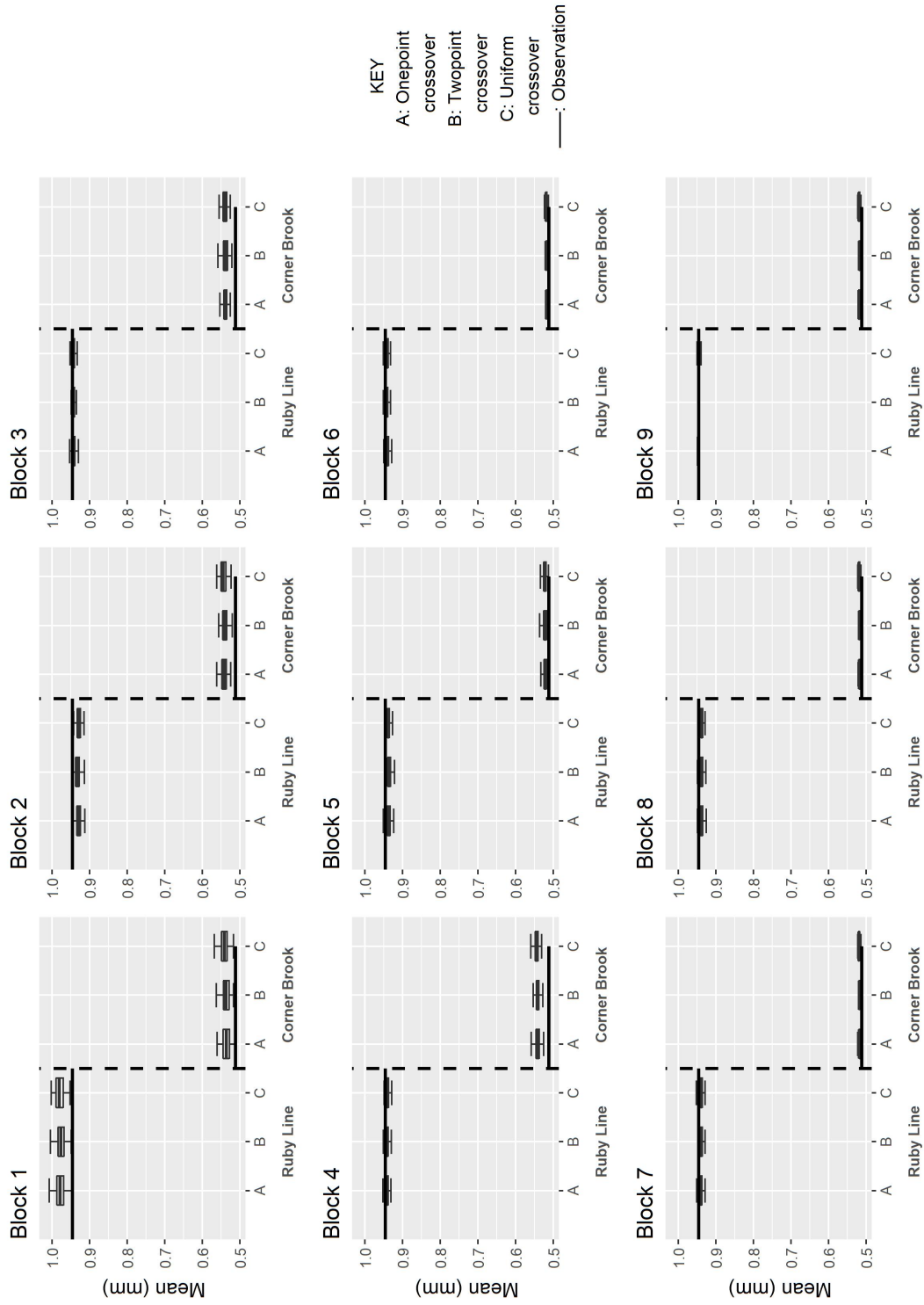
Figure A.6: Mean of observed and disaggregated data at 6hr for all blocks of available data (indicated at the top of the boxplot generated from 100 simulation runs). Station name indicated below the plot.

Figure A.7: Standard deviation of observed and disaggregated data at 6hr for all blocks of available data (indicated at the top of the boxplot generated from 100 simulation runs). Station name indicated below the plot.
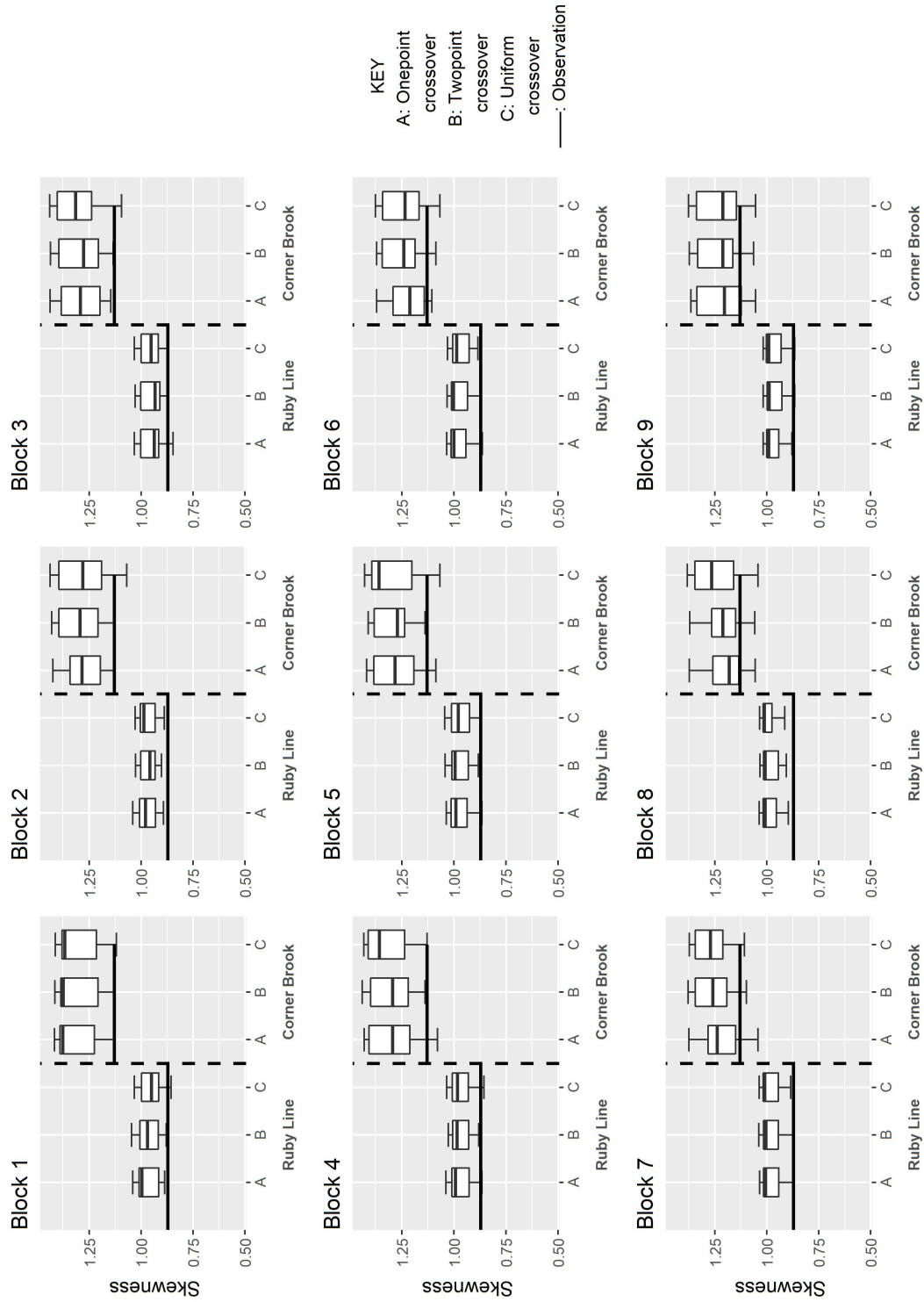
Figure A.8: Skewness of observed and disaggregated data at 6hr for all blocks of available data (indicated at the top of the boxplot generated from 100 simulation runs). Station name indicated below the plot.
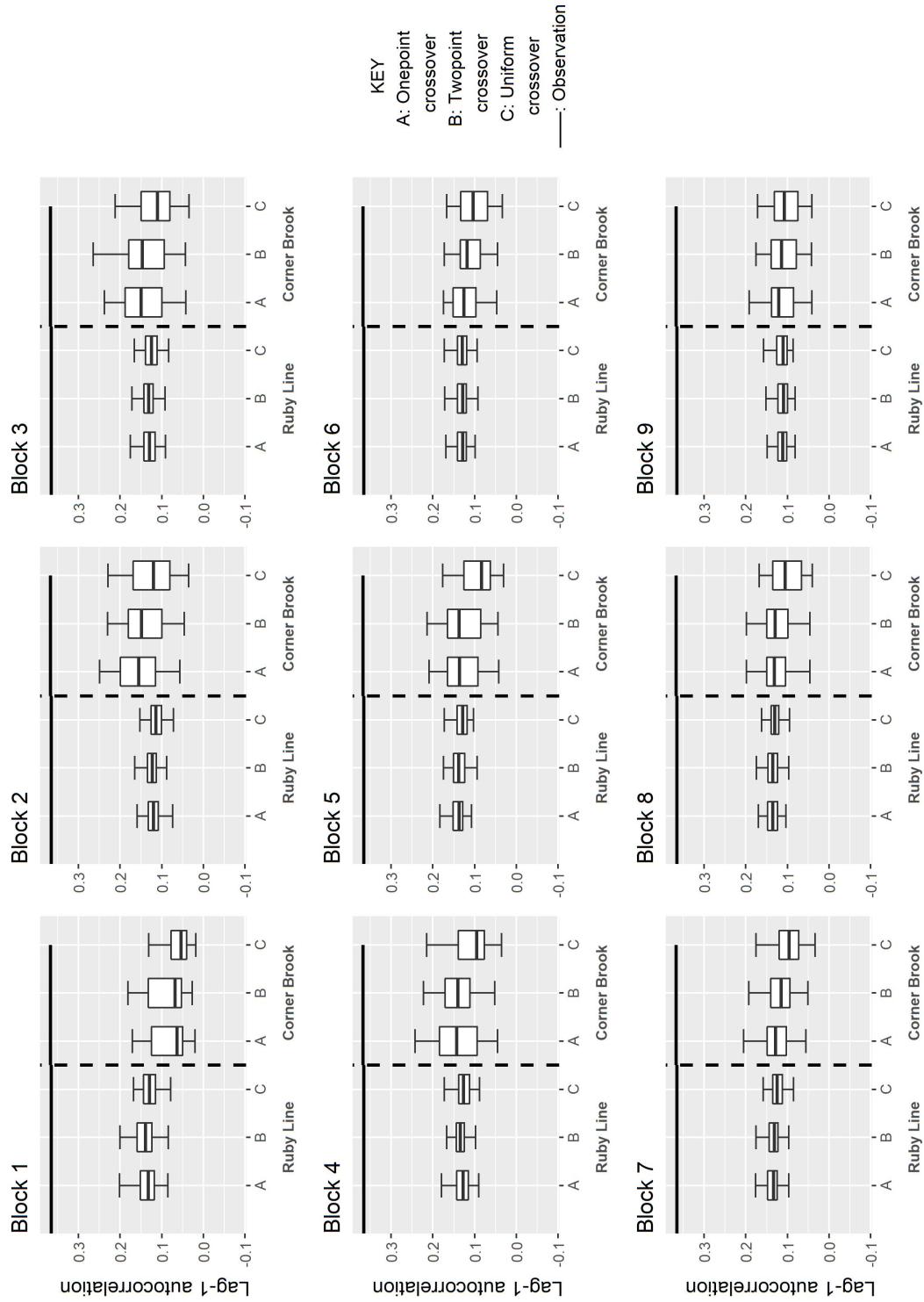
Figure A.9: Lag-1 autocorrelation of observed and disaggregated data at 6hr for all blocks of available data (indicated at the top of the boxplot generated from 100 simulation runs). Station name indicated below the plot.

219
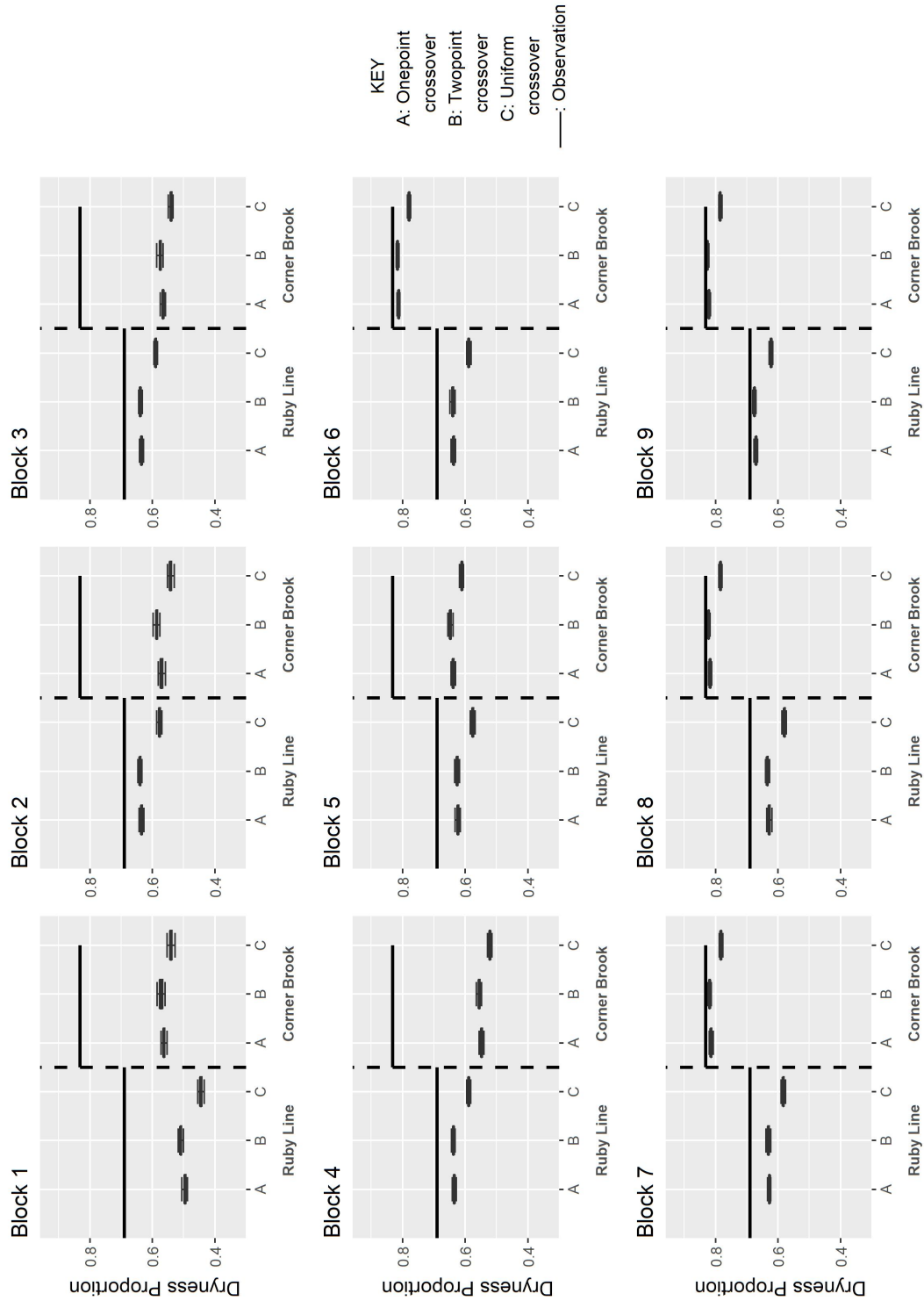
Figure A.10: Dryness proportion of observed and disaggregated data at 6hr for all blocks of available data (indicated at the top of the boxplot generated from 100 simulation runs). Station name indicated below the plot.
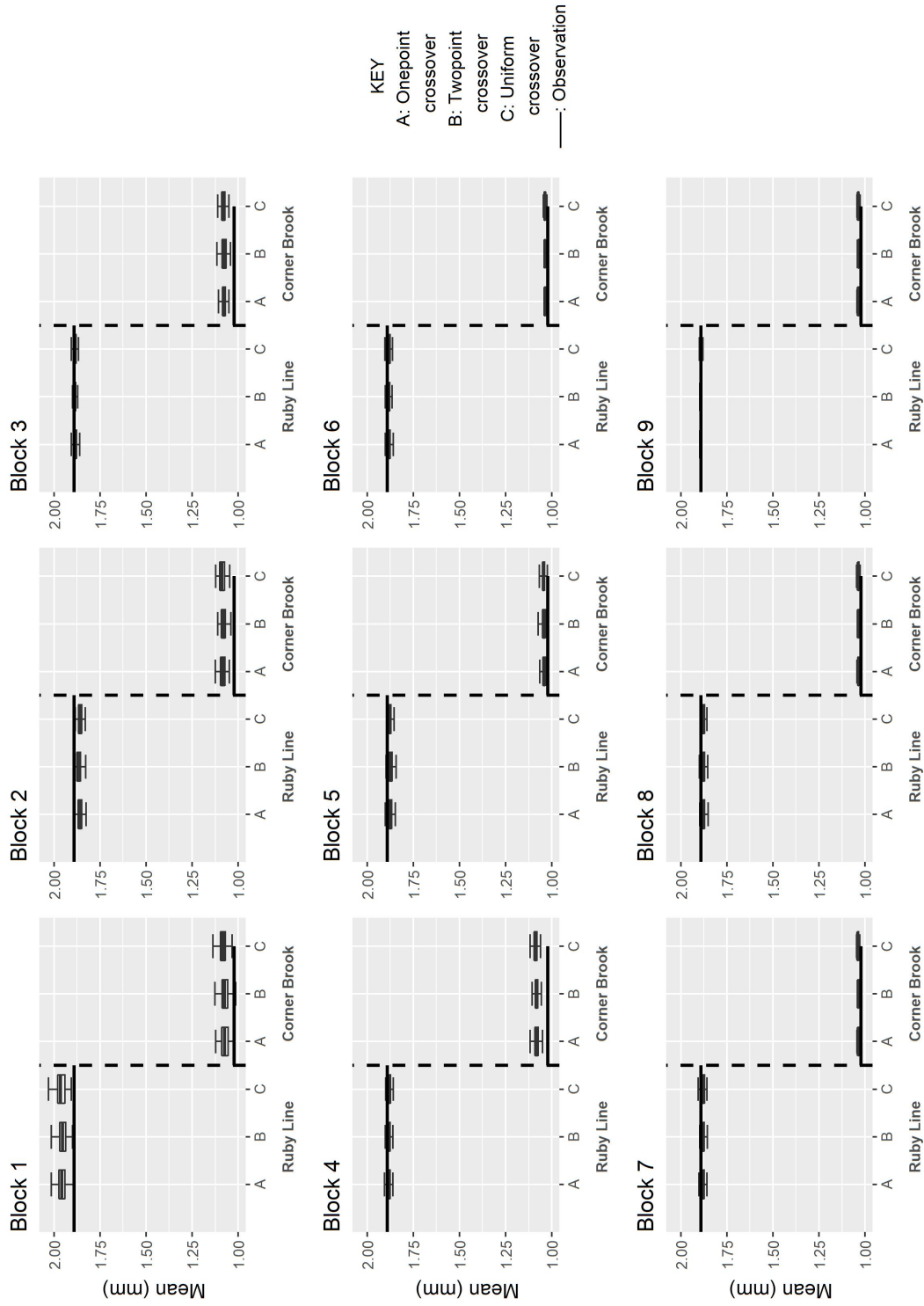
Figure A.11: Mean of observed and disaggregated data at 12hr for all blocks of available data (indicated at the top of the boxplot generated from 100 simulation runs). Station name indicated below the plot.

221

Figure A.12: Standard deviation of observed and disaggregated data at 12hr for all blocks of available data (indicated at the top of the boxplot generated from 100 simulation runs). Station name indicated below the plot.
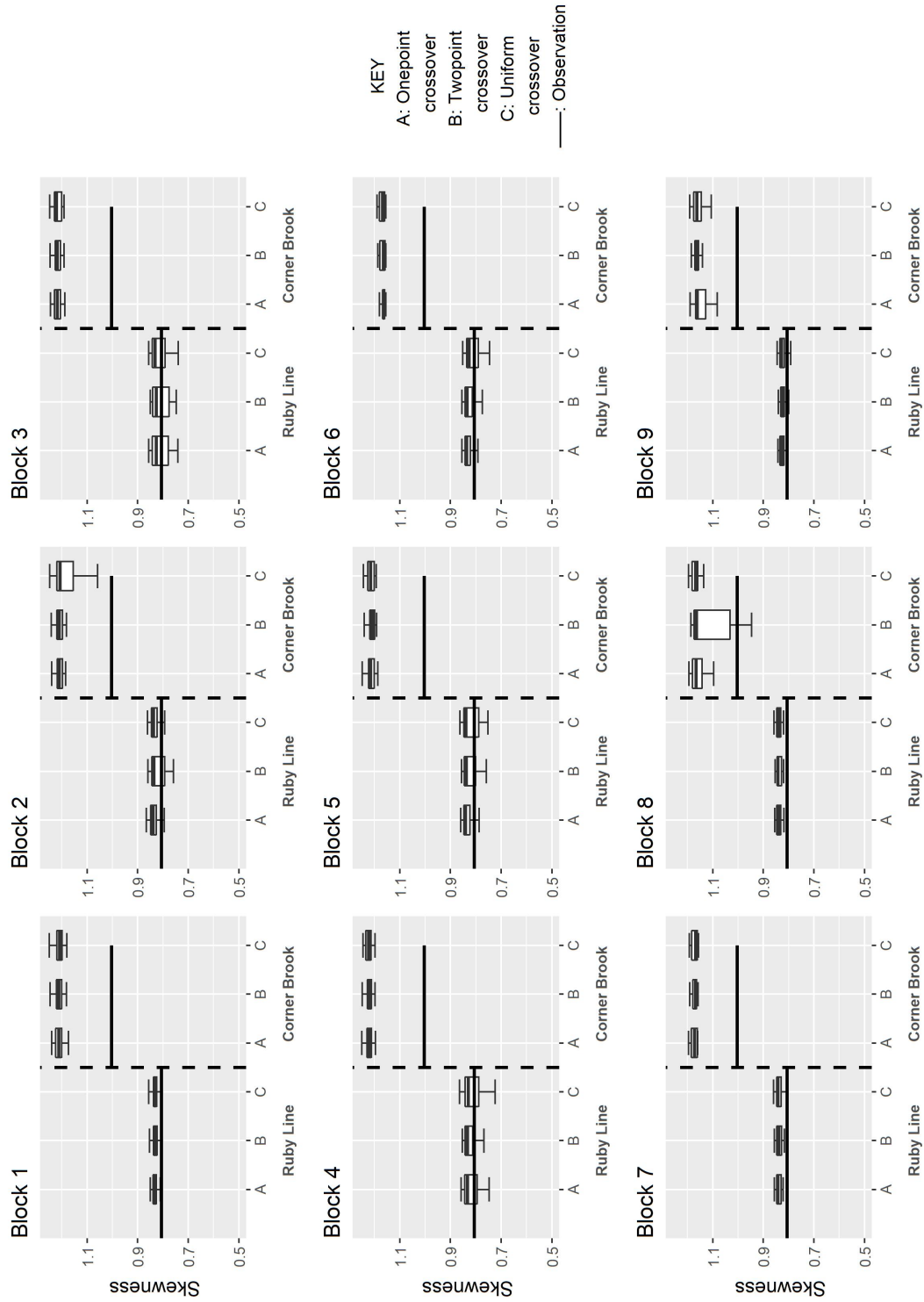
Figure A.13: Skewness of observed and disaggregated data at 12hr for all blocks of available data (indicated at the top of the boxplot generated from 100 simulation runs). Station name indicated below the plot.
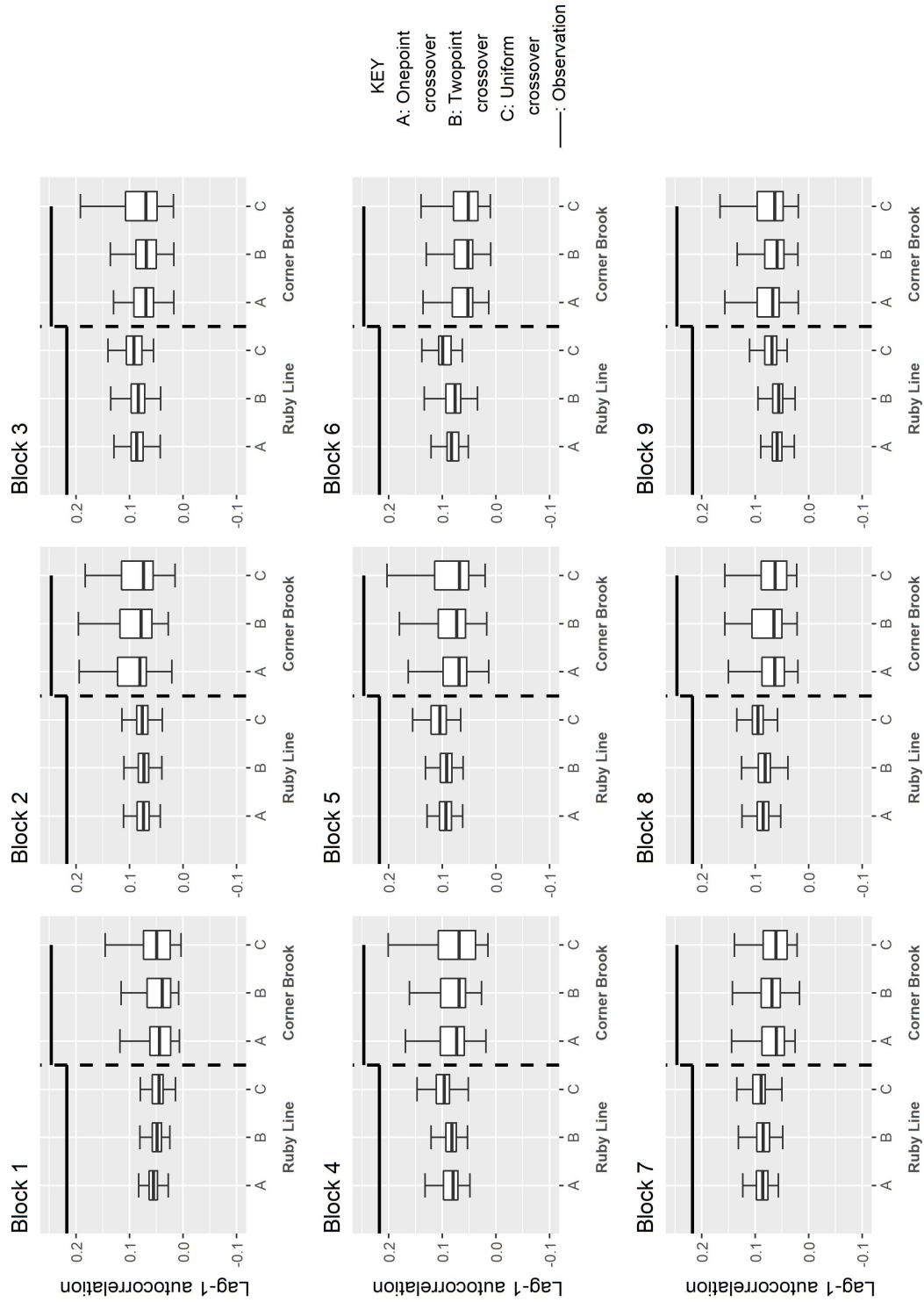
Figure A.14: Lag-1 autocorrelation of observed and disaggregated data at 12hr for all blocks of available data (indicated at the top of the boxplot generated from 100 simulation runs). Station name indicated below the plot.

224
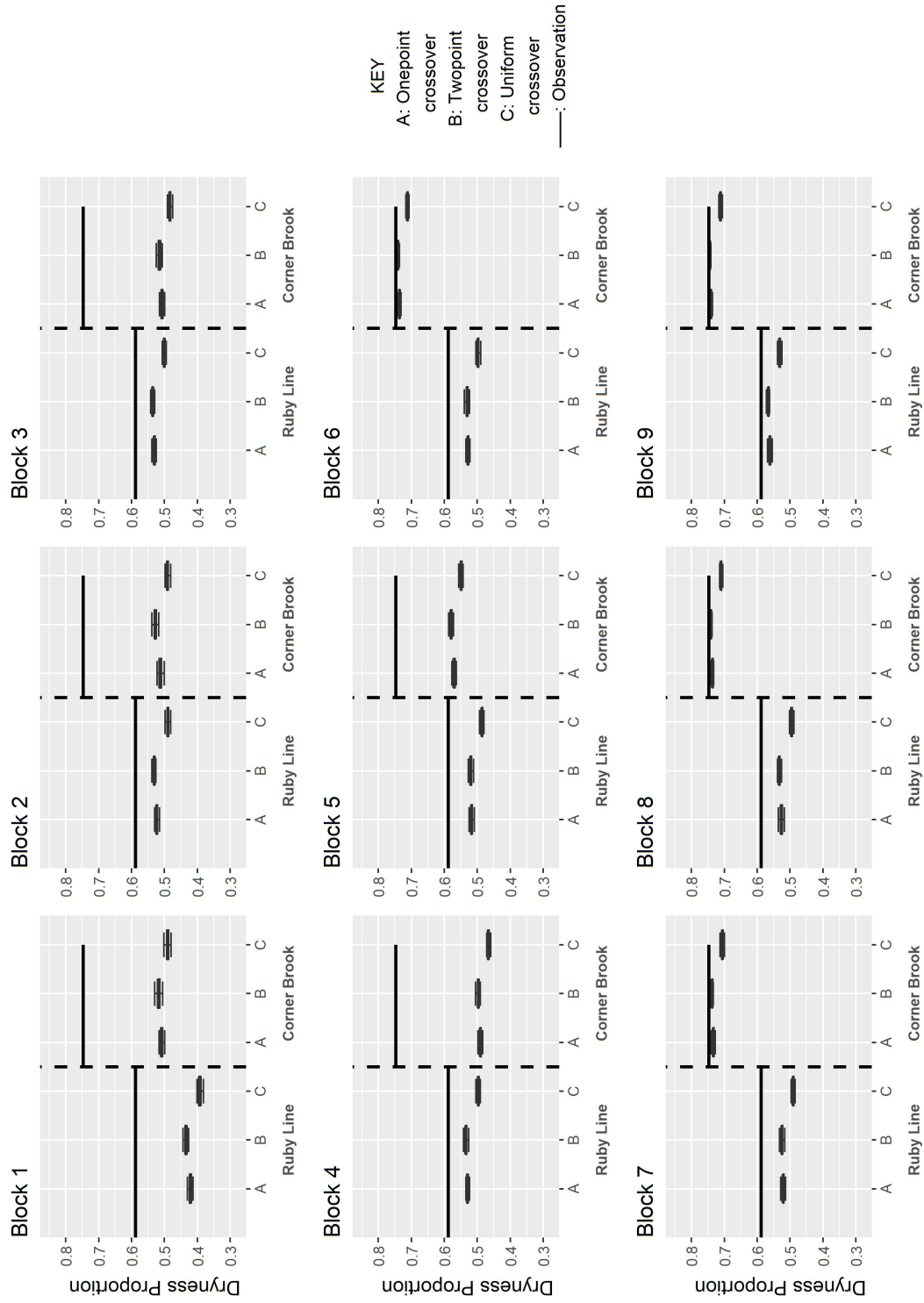
Figure A.15: Dryness proportion of observed and disaggregated data at 12hr for all blocks of available data (indicated at the top of the boxplot generated from 100 simulation runs). Station name indicated below the plot.

225
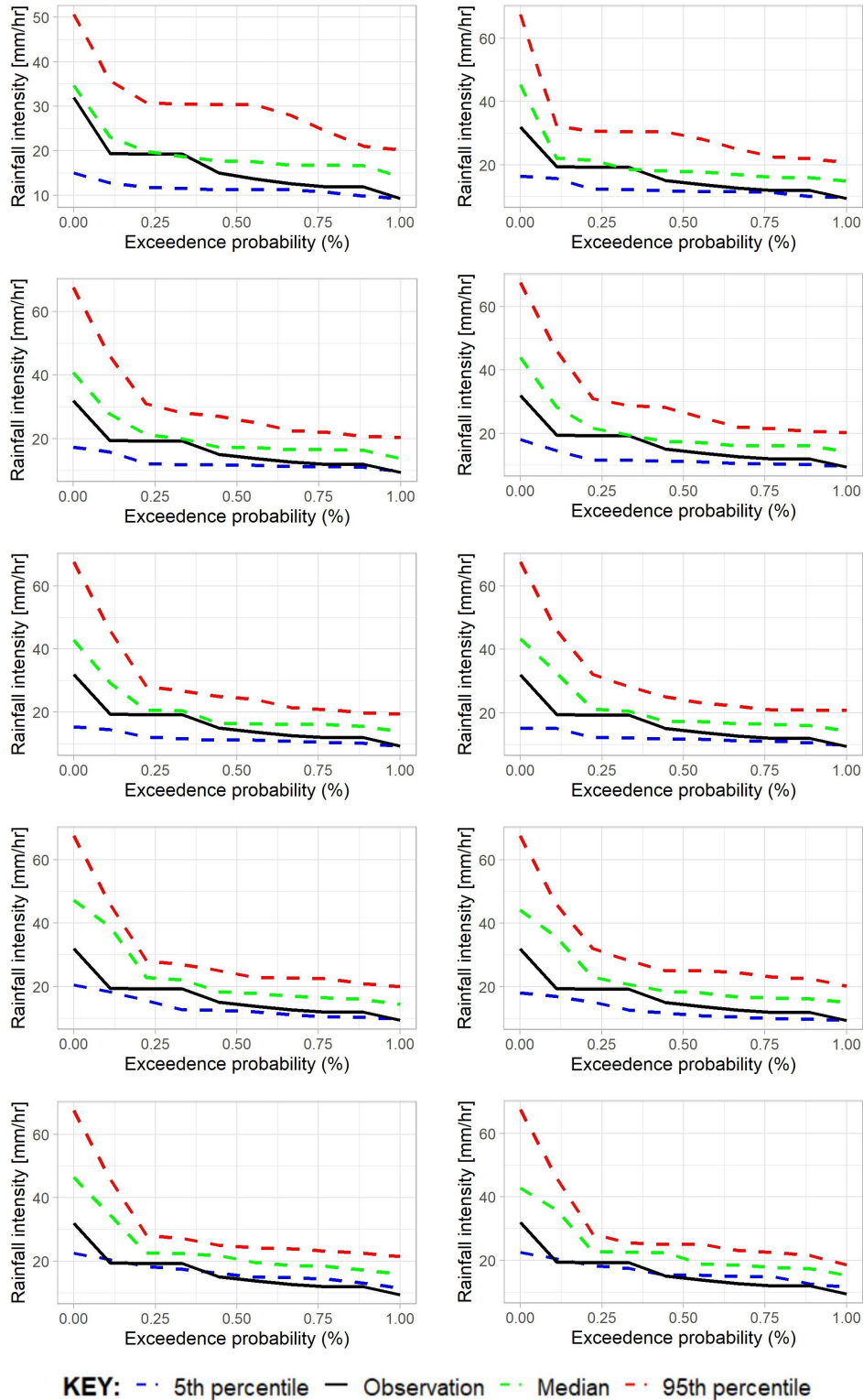
Figure B.16: Intensities of annual maximum precipitation for 1-hr against exceedence probability using the GA-MoF Onepoint crossover disaggregation model for all blocks of data at Ruby Line station.
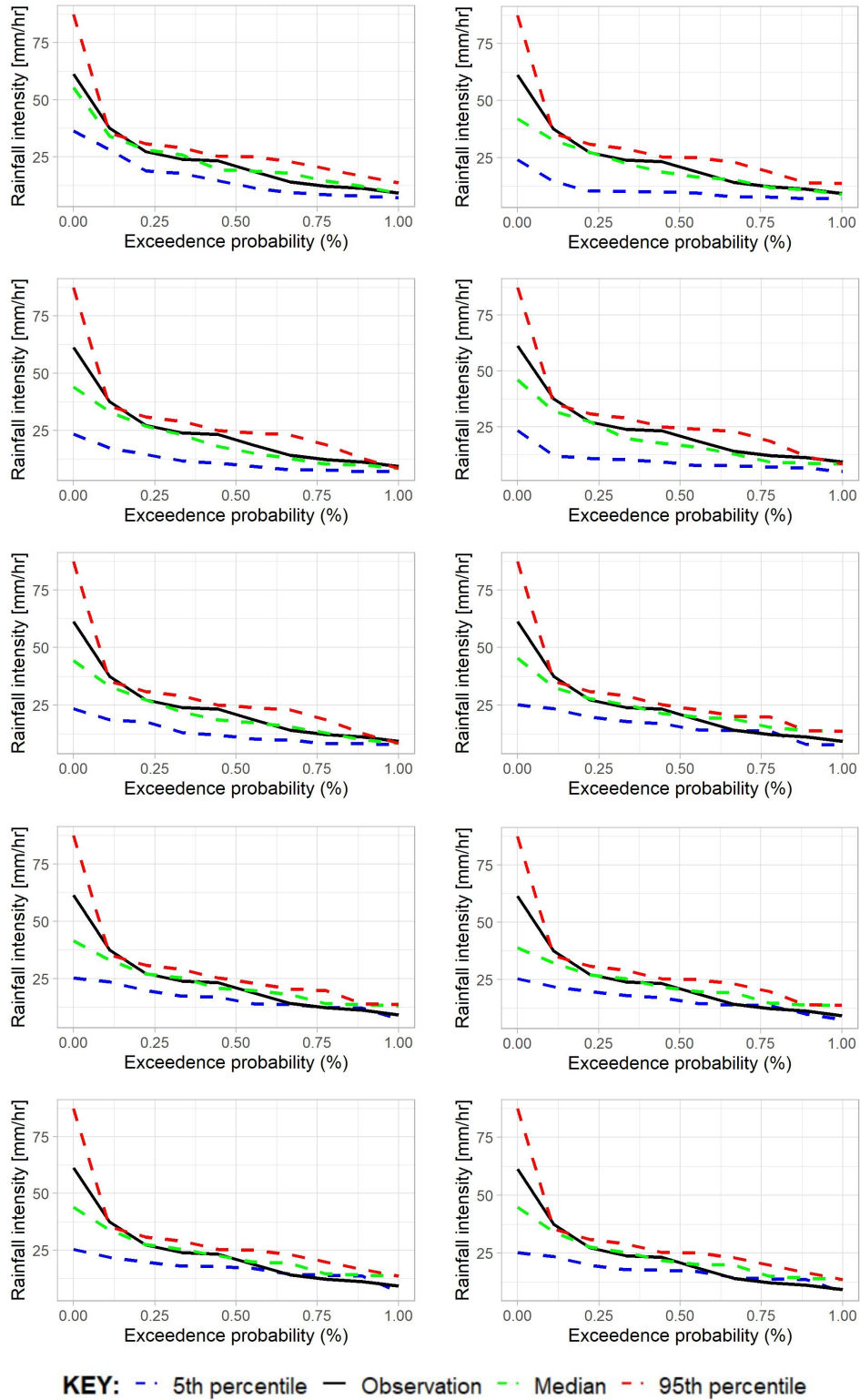
Figure B.17: Intensities of annual maximum precipitation for 1-hr against exceedence probability using the GA-MoF Onepoint crossover disaggregation model for all blocks of data at Corner Brook station.
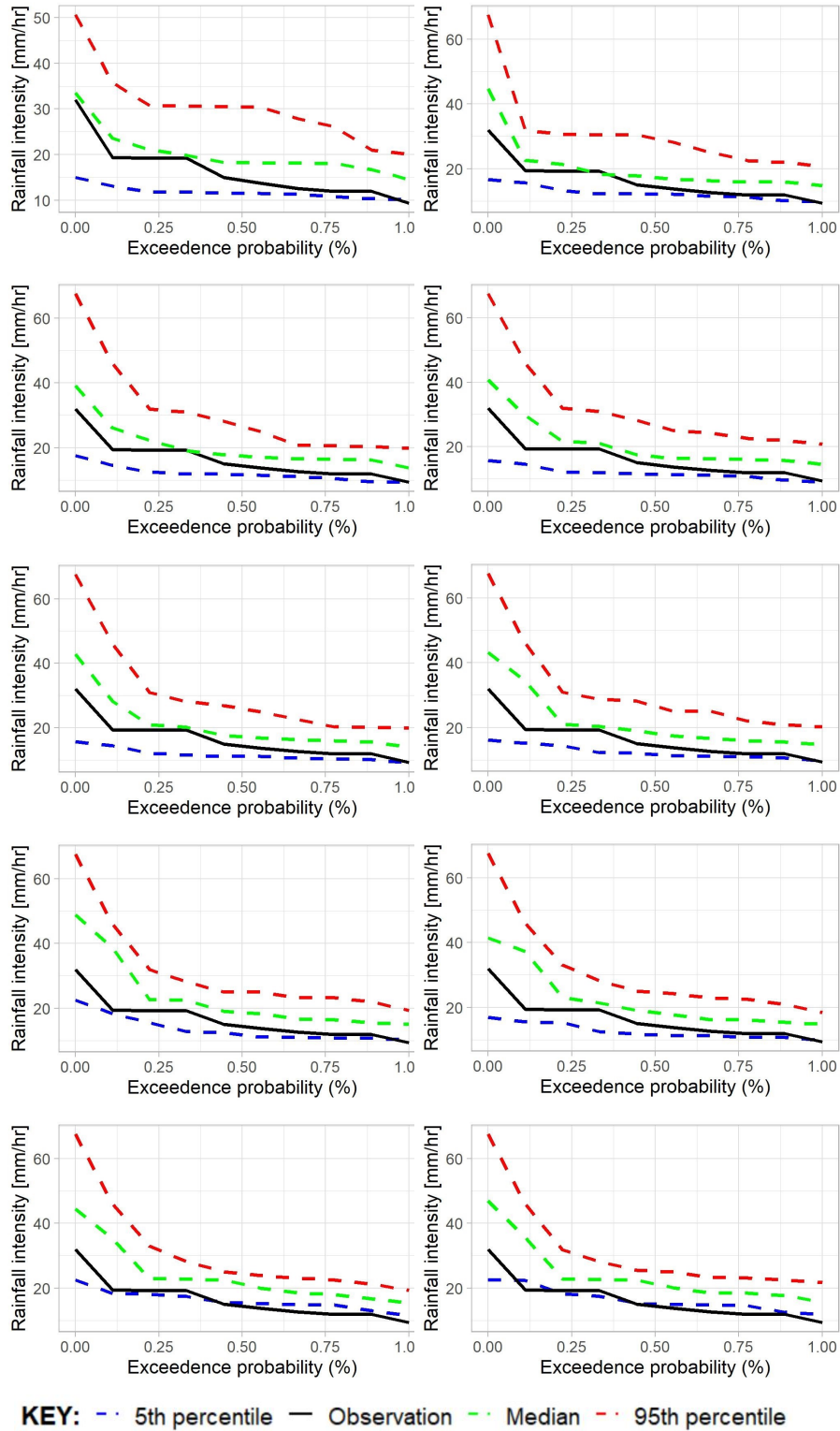
Figure B.18: Intensities of annual maximum precipitation for 1-hr against exceedence probability using the GA-MoF Twopoint crossover disaggregation model for all blocks of data at Ruby Line station.
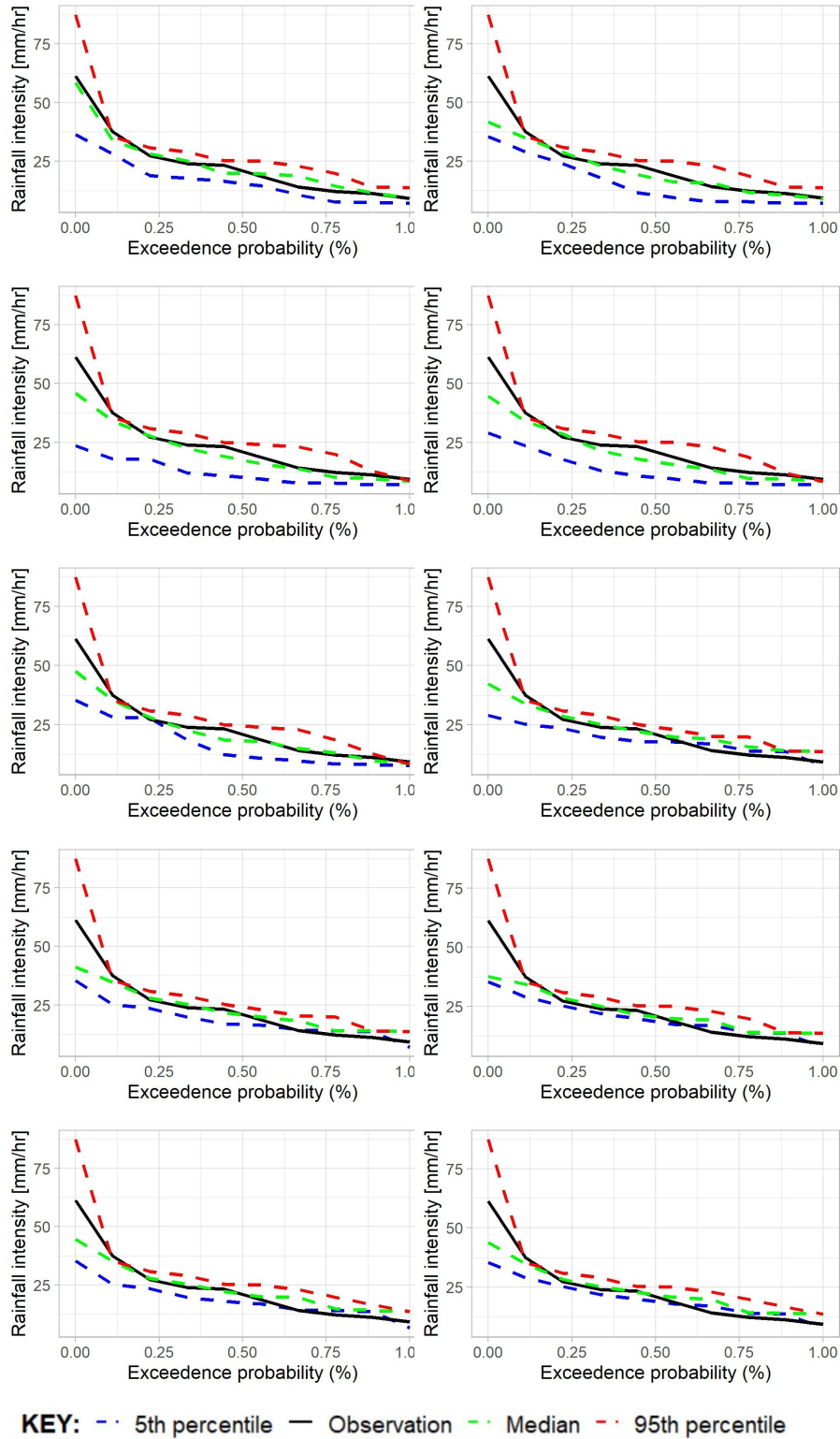
Figure B.19: Intensities of annual maximum precipitation for 1-hr against exceedence probability using the GA-MoF Twopoint crossover disaggregation model for all blocks of data at Corner Brook station.
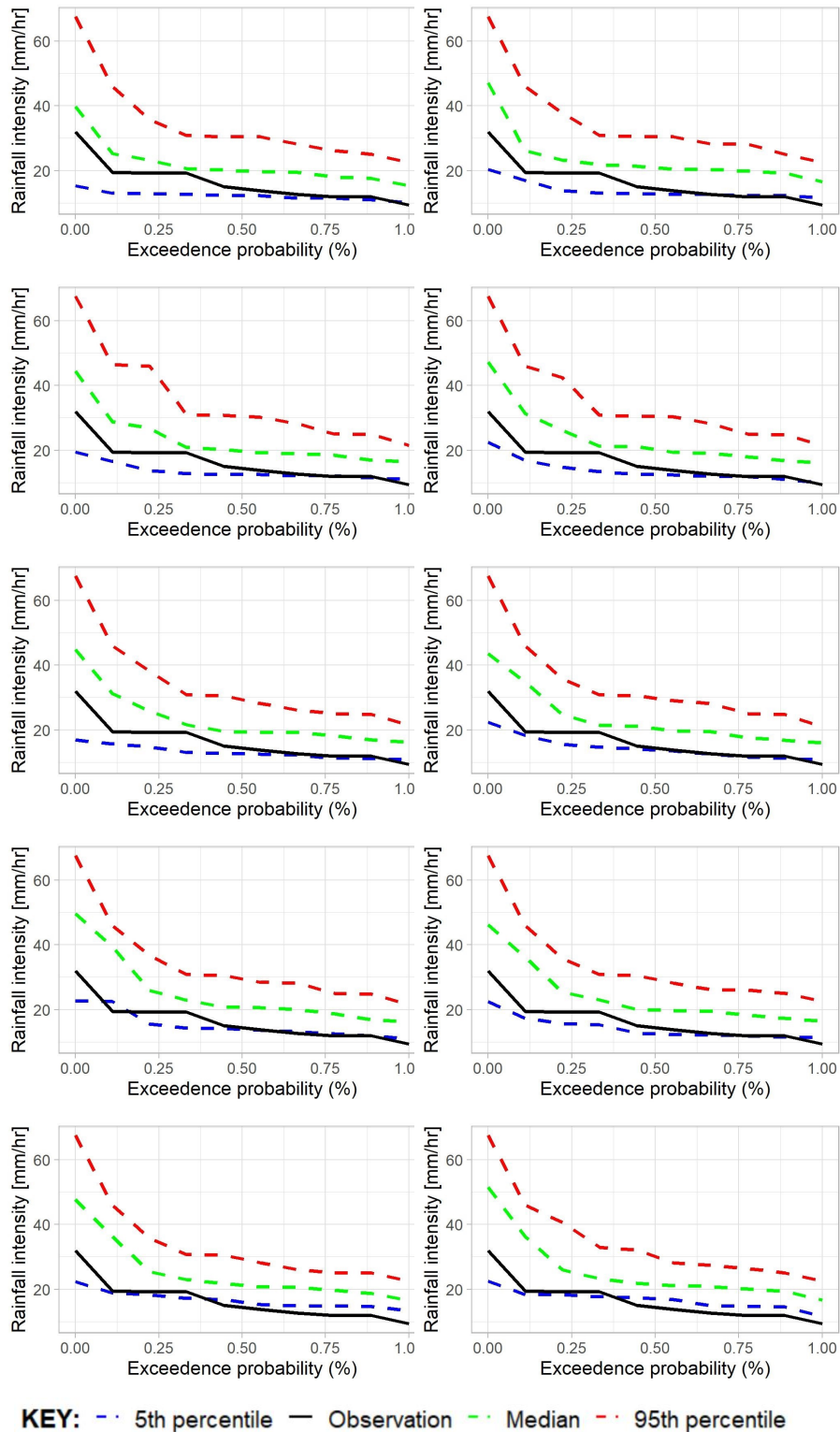
Figure B.20: Intensities of annual maximum precipitation for 1-hr against exceedence probability using the GA-MoF Uniform crossover disaggregation model for all blocks of data for Ruby Line station.
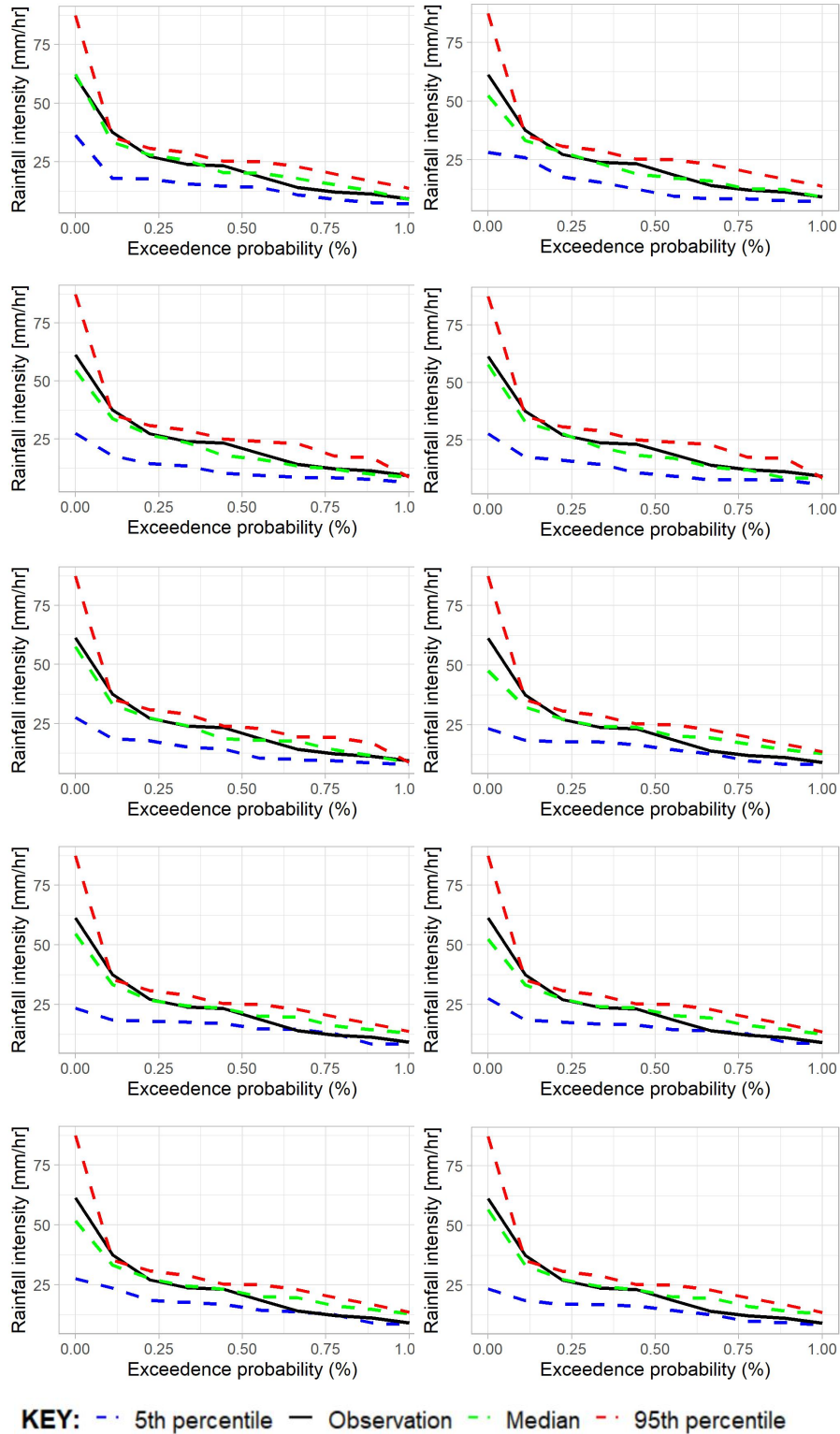
Figure B.21: Intensities of annual maximum precipitation for 1-hr against exceedence probability using the GA-MoF Uniform crossover disaggregation model for all blocks of data for Corner Brook station.
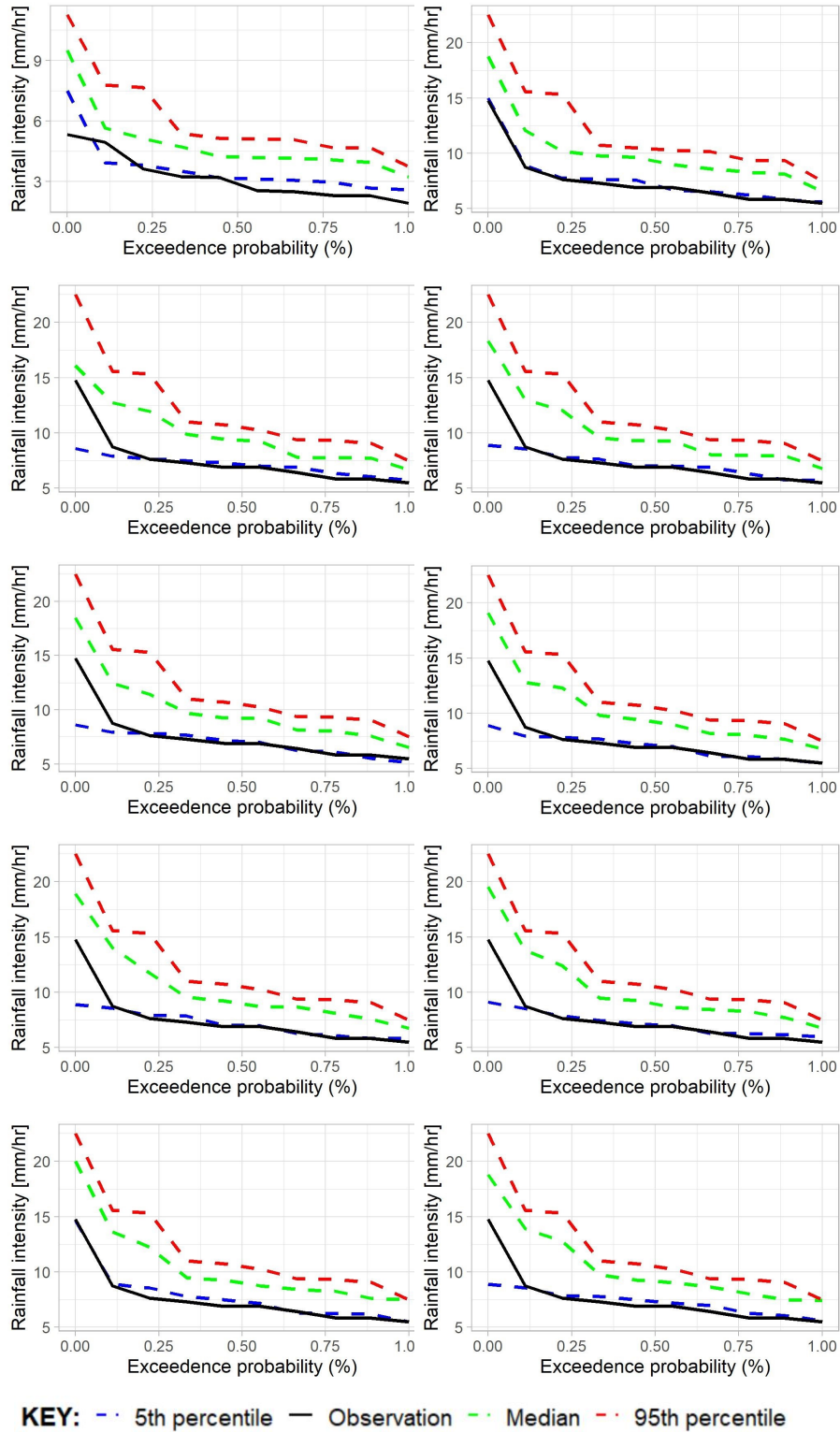
Figure B.22: Intensities of annual maximum precipitation for 6-hr against exceedence probability using the GA-MoF Onepoint crossover disaggregation model for all blocks of data at Ruby Line station.
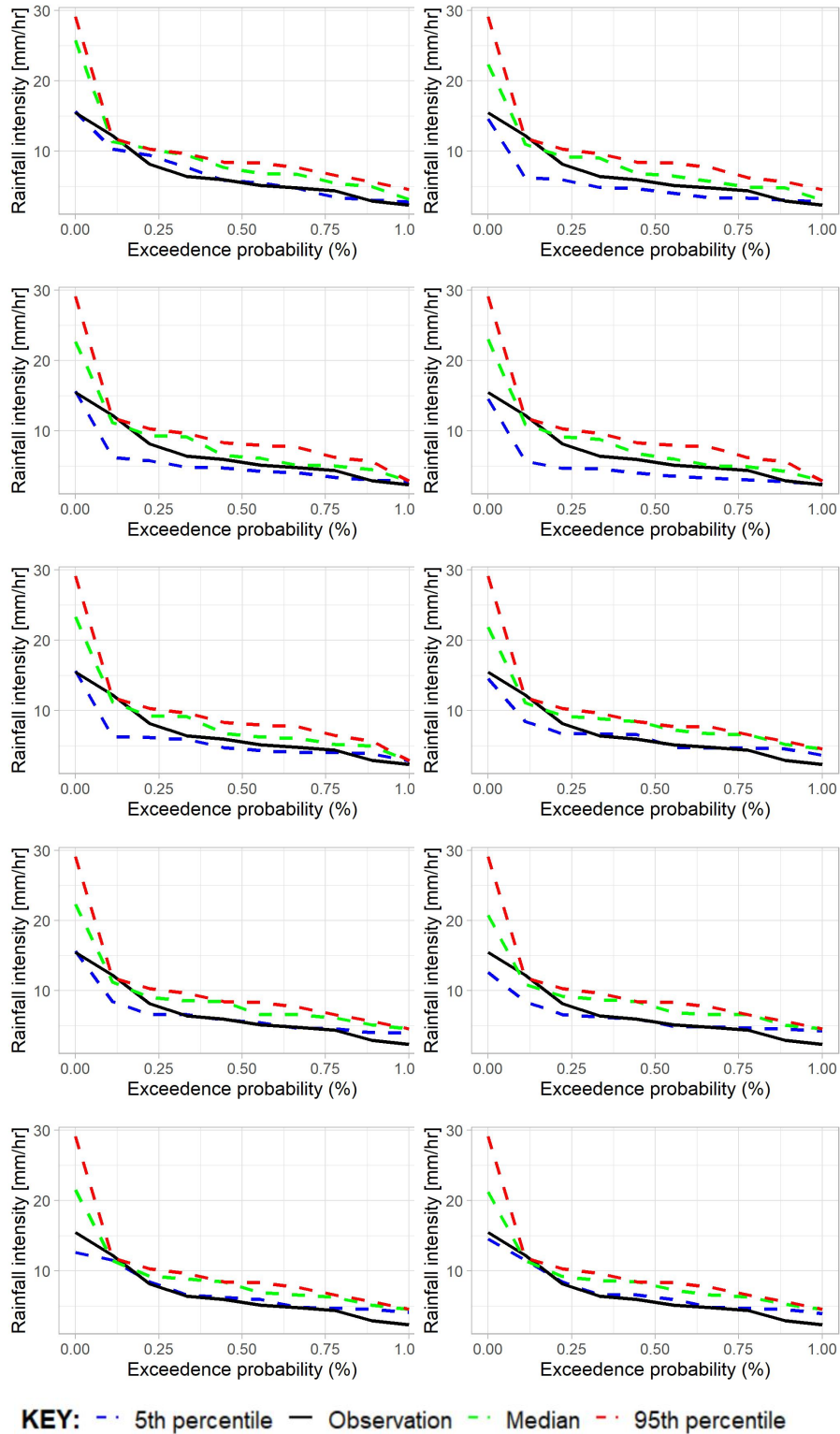
Figure B.23: Intensities of annual maximum precipitation for 6-hr against exceedence probability using the GA-MoF Onepoint crossover disaggregation model for all blocks of data at Corner Brook station.
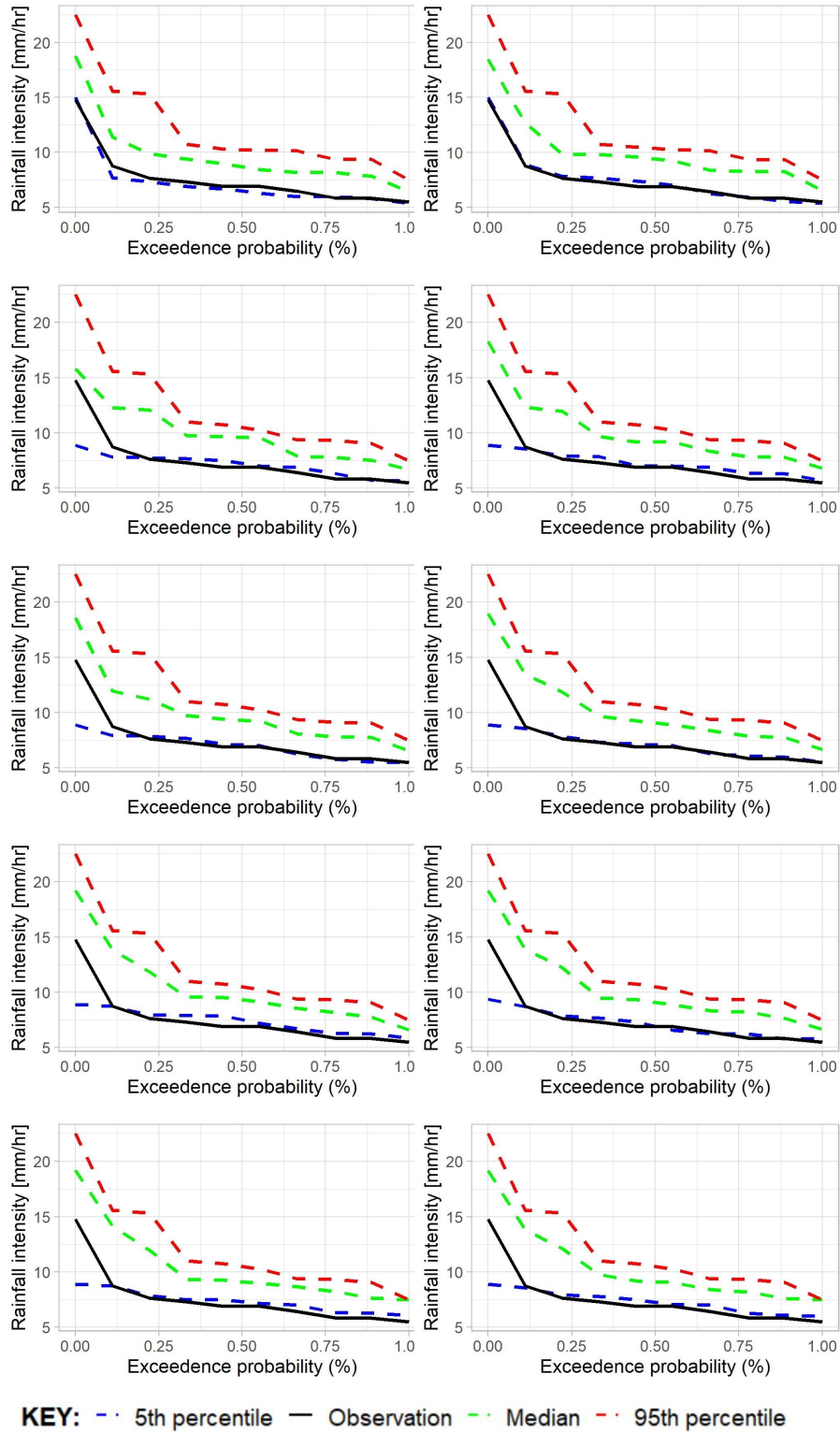
Figure B.24: Intensities of annual maximum precipitation for 6-hr against exceedence probability using the GA-MoF Twopoint crossover disaggregation model for all blocks of data at Ruby Line station.
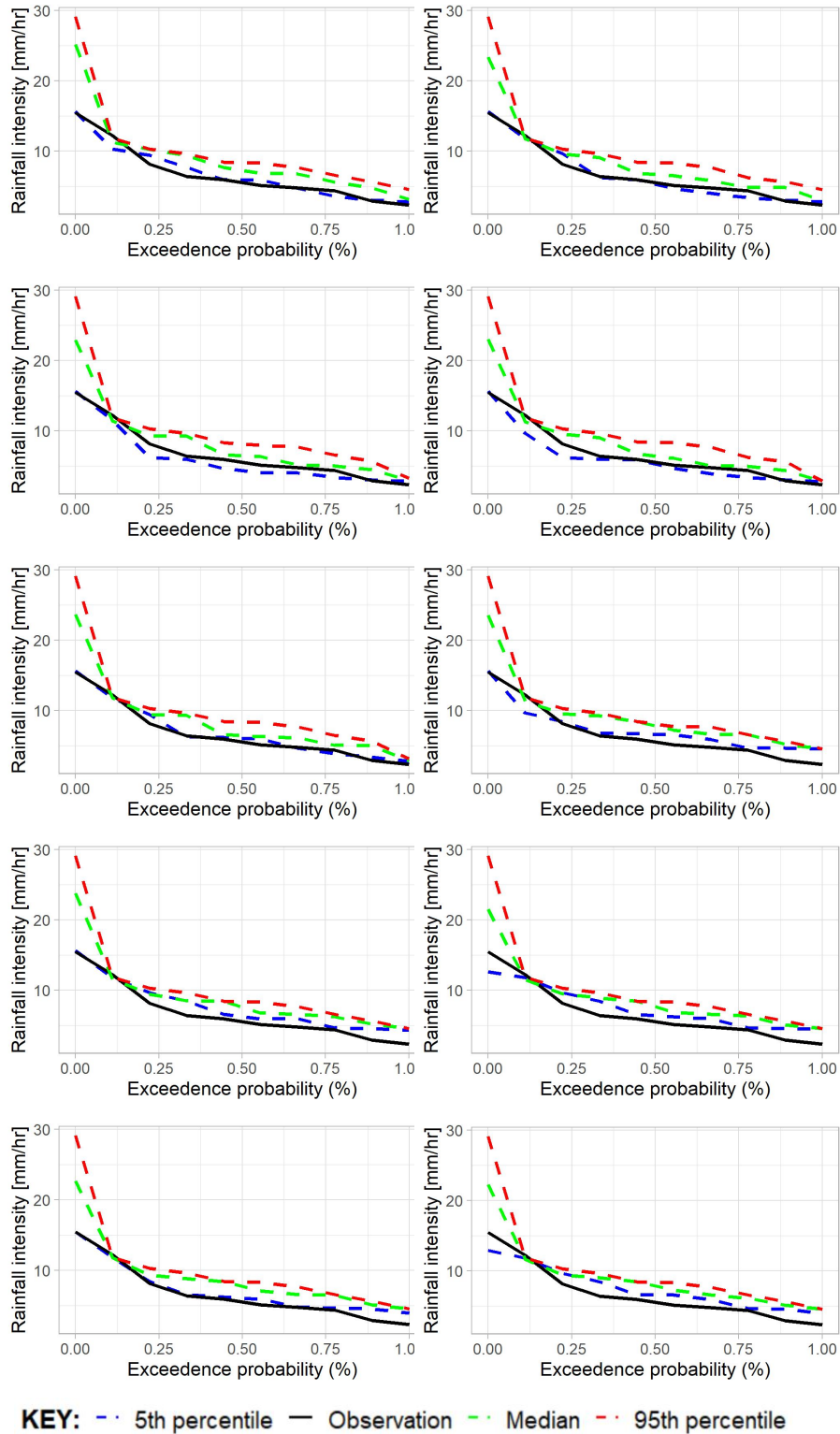
Figure B.25: Intensities of annual maximum precipitation for 6-hr against exceedence probability using the GA-MoF Twopoint crossover disaggregation model for all blocks of data at Corner Brook station.
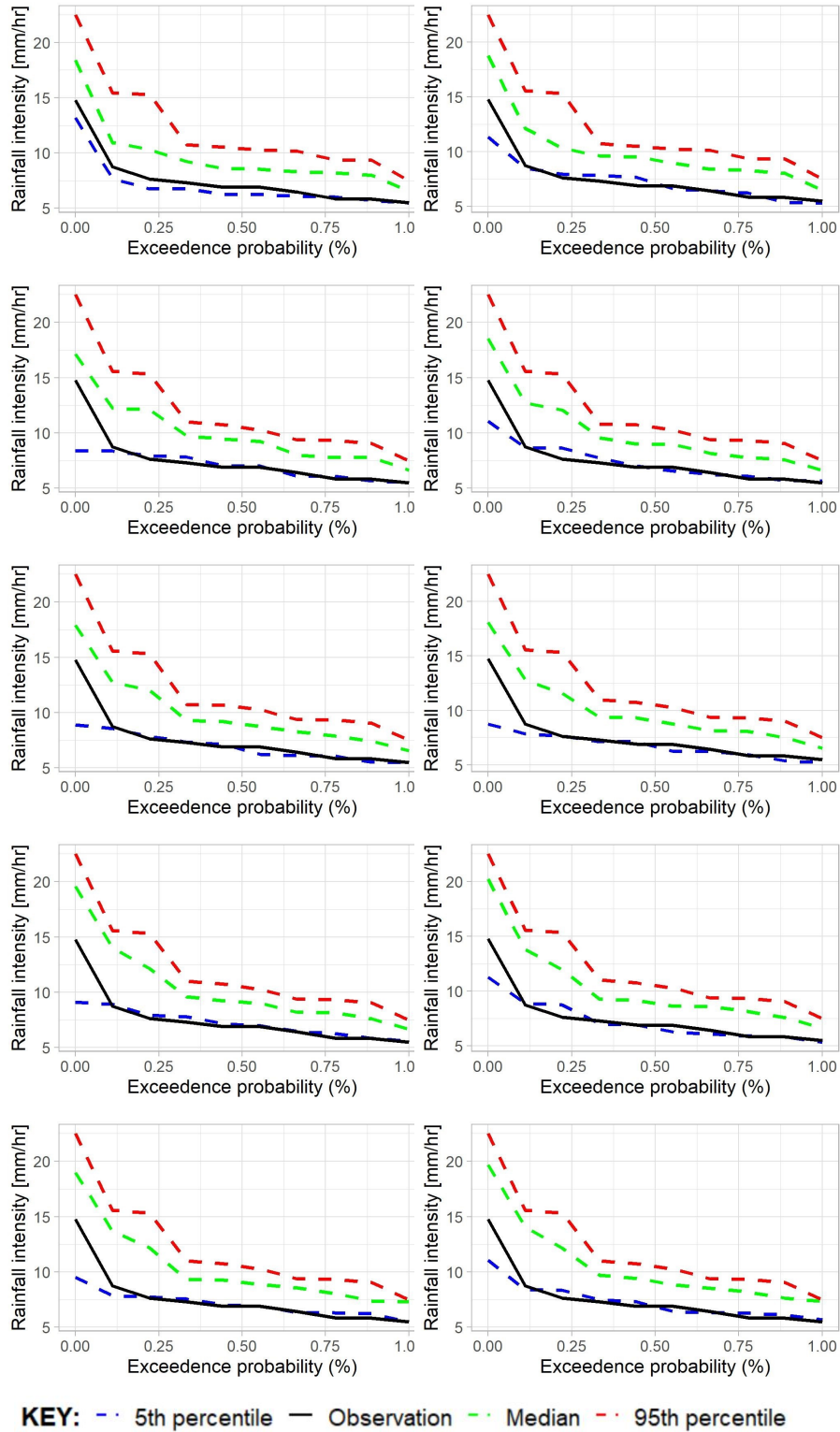
Figure B.26: Intensities of annual maximum precipitation for 6-hr against exceedence probability using the GA-MoF Uniform crossover disaggregation model for all blocks of data at the Ruby Line sattion.
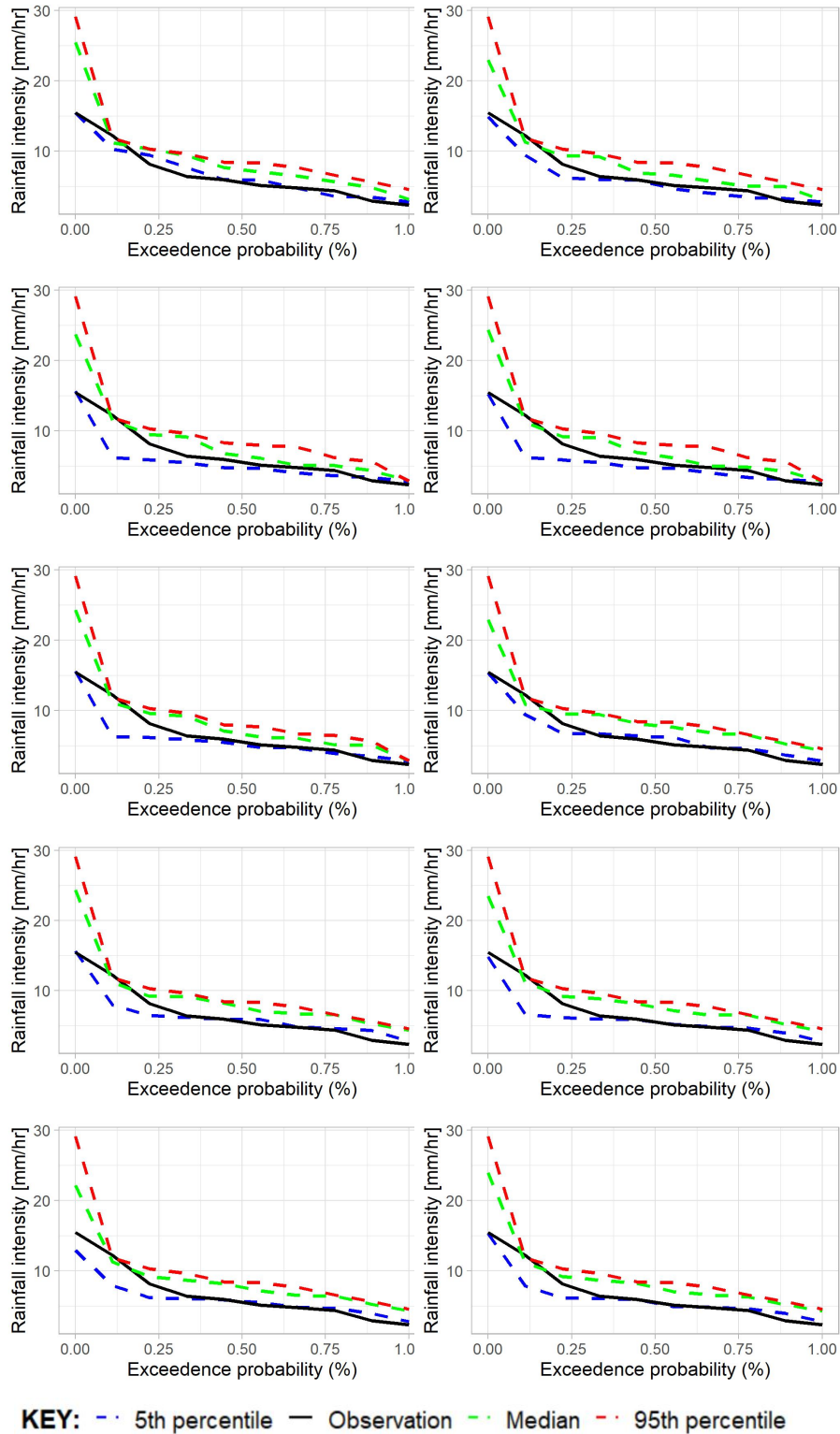
Figure B.27: Intensities of annual maximum precipitation for 6-hr against exceedence probability using the GA-MoF Uniform crossover disaggregation model for all blocks of data at the Corner Brook sattion.
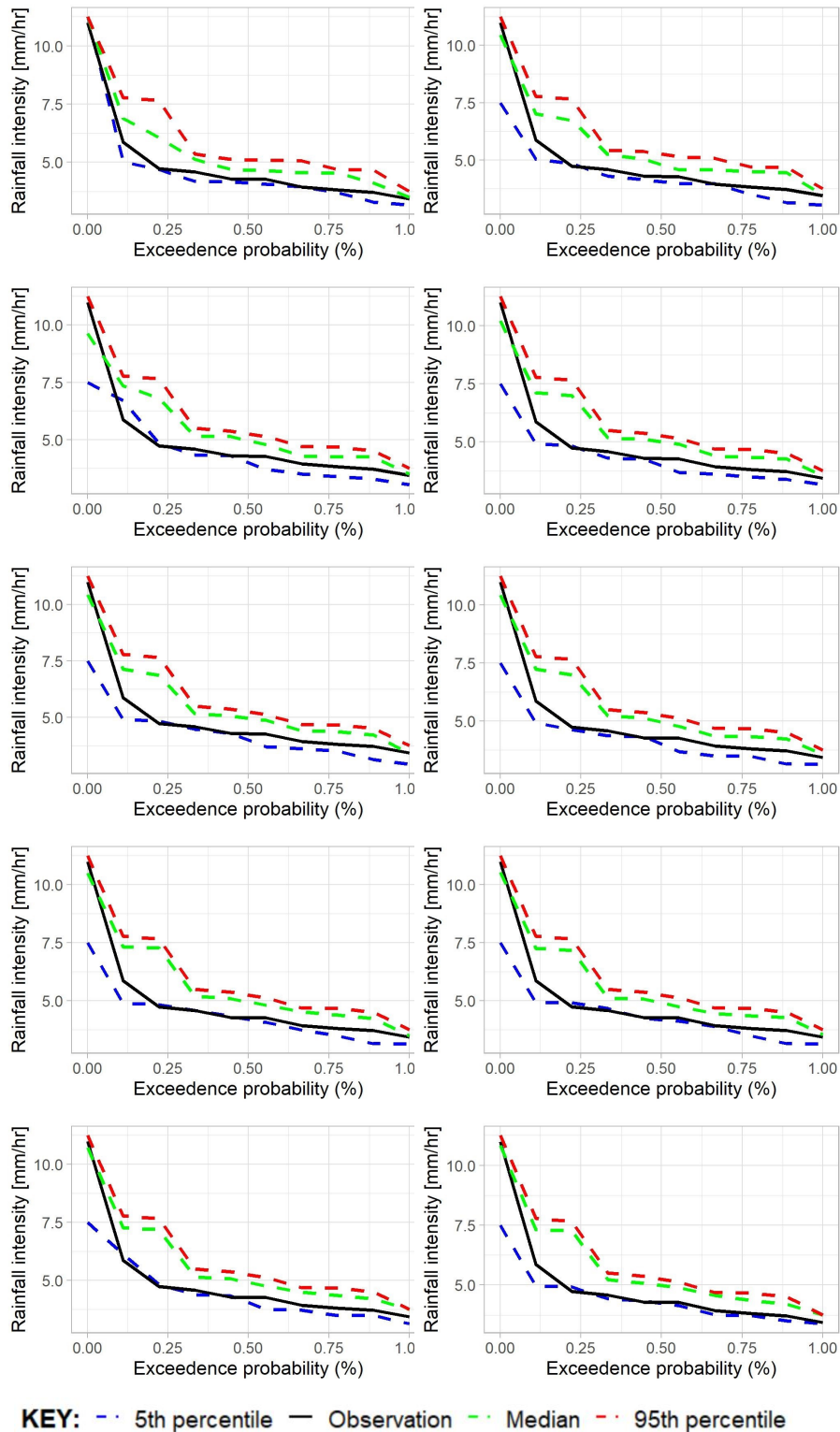
Figure B.28: Intensities of annual maximum precipitation for 12-hr against exceedence probability using the GA-MoF Onepoint crossover disaggregation model for all blocks of data at the Ruby Line station.
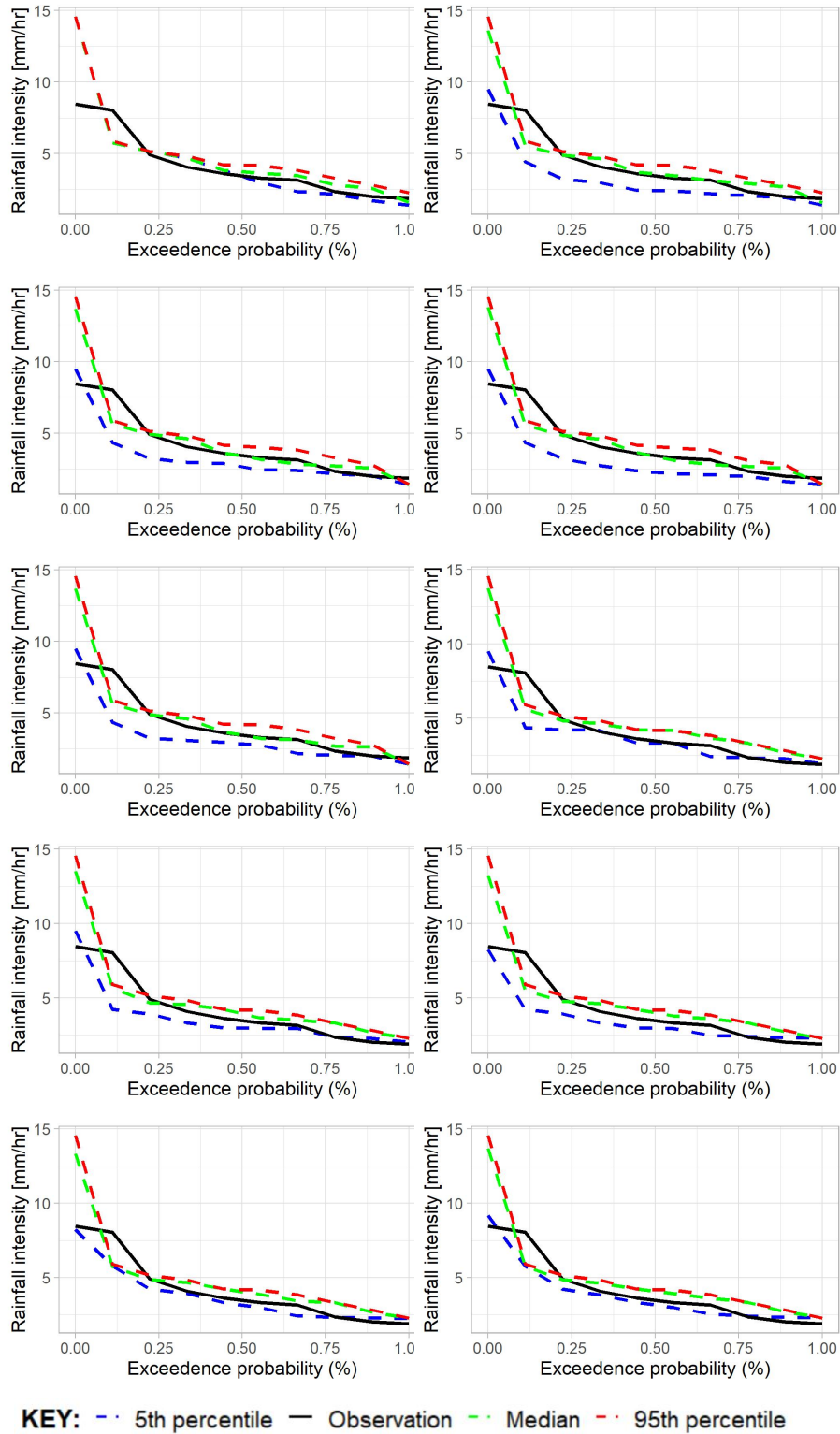
Figure B.29: Intensities of annual maximum precipitation for 12-hr against exceedence probability using the GA-MoF Onepoint crossover disaggregation model for all blocks of data at the Corner Brook station.
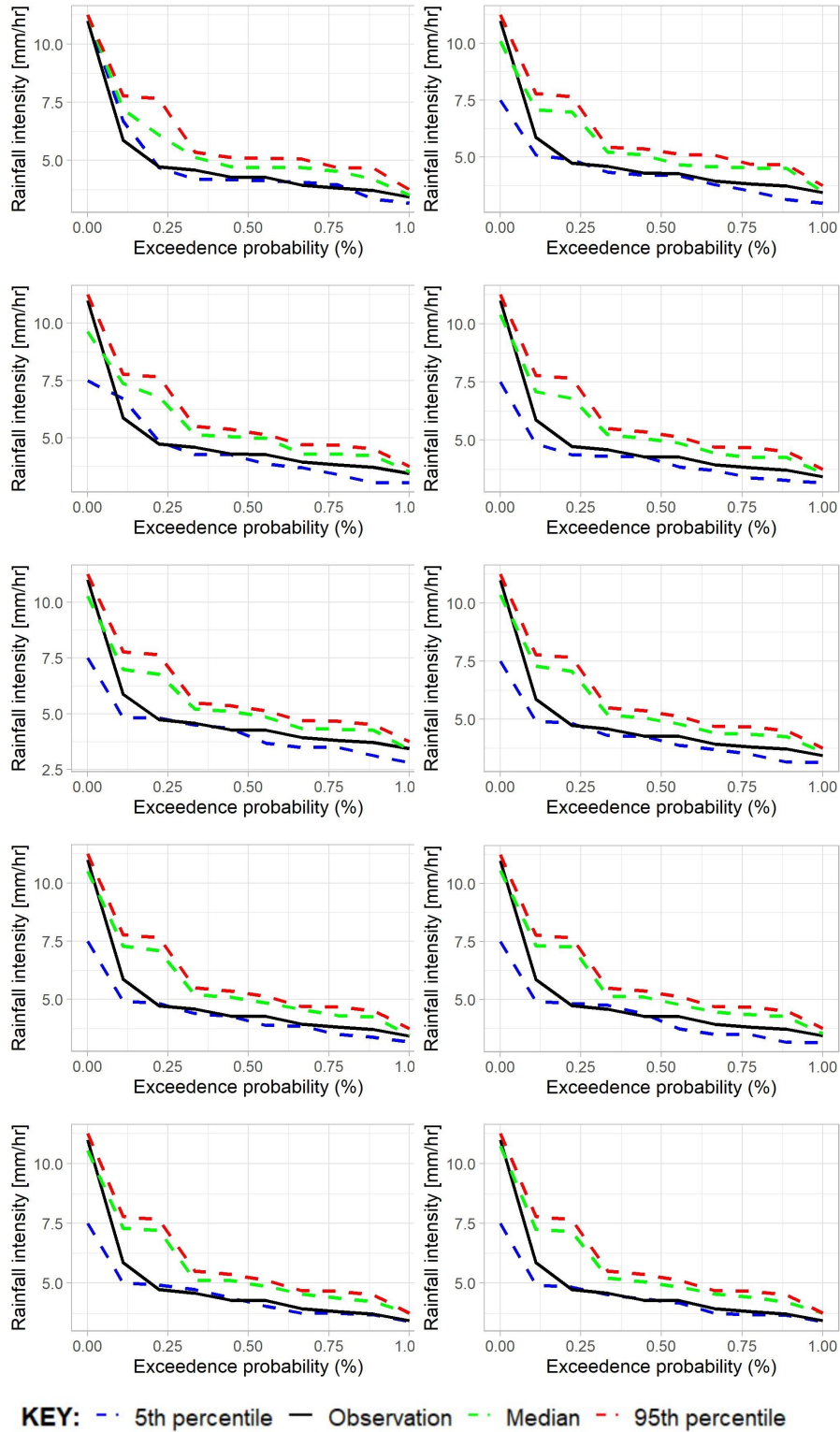
Figure B.30: Intensities of annual maximum precipitation for 12-hr against exceedence probability using the GA-MoF Twopoint crossover disaggregation model for all blocks of data at the Ruby Line station.
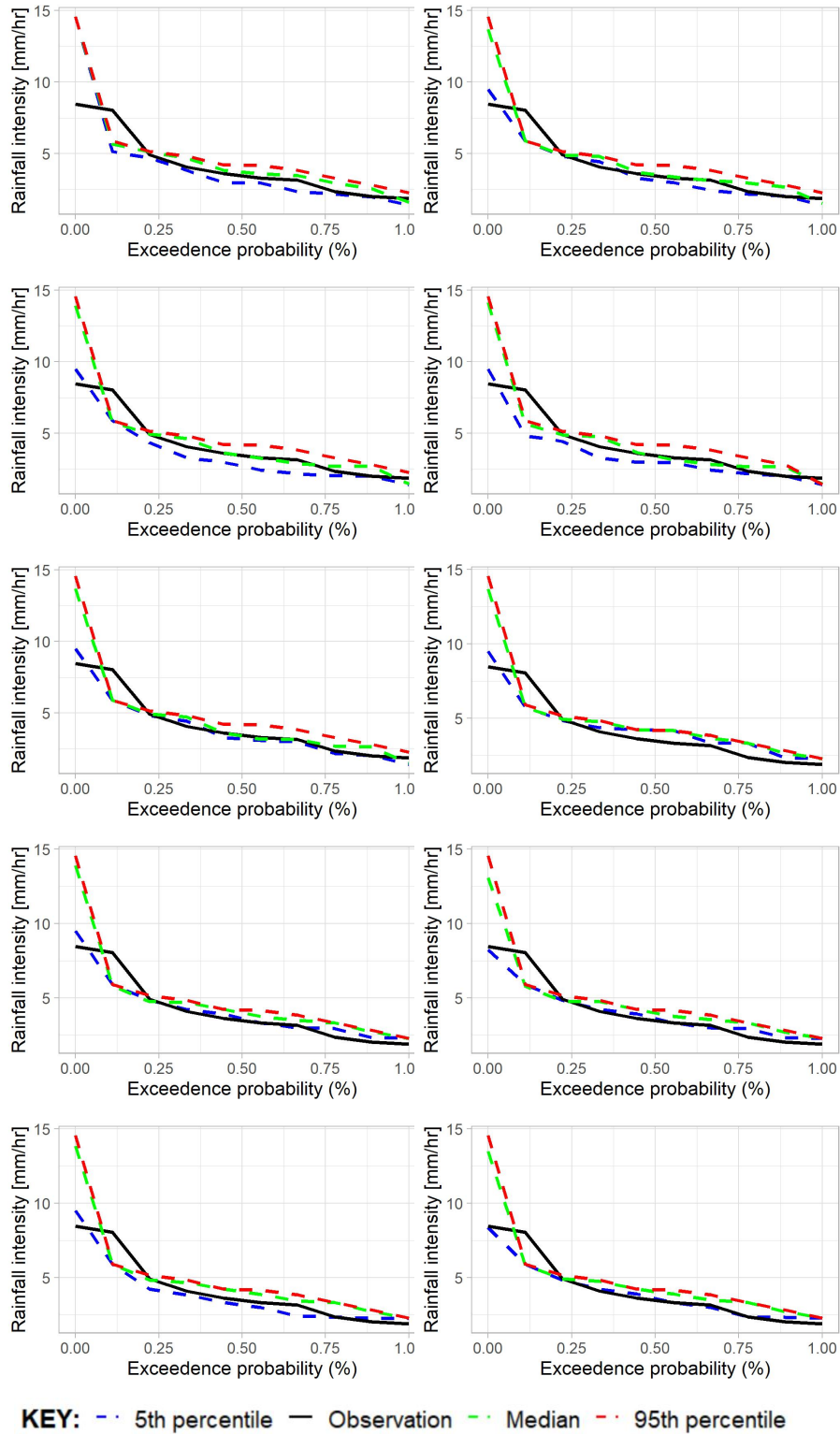
Figure B.31: Intensities of annual maximum precipitation for 12-hr against exceedence probability using the GA-MoF Twopoint crossover disaggregation model for all blocks of data at the Corner Brook station.
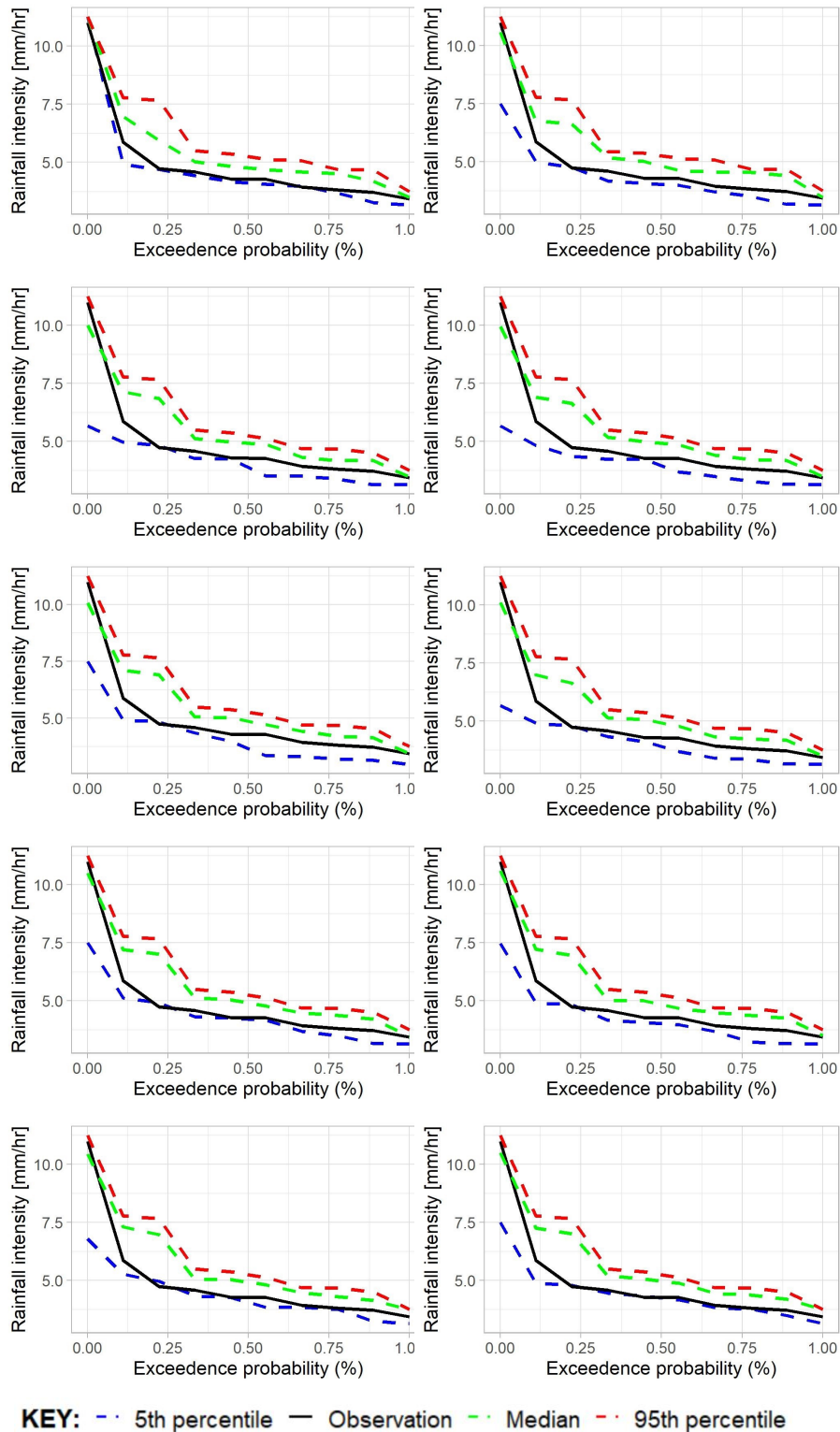
Figure B.32: Intensities of annual maximum precipitation for 12-hr against exceedence probability using the GA-MoF Uniform crossover disaggregation model for all blocks of data at the Ruby Line station.
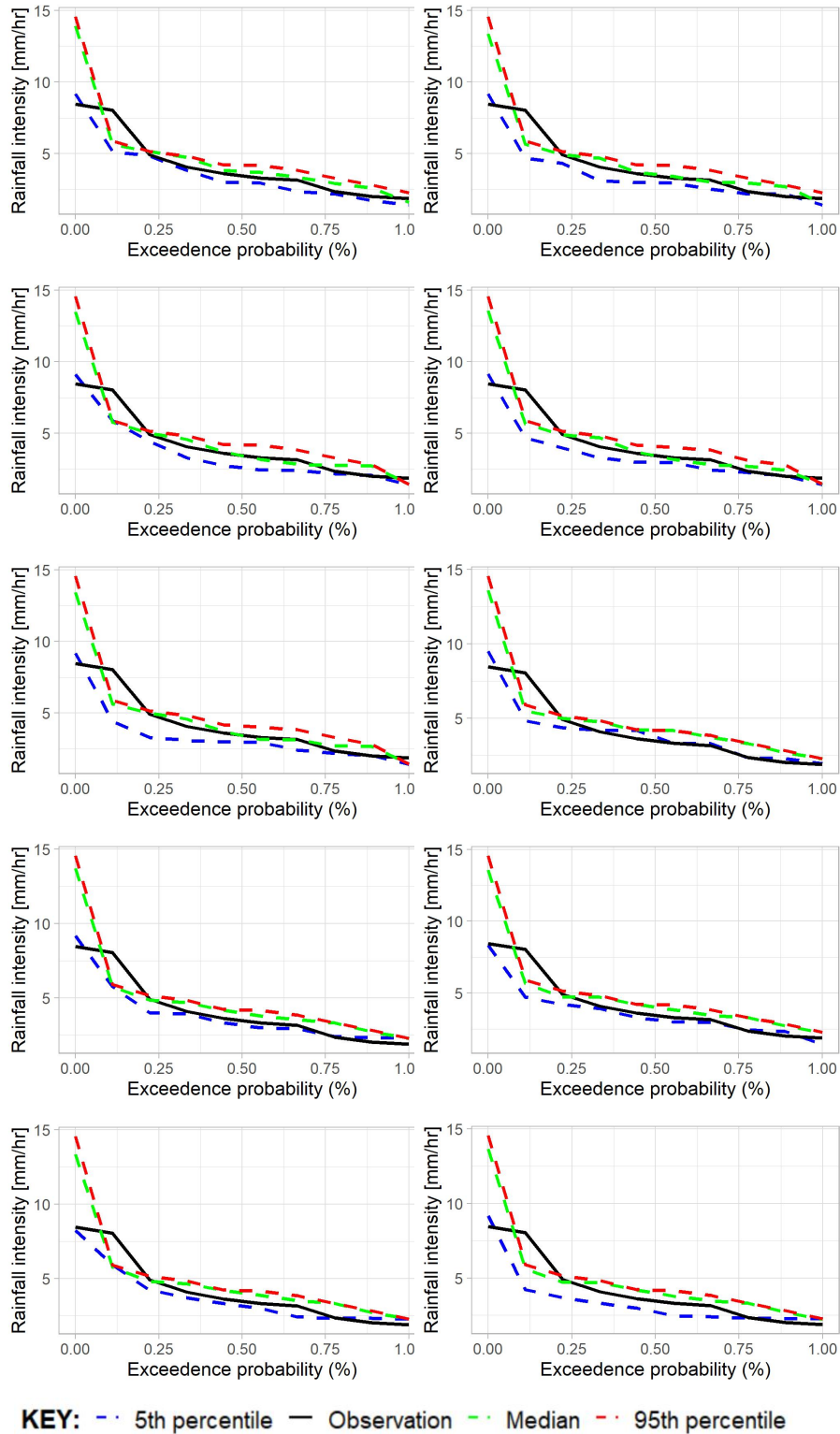
Figure B.33: Intensities of annual maximum precipitation for 12-hr against exceedence probability using the GA-MoF Uniform crossover disaggregation model for all blocks of data at the Corner Brook station.